DOE/LC/11057-2668
(DE89000946)

Recovery and Upgrading of Oil From Utah Tar Sands

DOE/LC/11057--2668

DE89 000946

Final Report

A.G. Oblad
J.W. Bunger
F.V. Hanson
J.D. Miller
J.D. Seader

December 1987

Work Performed Under Contract No.: DE-FG20-84LC11057

For
U.S. Department of Energy
Office of Fossil Energy
Morgantown Energy Technology Center
Morgantown, West Virginia

By
University of Utah
Salt Lake City, Utah

DISCLAIMER

Available from the National Technical Information Service, U. S. Department of Commerce, Springfield, VA 22161.

Price: Printed copy A17
Microfiche A01

Codes are used for pricing all publications. The code is determined by the number of pages in the publication. Information pertaining to the pricing codes can be found in the current issues of the following publications, which are generally available in most libraries: *Energy Research Abstracts (ERA), Government Reports Announcements* and Index (*GRA* and *I*); *Scientific and Technical Abstract Reports (STAR);* and publication NTIS-PR- 360 available from NTIS at the above address.

DOE/LC/11057-2668
(DE89000946)

Recovery and Upgrading of Oil From Utah Tar Sands

Final Report

A.G. Oblad
J.W. Bunger
F.V. Hanson
J.D. Miller
J.D. Seader

Work Performed Under Contract No.: DE-FG20-84LC11057

For
U.S. Department of Energy
Office of Fossil Energy
Morgantown Energy Technology Center
P.O. Box 880
Morgantown, West Virginia 26507-0880

By
University of Utah
Salt Lake City, Utah 84112-1183

December 1987

TABLE OF CONTENTS

LIST OF TABLES

LIST OF FIGURES

EXECUTIVE SUMMARY

This report covers the work carried out at the University of Utah during the period October 1, 1984 through December 31, 1987, on Utah's tar sands. The program has advanced significantly towards our long-term objectives. These are concerned with the selection of optimal process concepts for bitumen recovery and upgrading via above-ground methods and the development of the scientific and engineering data base necessary for the eventual commercialization of domestic tar sands.

The main areas for study in this report are bitumen upgrading by hydropyrolysis, a low coke-producing process pioneered at the University; bitumen recovery by pyrolysis of tar sand in a fluidized-bed retort; bitumen recovery in coupled fluidized-beds with interbed heat transfer via heat pipes; and bitumen recovery by water-assisted separation methods of bitumen from ore.

The principal reactions occurring in hydropyrolysis have been defined and grouped. The reaction kinetics (mathematical models) have been determined for the individual reaction types, thus making it possible to predict product distribution obtainable from bitumens and hydrogen consumption as a function of process variables.

Results from the 2 liter per hour process development unit (PDU) have shown that heavy residual feeds and bitumens can be converted to high yields of liquid products (>90%) with low coke and gas production. Even better yields are expected on a larger scale reactor model which is planned for the next phase of our study.

A large-scale fluidized-bed tar sand pyrolysis reactor system has been designed, erected, and preliminarily tested. While operation for longer time periods has not yet been achieved, the tests carried out thus far have indicated that results are consistent with previous results obtained with the small reactor system. Further testing after modifications to the equipment, particularly the front end materials handling equipment, will be carried out. Of particular importance will be the corroboration of

the effect of the main variables on yield structures. The unit is currently being operated on Whiterocks tar sand to produce barrel quantities of liquid product for the Department of Energy.

The small-scale reactor system has been operated on several additional Utah tar sands. Those investigated are three samples from different areas of the PR Spring deposit and one from the Circle Cliffs deposit. Yield structures as a function of temperatures and retention time were determined. The Circle Cliffs tar sand was found to contain sand along with feldspar and kaolinite. The results obtained with the PR Spring samples were consistent with previous results obtained with other tar sands. However, the Circle Cliffs material was quite different in that the pyrolysis resulted in the production of water along with the hydrocarbon liquid usually obtained. Furthermore, an unusual decrease in product liquids at higher pyrolysis temperatures was found. Both the excess water found and the loss of yield encountered may result from the kaolin mineral present in the sand.

As a follow-up of the finding of an increase of liquid product yield at short residence times, a theoretical study was made of a cyclone separator reactor concept. A study of cyclone size, particle size, pyrolysis temperature, and reaction time indicated that tar sands of particle sizes as low as 0.03 cm could be successfully pyrolyzed in a cyclone reactor of 400 cm diameter, while pyrolysis of tar sands of particle sizes greater than 0.1 cm diameter would not be successful. The study indicated that a transport reactor coupled with cyclone separators would be more attractive than the cyclone alone.

A mathematical model of tar sand bitumen pyrolysis has been developed. The model is based on a hypothetical reaction matrix in which reaction kinetics and mass transport via convective and diffusion processes are occurring. Extensive data from thermogravimetric analysis studies were carried out to provide a data base for the model studies.

Studies of the coupled bed pyrolysis of tar sands using heat pipes were carried out. Included were (1) determinations of the effect of pressure on the upgrading of oil obtained the laboratory unit; (2) the design and estimate of investment and operating costs for tar sand processing plants of 15,000 and 50,000 bbls/day capacity; (3) the effect of bitumen content on the costs for a 50,000 bbl/day plant;

(4) the energy efficiency analyses of several different coupled-bed tar sand processing schemes; and (5) the development of a mathematical model for the minimum fluidization velocity of tar sands at high temperatures.

Extensive studies have been carried out to advance the technology of the modified hot-water process developed at the University of Utah. These studies have been concentrated in three main areas: (1) fundamental research to elicit a broader understanding of bitumen displacement from the sand surfaces; (2) research to achieve lower energy use in the digestion step in a stirred reactor; and (3) studies leading to diluents of improved properties for altering bitumen properties which are of importance in the disengagement and separation steps of the hot-water separation process. Some of the important conclusion from this work are: (1) bitumen disengagement from a coated surface takes place only when the shear stress on the bitumen layer exceeds the adhesive or cohesive forces occurring in the layer; (2) tar sand shape factors play an important role in bitumen recovery efficiency; and (3) efficiency of diluent for altering bitumen viscosity has been found to be related to both physical and chemical properties of the diluent.

SECTION A

BITUMEN UPGRADING

J.W. Bunger

BITUMEN UPGRADING

J.W. Bunger	Research Assistant Professor
P. Devineni	Graduate Student
H. Ryu	Graduate Student
C.H. Tsai	Graduate Student
R. Umoh	Graduate Student
J. Wiser	Research Assistant

INTRODUCTION

The upgrading of bitumen and bitumen-derived liquids can be accomplished by a variety of thermal and catalytic processes.[1,2] In recent years, attention has been focused on hydropyrolysis as a novel approach for the production of crude.[3-9] Hydropyrolysis upgrading of bitumen has been studied at the University of Utah for the past eleven years. In that time, we have demonstrated that hydropyrolysis will convert residual bitumen to high-grade distillate products in high yields. The high liquid yields achieved in hydropyrolysis result not only in better economics for the upgrading step, but also have a beneficial impact on the economics of the overall process, including the mining and bitumen recovery steps.

In previous reporting periods, we have described the design and construction of a 2 l/h hydropyrolysis unit. A schematic of this unit is presented in Figure 1. During the current reporting period we have gained operational experience on this process development unit and have conducted a more systematic study of the effect of process variables on yields and product distribution.

In the course of this work we have discovered that certain reactor variables are more important than previously thought. These variables included gas composition, gas preheater temperature, reactor wall temperature, and reactor and nozzle configuration. Also, the rate of the hydropyrolysis reactions, as contrasted with thermal reactions, were more dependent upon atomization quality than previously suspected. As a result, considerable effort was spent in establishing the operating procedures required to optimize the performance of the system. Once the operating procedures were established, a series

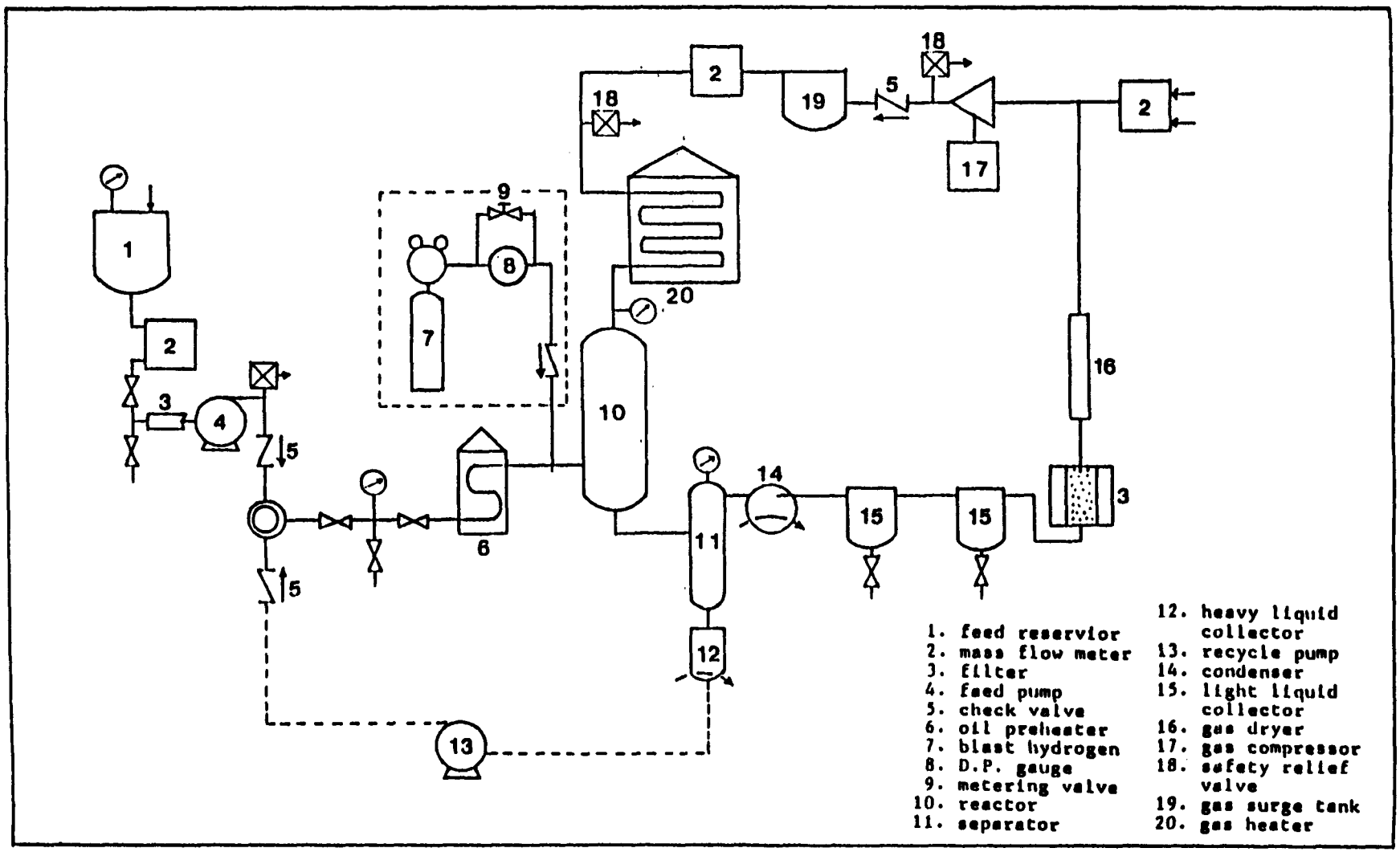

Figure 1. Hydropyrolysis process development unit process flow diagram.

of runs were performed to ascertain the effect of process variables on yield and product quality. This work is done in anticipation of the development of a model which is to be used for process design and optimization.

These engineering studies have been highly instructive as to the application of hydropyrolysis for upgrading of bitumen, but prior to this present study, there was a notable deficiency in our understanding of the fundamental chemistry that gives rise to the remarkable results.

A significant portion of our recent effort has emphasized the research on the fundamental chemistry involved in hydropyrolysis. The purpose of this effort was to provide a theoretical basis for hydropyrolysis optimization. There are many variations of hydropyrolysis, or thermal hydrocracking, currently under development in various laboratories around the world. In none of the cases is the chemistry associated with the hydrogen activity very well understood. It was our intent to learn the nature of the hydrogen involvement by identifying important reaction pathways and kinetics. This information will lead to a better engineering optimization of hydropyrolysis.

To accomplish this objective, a new look at free radical chain reactions in complex mixtures has been necessary. This view has utilized carbon-type composition as a basis for study. The assumption inherent in this approach is that a given carbon-type will exhibit similar hydropyrolytic behavior irrespective of the other bonding in the molecule in which it is found. Examples of carbon-types that, as classes, will behave in a similar chemical fashion are paraffin or alkyl carbon, naphthenic carbon, monoaromatic carbon, diaromatic carbon, polynuclear aromatic carbon, and special cases, such as olephinic carbon, benzylic carbon and methyl carbon.

A kinetic and mechanistic model based on carbon-type has led to an important new understanding of hydropyrolysis processing. First and foremost, optimum reactor configuration is determined by the physical and chemical kinetics that occur during hydropyrolysis. It is clear from the variations reported in the literature that the optimum reactor configuration has not yet been determined, and studies on less than optimum reactors are resulting in data which may not be of optimum economic or commercial value. Second, an understanding of the carbon-type reaction chemistry leads to an assessment of the application of hydropyrolysis to residual feeds, in general. This is of great

usefulness in determining the influence of feedstock composition on reaction results. Third, a mechanistic modeling leads to a more fundamental assessment of the effect of gas composition. Gas composition is a variable which is extremely difficult to control experimentally in a recycle system. Gas composition has a major impact on process economics in that the gas processing step is an important economic variable. Fourth, understanding of the mechanism and kinetics leads to a better theoretical basis for understanding the relationship and tradeoffs between reaction variables and product yield and quality. The results reported represent a definitive step toward hydropyrolysis optimization.

As a result of this work, we are now in a position to commence detailed engineering studies which will result in a conceptual design of a commercial facility and the design and economic studies necessary to support a pilot plant program.

SUMMARY OF PREVIOUS STUDIES

Our early reports emphasized the fact that hydrogen acts both as a diluent and as a participant in the hydropyrolysis reactions.[10-12] As a participant, hydrogen engages in the metathesis reaction

$$R\bullet + H_2 \rightleftharpoons RH + H\bullet$$

The primary effect of molecular hydrogen is the termination of free radicals before they can engage in secondary, retrogressive reactions. Later reports[1,2,4,13] emphasized the comparison of hydropyrolysis results with other alternative upgrading processes. A detailed comparison was made between hydropyrolysis and coking, with coking representing thermal cracking in the absence of hydrogen. The use of hydropyrolysis for examination of the nature of asphaltenes was reported in 1981.[3] Hydropyrolysis results in a total product yield which is analyzable by conventional methods and reduces the ambiguity associated with loss of asphaltenes to coke.

On the basis of this earlier work, a preliminary economic analysis was conducted.[14] The economic analysis showed that the principal economic variables were the gas processing requirements and the reactor space utilization. Based on the economic analysis, a new hydropyrolysis process development unit used for the current study was designed and constructed.

In 1983, at the Seattle ACS Meeting, we reported some new findings that suggested that an important hydropyrolysis reaction was the thermal hydrogenation of aromatics.[15] This finding was very significant in that high temperature reactions favor the formation of aromatics through dehydrogenation reactions. The fact that hydropyrolysis results in thermal hydrogenation of aromatics promised to be very significant in explaining the low coke production.

Three subsequent papers have now dealt with the preliminary understanding of the role of hydrogen.[6,8,9] In the first of these papers,[9] the elementary reaction in coke formation was postulated to be the addition of an aryl radical to the aromatic ring forming an aryl-aryl bond. This bond is stronger than a hydrogen-aryl bond and is not susceptible to thermal hydropyrolysis. Hydropyrolysis prevents the formation of this bond, both through the participation of molecular hydrogen to terminate the aromatic free radical, and the attack of hydrogen on polynuclear aromatic rings, initiating hydrogenation and thereby reducing the overall aromaticity in the system. A very important element of the University of Utah approach to hydropyrolysis is also the dilution of aromatic through the maximization of vapor phase reactions.

The second of these papers[8] further discussed the role of hydrogen in hydropyrolysis. This paper suggested that, in addition to participation of molecular hydrogen in the metathesis reaction, as discussed above, atomic hydrogen could act as an accelerator for the cracking reactions and as an instrument for dealkylation of aromatic rings. The semiquantitative relationship between these various reactions was described in a paper at the WRI-DOE Tar Sands Symposium.[6] In this paper, it was pointed out that dealkylation reactions may be an important source of cracking of naphthenoaromatic rings, and that the hydrogen-atom concentration represented the main determinant for the rate at which these beneficial reactions occurred.

As a consequence of these studies, it was realized that any kinetic or mechanistic model for hydropyrolysis must account for the hydrogen-atom concentration. The hydrogen-atom concentration is the main determiner of the hydropyrolysis reaction rates. Correspondingly, kinetics of hydropyrolysis reactions must account for (H•). This has been addressed in the present study.

EXPERIMENTAL DESCRIPTION

Bench Scale Hydropyrolysis Apparatus

Figure 2 shows the flow diagram of the bench scale unit for hydropyrolysis studies of model compounds and distillate from heavy crude oil. The reactor used was the same 3/16 in. I.D. x 216 in. long coiled tube reactor reported previously.[16,17] The basic flow pattern is similar to the previously described system, except that additional flow control valves were installed in order to obtain a better handling of gas flow rate and a better material balance. A Milton Roy minipump was used to pump liquid feed. Two GCA/Precision wet test meters were connected in parallel to increase the capacity for higher gas flow rate and lower residence time.

Process Development Unit

Reactor and Nozzle: The reactor used in this process development unit is a 1 in. I.D. x 1-1/4 in. O.D. x 18 in. long 316 stainless steel tube equipped with a spray-type nozzle. In some experiments, a 30 in. long reactor was used. The custom-made nozzle is a hydrogen-blast atomizer employing a high velocity hydrogen stream to disperse the bitumen into small droplets. The dimensions of the nozzle are included in Figure 3.

Heater and Temperature Control System: There were three heater assemblies incorporated into the process development unit: 1) an oil preheater; 2) a gas preheater; and 3) the reactor heater. The feed oil was preheated to 420°C in a 1/4 in. O.D. x 20 ft. long stainless steel tube, which was coiled in a brass-alundum block surrounded by two semicircular 900-watt heaters. The reactor was held at a constant temperature by a 1650-watt multiple unit furnace. A 5,000 cubic inch fluidized-bed sand bath, with 8,030 watts heating capacity, was used to preheat the gases. The temperature of the sand bath was controlled by a Barber-Colman 560 controller. This heater could heat hydrogen flowing at a rate of 15 SCF/min from ambient temperature to 650±1°C. The heat contained in the hydrogen feedstream is the principle source of heat in the system. All tubing from the feed reservoir to reactor exit was wrapped with heating tapes. Type K thermocouples were used to monitor the temperatures. The temperature readings were recorded with a Leeds & Northrup Speedomax Recorder.

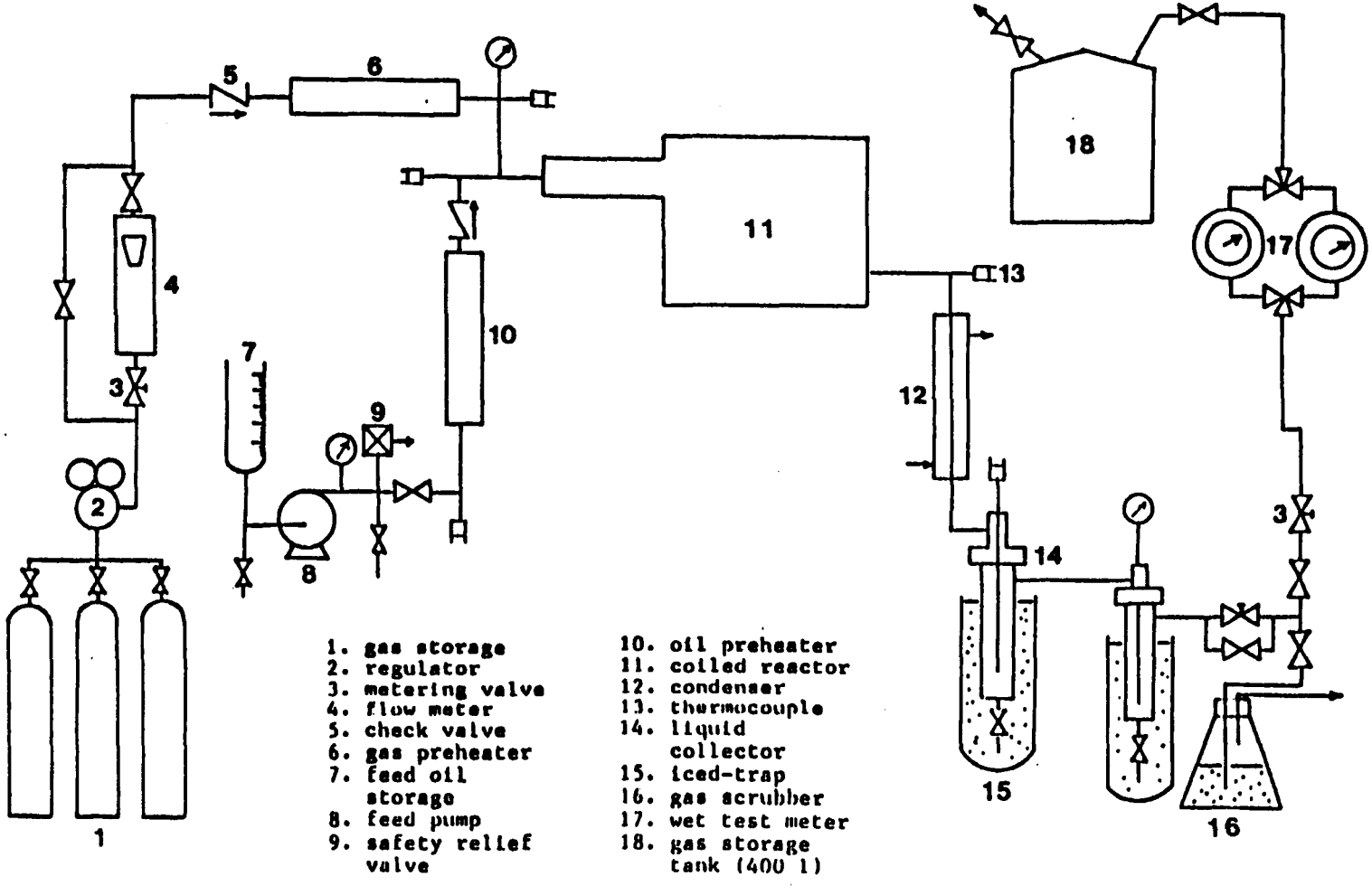

Figure 2. Bench scale hydropyrolysis apparatus flow diagram.

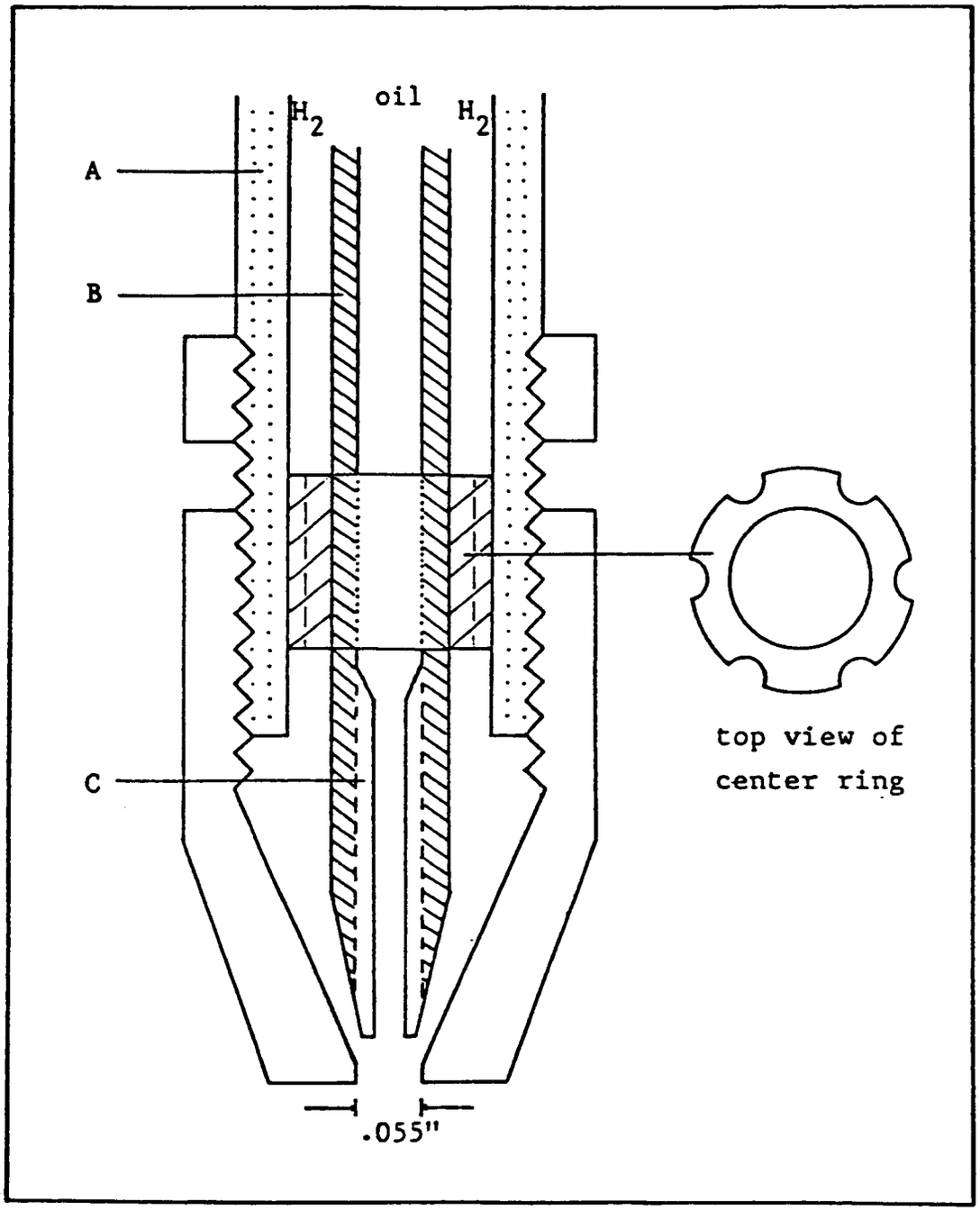

Figure 3. Spray nozzle configuration.

Tube A: .375" O.D. ; .259" I.D.
Tube B: .125" O.D. ; .055" I.D.
Tube C: .0625" O.D. ; .03" I.D.

Gas Handling System: The gas handling system is presented in Figure 4. The system is driven by a PPI model 3060 compressor (#14). Fresh hydrogen is pumped into the system to the desired pressure, then the pressure is maintained by two nitrogen-controlled back-pressure-relief-valves (BPRV). The amount of hydrogen flowing in or out was monitored by a Micro Motion model C6 mass flow meter. If the system pressure is higher than the desired pressure, the back-pressure-relief-valves will open and vent the excess gas; if the system pressure is lower than the desired pressure, the compressor will add fresh hydrogen to the system from the make-up line. The amount of hydrogen added can be estimated by the differential pressure gauge (#3) and metering valve (#4). The regulator (#6) and a regulating flow control valve (#7) in the recycle loop are used for controlling the constant gas flow rate (within ±0.2 g/min). A check valve and a one-liter gas surge vessel (#16), located after the compressor head, are used to dampen the pressure pulses from the compressor.

Operation of Unit: Introducing bitumen into a high temperature zone without forming coke in the nozzle is not a trivial task. First, the bitumen itself is quite viscous, and must be heated and pressurized in order to be pumped. In-line filters are required to remove small particles that may cause nozzle plugging. Cold spots in the feed system will result in solidification of the bitumen and the concomitant cessation of flow. The electronic flow-meters limit the temperature of the feed at the point of metering, and are especially susceptible to plugging. These difficulties are particularly troublesome for a small scale process development unit operating intermittently, and would not be expected to be a problem for a large-scale, continuously operating unit.

Second, temperature of metal surfaces with which oil comes in contact must always be maintained below coking temperature (<420°C). This requires special start-up and shut-down procedures to cool the nozzle and feedstream, which are housed in a reactor through which hydrogen preheated to over 600°C is flowing. Once the oil is flowing, the cooling effect of the oil and the vaporization process keep the nozzle cool and free from coking. Even so, the heat transfer aspects of the nozzle design have proven to be complex problems, some of which could only be solved through

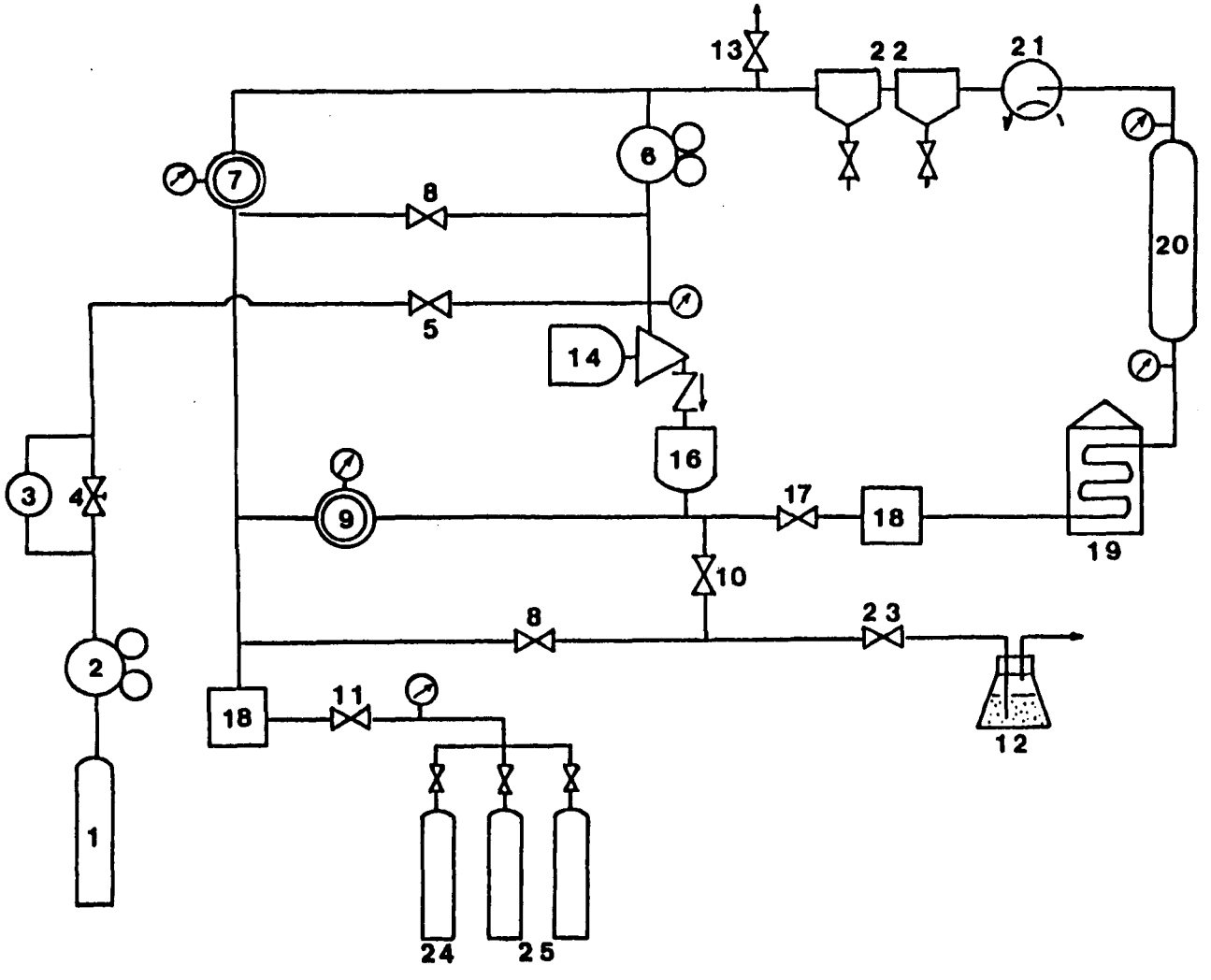

1. make-up hydrogen
2. regulator
3. D. P. gauge
4. metering valve
5. make-up on/off
6. regulator
7. system B.P.R.V.
8. system on/off
9. compressor BPRV
10. system in/out
11. system inlet
12. gas scrubber
13. gas sampler
14. gas compressor
15. check valve
16. gas surge tank
17. recyle flow control
18. mass flow meter
19. main gas heater
20. reactor
21. condenser
22. liquid collector
23. main vent
24. fresh hydrogen
25. gas storage

Figure 4. Gas handling system of the hydropyrolysis process development unit.

experimental trial and error. Again, these problems are not expected to be significant in a properly designed, continuously operating unit.

A run can be conducted in 1 day and consists of a 4 to 6 hour start-up period, a 1 - 2 hour hydropyrolysis run, and a 1 - 2 hour shut-down period. One to two days are required for sample work-up and design of the subsequent experiment. Two days are required to obtain the material balance, which involves disassembly and weighing of all the critical reactor and nozzle parts. The reactor parts are then cleaned and reassembled. The reactor must pass stringent pressure tests prior to the next run since small leaks can have a major influence on the material balances, as well as posing a safety hazard. More recent results have revealed much lower coke production and for these runs a procedure of in-situ burning of the coke has been adopted. This has resulted in a streamlined schedule and has lessened the problems associated with disassembly of high pressure fittings.

Feedstocks

TS-IIC tar sand bitumen[18] was used as the primary feed material. The feedstock was confined to an eight-liter 304 stainless steel cylinder, which was heated to 100°C and pressurized with hydrogen to 125 psig. A Milton Roy type A pump was employed to pump the feed oil from the reservoir to the reactor system. The same type of pump was used to circulate heavy liquid as a recycle stream. The liquid feed rate and accumulated amount fed was monitored and recorded by a Micro Motion model C6 electronic mass flow meter.

Later runs were made utilizing a 14 API Wilmington crude oil. Wilmington crude oil was previously determined to possess a composition similar to Uinta Basin tar sand bitumen.[19] Except for a small amount of light ends (<10% below 225°C), the Wilmington crude oil exhibits properties remarkably similar to TS-IIC oil. The switch to Wilmington crude to simulate tar sands was made on the basis of availability and ease of handling.

Distillation Apparatus

A laboratory scale distillation plant, Leybold-Heraeus model KDT-6, was assembled for the purpose of obtaining fractions of heavy crude oil for use in this study. The configuration of this short

path distillation apparatus is shown in Figure 5. The heat exchange surface area of the evaporator is 600 cm^2, and for the internal condenser, the area is 400 cm^2. The vacuum system is equipped with an LH model D4A mechanical pump and an LH 40 diffusion pump. With all the joints properly sealed and proper use of cold traps, the system can be evacuated to below 10^{-3} torr during distillation. The three rows of roller-wipers are driven by a Janke & Kunkel RW 20 motor. The feed material is preheated in a double-wall glass reservoir by a Haake Pt 1000 water bath in order to reduce viscosity. The evaporator body is heated by a Neslab Exacal EX-250 HT oil bath and the temperature can be controlled within ±0.1°C up to 250°C.

Materials

Model Compounds: High purity (≥99%) model compounds were used in this study. The properties of these compounds are listed in Table 1.

Table 1. Properties of Model Compounds Used in Hydropyrolysis Study

Compound	Formula	M.W.	Density	B.P.°C
Decane	$C_{10}H_{22}$	142.3	.73	174
Methylcyclohexane	C_7H_{14}	98.2	.77	101
Methylnaphthalene	$C_{11}H_{10}$	142.2	1.00	242-3
Mixture*	--	122.2	.766	--

* The composition of the model compound mixture used in this study is: 60% decane, 30% methylcyclohexane, 10% methylnaphthalene, based on number of carbon atoms. Density was experimentally determined.

Petroleum Distillate

The short path distillation apparatus was used to obtain a fraction boiling from 100-320°C from a Wilmington, California, crude oil. The boiling point distribution of the Wilmington crude oil and the distillate fraction, as determined by simulated distillation gas chromatography, is shown in Figure 6.

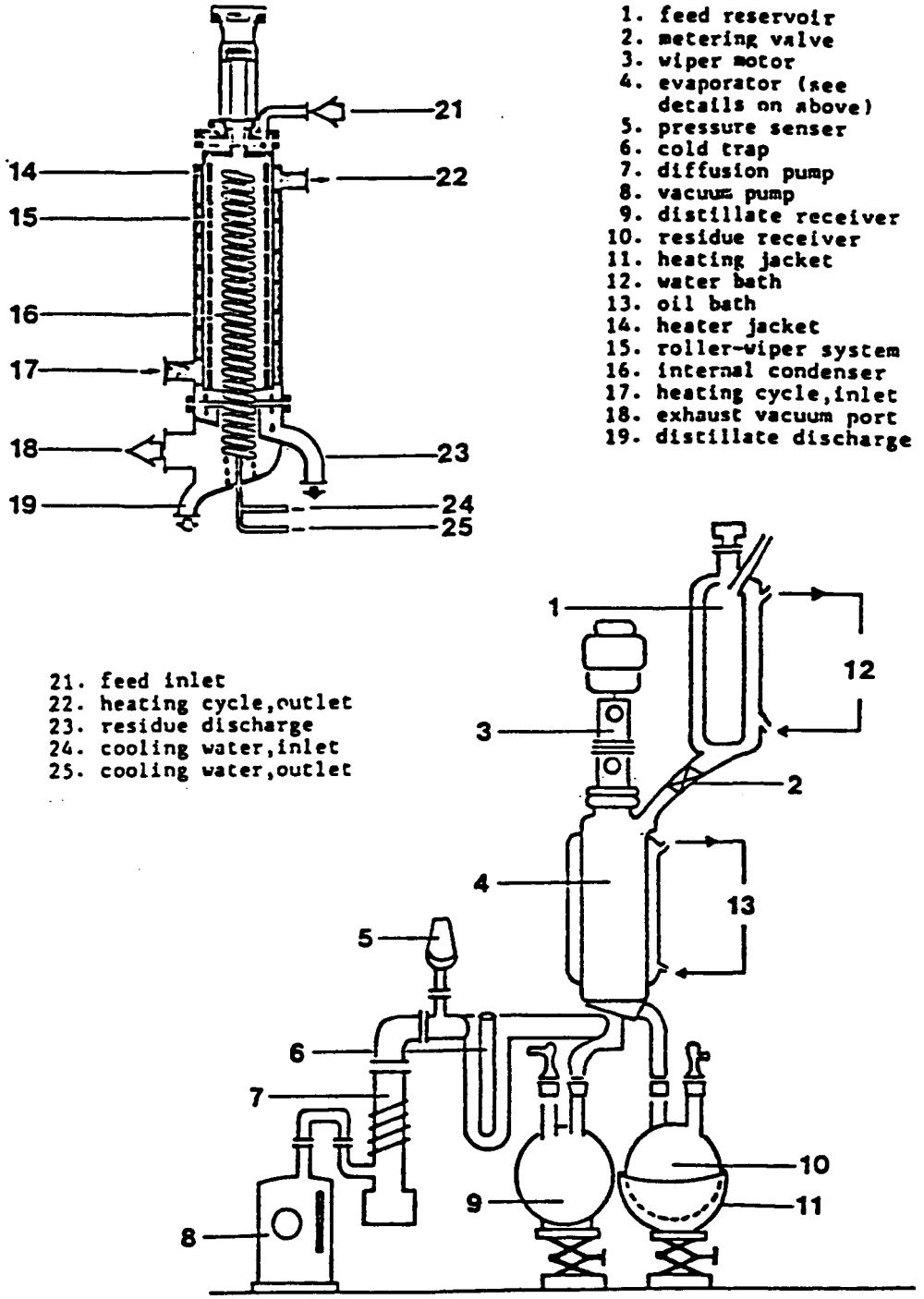

Figure 5. Leybold-Heraeus KDT 6 short-path distillation laboratory system.

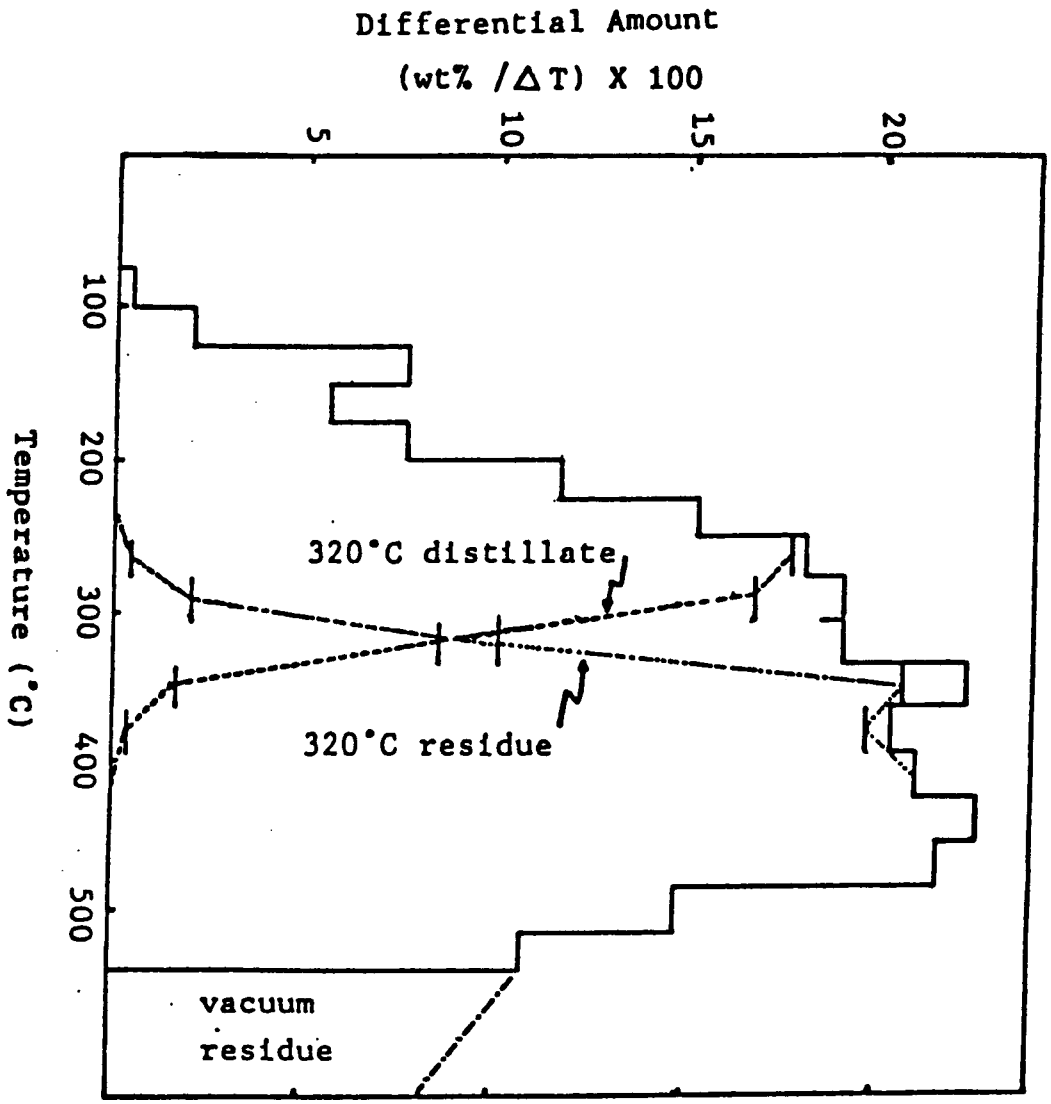

Figure 6. Boiling point distribution of Wilmington crude oil (API = 14.3) showing short path distillation cut point.

The fraction was used as distilled as the starting material for hydropyrolysis runs and for spectroscopic analysis. Small amounts of heteroatoms present were not removed and were ignored in this exploratory stage of the study. Details of the distillation procedure have been previously reported.[20] An example of the distillation results applied to the Wilmington crude oil is shown in Figure 7.

Hydropyrolytic Processing of Model Compounds and Petroleum Distillate

The reactor was preheated to a temperature between 510°C and 530°C. A low flow (under 100 ml/min) of air was passed through the reactor for at least 1 hour to burn out carbon deposits on the reactor wall. The reactor was then flushed with nitrogen to displace oxygen from the reactor tube. A 5% H_2S/95% H_2 mixture was passed at a flow rate of 250 ml/min through the reactor for 30 minutes. The system was then flashed with H_2 for 30 minutes at the rate of 3 l/m at just above atmospheric pressure. This sulfiding procedure was used to reduce the catalytic effects of the reactor surface.

The system was brought to the desired pressure with compressed H_2 and the temperature was adjusted to the desired reactor temperature. Hydrogen flow was begun and controlled by adjusting two metering valves on the downstream side of the reactor. Liquid feed was then pumped into the system.

The gas products, including the unreacted H_2, were collected in a 500 liter gas tank at near-atmospheric pressure. The liquid product passed through a water-cooled condenser and was collected at reaction pressure in a trap cooled with ice. After the reaction was complete, the system was depressurized slowly to atmospheric pressure. The quantities of the liquid and gaseous samples were measured and the samples were collected for analysis. The downstream section of the system (beyond the reactor) was disconnected and washed with pentane; the pentane solution was saved for later analysis. Coke deposited in the reactor was measured by analyzing the combustion gas for CO_2. Virtually no coke was produced in the model compound studies.

Analysis of Feeds and Products

Quantitative analyses of gaseous and liquid products from hydropyrolysis of model compound mixtures were obtained by gas chromatography. Co-injection of known compounds was used for initial

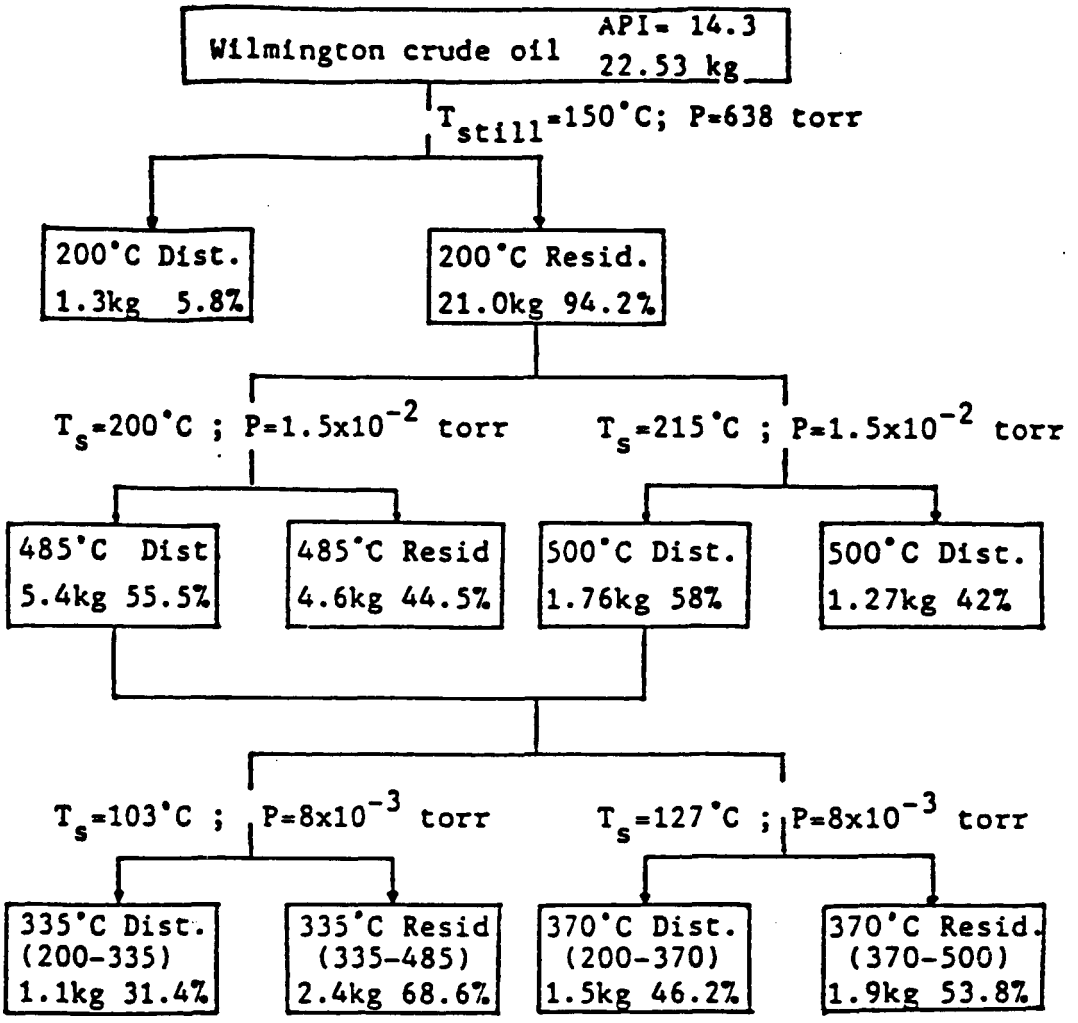

Figure 7. Example of short path distillation applied to crude oil.

identification of the chromatographic peaks. GC-MS was used to confirm the identity of the peaks. Average molecular weight and boiling point distribution of petroleum distillates and tar sand bitumen were determined by vapor pressure osmometry and simulated distillation, respectively. Elemental analysis for C, H, N, S, and O on the feedstock and products were obtained by conventional microanalytical techniques. Carbon-13 NMR and proton NMR provided information about carbon types and structural parameters in the distillate samples.

Gas Chromatography

Four different gas chromatographic samples were used to analyze the feedstocks and reaction products. The typical operating conditions for these systems are summarized in Table 2. Typical gas chromatograms of gaseous and liquid products from the hydropyrolysis of a mixture of model compounds are shown in Figures 8 and 9.

Simulated Distillation

The boiling point distributions of petroleum distillate and its hydropyrolyzed products were determined by a simulated distillation using a Hewlett-Packard model 5880A Gas Chromatograph according to the ASTM D 3710 method. The wide boiling point distributions for tar sand bitumen were determined by using a Hewlett-Packard model 5730A Gas Chromatograph and followed a procedure previously described.[12] A Hewlett-Packard 3550 Data Acquisition System, programmed with appropriate software, was used to electronically record, calculate, and report the data. Typical simulated distillation curves for the above-mentioned samples are shown in Figure 10.

NMR Spectral Analysis

NMR spectra of the hydrocarbons were obtained on a Varian SC-400 Spectrometer operating in the Fourier transform mode at 100.3 MHz for ^{13}C and 400 MHz for ^{1}H. Concentrations of approximately 75/25 by volume of sample to solvent ($CDC1_3$) in 5 mm o.d. samples tubes were used. A small amount of tetramethylsilone (TMS) was added as the internal reference. For carbon-13 spectra, gated decoupling was used to suppress the nuclear Overhauser effect (NOE) and 45° pulses and 15

Table 2

Typical Gas Chromatograph Operating Conditions

Usage	Simulated Distillation	Simulated Distillation	Gas Analysis	Model Compd Liq. Product
Model	HP 5730	HP 5880A	HP 5830	HP 5890
Detector	FID	FID	FID	FID
Col. Length	18"	20"	20"	25 m
Col. o.d.	1/4"	1/8"	1/8"	a
Packing Materials	3% Dexsil 400 on 90/100 mesh Anakrom Q	10% Dexsil 300 on 80/100 mesh Chrom. W HP	Chromasorb 102 MeOH wash	b
Temperature Program (^{o}C)	350^{o}C, 4 min 11^{o}C/min -30^{o}C	320^{o}C, 5 min 6^{o}C/min 40^{o}C	235^{o}C, 15 min 10^{o}C/min 80^{o}C	c
Inj Temp ^{o}C	350	300	200	225
Det Temp ^{o}C	400	350	250	275
Sample Size	0.2 μl	0.1~0.2 μl	1~2 CC	0.1 μl *d
Carrier Gas	He	He	He	He *e
Flow Rate (cc/min)	50	30	20	4

a. 0.32 mm i.d. x 0.52 m film thickness glass capillary column

b. crosslinked 5% phenylmethyl silicone gum phase

c. 0^{o}C hold for 1 min, rate 1=20^{o}C/min, 60^{o}C hold for 0.5 min, rate 2-15^{o}C/min, 175^{o}C hold for 3 min

d. split ratio, 20:1

e. with nitrogen as detector make-up gas

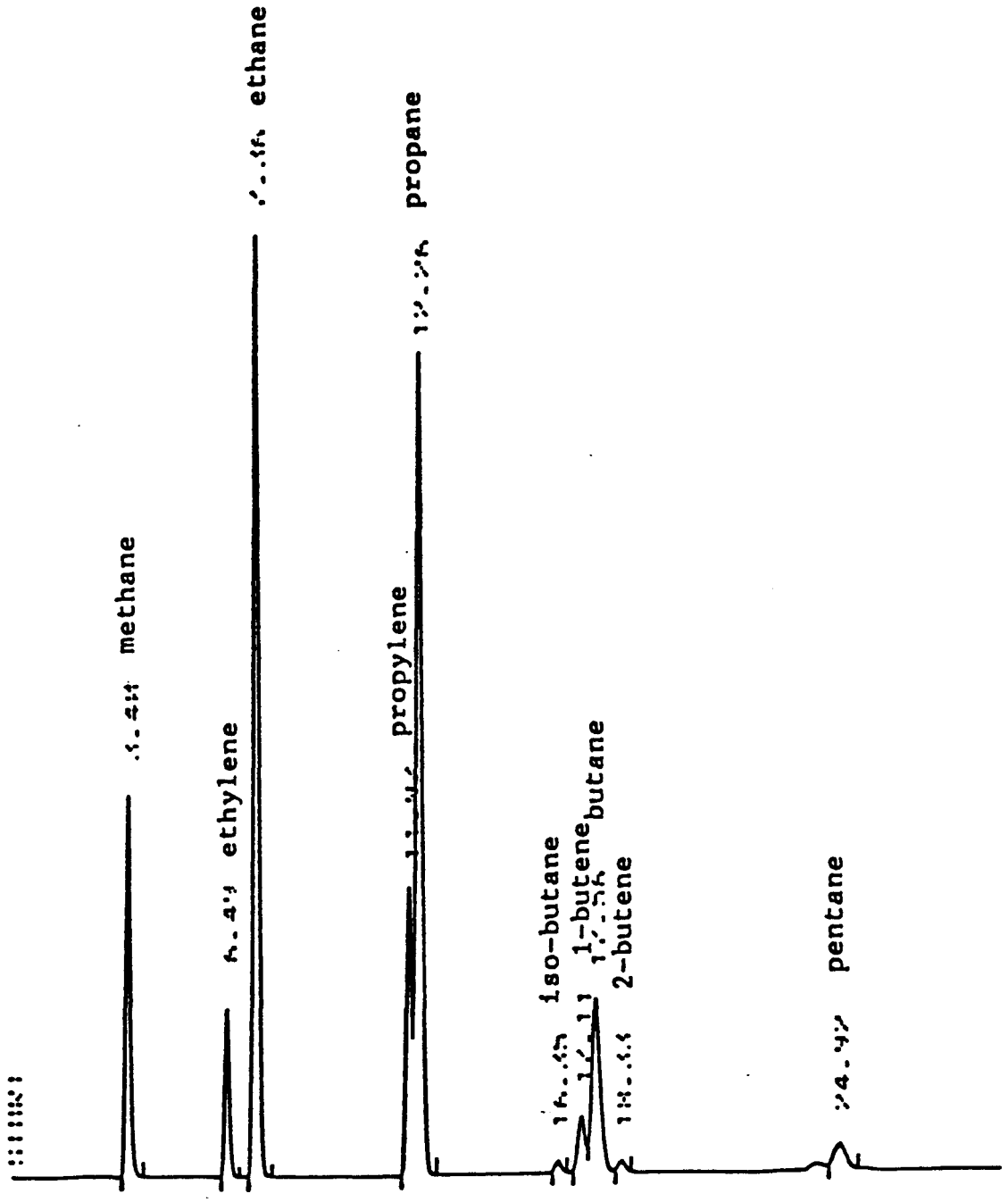

Figure 8. Gas chromatogram obtained from gaseous product of hydropyrolysis model mixture at 525 C, 30 sec residence time.

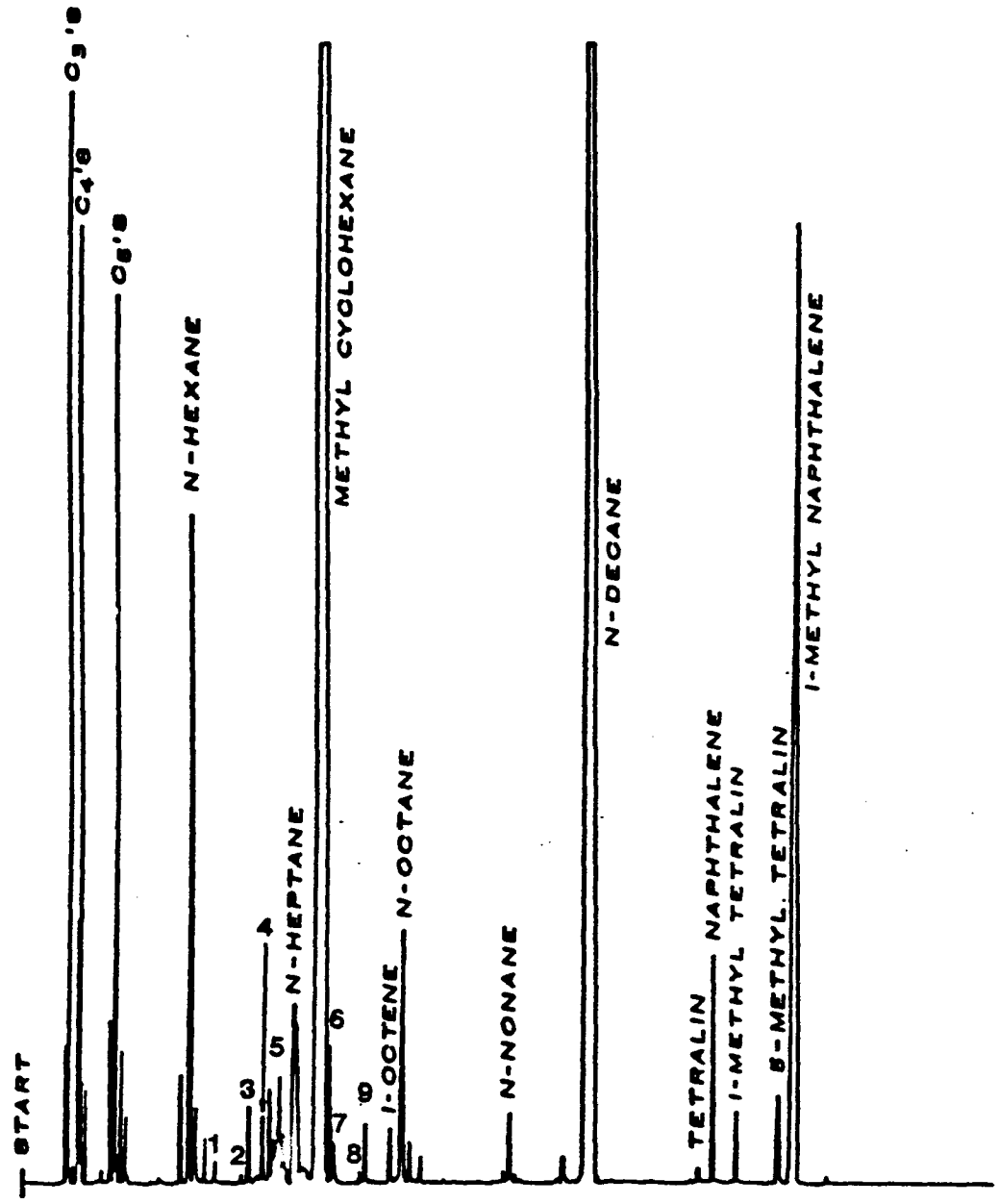

Figure 9. Reaction products of hydropyrolysis of n-decane, methylcyclohexane and 1-methylnaphthalene (60:30:10 mixture) in which, 1: benzene; 2: cyclohexadiene; 3: cyclohexane; 4: cyclohexene; 5: heptenes; 6: methylhexene; 7: methylcyclohexenes; 8: toluene; 9: 1-methylcyclohexene.

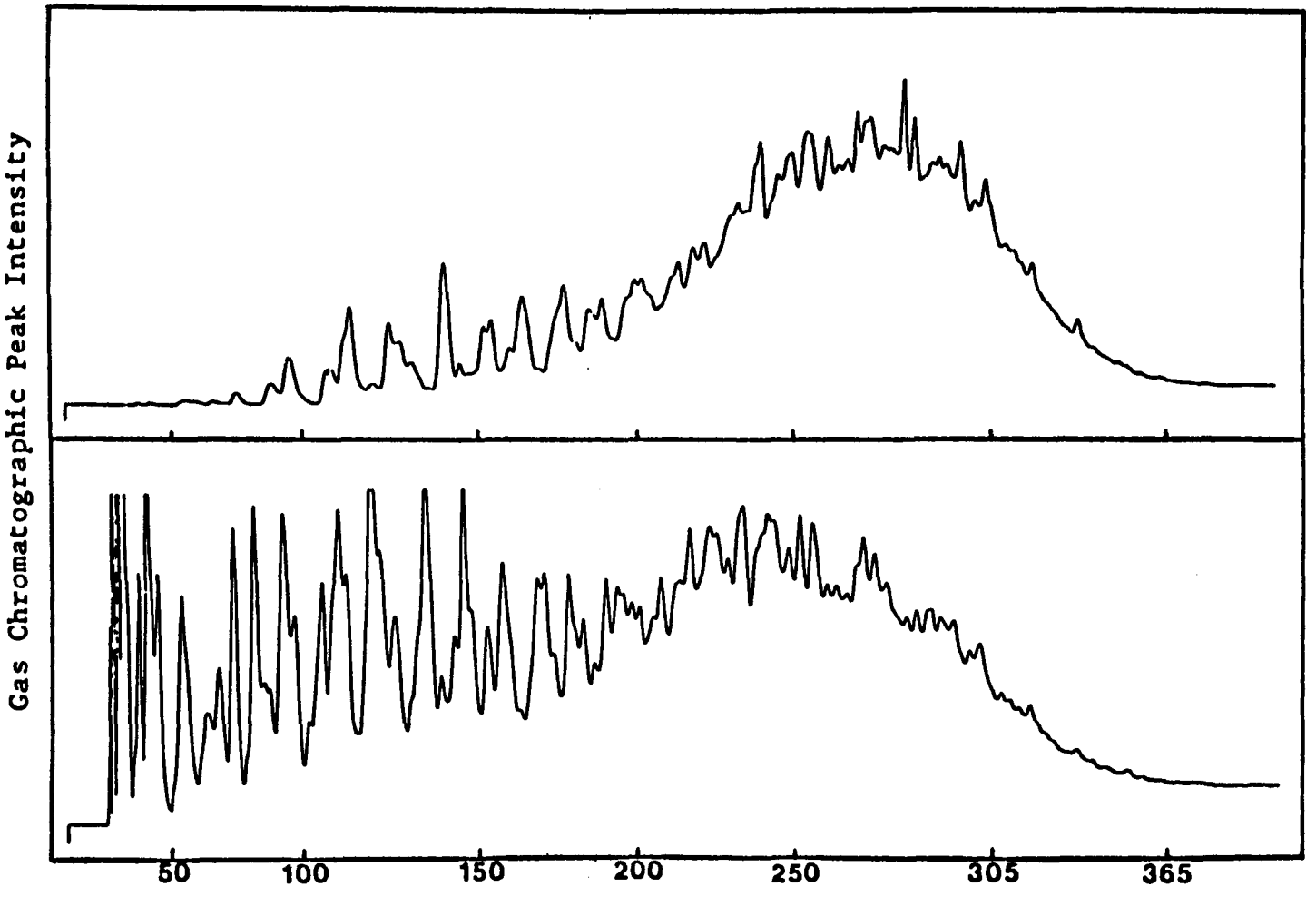

Figure 10. Simulated distillation curves of (A) Wilmington crude oil boiling range under 320°C fraction; (B) liquid product obtained from hydropyrolysis of this distillate at reaction temperature 535°C and 30 seconds residence time.

seconds pulse delay were used. For proton spectra, a pulse delay of 60 seconds was employed. Typical NMR spectra are shown in Figures 11 to 14.

GC-MS Analysis

The hydrocarbons have been analyzed by a GC-MS system which consisted of a Tracor-MT 560 GC equipped with a 15 m x 0.32 mm x 0.52 m DB-5 (crosslinked phenylmethyl silicone gum phase) capillary column, a Finnigan MAT 700 Ion Trap Detector, and an IBM PC-XT data acquisition system. Samples were ionized both at 80 e.v. to obtain fragmentation patterns, and 12 e.v. for parent peak identifications. A mass spectra of an 80 e.v. run is shown in Figure 15.

RESULTS AND DISCUSSION

It has been observed in hydropyrolysis processing of bitumen that hydropyrolysis reactions are enhanced with increasing free radical populations in the presence of H_2. Unsaturation tends to deplete the free radicals while saturation increases the population. It has also been observed that representative chain reactions cannot occur in systems of pure model compounds. For example, processing naphthalene in the presence of H_2 at 500°C results in virtually no reaction, but when n-hexadecane is added, chain reactions leading to the hydrogenation of naphthalene to tetralin occur.

Based on this knowledge, a mixture of model compounds was devised such that each of the major hydropyrolysis reactions would be studied simultaneously. These reactions are cracking of paraffins and naphthenes, dehydrogenation of naphthenes to aromatics, hydrogenation of aromatics to naphthenes, and dealkylation of aromatic side chains.

A model compound system was selected which consisted of n-decane as a representative paraffin (P), methylcyclohexane as a representative naphthalene (N), and 1-methylnaphthalene as a representative aromatic (A). This model compound mixture was blended in ratio of P:N:A = 60:30:10, based on carbon. This carbon composition is not atypical of that found in the middle to high boiling distillates of petroleum.

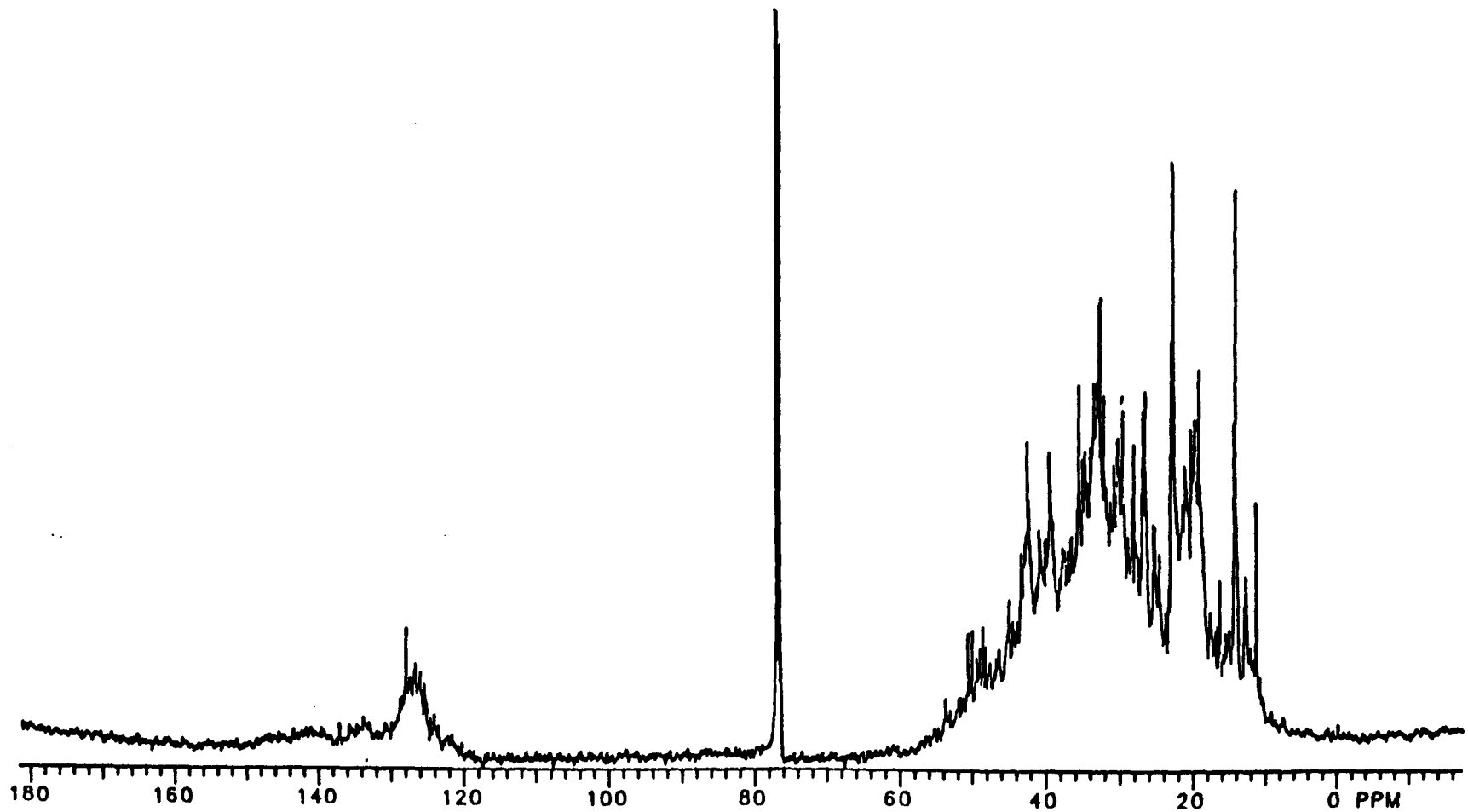

Figure 11. ^{13}C NMR spectrum of Wilmington crude oil distillate - boiling range under 320^{o}C fraction.

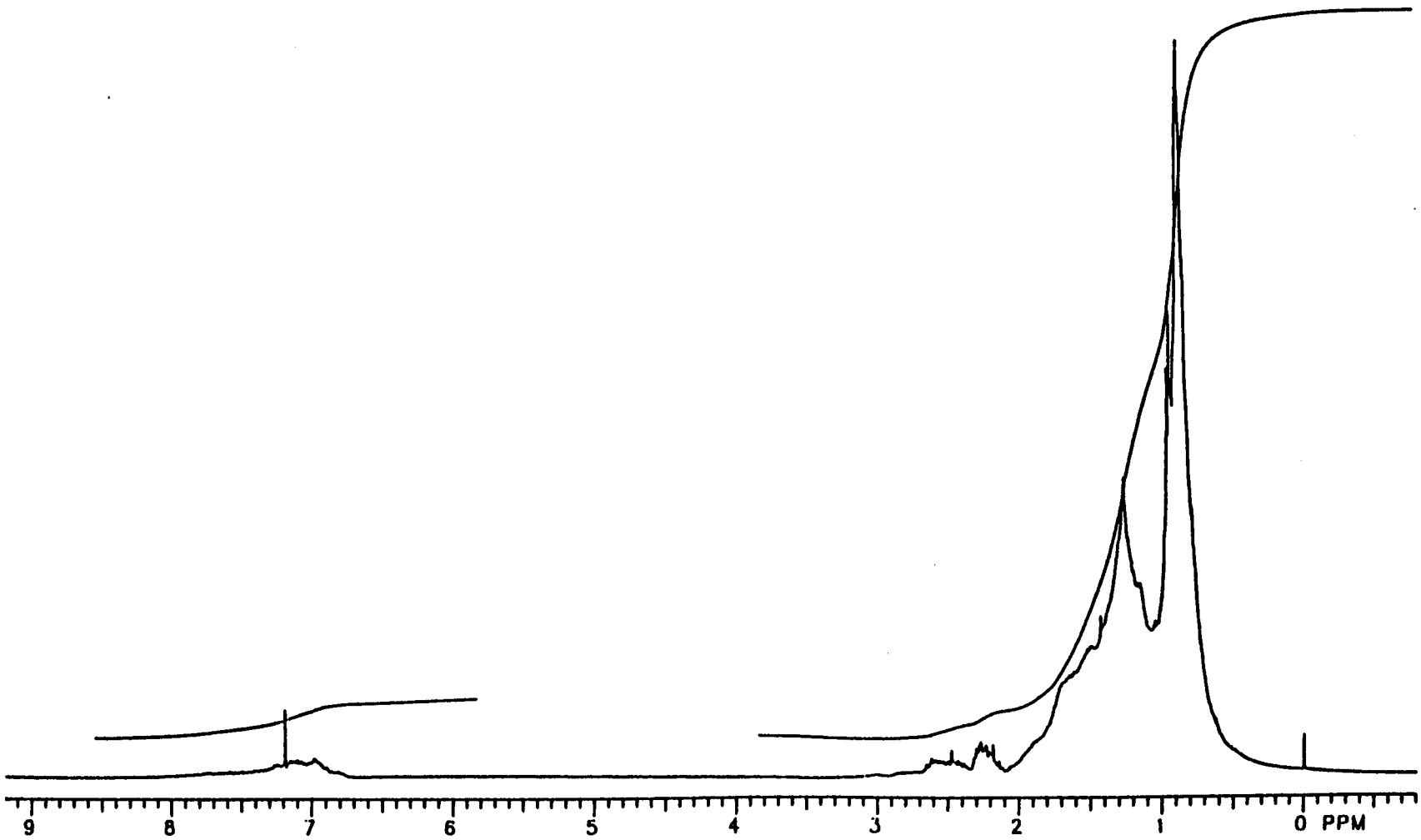

Figure 12. Proton NMR spectrum of Wilmington crude oil distillate - boiling range under 320°C fraction.

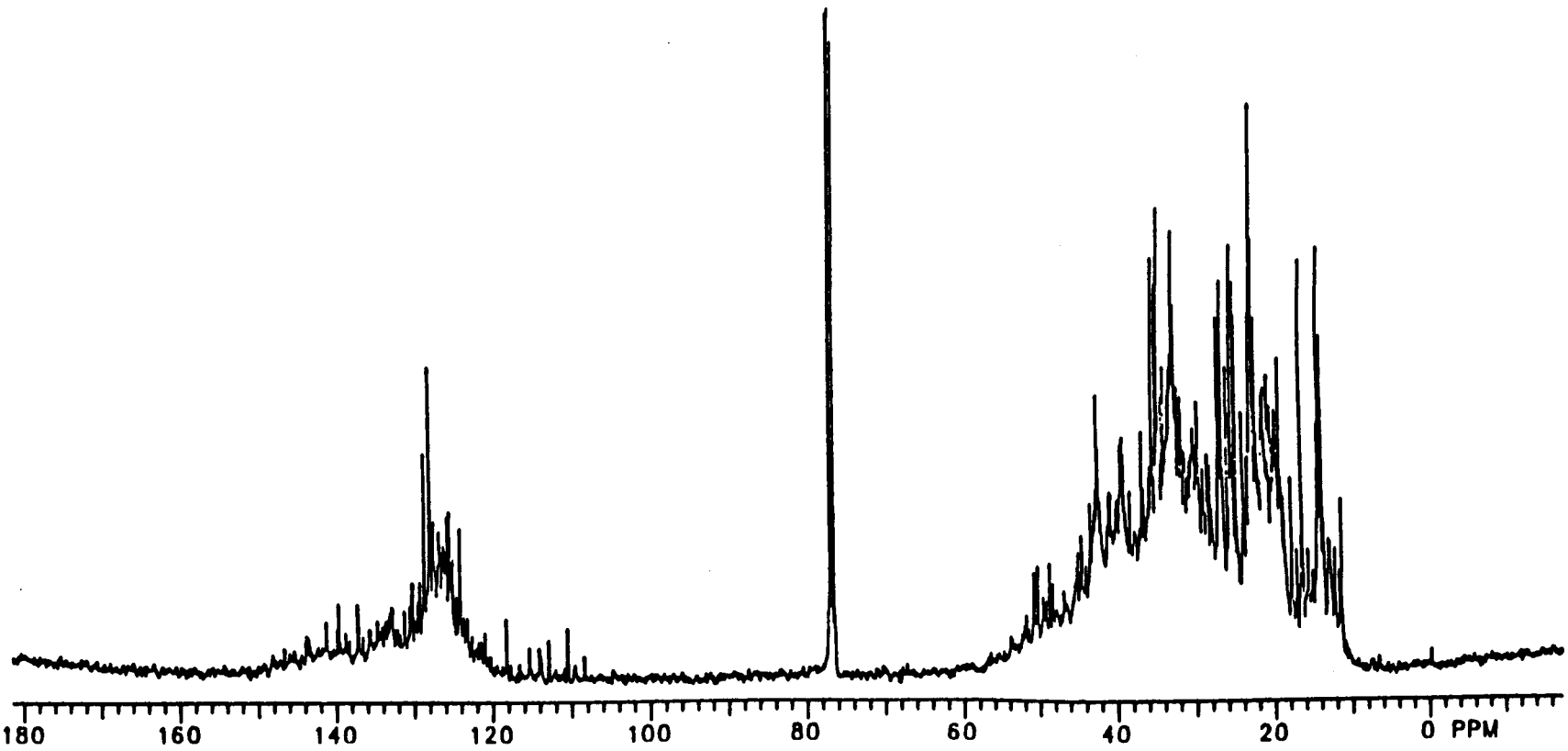

Figure 13. ^{13}C NMR spectrum of liquid product obtained by hydropyrolysis of Wilmington crude oil distillate at 535°C, 30 sec residence time.

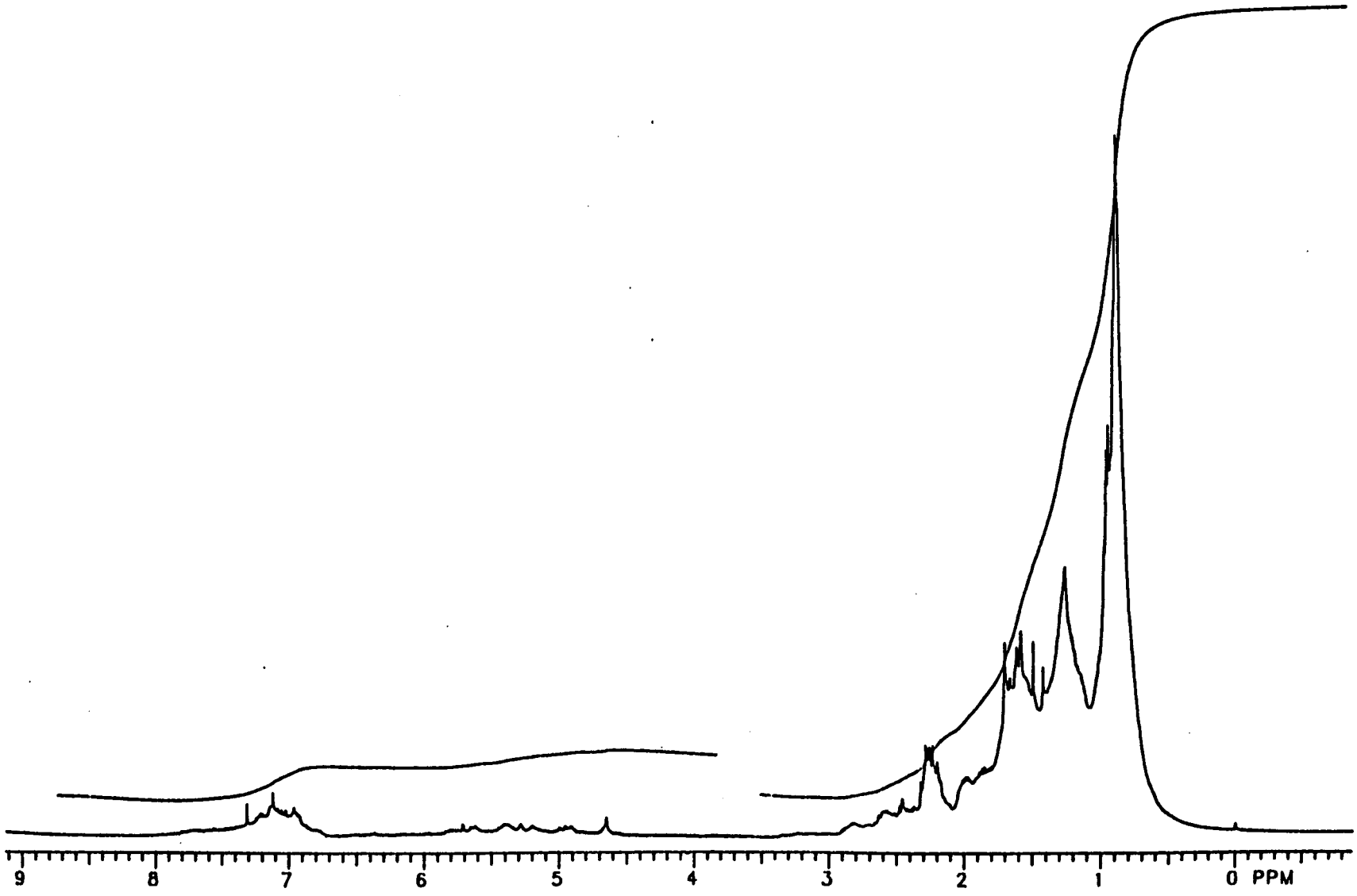

Figure 14. Proton NMR spectrum of liquid product obtained by hydropyrolysis of Wilmington crude oil distillate at 535°C, 30 sec residence time.

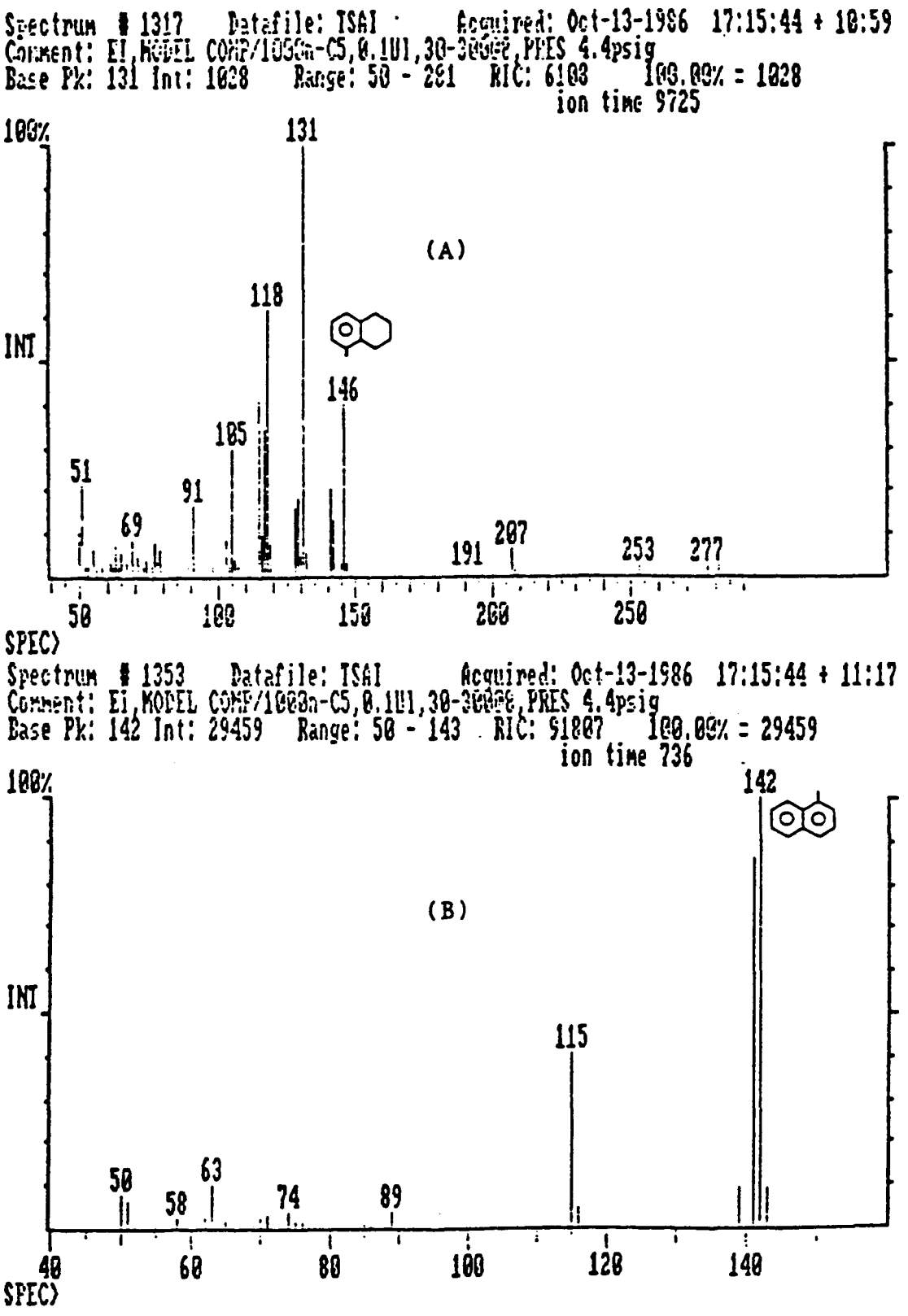

Figure 15. Mass spectrum of (A) 5-methyltetralin; (B) 1-methylnaphthalene.

A systematic investigation of hydropyrolysis reactions was carried out in a coiled tube flow reactor at 1800 psig hydrogen pressure, liquid hour space velocity of 3.1 per hour and under operation conditions indicated in the following matrix:

Matrix of Reaction Conditions

Temperatures, °C	Calculated Residence Time, Sec[a]				
	15	20	30	40	50
510	X	X	X	X[b]	X
525	X	X	X[c]	X	X[d]
540	X	X	X	X	X

a. residence times of less than 1 second could not be achieved with the current reactor hardware

b. duplicate run without burning coke prior to the run

c. individual model compounds and mixtures of pairs of compounds were also investigated at this condition

d. duplicate run at different gas-to-feed ratio

Products obtained were identified by gas chromatography and peak identification was established by GC-MS.

Reactions of Model Compounds

Hydropyrolytic reactions of the individual model compound described above and their binary and ternary mixtures were carried out under identical reaction conditions to investigate the products and the interaction between the compounds.

The reaction conditions and results are summarized in Table 3. Product analyses indicate the following:

Table 3

Reaction of Model Compounds

Run No.	Feed % Wt	Rxn Temp°C Res Time, sec	Wt% of Gas Make	Individual Conversion %	Overall Conversion %
86-M03	100% P	525°C 30 sec	18.2	50.3	50.3
86-M06A	100% N	525°C 30 sec	1.1	6.0	6.0
86-M04	40% P 60% N	525°C 30 sec	6.6	45.4 11.2	24.5
86-M05	50% P 50% A	525°C 30 sec	3.6	22.6 16.7	19.7
86-M07	70% P 25% N 5% A	525°C 30 sec	12.7	43.5 7.5 22.5	33.5
86-M01	100% P	500°C 30 sec	6.2	22.8	22.8
86-M02	80% P 20% N	500°C 30 sec	3.8	17.1 5.2	14.7

P: decane as a representative paraffin

N: methylcyclohexane as a representative naphthene

A: 1-methylnaphthalene as a representative aromatic.

1. The principal products of hydropyrolysis of decane are lower molecular weight paraffins and related olefins. Mono-olefins, both terminal and internal, are found and lesser amounts of di-olefins are present.
2. The principal products of hydropyrolysis of methylcyclohexane are its dealkylated products (methane & cyclohexane), ring opening and cracked products (C_2 to C_7 paraffins and olefins), and dehydrogenation ring products (mono-, di-enes, and aromatics).
3. The principal products of hydropyrolysis of 1-methylnaphthalene (reacted in the presence of decane) are its dealkylated products (methane and naphthalene) and hydrogenation products (1-methyltetralin, 5-methyltetralin, and tetralin).
4. Products from binary or ternary feeds are those expected from individual compounds, but individual reaction rates are modified by the presence of other compounds.
5. The presence of naphthenes and aromatics suppresses the paraffin conversion; conversely, the conversion of naphthenes and aromatics increases with the proportion of paraffin present. The presence of aromatics suppresses paraffin conversion more than does the presence of naphthene.

These observations tend to confirm the original hypothesis: the interaction between different hydrocarbons during hydropyrolysis is directly related to the population of free radicals, especially the hydrogen atoms. A detailed study of the mechanisms and kinetics of hydropyrolysis reactions must necessarily account for the instantaneous hydrogen atom concentration.

Effect of Reactor Surface Condition on Hydropyrolysis Results

The condition of the reactor surface is suspected of having an appreciable effect on hydropyrolysis results. In the process development unit, for example, freshly burned surfaces, resulted in high production of gases at the initial stages of a run.

In the model compound study the reactor was routinely burned with air and then treated with H_2S prior to each run as described in the experimental section. The burning removes any coke from previous runs, and the sulfiding helps attenuate catalytic effects of the reactor surface.

An attempt was made to qualitatively determine the magnitude of the surface effects. Results of a run conducted over a freshly prepared surface were compared with those in which no burning procedure was done prior to the run.

Table 4 shows the comparison of product distribution and its characteristics obtained from two reactions with similar operating conditions, but different pretreatment procedures. The freshly conditioned reactor wall results in less olefin, lower average molecular weight of the gaseous product and more hydrogenated aromatic products than that from the reactor with a preexisting coke film on the wall.

The overall conversion for these two reactions does not appear to be very different. The change in the hydrogen index of $[C_3\ P/(P+O)]$ is reduced by 14% in the presence of a coke "sink." These results show that the reactor surface may be playing a catalytic role and, conversely, that coke formation will inhibit the hydropyrolysis reaction rates. In a large scale, "wall-less" reactor, both of these effects will be minimized.

In previous studies of hydropyrolysis of hexadecane and decalin, no coke was formed. Hydropyrolysis of SRC-II coal-derived liquid produced only small amounts of coke (0.12 wt.% at hydrogen pressure 1800 psig and reaction temperature 500°C). In the presence of hydrogen, the coke yield is suppressed significantly. From a kinetic standpoint, even trace amounts of coke are expected to deplete the hydrogen free radical population. The effect is to change the product distribution from the characteristics of hydropyrolysis to those of thermal cracking.

Hydrogen Atom as a Key Reaction Intermediate

The major hydropyrolysis reactions involve (H•) and therefore, a complete kinetic treatment must include a term for (H•). However, the (H•) are very active intermediates, so direct measurement of (H•) is not possible at reaction conditions.

In order to include (H•) in kinetic expressions, it may be postulated that (H•) is reflected in the products and that some index based on the products is possible. Hydrogen free radicals are likely to hydrogenate olefins. This suggests an index for (H•) that involves paraffin and olefin concentrations.

Table 4

Comparison of Product Yield Obtained from a "Clean" Reactor (Run No. M20) and from a Reactor with Coke-Film (Run No. M25), Both at Reaction Temperature 510°C, Residence Time 40 Seconds, With Hydropyrolyzing Model Mixtures

Product Yield or Characteristics	Run Number M20 "Clean"	Run Number M25 "Coke-Film"
Gas Yield (g/100g oil fed)	7.91	8.25
Average m.w. of gas product	31.63	32.43
Mole % in gas product		
Methane	27.4	24.9
Ethane	37.1	33.7
Ethylene	1.9	5.2
Propane	22.6	20.9
Propylene	5.2	8.1
P/(P+O) of C 3 in gas	0.812	0.697
Mole fractions of reactant left:*		
Naphthalene	0.00735	0.00725
5-methyltetralin	0.00725	0.00314
1-methyltetralin	0.00375	0.00170
Tetralin	0.00115	0.00045

* feed compositions are P:N:A = 0.454:0.454:0.091

A choice of propane and propylene was made because C_3 fragments probably develop from reactions energetically similar to higher carbon number fragments. For the unique case of C_3, there is no ambiguity between isomers as there is for C_4 and higher paraffins and olefins. Propane and propylene are easily analyzed by gas chromatography. For simplicity, it was assumed that the proportion of propane to total C_3 was a linear function of (H•), thus:

$$(H\bullet) = aY + b \tag{1}$$

where

$$Y = C_3/(C_3+C_3^=)$$

C_3 and $C_3^=$ are the concentrations in the gaseous product of propane and propylene, respectively; a and b are constants for a reaction, dependent only on temperature. Following is a description of a kinetic analysis which utilizes this index. If the kinetic treatment accurately describes the data, then a partial test of the above assumptions will have been made.

Kinetic Treatment

Consider the general reaction $C_i + (H\bullet) \longrightarrow P_i$, and where (H•) is a limiting reactant. It is assumed that the reaction is first order with respect to reactant and first order with respect to hydrogen free radicals. Thus the rate expression for a model compound (C_i) in the feed is

$$dC_i/dt = -k\, C_i\, (H\bullet) \tag{2}$$

or, assuming $(H\bullet) = aY + b$ gives:

$$\begin{aligned} dC_i/dt &= -k\, C_i\, (aY + b) \\ &= -k_a\, C_i\, Y - K_b\, C_i \end{aligned} \tag{3}$$

in which $K_a = K\bullet a$

$K_b = K\bullet b$

the integration of equation (3) gives:

$$C_i - C_{io} = -K_a \int_{to}^{t} C_i Y \, dt - K_b \int_{to}^{t} C_i dt.$$

Now let

$$W = C_i - C_{io}$$

$$Z_1 = \int_{to}^{t} C_i Y dt$$

$$Z_2 = \int_{to}^{t} C_i dt$$

then $W = -K_a Z_1 - K_b Z_2$. (4)

The constants K_a and K_b can be obtained by plotting W/Z_2 vs Z_1/Z_2, which should give a straight line with a slope of $-K_a$ and an intercept of $-K_b$. This is illustrated in the following section.

For comparison, the case is considered where (H•) is not limiting and does not vary during the reaction. In this case, the rate expression for a model compound in the feed is

$$dC_i/dt = -K_i C_i$$

The rate constant K_i is obtained from the usual integration of this equation to give the following:

$$K_i = -1n(1-X_i)/t \quad (5)$$

where

t = residence time

X_i = conversion = $(C_{io}-C_{if})/C_{io}$

C_{io} = initial concentration of reactant i.

C_{if} = final concentration of reactant i.

Both treatments were applied to the data presented below.

Model Paraffin and Model Naphthene

The kinetic treatment for the reactions of n-decane and methylcyclohexane are based on their disappearance during hydropyrolysis of a ternary model compound system. First order rate constants determined using equation (5) are summarized in Tables 5 and 6. The activation energies were calculated to be 58.6 and 50.5 Kcal/mole for the disappearance of decane and methylcyclohexane, respectively. The corresponding pre-exponential factors were 1.88×10^{14} and 5.20×10^{11} $(mol/l)^{-0.5} \cdot s^{-1}$.

The activation energy for thermal cracking of n-hexadecane is 60 kcal/mol, while the activation energy for hydropyrolysis of n-hexadecane is estimated to be 50 kcal/mol.[17] The activation energy for thermal cracking of decane is 65 kcal/mol.[17] Thus, an activation energy of 58.6 kcal/mol for the hydropyrolysis of n-decane is reasonable. The activation energy for thermal cracking of cyclohexane is reported to be 60-65 kcal/mol, while the activation energy for steam cracking of methylcyclohexane is reported to be 48 kcal/mol.[21] Thus, the value of 50.5 kcal/mol for hydropyrolysis of methylcyclohexane using the same kinetic treatment is also consistent with literature values.

In an attempt to account for the hydrogen atom concentration (H•), equation (4) was applied. Figure 16(a) shows the hydrogen index as a function of residence time in the hydropyrolysis of the model mixture. A graphical method was applied to obtain the parameters k_a and k_b. If Y is a linear function of (H•), then a plot of W/Z2 vs Z1/Z2 should be with a slope of $-k_a$ and an intercept of $-k_b$. The plot shown in Figure 16(b) does follow a straight line.

Values for k_a and k_b in hydropyrolysis of n-decane and methylcyclohexane are given in Tables 5 and 6. It may be noted that k_a and k_b are of opposite signs but are of approximately equal absolute value. Activation energies calculated on the basis of k_b are 73.7 and 60.0 kcal/mol for decane and methylcyclohexane, respectively. These values bear the same general relationship to each other as was observed with kinetic treatment that did not consider the hydrogen atom concentrations. The higher values considering the hydrogen atom may be a more accurate reflection of the rate limiting step involved in the hydropyrolysis reactions.

Table 5

Kinetic Parameters Obtained from Hydropyrolysis of Decane**

Reaction Temp ^{o}C	Residence Time, Sec	Mole Fraction	Conver. Percent	Parameters include (H) k_a	k_b	First Order Rate Const. (s^{-1})
	15	0.375	17.4			
	20	0.356	21.6			
510	30	0.324	28.6	-0.033	0.034	0.008
	40	0.304	33.0			
	50	0.281	38.1			
	15	0.294	35.2			
	20	0.263	42.1			
525	30	0.218	52.0	-0.076	0.076	0.017
	40	0.190	58.2			
	50	0.163	64.1			
	15	0.179	60.5			
	20	0.142	68.7			
540	30	0.100	78.0	-0.206	0.195	0.032
	40	0.071	84.4			
	50	0.059	87.0			

** feed mole fraction of decane = 0.454

Table 6

Kinetic Parameters of Hydropyrolysis of Methylcyclohexane**

Reaction Temp ^{o}C	Residence Time, Sec	Mole Fraction	Conver. Percent	Parameters include (H) k_a	k_b	First Order Rate Const. (s^{-1})
	15	0.400	11.9			
	20	0.388	14.5			
510	30	0.370	18.5	-0.029	0.028	0.0040
	40	0.356	21.6			
	50	0.344	24.2			
	15	0.380	16.3			
	20	0.356	21.6			
525	30	0.325	28.4	-0.065	0.059	0.0080
	40	0.304	33.0			
	50	0.284	37.4			
	15	0.301	33.7			
	20	0.269	40.7			
540	30	0.231	49.1	-0.128	0.116	0.0132
	40	0.200	55.9			
	50	0.186	59.0			

** feed mole fraction of methylcyclohexane = 0.454

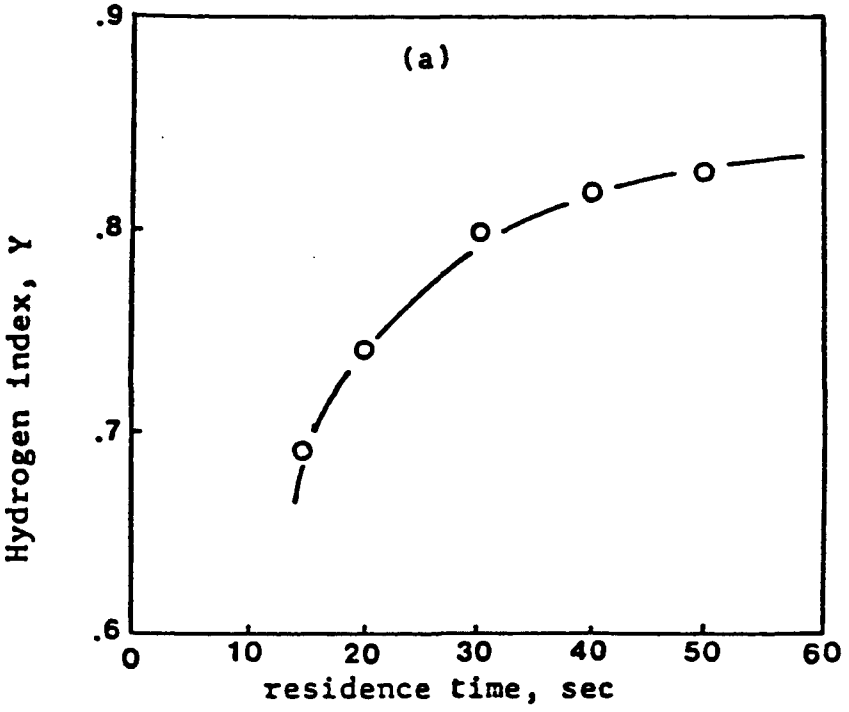

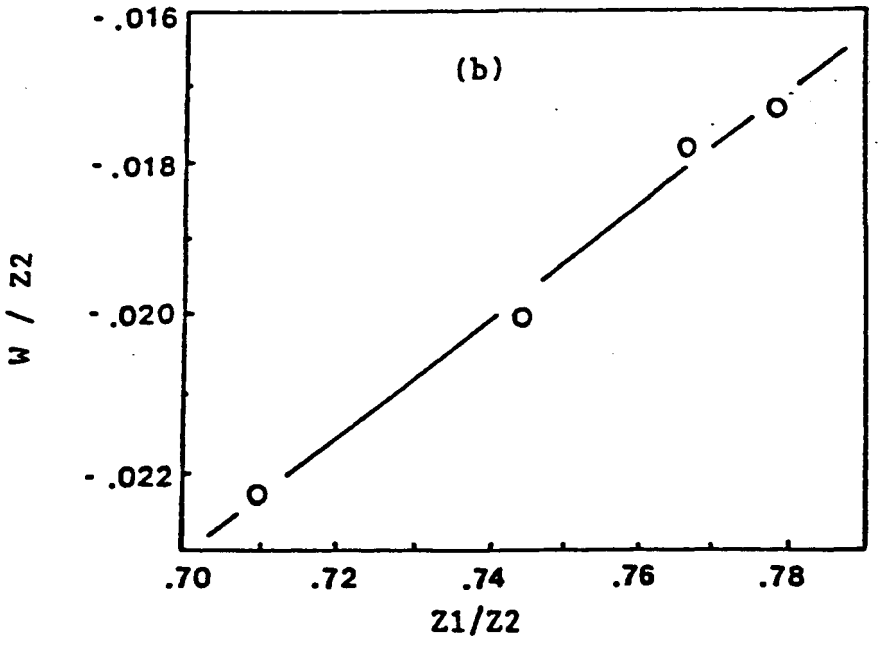

Figure 16. (a) Hydrogen radical index Y as a function of residence time of hydropyrolysis model mixture at reaction temperature 525°C.

(b) Use graphic method to obtain ka and kb. Example shown is hydropyrolysis of decane in the model mixture at reaction temperature 525°C, in which the straight line expected:

$$\frac{W}{22} = -k_b - k_a \frac{Z1}{Z2} = -0.076 + 0.076 \frac{Z1}{Z2}$$

Model Aromatics

The major products from hydropyrolysis of 1-methylnaphthalene reacted in the model mixture were found to be naphthalene and 5-methyl-1,2,3,4-tetrahydronaphthalene (or 5-methyltetralin). Also tetralin and 1-methyltetralin were found in minor quantities. The primary reactions observed are dealkylation of aromatics, hydrogenation of aromatic rings, and cracking of hydrogenated rings. Therefore, the aromatic reaction network can be indicated as follows:

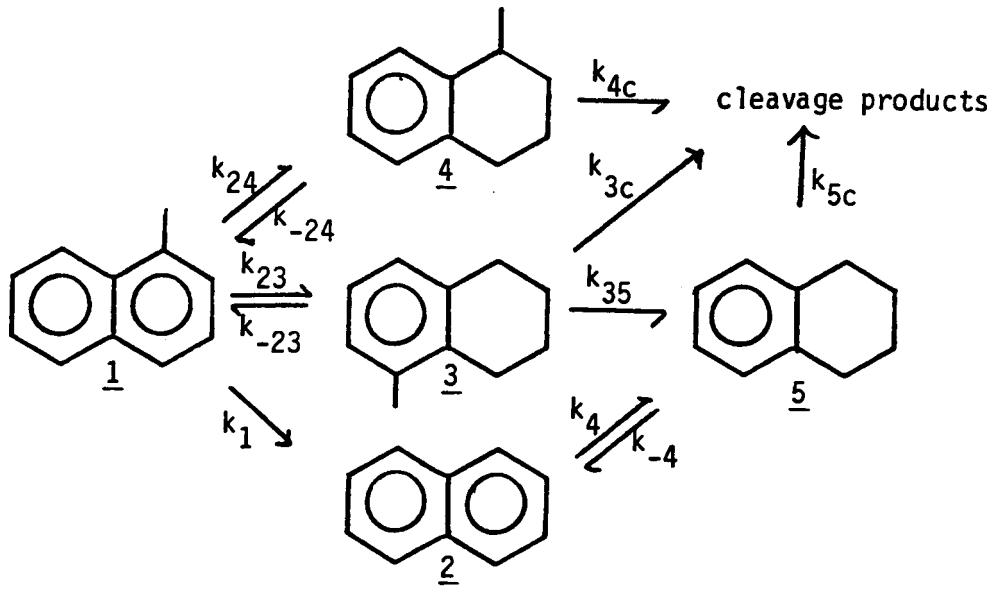

Figure 17. Reaction Network for Hydropyrolysis of 1-methylnaphthalene

Figure 18 shows the change of product concentration as a function of time. The appearance of maximum concentrations for the tetralins shown indicates there are successive and reversible reactions taking place. By using the Van Krevelen group contribution method to obtain the free energy of formation of each species, the equilibrium constant of k_4/k_{-4} is estimated to be 0.77, 0.56, and 0.33

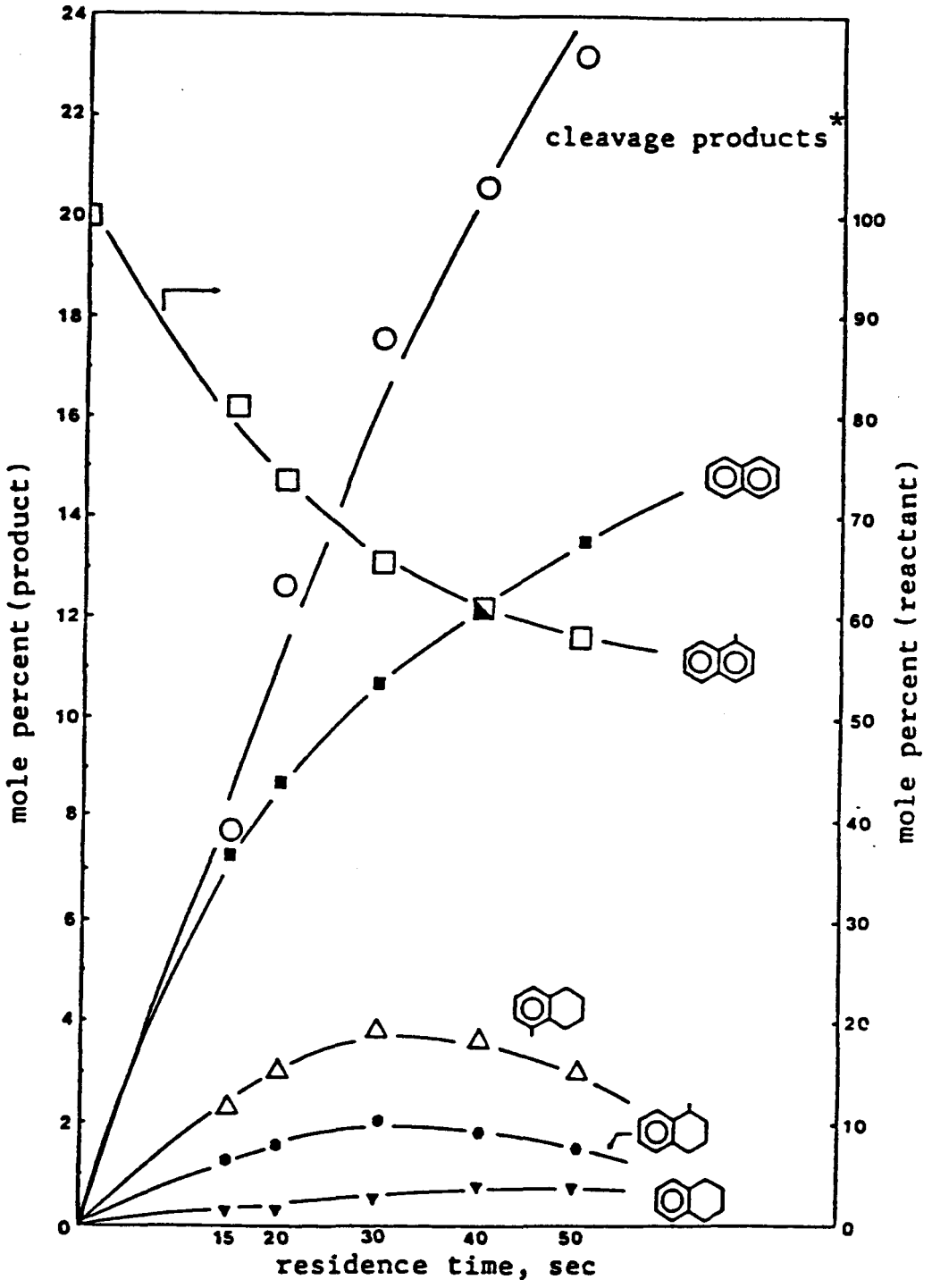

Figure 18. Change of product distribution as a function of residence time of hydropyrolysis of 1-methylnaphthalene in the model mixture at reaction temperature 525°C. [H_2 pressure 1800 psig, LHSV=3.1 hr^{-1}.]

*Obtained by difference.

at 510°C, 525°C, and 540°C, respectively. These values will be close to those of k_{23}/k_{-23} and k_{24}/k_{-24}, because of their similar geometric structures.

The corresponding rate constants in the aromatic reaction network can be obtained by solving the following five equations:

$$dC_1/dt = -(k_1+k_{23}+k_{24})\cdot C_1 + k_{-24}C_4 + k_{-23}C_3 \quad (6)$$

$$dC_2/dt = -k_4C_2 + k_1C_1 + k_{-4}C_5 \quad (7)$$

$$dC_3/dt = k_{23}C_1 - (k_{-23}+k_{35}+k_{3c})\cdot C_3 \quad (8)$$

$$dC_4/dt = k_{24}C_1 - (k_{-24}+k_{4c})\cdot C_4 \quad (9)$$

$$dC_5/dt = k_{45}C_4 + k_{35}C_3 + k_4C_2 - (k_{-4}+k_{5c})\cdot C_5 \quad (10)$$

in which

C_1 = concentration of 1-methylnaphthalene

C_2 = concentration of naphthalene

C_3 = concentration of 5-methyltetralin

C_4 = concentration of 1-methyltetralin

C_5 = concentration of tetralin

Each rate constant includes the hydrogen free radical concentration. It is assumed that the k_a/k_b ratio obtained from decane kinetics will apply for any of the hydrogen atom involving reactions.

Using the same expression for (H•) and using the same integration techniques as described previously, the following expressions result:

$$W_1 = -(k_1+k_{23}+k_{24})\, Z_1 + k_{-24}Z_4 + k_{-23}Z_3 \quad (11)$$

$$W_2 = -k_4Z_2 + k_1Z_1 + k_{-4}Z_5 \quad (12)$$

$$W_3 = k_{23}Z_1 - (k_{-23}+k_{35}+k_{3c})\, Z_3 \quad (13)$$

$$W_4 = k_{24}Z_1 - (k_{-24}+k_{4c})\,Z_4 \quad (14)$$

$$W_5 = k_{45}Z_4 + k_{35}Z_3 + k_4Z_2 - (k_{-4}+k_{5c})\,Z_5 \quad (15)$$

in which

$$Z_j = \int_{to}^{t} C_j dt$$

$$W_j = C_j - (C_j)_o$$

$$k_i = k_{b,i}\,(R_T Y+1)$$

Y = hydrogen free radical index

$R_T = k_a/k_b$ from hydropyrolysis of decane at temperature T.

The resulting rate constants in the aromatic reaction network are listed in Table 7. Also shown in the table are kinetic rate constants for the more typical case of kinetic treatment which does not consider the (H•) concentration. From this table, the following observations can be made:

1. The rate of hydrogenation of 1-methylnaphthalene to 5-methyltetralin is about twice the rate of hydrogenation to 1-methyltetralin.
2. The rate of dehydrogenation of naphthenic rings (k_{-23}, k_{-24}, and k_{-4}) are faster than that of the reverse reaction of hydrogenation of aromatic rings (k_{23}, k_{24}, and k_4).
3. The rate of dealkylation is nearly an order of magnitude faster than the rate of hydrogenation.

This latter point is especially important in that a major reaction for molecular weight reduction could be the hydrogen-induced cracking of naphthenoaromatics. The fact that some hydrogenation of aromatics occurs is probably significant for the important fact that the reverse reaction, dehydrogenation of naphthenes, is virtually inhibited.

Application to Mixtures

It is important to determine whether the general kinetics describing hydropyrolysis of a model mixture can also describe hydropyrolysis of a petroleum-derived system. A mathematical model was

Table 7

Kinetic Parameters Obtained from Hydropyrolysis of 1-Methylnaphthalene (a)

Kinetic Parameters X 10^{-3}	Reaction Temperature			Ea (kcal/mol) X 10^{-3}
	510°C	525°C	540°C	
Dealkylation:				
k_1	16.0	30.5	58.8	55,000
$k_{1,b}$(b)	46.7	88.6	151.2	50,000
Hydrogenation:				
k_{24}	1.4	2.4	4.0	44,600
$k_{24,b}$	4.5	8.2	14.9	52,000
k_{23}	2.8	4.7	7.8	44,200
$k_{23,b}$	9.0	16.2	28.9	49,200
k_4 (c)	3.0	6.0	8.0	41,800
Dehydrogenation:				
k_{-24}	1.8	4.7	12.0	80,600
$k_{-24,b}$	5.8	16.2	45.0	86,600
k_{-23}	3.6	8.4	23.6	80,000
$k_{-23,b}$	11.7	28.9	87.6	85,000
k_{-4} (c)	4.0	10.7	24.2	76,600

a. k_{35}, k_{3c}, k_{4c}, and k_{5c} cannot be obtained because of limited amount of data.

b. footnote "b" means parameters are obtained which consider the hydrogen radicals concentration.

c. numbers obtained may not be reliable because the quantities of tetralin produced are relatively small.

developed to predict the product distribution from the reaction of a petroleum distillate based on kinetic rate constants for model compounds.

Because of the complex nature of the distillate, a simple means of describing the important chemistry was chosen. This system utilized carbon-type analysis, the underlying assumption of this approach being that a given carbon type will behave similarly in hydropyrolysis, irrespective of the remaining molecular structure to which it is attached. The carbon types of interest are defined as follows:

C_A = aromatic carbon

C_N = naphthenic carbon

C_P = paraffinic carbon, but not including terminal or benzylic carbon

C_m = terminal paraffinic carbon - $\underline{C}H_3$

C_α = benzylic carbon but not including C_m

The main reactions in the hydropyrolysis of hydrocarbons have been grouped as follows:

1. hydrogen abstraction
   a. cracking of paraffins and naphthenes
   b. dehydrogenation of naphthenic rings
2. hydrogenation addition
   a. hydrogenation of olefins and aromatics, and
   b. dealkylation of alkyl-substituted or naphthenoaromatics

The main reaction types involved in the model compound study can then be expressed as:

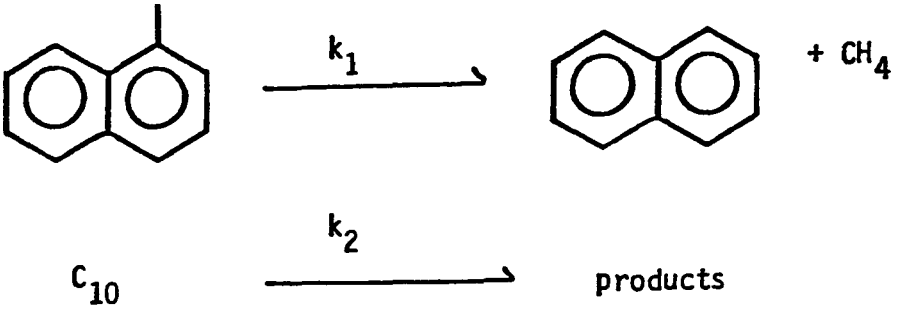

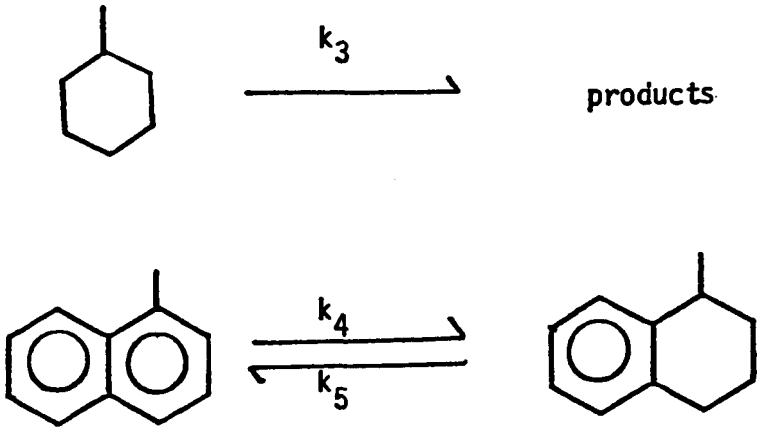

These reaction steps have the following meanings regarding the carbon types:

k_1: Lose one C_α, gain one C_m, and the reaction occurs where there is a C_α.

k_2: Lose two C_p, gain two C_m, and the reaction occurs where there are two adjacent internal C_p; since there are 7 internal C_p pairs in decane, use 1/7 K_2 from above.

k_3: Lose 6 C_N, gain 2 C_m, gain 4 C_p and the reaction occurs where there are 6 C_N.

k_4: Lose 6 C_A, and (C_α/C_A) C_α's for each C_A lost, gain 6 C_N, gain (C_α/C_A) C_p's for each C_A lost, and the reaction occurs where there are 6 C_A.

k_5: Lose 6 C_N, gain 6 C_A and (C_α/C_A)C_α's for each C_A gained, lose (C_α/C_A)C_p's for each C_A gained, and the reaction occurs where there are 6 C_N.

Now assume the following:

1. there are only single aromatic rings, possibly connected to naphthenic rings, i.e., no naphthalene, phenanthrene, etc.

2. cracking of a paraffin occurs only internally, i.e.,

$$R - CH_2 - CH_2 - R'$$

3. cracking of naphthene opens the ring

4. most naphthenic rings do not share a bond with an aromatic ring.

5. the degree of aliphatic substitution is about the same on naphthenic rings as on aromatic rings.

Now the rate expressions with regard to carbon types become the following:

$$d\,C_A/dt = -6\,k_4\,(C_A/6) + 6\,k_5\,(C_N/6) \qquad (16')$$

$$d\,C_N/dt = -6\,k_3\,(C_N/6) + 6\,k_4\,(C_A/6) - 6\,k_5\,(C_N/6) \qquad (17')$$

$$d\,C_p/dt = -2\,k_2\,(C_p) + 4\,k_3\,(C_N/6) + 6\,k_4\,(C_A/6)\,(C\alpha/C_A) - 6\,k_5\,(C_N/6)(C\alpha/C_A) \qquad (18')$$

$$d\,C_m/dt = k_1\,(C\alpha) + 2\,k_2\,(C_p) + 2\,k_3\,(C_N/6) \qquad (19')$$

$$d\,C\alpha/dt = -k_1\,(C\alpha) - 6\,k_4\,(C_A/g6)(C\alpha/C_A) + 6\,k_5\,(C_N/6)(C\alpha/C_A) \qquad (20')$$

or

$$d\,C_A/dt = -k_4C_A + k_5C_N \qquad (16)$$

$$d\,C_N/dt = -(k_3+k_5)\,C_N + k_4C_A \qquad (17)$$

$$d\,C_p/dt = -2k_2C_p + k_4C\alpha + (2k_3/3 - k_5C\alpha/C_A)\,C_N \qquad (18)$$

$$d\,C_m/dt = k_1C\alpha + 2\,k_2C_p + k_3C_N/3 \qquad (19)$$

$$d\,C\alpha/dt = -(k_1+k_4)\,C\alpha + k_5C_NC\alpha/C_A \qquad (20)$$

If the kinetic parameters determined from the model compound study are valid for mixtures, then applying these to the above equations followed by integration should describe the precursor-product relationship for hydropyrolysis of a petroleum distillate. Before this is accomplished, a means for analyzing and interpreting carbon-type structure must be adopted. The most obvious choice is the average structural parameters analysis by means of ^{1}H and ^{13}C NMR spectroscopy.

Structural Analysis

Recent work on upgrading of heavy crudes and the development of alternate fuels technology has created a need for additional analytical methodology. Techniques for characterization of petroleum and its derivatives have been well-developed. Individual quantification of each component is theoretically possible; however, it is too detailed and time-consuming for routine guidance of process development. An alternative approach involves characterization in terms of selected average structures through NMR techniques. Such an analysis gives an easily interpreted picture of the sample and significant quantitative information.

Before the introduction of ^{13}C NMR spectroscopy, complex hydrocarbon mixtures from fossil sources were often characterized in terms of average structural parameters derived mainly from ^{1}H NMR and elemental analysis. The development of ^{13}C NMR spectroscopy has made it possible to obtain information directly about the average carbon skeletons. When these results are used in conjunction with those obtained form the ^{1}H NMR spectra, an excellent characterization of petroleum fractions in terms of molecular structure parameters can be achieved.

Based on the chemical shift of various model compounds and some reference data,[23-29] the carbon types present in the hydrocarbons can be divided into two major categories--aliphatic and aromatic--and several subclasses within the chemical shift range of 10-170 ppm from TMS. These are listed in Table 8. The hydrogen types can also be divided into three major categories--aliphatic, olefinic, and aromatic--and eight subclasses within the chemical shift range of 0.3-9.0 ppm from TMS. These are listed in Table 9.

The five carbon types modeled were determined quantitatively from ^{1}H and ^{13}C NMR spectra as follows.

Table 8

^{13}C NMR Spectroscopy Interpretation for Petroleum and Related Materials

Symbol	Assignment	Shift Range ppm from TMS
C_{Ar}	Aromatic carbon	160 -- 110
C_{Al}	Aliphatic carbon (carbon in aliphatic chains and naphthenic rings)	60 -- 10
* Data from Dickinson, 1980		
C_{Al}	Aliphatic carbon	70 -- 0
C_N	Naphthenic carbon	20 -- 45
C_{ArH}	Aromatic protonated carbon	118 -- 130.5
C_{ArArAr}	C at the junction of three Ar rings	123.5- 126
C_{ArAr}	C at the junction of two Ar rings	128.5- 136
$C_{Ar,CH3}$	Methyl-substituted Ar C	129 -- 137
$C_{Ar,n}$	C at the junction of Ar and Naph. rings	132 -- 137
$C_{Ar,alk}$	alkyl(ex.CH_3)-subs. Ar. C	137 -- 160
* Data from Gillet, 1981		
A_o	Ar. C subs by -OH, -CO, ether, and C in carbonyls	170 -- 150
A_1	ring junc. C, subs Ar. ring C. and one half of the unsubs. C. (Ar. C subs by alkyl groups a/o in condensed point)	150 -- 130
A_2	the other half of unsubs (protonated) Ar. ring C	130 -- 100
A_3	paraffinic, including cycloparaffinic and C of methyl and alkyl subs on Ar rings	60 -- 9
$A_{14.1}$	terminal methyl C $-CH_3$	~ 14.1
A_{23}	first methylene C $\sim C-CH_2-CH_3$ in long alkyl	~ 23

Table 8, continued

A_{32}	second methylene C ~CH_2-CH_2-CH_3 in long alkyl	~32
$A_{29.7}$	third and further methylene C ~$(CH_2)_n$-CH_2-CH_2-CH_3 in long alkyl groups	~29.7
$A_{19.5}$	internal methyl -CH_2-CH(CH_3)-CH_2- in long alkyl groups	~19.5

* Data from Gupta, 1986

Aromatic C-O	148 -- 168
Aromatic C-C	129 -- 148
Aromatic C-H	118 -- 129
Aromatic C-H ortho to aromatic C-O	100 -- 118
CH_2 in Ar-CH_2-Ar, CH in naphthenic rings and alkyl group, CH_2 in alkyl group adj. to CH	37 -- 60
CH_2 in long chain, CH_2 in naphthenic rings, CH_2 in hydroaromatic ring at α to Ar. ring, CH in hydroaromatic rings	27.5- 37
δ and ε CH_2 groups of long chains	29 -- 30
CH_2 adj. to terminal CH_3 in alkyl group $>C_4$, CH_2 in hydroaromatic rings and in propyl group at β to Ar. ring	27.5- 22.5
α-CH_3	18 -- 22.5
β-CH_3 of ethyl group	15 -- 18
CH_3 τ or further from aromatic ring, terminal CH_3 of long chains	10 -- 15

* Data from Snape,[22] and Kershaw[21]

Table 9

^{1}H NMR Spectroscopy Interpretation for Petroleum and Related Materials

Symbol	Assignment	Shift Range ppm from TMS
H_{dar}	H on condensed di- and polyaromatic rings	9.0 - 7.2
H_{mar}	H on monoaromatic rings	7.2 - 6.0
H_{Ar}	Aromatic H and phenolic H	9.0 - 6.0
H_O	Olefinic hydrogen	6.0 - 4.0
$H_{\alpha 2}$	H in CH_2 and CH of alkyl groups α to Ar ring	4.0 - 2.35
$H_{\alpha 1}$	H in methyl group α to Ar. rings	2.35 - 2.1
H_α	H in saturated group α to Ar. rings	4.0 - 2.1
H_{CH}	H in CH groups of saturates	2.1 - 1.6
H_{CH2}	H in CH_2 groups of saturates (including cycloparaffins)	1.6 - 1.1
H_β	H of paraffinic methylene, methine and naphthenes or methylene groups β or further from Ar. rings	2.1 - 1.1
H_τ or H_{CH3}	H in terminal or isolated CH_3- of saturates or methyl τ or further from Ar. rings	1.1 - 0.3
$H_{\beta+\tau}$	H other than α on side chains	2.1 - 0.5
H_{A1}	aliphatic hydrogen	4.0 - 0.3

Determination of Carbon Types

^1H and ^{13}C NMR were used to define key carbon types used in the reaction network model. The five types of carbon are C_A, C_m, C_N, C_p, and C_α as previously defined. The fraction of C_A is determined directly from the ^{13}C NMR integration of the aromatic band (110-160 ppm), terminal methyl carbon (C_m) is likewise obtained from the ^{13}C NMR spectrum (10-22.5 ppm). The fraction of naphthenic carbon (C_N) is obtained using the empirical equation,[20]

$$C_N = 54.3\ [(H_\gamma + H_\beta) + 0.12]/100$$

where H_γ is ^1H NMR integral for methyl hydrogen (0.3 - 1.1 ppm)

H_β is the total secondary hydrogen present in the ^1H NMR spectrum (1.1 - 2.1 ppm)

The number of benzylic carbon (C_α) is obtained as follows,[22]

$$\#C_\alpha = (RS/6) \bullet \#C_A$$

where RS is the number of α carbon per aromatic molecule

and

$$RS = \frac{(8 - 2\ f_{mo})\ (H_{\alpha 1}/2 + H_{\alpha 2}/3)}{H_{Mo} + H_{Di} - (H_{\alpha 1}/2 + H_{\alpha 2}/3)}\ .$$

f_{mo} is the fraction of monoaromatic rings, determined by

$$f_{mo} = \frac{H_{Mo}}{H_{Mo} + [(6 - RS)/(8 - RS)]\ H_{Di}}$$

where

$H_{\alpha 1}$ = H in methyl α to aromatic rings (2.1 - 2.35 ppm);

$H_{\alpha 2}$ = H in CH_2 or CH α to aromatic rings (2.35 - 4.0 ppm;

M_{Ho} = fraction of H on monoaromatic ring (6.0 - 7.2 ppm); and

H_{Di} = fraction of H in diaromatic ring (7.2 - 9.0 ppm).

The fraction of paraffinic carbon not including terminal carbon (C_p) is determined by difference.

$$C_p = 1 - C_N - C_A - C_m - C_\alpha$$

The weight fraction of (type,i) carbon, C_i, is determined by

C_i = fraction of (type,i) carbon X C

where C = weight fraction of carbon in the sample

and the number of (type,i) carbon, $^{\#}C_i$, is determined by

$^{\#}C_i = C_i$ X average molecular weight of sample / 12.

Reactions of Petroleum Distillates

A Wilmington crude oil fraction with a boiling range from 100 to 320°C was selected to perform the kinetic study. Reactions were carried out in the same coiled tube flow reactor as was used in the model compound study. A reaction temperature range from 485 to 585°C and residence times from 12 to 40 seconds were studied.

The Wilmington crude oil is rich in naphthenic compounds. As a feedstock, it is similar to tar sand bitumen and both are excellent feedstocks for hydropyrolysis processing.[11,12] The high naphthenic content is expected to result in products amenable to the production of high density jet fuels. The boiling range under 320°C was selected because it represented a simpler fraction than a broad range material. This allowed for easier analysis. Also, the molecular weight present was closer to that of the model compounds used. Some heavier material needed to be included to provide sufficient aromatic content for good quantitative analysis.

A petroleum distillate was selected for study by hydropyrolysis also because work with residual materials has proven time consuming and experimentally cumbersome. It was felt that a study of a simpler material would provide important insight into the reaction chemistry and the effect of process variables related to hydropyrolysis. It may be properly emphasized that the theory relying on a carbon-

type description is independent of composition. Thus, a Wilmington distillate is an adequate model for tar sand oils or other petroleum samples. Differences in composition relate effectively to differences in concentration of carbon types for which the model accounts.

Results of Hydropyrolysis of Wilmington Distillate

Figure 19 shows the change in gas composition as a function of reaction temperature at a residence time of 40 seconds. It is observed that the amount of CH_4 and C_2H_6 increases as the temperature increases, possibly indicating that secondary cracking of C_3 and C_4 compounds is occurring. The relatively larger increase in methane is expected on the basis of thermodynamic considerations. The decrease in olefin content with increasing temperature indicates hydrogenation reactions are occurring. This is due to the increased population of (H•), and is reflected in the hydrogen index.

Figure 20 shows the change in boiling point distribution of the liquid product obtained at different reaction temperatures. As the reaction temperature goes up, more low boiling material (boiling range from 75 to 175°C) is produced. This is indicative of more extensive cracking, as expected. As has been previously reported, there is no evidence for the production of coke or condensation products with molecular weight higher than the starting material.[4] The small heavy ends tail for the 585°C produced material is an artifact of normalizing the areas under the curves to unity (the liquid product yield for the 585°C run is 53.8% of the feed).

Figure 21 shows the change in product distribution as a function of reaction temperature for several residence times. Products are defined as gasoline (boiling < 200°C), kerosene (200-275°C), gas oil (275-325°C) and heavy gas oil (325-400°C). First, it is observed that irrespective of residence time production of heavy (gas oil) and middle (kerosene) distillates decreases with increasing temperature. Gas production increases, particularly above 535°C, with increasing temperature. The light distillate (gasoline) exhibits a maximum with respect to temperature. For a 40 seconds residence time, the gasoline yield reaches a maximum at about 535°C; this point shifts to lower temperatures as the reaction time decreases.

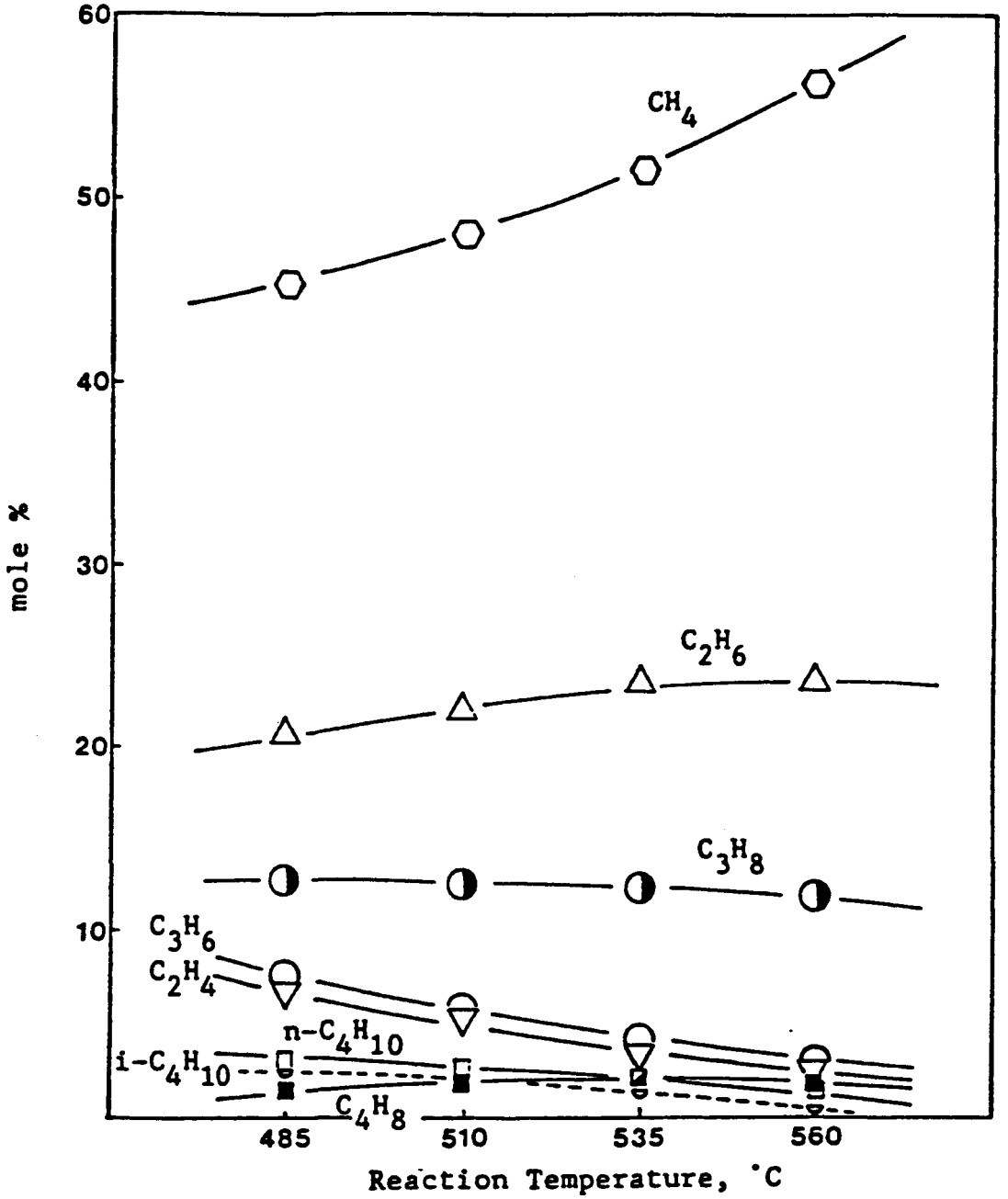

Figure 19. Change in the composition of gases products from hydropyrolysis of Wilmington crude distillate as a function of reaction temperature. [H_2 pressure 1800 psig; residence time, 40 sec; LHSV, 3.1 hr^{-1} H_2/oil mole ratio, 10.6.]

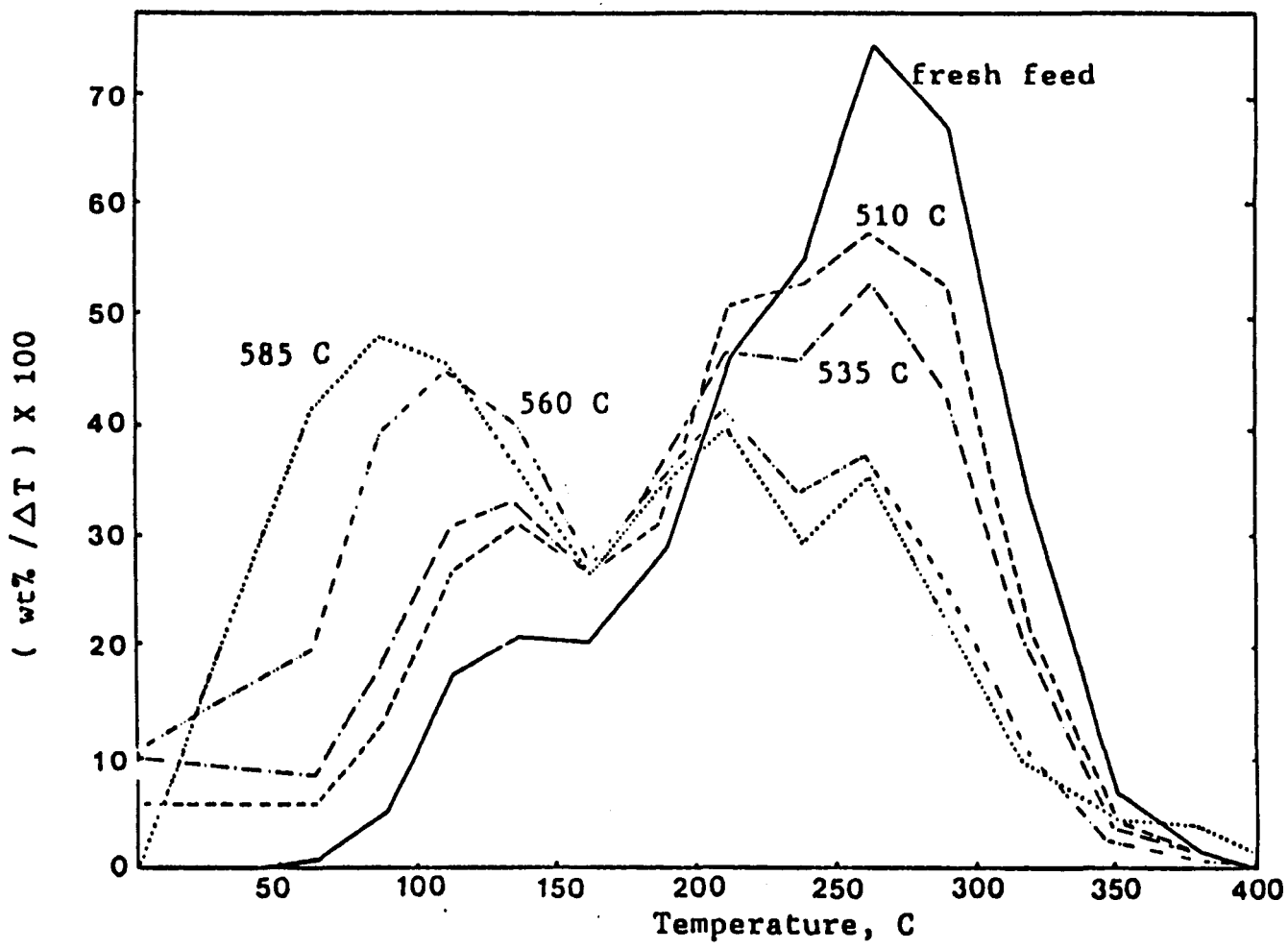

Figure 20. Boiling point distribution of liquid products obtained from hydropyrolysis of Wilmington crude distillate at different reaction temperature [H_2 pressure, 1800 psig; LHSV, 3.1 hr^{-1}; residence time, 12 sec].

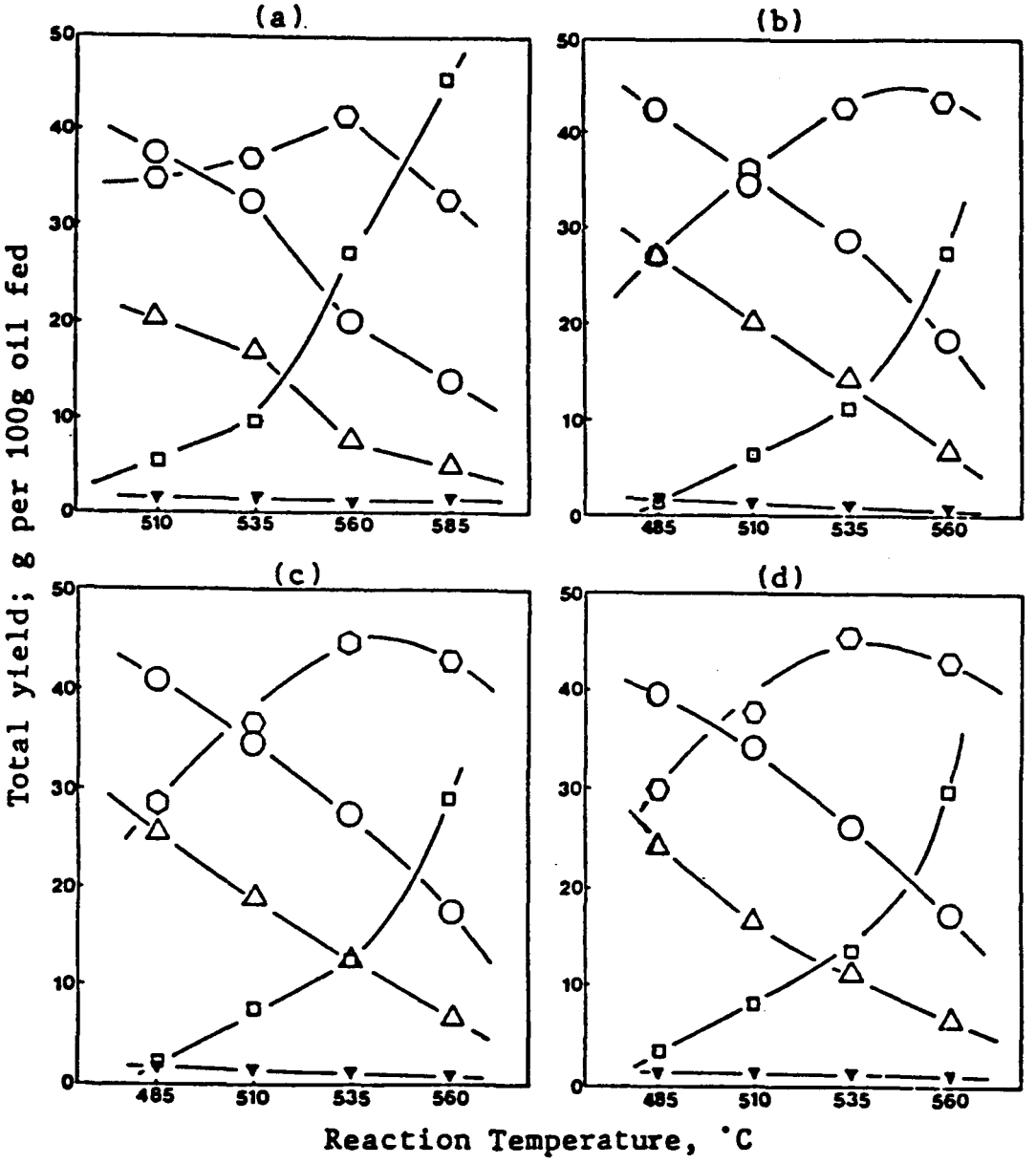

Figure 21. Total yield versus reaction temperature obtained from hydropyrolysis of Wilmington crude boiling less than 320°C distillate, at H_2 pressure 1800 psig, LHSV=3.1 hr^{-1}, residence time (a) 12 sec, (b) 20 sec, (c) 30 sec, (d) 40 sec. in which : gases; : gasoline fraction; : kerosene fraction; : gas oil fraction; :heavy gas oil fraction, in the liquid product.

Figure 22 shows the data replotted with respect to residence time. In general, as residence time is increased, the lighter fractions increase and heavier fractions decrease. The reaction temperature affects product yields more than does residence time over the range of values studied.

For a feedstock of commercial significance data such as this could be reduced to a mathematical model, economic parameters could be placed on the value of the products and an optimum time and temperature for the reaction can be determined.

Hydrogen Consumption

It was the purpose of the study with Wilmington distillate to examine the reaction chemistry through careful analysis of the data and characterization of the products. An important aspect of hydropyrolysis is the consumption and fate of hydrogen. A hydrogen balance can be calculated quite accurately by comparing the hydrogen present in the starting material with that in the products, thus

(Hydrogen) = (Hyd)liq. prod. + (Hyd)gas. prod. = (Hyd)feedstock.

Results are shown in Table 10 for four different reaction temperatures at a constant residence time of 20 sec. With increasing reaction temperature, there is observed an increase in hydrogen content of gases and correspondingly an increase in hydrogen consumption. Hydrogen content of the liquids declines slightly. While hydrogenation of aromatics is expected to occur, the effect is offset by loss of hydrogen to hydrogen rich gases by more favored cracking of paraffinic species. As has been previously reported, hydrogen consumption and gas production are nearly a linear proportion of each other.[12] This is shown in Figure 23 which exhibits a remarkable linearity over a wide range of values. The negative intercept suggests that at lower temperatures there is, as may be expected, a net dehydrogenation occurring. For this particular feedstock and the reaction conditions stated, the rates of hydrogenation and dehydrogenation reactions are equal at about 485-490°C.

Additional information about the relative reaction rates for hydrogenation and dehydrogenation can be obtained from the hydrogen balance. The major reactions involving hydrogen are cracking (consumption of up to one molecule of H_2 per event), hydrogenation (consumption by aromatic or

Table 10

Hydrogen Consumption Obtained from Hydropyrolysis of Wilmington Crude Oil Distillate[a]

Run Number	W 08	W 02	W 03	W 04
Reaction Temperature, °C	485	510	535	560
Residence Time, sec	20	20	20	20
Liquid Yield (g per 100g oil fed)	97.8	93.3	88.7	71.4
H wt % in liquid (b)	12.74	12.68	12.55	11.96
C wt % in liquid (b)	85.64	86.25	85.75	84.68
(H/C) liq.	1.771	1.750	1.742	1.681
Gas Yield (g per 100g oil fed)	1.3	5.5	12.2	26.5
H wt % in gases (c)	19.11	19.16	19.7	20.03
C wt % in gases (c)	80.89	80.84	80.3	79.97
(H/C) gas	2.812	2.822	2.921	2.982
H/C of Total Prod. (d)	1.785	1.810	1.885	2.033
Calc. H Consumption g per 100g oil fed	-0.026	0.188	0.570	1.267
SCF/bbl	-14	101	305	680

(a) (H/C) wt of fresh feed = 12.85 / 85.52; (H/C) atomic = 1.789; feed density = 0.85
(b) number obtained from elemental analysis
(c) calculated from composition by gas chromatographic analysis
(d) calculated from weighted average H/C of liquid and gaseous products

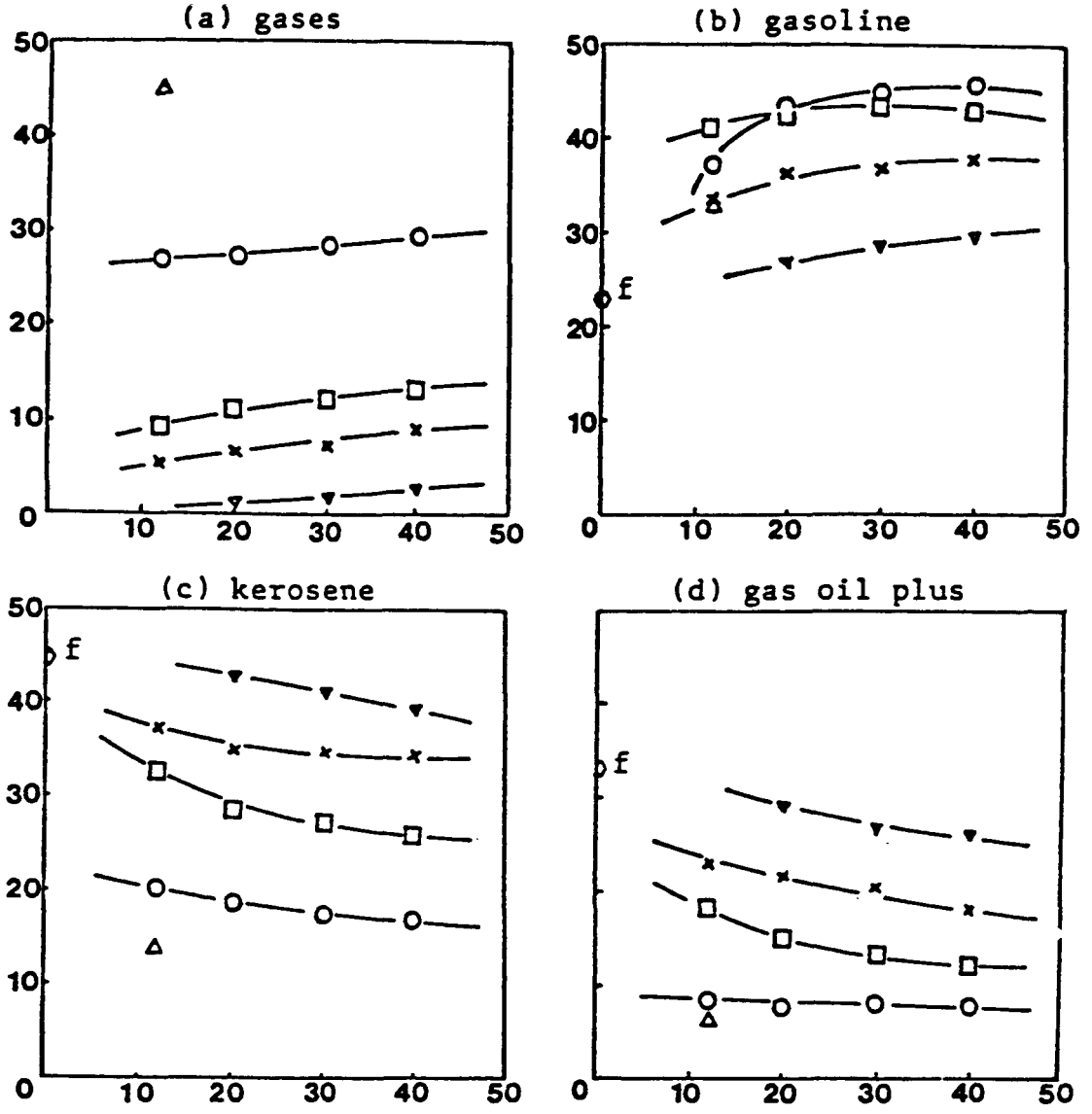

Figure 22. Total yield as a function of residence time at various reaction temperatures; : 485°C; x: 510°C; : 535°C; : 560°C; : 585 C; for which (a) gases, (b) gasoline fraction, (c) kerosene fraction, (d) gas oil and heavy gas oil fractions; obtained from hydropyrolysis of Wilmington crude oil boiling under 320°C distillate, at H_2 pressure 1800 psig, LHSV = 3.1 hr^{-1}.
"f" referred to the feed compositions.

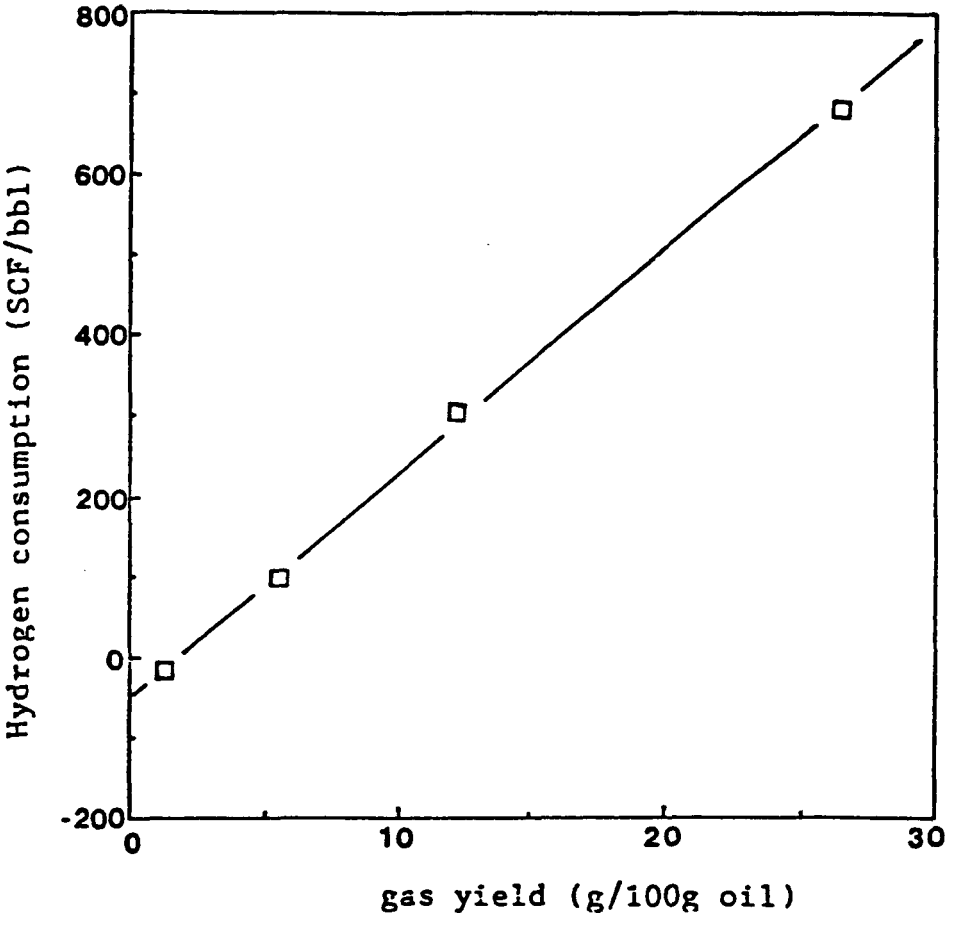

Figure 23. Hydrogen consumption is a linear function of gas production in hydropyrolysis of Wilmington distillate.

olefinic structures), and dehydrogenation (loss of hydrogen from naphthenic or paraffinic structures). Condensation and polymerization reactions can be ignored under hydropyrolytic conditions. The material balance equation describing these reactions is

$$\Delta H_{net} = \Delta H_{c,g} + \Delta H_{C,1} + \Delta H_{hyd} \qquad (21)$$

where ΔH_{net} is the net consumption determined experimentally;

$\Delta H_{c,g}$ is the hydrogen required for cracking of liquid to gas;

$\Delta H_{C,1}$ is the hydrogen required for cracking of liquid to lower molecular weight liquid; and

ΔH_{hyd} is the net hydrogen required for hydrogenation-dehydrogenation reactions occurring in the liquid.

The amount of hydrogenation required for cracking can be calculated from the change in molecular weight. Assume that each cracking event results in an average molecular weight reduction of 50%. The average number of cracking events can be calculated from the following formula.

$$\text{\# of event} = \frac{\text{amu carbon in feed molecules}}{\text{amu carbon in product molecules}} - 1$$

For each event two atoms (one molecule) of hydrogen is required. By weighting each fraction (gas and liquid) to account for the amount produced the $\Delta H_{c,g}$ and $\Delta H_{c,1}$ can be estimated. ΔH_{hyd} can then be calculated from equation 21.

The data for the Wilmington distillate were treated by this method. Results for the four parameters of equation 21 are given in Figure 24. Results reveal that the majority of hydrogen is required for gas production. Smaller amounts are required for liquid cracking.

It is evident that for the liquids net dehydrogenation is occurring. Previous results have suggested that naphthenes are being dehydrogenated to monoaromatics while PNA's have been hydrogenated to lower ring aromatics. It is apparent from the current results that the net reaction is that of dehydrogenation and that an increase in temperature does not reverse the trend.

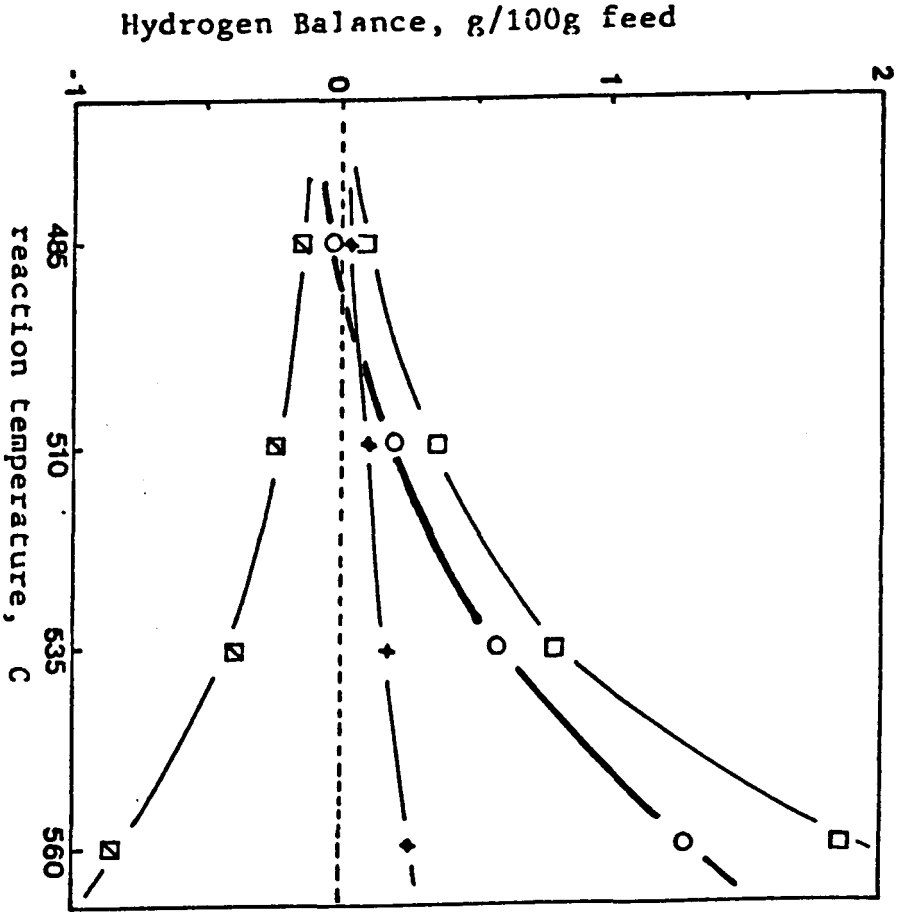

Figure 24. Hydrogen consumption based on feed as a function of reaction temperature in hydropyrolysis of Wilmington distillate, in which : ΔH_{net}; : $\Delta H_{c,g}$; : $\Delta H_{c,1}$; : ΔH_{hyd}.

The data presented above were recalculated on a product basis and replotted against reciprocal temperature. Results shown in Figure 25 are quite linear. Results are quite linear. The shallow slope for all the lines is significant and suggests that the dominant mechanisms for the gas production and liquid cracking/hydrogenation/dehydrogenation reactions do not change over the temperature range studied. Lack of curvature also suggests that new and competing reactions are not introduced at higher temperatures. The slight curvature seen at the high temperature end can be easily explained by the expected increase in methyl cracking reactions.

NMR Analysis of Wilmington Distillate

Liquid products representing a range of process severity were subjected to NMR analysis. Tables 11 and 12 summarize the structural parameters obtained. Inspection of the results reveals that net aromaticity increases with increasing temperature but most substantially for the severest case of 560°C and 40 sec. The number of methyl substituents as indicated by H_α parameters rises substantially with increasing severity. The naphthenes reveal a possible maximum as indicated by the naphthenic carbon content. The results shown in Tables 11 and 12 were compared with that which would be predicted from the kinetics of the model compound study.

Validation of Kinetic Model

A kinetic model based on the carbon type and derived from hydropyrolysis of model compounds has been described in a previous section. The temperature conditions and the related kinetic parameters are given in Table 13. The rate constants given in the table are those calculated from the model compound study. These are to be used under the process conditions of the distillate feed to calculate the product composition on a feed basis.

After stepwise integration of equations 16 through 20, the calculated carbon composition is then compared with that obtained by structural analysis. Table 14 shows this comparison for both the cases when (H•) is accounted for and that in which it is not. In the case for which the hydrogen free radical concentration is taken account, the rate constant (k_b) is treated as follows:

$$k_i = k_{b,i} (R^* Y + 1)$$

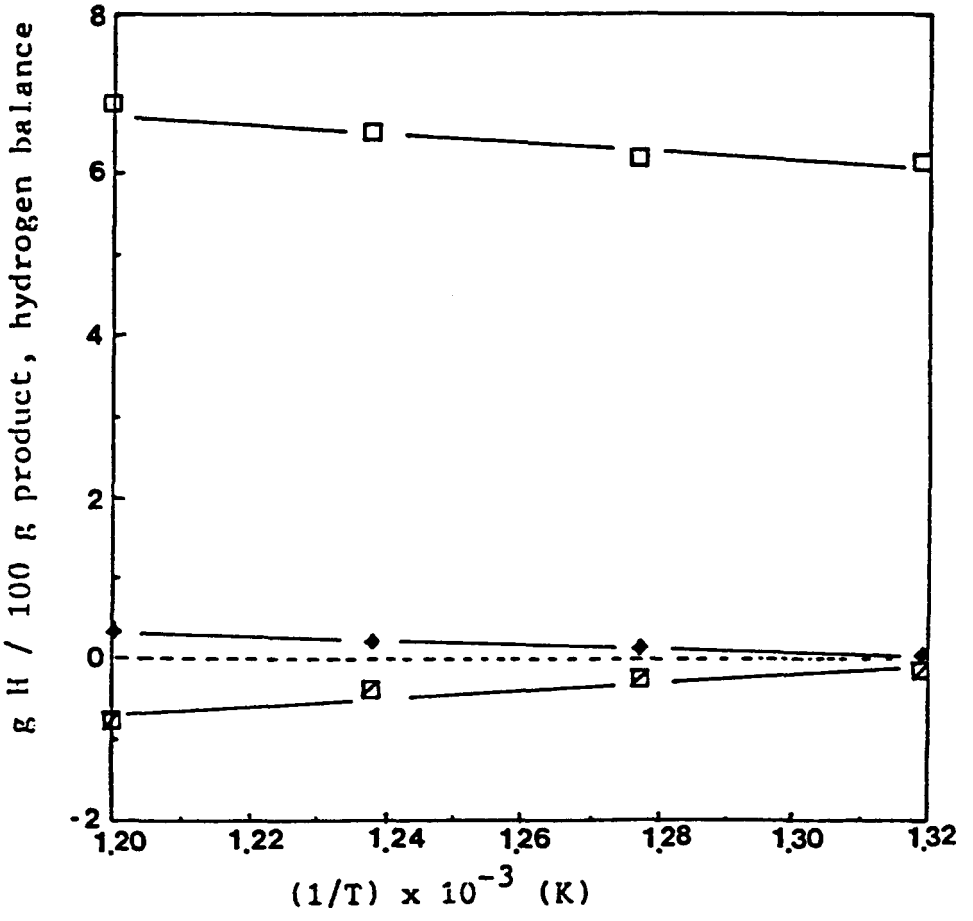

Figure 25: Hydrogen consumption based on product as a function of reciprocal reaction temperature, in which : $\Delta H_{c,g}$; : $\Delta H_{c,1}$; : ΔH_{hyd}.

Table 11

Structure Parameters of Wilmington Crude Oil Distillate and its Hydropyrolysis Liquid Products Obtained by NMR Spectra

Parameters	<320°C Distillate	HP Product 510°C,20 sec	HP Product 535°C,30 sec	HP Product 560°C,40 sec
H dar	0.02	0.02	0.02	0.05
H mar	0.03	0.02	0.02	0.05
H Ar	0.05	0.04	0.04	0.11
H o	0	0.01	0.02	0.04
H α1	0.02	0.02	0.03	0.05
H α2	0.02	0.04	0.05	0.08
H α	0.04	0.06	0.08	0.14
Hβ	0.47	0.45	0.45	0.40
H	0.44	0.44	0.42	0.32
A1	0.03	0.03	0.06	0.08
A2	0.04	0.06	0.12	0.20
A1+A2+C Ar	0.08	0.09	0.18	0.27
A3=C A1	0.92	0.91	0.82	0.73
Aromaticity	0.09	0.11	0.21	0.32
Avg. M.W.	184	167	154	138
Wt C	0.855	0.855	0.852	0.846
Wt H	0.128	0.122	0.129	0.12

Table 12

Structural Parameters of Wilmington Crude Distillate and its Hydropyrolysis Product Data Obtained from NMR Spectra Interpretation and Gas Analysis

Structural Parameters	<320°C Distillate	Hydropyrolysis Product 510°C,20 sec	535°C,30 sec	540°C,40 sec
Fractions of (type) carbon in liquid product				
Aromatic C	0.08	0.09	0.18	0.27
Aliphatic C	0.92	0.91	0.82	0.73
Naphthenic C	0.57	0.59	0.57	0.50
Paraffinic C	0.35	0.32	0.25	0.23
# of Carbon in Liquid Product	13.11	11.90	10.93	9.73
in Gas Prod.*	--	1.21	2.18	3.38
Mole % of Cm in gas	--	88.0	90.8	93.2
Cp in gas	--	12.0	9.2	6.8

* number obtained by difference

Table 13

Initial Conditions[a] and Kinetic Parameters
Used in the Carbon Type Kinetic Model

Reaction Temperature	510°C	535°C	560°C
Hydrogen Index:			
Y,o (extrapolated)	0.560	0.606	0.687
Y, 12 sec (exptal)	0.629	0.684	0.761
Y, 20 sec (exptal)	0.655	0.714	0.791
Y, 30 sec (exptal)	0.673	0.733	0.810
Y, 40 sec (exptal)	0.684	0.759	0.835
Kinetic Parameter (Conventional):			
k_1 (dealkylation)	0.016	0.0474	0.1326
k_2 (decane crac.)[b]	0.00114	0.00378	0.0113
k_3 (m.c. crac.)	0.004	0.0113	0.0292
k_4 (hydrogenation)[c]	0.0014	0.0028	0.0065
K_5 (dehydrogenation)[c]	0.0018	0.00625	0.0282
Kinetic Parameters Involving (H) Index:			
K_{1b} (dealkylation)	0.467	0.105	0.267
K_{2b} (decane crac.)[b]	0.00486	0.0212	0.084
K_{3b} (m.c. crac.)	0.028	0.0965	0.296
K_{4b} (hydrogenation)[c]	0.0045	0.00944	0.025
K_{5b} (dehydrogenation)[c]	0.0058	0.032	0.162

a initial conditions of feedstock: C A=1.05, C N=7.47, C p=3.04, C m=1.32, C α=0.23, in terms of carbon numbers

b use 1/7 of rate constant obtained from cracking of decane. (the rate constant must be normalized to a unit carbon basis to avoid influence of structure, e.g., n-decane provides seven internal bonds available for cracking)

c use k_{24} and k_{-24} in the model aromatic reaction network

Table 14

Comparison of Carbon Number Obtained from Experimental Values and Predicted Values in Hydropyrolysis of Wilmington Distillates

Samples	Fresh Feed	510°C,20 sec	535°C,30 sec	560°C,40 sec
C A				
exptal	1.05	1.07	1.96	2.77
p (H)	--	1.31	2.25	3.19
p (conv)	--	1.27	2.03	3.83
C N				
exptal	7.47	7.09	6.25	4.86
p (H)	--	5.75	2.17	0.24
p (conv)	--	6.68	4.48	1.01
C p				
exptal	3.04	2.27	0.84	0.36
p (H)	--	3.71	4.06	1.66
p (conv)	--	3.23	3.50	2.48
C m				
exptal	1.32	2.31	3.25	4.24
p (H)	--	2.14	4.50	8.00
p (conv)	--	1.72	2.99	5.79
C α				
exptal	0.23	0.37	0.81	0.88
p (H)	--	0.20	0.13	0.17
p (conv)	--	0.20	0.22	0.003

1 exptal: number obtained from NMR spectra interpretation and gas analysis

2 p (conv): predicted values, number obtained from kinetic model in which hydrogen radical index was not considered.

3 p (H): predicted values, number obtained from kinetic model in which hydrogen radical index was considered.

in which $R = k_a/k_b = -1.0$ for all three temperatures.

Y = hydrogen radical index, obtained from experimental data.

Results in Table 14 show the prediction is generally good at low reaction temperatures, but it is not as good at higher temperatures, especially for the naphthenic and paraffinic carbon. It is probable that this error derives from errors in the quantitative determination of C_N from the NMR analysis. If C_N is underestimated, then by difference C_p is over-estimated. By simply dividing C_N by a constant factor of 6, a much better fit of the data is forced. These results are shown in Table 15.

While the agreement with experimental results is not perfect, the trends predicted by the models are accurate. Both models successfully predict the increase in aromatic carbon and terminal methyl carbon. Both models predict the decrease in paraffinic and naphthenic carbon, with the naphthenic carbon showing greater resistance to cracking. The model does not predict the increase in benzylic carbon due to lack of an appropriate model compound in the base study.

Overall, the model which considers the effect of the hydrogen atom concentration improves the accuracy of the predictions. Both models tend to underestimate the rate of dehydrogenation to form aromatics. The model accounting for (H•) does better at predicting the rate of cracking for naphthenes and paraffins.

The rate constants obtained from the model compound work may not be directly applicable to a distillate and some factor may be needed to correct the rate constants. The kinetic meaning of each reaction (or each rate constant) may not be as simple as described before; i.e., a more complex model may be needed to better describe the system. It may be that the (H•) parameter is more important to some reactions than others and a combination of conventional kinetic treatment and that developed in this work will better describe the reactions occurring in hydropyrolysis.

Complex models are not suitable for general process design work. However, the current model shows promise in that its foundation is based on fundamental chemical reactions. One way to improve the carbon-type model would be to obtain the kinetic rate constants from authentic distillates. Such results may be more generally applicable to heavy oil processing. Because of the complex nature of

Table 15

Comparison of Carbon Number Obtained from Hydropyrolysis of Wilmington Distillate Between Experimental Values and Predicted Values Modified Model*

Samples	Fresh Feed	510°C,20 sec	535°C,30 sec	560°C,40 sec
C A				
exptal	1.05	1.07	1.96	2.77
p (H)	--	1.07	1.29	2.05
p (conv)	--	1.07	1.89	1.87
C N				
exptal	7.47	7.09	6.25	4.86
p (H)	--	7.18	6.17	4.01
p (conv)	--	7.36	6.93	5.41
C p				
exptal	3.04	2.27	0.84	0.36
p (H)	--	2.98	2.56	1.36
p (conv)	--	2.96	2.64	1.72
C m				
exptal	1.32	2.31	3.25	4.24
p (H)	--	1.71	3.01	5.65
p (conv)	--	1.55	2.29	4.12
C α				
exptal	0.23	0.37	0.81	0.88
p (H)	--	0.17	0.07	0.03
p (conv)	--	0.17	0.06	0.001

* model was modified by dividing each Cn by 6.

1 exptal: number obtained from NMR spectra interpretation and gas analysis

2 p (conv): predicted values, number obtained from kinetic model in which hydrogen radical index was not considered

3 p (H): predicted values, number obtained from kinetic model in which hydrogen radical index was considered

the distillates even this simple model is nonlinear. Thus, development of an improved model will require more extensive work and analysis.

Results from Process Development Unit

The results have been applied, insofar as currently possible to the operation of the 2 l/h process development unit. Both previously reported results[30] and current results are included.

A summary of the hydropyrolysis yields using TS-IIC oil as the feed is presented in Table 16. Run numbers not included in the table represent those experiments which failed for operational reasons, or for which quantitative yield results were not obtained. Operating experience was gained from these runs, and this information was incorporated into the overall process development unit operating procedures.

It is evident from the results that without proper atomization, larger droplets tend to undergo thermal reactions resulting in greater coke production. This observation applies to all of the "fountain" type nozzle runs (3H and 1H). It is only in runs 85-63 through 86-2 that the potential of hydropyrolysis can be seen. In these runs, the internal walls of the reactor were not allowed to go over 510°C, atomization quality was good, and residence times were short. At the moderately low reactor temperatures utilized in these experiments high conversion to liquid products was achieved.

The list of important variables in hydropyrolysis has been found to be greater than anticipated. In addition to outlet temperature, pressure, residence time, and gas/oil ratio, several other variables need to be considered. These are gas composition, reactor and nozzle configuration, reactor wall temperature, blast rate, and blast temperature. Oil properties such as viscosity and surface tension are also expected to be important, due to their influence on the quality of atomization. The range and influence of each of the above-mentioned variables is discussed in the following sections:

Reactor Configuration

Two straight tube reactors, with different length but the same radius, were used in this study. The long tube was 28 inches long and the volume, including fittings, was 22.0 in^3 (or 360 c.c.). The short tube was 16 inches long with a volume of 12.8 in^3 (or 210 c.c.).

Table 16

Product Distribution and Reaction Conditions for Hydropyrolysis Process Development Unit Runs

Run #	%Coke	%Gas	%Light	%Heavy	%Liquid	API of lt	R.I.	Fl/Nz	Tin	Tout	Trxt	(H)t	R.T.	Bl.H	gas	oil	G/O
85-17	1.9	10.1	74.3	13.7	88.0	25.9	1.5100	C/3	594	497	546	9.8	7.9	-	11.0	28.9	0.36
85-18	1.9	11.2	81.2	5.8	87.0	28.8	1.5127	C/3	605	521	563	14.9	5.1	-	17.3	30.4	0.57
85-19	1.9	9.8	81.1	7.2	88.3	23.7	1.5125	C/3	602	507	555	10.1	7.7	-	11.0	30.0	0.38
85-20	3.5	15.9	81.8	2.3	84.1	24.0	1.5090	C/3	608	552	577	15.0	5.0	-	19.4	30.4	0.64
85-22	1.2	1.5	81.6	15.7	97.3	24.1	1.5087	C/3	601	496	549	10.1	7.5	-	10.0	30.0	0.33
85-23	0.9	3.9	75.8	19.4	95.2	23.9	1.5105	C/3m	600	513	556	10.1	7.4	-	12.0	30.0	0.40
85-27	2.2	8.1	79.7	10.0	89.7	25.2	1.5120	C/1	602	495	549	10.5	7.2	-	12.2	30.5	0.40
85-28	3.2	14.6	75.4	6.8	82.2	24.3	1.5095	C/1m	604	506	555	11.5	6.5	(2.1)	12.3	35.0	0.40
85-29	5.6	8.9	82.5	3.0	85.5	25.1	1.5090	P/1	570	538	554	10.0	7.8	-	15.1	28.3	0.53
85-30	5.2	6.6	79.4	8.8	88.2	25.0	1.5060	P/1	542	502	522	9.4	8.8	-	10.0	29.2	0.34
85-31	2.7	9.8	76.2	11.3	87.5	23.6	1.5083	P/1	552	479	516	13.7	6.1	-	14.7	30.4	0.48
85-34	5.9	11.0	78.5	5.7	84.2	25.7	1.5056	P/1	578	510	544	9.9	8.0	-	13.8	41.5	0.33
85-35	5.9	9.9	78.5	3.4	81.9	25.2	1.5130	P/1	596	530	560	10.5	7.4	-	15.2	29.9	0.51
85-36	5.5	12.1	78.3	4.1	82.4	25.3	1.5105	P/1	598	534	566	15.0	5.1	-	20.5	43.7	0.47
85-37	6.1	17.8	77.3	3.1	80.4	25.9	1.5135	P/1	607	544	576	12.0	6.3	-	18.8	39.8	0.47
85-38	1.6	2.1	84.3	12.0	96.3	24.0	1.5070	C/1	579	498	539	10.1	4.5	-	11.8	31.0	0.38
85-39	1.2	4.0	84.6	10.2	94.8	22.2	1.5680	C/1	566	488	527	9.8	4.7	-	11.5	28.5	0.40
85-40	1.9	3.1	48.8	46.2	95.0	26.6	1.5050	C/1	596	499	548	9.5	4.8	-	11.3	47.6	0.24
85-41	3.6	4.5	81.6	10.3	91.9	23.5	1.5100	C/1	613	512	563	15.0	3.0	-	17.6	41.0	0.43
85-42	4.5	6.3	80.7	8.5	89.2	24.0	1.5065	C/S*	578	478	528	9.5	-	1.5	11.0	31.0	0.40
85-43	2.8	7.6	79.4	10.2	89.6	23.5	1.5110	C/S*	583	509	546	11.8	-	2.0	13.9	36.7	0.43
85-44	1.4	3.5	84.0	11.1	95.1	22.2	1.5670	C/S*	570	494	532	12.0	-	2.0	13.1	37.0	0.41
85-45	1.5	5.9	81.2	11.4	92.6	23.6	1.5760	C/S*	559	487	523	11.4	-	2.2	12.7	36.5	0.41
85-46	5.2	11.1	80.1	3.7	83.8	22.9	1.5160	C/S*	578	513	546	17.6	-	2.8	26.1	21.9	1.32
85-47	5.5	8.6	71.5	14.4	85.9	21.4	1.5200	C/S/A	550	492	521	11.3	-	2.6	13.9	35.9	0.48
85-48	3.7	11.1	63.0	22.2	85.2	20.0	1.5300	C/S/A	576	506	541	9.3	-	2.9	11.7	31.2	0.47
85-49	1.7	6.6	73.3	18.4	91.7	17.7	1.5630	C/S/A	544	487	516	9.0	-	1.9	9.2	38.2	0.29
85-51	4.1	14.9	69.6	11.4	81.0	19.7	1.6265	C/S/A	621	524	573	12.0	-	5.4	16.8	36.7	0.58
85-52	3.6	15.7	7.6	3.1	80.7	23.5	1.5220	C/S	636	548	592	10.3	-	4.6	14.3	31.0	0.61
85-54	4.5	13.5	77.0	5.0	82.0	22.9	1.5155	C/S**	663	549	606	15.0	-	10.5	16.6	40.5	0.67
85-55	4.8	9.7	80.5	5.0	85.5	22.6	1.5180	C/S**	662	530	596	13.0	-	11.6	13.9	40.7	0.63
85-58	2.1	11.6	72.2	14.1	86.3	22.5	1.5180	P/S	552	507	530	27.0	1.8	-	31.8	15.0	2.10
85-59	1.1	6.8	80.0	12.1	92.1	23.5	1.5120	P/S	551	506	529	25.0	1.9	-	36.1	44.0	0.82
85-60	2.9	8.7	67.6	20.8	88.4	22.5	1.5136	P/S	564	512	530	21.5	2.2	-	20.7	38.3	0.75
85-62	3.9	14.0	81.0	1.1	92.1	21.9	1.5215	P/S	560	530	545	23.0	1.9	-	32.5	22.8	1.42
85-63	0.2	4.7	84.5	10.6	95.1	24.5	1.5080	P/S	532	505	519	24.0	2.1	-	29.5	34.6	0.85
86-1	0.2	2.8	92.4	4.6	97.0	19.3	1.5950	P/S	515	493	504	22.4	2.2	-	26.3	61.5	0.43
86-2	0.2	7.3	83.8	8.7	92.5	24.2	1.5100	P/S	524	499	512	25.0	1.9	-	32.7	59.0	0.55

Definitions of Headings Used in Table 16

Reaction Conditions of Hydropyrolysis Process Development Unit Runs

%	All percentages are weight percents based on feed
API of lt	API gravity of overhead condensable products
R.I.	Refractive index of overhead condensable products
Fl/Nz	Reactor flow pattern/nozzle design code
C/3	Countercurrent flow mode, three-orifice nozzle
C/3m	Countercurrent flow mode, three-orifice nozzle, with make-up H_2
C/1	Countercurrent flow mode, one-hole nozzle
C/1m	Countercurrent flow mode, one-hole nozzle, with make-up H_2
P/1	Parallel (co-current) flow mode, one-hole nozzle
C/S*	Countercurrent flow mode, spray nozzle, low blast H_2 rate
C/S/A	Countercurrent flow mode, spray nozzle, low blasting rate with Athabasca bitumen as feedstock; otherwise TS IIC oil as feed
P/S	Parallel (co-current) flow mode, spray nozzle, total recycle gas stream as blast gas passed through inside of nozzle.
Tin	Reactor (gas) inlet temperature, averaged (^oC)
Tout	Reactor outlet temperature, averaged (^oC)
Trxt	Average reactor temperature = (Tin + Tout)/2 (^oC)
(H)i	Initial hydrogen recycle flow rate (g/min)
R.T.	Calculated gas residence time based on (H)i (sec)
Bl H	Blast hydrogen flow rate (g/min)
gas	System recycle gas flow rate, averaged (g/min)
oil	Oil feed rate (g/min)
G/O	Gas to oil mass ratio, gas including recycled and blasting gases

Note that runs from #85-17 to #85-37 were made with the long (28") reactor; and runs after #85-38 were made with the short (16") reactor.

The long reactor tube was used in Runs 85-17 through 85-37, and 17 successful runs were made. In these runs, it was found that consistently high coke yield (more than 5%) occurred in the parallel flow mode (Runs 85-29 through 85-37). The coke formed was located mainly on the reactor wall on the outlet side. As unconverted heavy oil travelled through the tube, the radial momentum became significant, and the droplets impinged on the wall. Coke yield was unacceptably high in these runs. Coke yield was reduced with the counter-current flow mode compared to that in the parallel flow mode (Runs 85-17 through 85-28). The coke was deposited 2 to 8 inches above the nozzle, and as the reaction proceeded, the pressure drop across the reactor increased and the gas flow decreased. Inspection after the run revealed a solid but porous plug of coke. It was apparent from these results that reactor space above about 10 inches was not being utilized. Beginning with Run #85-38, the long tube reactor was replaced with the 16 inch, shortened version, and runs concentrating on improved nozzle performance were begun.

The original concept of an open tubular reactor of moderately high length-to-diameter ratio appears to be sound. Economics dictate that a high rate of reactor space utilization must be maintained. Thus, the trade-off is between space utilization and impingement of oil droplets on the walls, which may result in coke formation. This trade-off is expected to be less severe in scale-up. Recent work has suggested that in scale-up, a "wall-less" reactor may be possible, thus reducing coke formation to negligible amounts. The concept of counter-current flow (oil up, gas down) has also been shown to be theoretically sound. Work in this mode will require a change in length-to-diameter ratio, and other significant modifications, and it is currently felt that such work must await future funding.

Nozzle Design

It now seems clear that oil droplets must be reduced to the smallest diameter feasible. This indicates that a blast atomizer nozzle will be required for injection of the oil. The optimization problem here is the trade-off between the gas-to-oil ratio and droplet size.

Three types of nozzles have been used in this study: (1) a three-orifice nozzle; (2) a one-orifice nozzle; and (3) a spray nozzle. The three-orifice nozzle is doughnut shaped (3/4 inch O.D. and 7/16

inch I.D.) with three 0.007 inch I.D. orifices equidistant from each other. total orifice area of this nozzle is 1.15×10^{-4} in^2. During the atomization process, hydrogen passes through the center and surrounds the nozzle. The one-hole nozzle is bullet-shaped (1/4 inch O.D.) with one 0.010 inch orifice in the center. The area of this orifice is 7.85×10^{-5} in^2. Oil passes through both of these nozzles and is dispersed in the reactor. In laboratory tests, water passed through these two nozzles was observed as jet streams. The spray nozzle was previously described. Laboratory tests using water and air have been used to obtain visual confirmation of the blast efficiency. The nozzle is capable of producing a cloud of fine droplets that is radially symmetrical. Results from Run 86-2 demonstrate the potential effectiveness of the atomizing nozzle.

Reactor Wall Temperature

The original design concept regarding the reactor wall was to maintain the wall temperature at or above the reaction temperature to avoid oil vapor condensation on the walls. However, due to the low partial pressure of the oil (lower dew point), this has not been a problem. Lower wall temperatures have resulted in significantly reduced coke formation. Runs 85-63, 86-1, and 86-2 were made with the wall temperatures in the range 490-500°C. This variable will be studied more quantitatively in the next phase of the project. The question of catalytic effects of the wall or trace minerals present in the bitumen has been raised throughout these studies. At the present time, insufficient data is available to quantify these effects, if they exist at all. Runs made in 4 different reactor units of differing aspect ratios have failed to show measurable differences in results. Also, solid surfaces tend to become quickly attenuated by small amounts of carbon deposits. The current opinion is that catalytic effects, if they exist, are small.

Blast Hydrogen Rate and Temperature

A high blast hydrogen rate is required for improved atomization. A high rate increases the gas-to-oil ratio, which results in higher gas processing costs. Blast composition is thought to be important, as higher density, higher viscosity gases result in greater shear stresses, leading to enhanced atomization. This advantage is partially offset by reduced heat transfer and lower

hydropyrolysis reaction rates. Blast temperature may be limited by the heat transfer characteristics in the nozzle jet. For a given nozzle, this temperature may need to be ascertained experimentally by increasing the blast stream temperature until coking occurs.

Reactor Pressure

This variable has proven to be easily controlled. Most runs to date have been conducted at 1800 psig. In previous reports, it has been suggested that a minimum critical pressure in the range of 1200 psig may exist. Below this pressure, cokeless conditions may not exist. Future runs will study the effect of this variable, once the influence of other variables has been better defined.

Liquid Feed Rate

This variable has been easily controlled. However, the target of 40 reactor volumes/hour established by economic analysis has not yet been achieved under non-coking conditions. The encouraging results of the latest runs indicate that this objective will be achievable, if not at the current reactor scale, then certainly at a larger scale where the reactor surface to volume ratio is reduced.

Gas Feed Rate and Composition

The volumetric and the gravimetric gas feed rate have been amenable to control, the latter by regulating the hydrogen purge rate. Fixing both the volumetric and gravimetric rate does not, however, specify the hydrogen concentration. Throughout the reaction, there is a slow cracking of C_3's and C_2's to C_1, and a steady state with respect to composition has not been achieved. In a commercial reactor, steady state would be easily achieved. Under experimental conditions, and with the funding available, the effect of gas composition will necessarily have to be made by analysis after the run. Precise control appears to be very difficult to achieve, and would require a highly responsive online hydrogen concentration monitor, which is currently not available.

Gas to Oil Ratio

The gas to oil ratio in the hydropyrolysis process not only affects the chemistry, but also the economics. It is important that excess hydrogen is available in the system. The hydrogen molar percent has been set at 90 for the experiments conducted to date.

The influence of the oil feed rate has been investigated in the range of 15 to 60 grams per minute. It has been found that the nozzle coked up at oil feed rates under 20 grams per minute at gas temperatures above 500°C due to insufficient cooling of the nozzle at low oil flow rates.

The most common oil feed rate selected in this study was 30 g/min, with an average recycle gas rate of 12 g/min. The gas to oil mass ratio was 0.4. The gas-to-oil molar ratio is about 70 to 1 for an average oil molecular weight of 410 and 85 weight percent of hydrogen in the recycle stream. This is equivalent to approximately 30,000 SCF of hydrogen per barrel of oil, which is somewhat higher than the 20,000 SCF/bbl currently practiced in hydrocracking technology. Hydropyrolysis may not be as economically limited with respect to gas/oil ratio as is catalytic hydrocracking, due to the shorter residence times with hydropyrolysis.

The influence of the gas-to-oil ratio on yields and product distribution in the short tube reactor operated in the counter-current flow mode may be determined from the following data:

Run No.	Temp(°C)	Gas/Oil	% Coke	% Gas	Lt/Hvy	% Liquid
85-40[a]	548	0.24	1.9	3.1	48.8/46.2	95.0
85-43[b]	546	0.4	2.8	7.6	79.4/10.2	89.6
85-46[b]	546	1.32	5.2	11.2	80.1/3.7	83.3

a. one-hole nozzle b. spray nozzle, low blast rate

An increase in gas-to-oil ratio resulted in an increase in coke and gas yield, and a decrease in heavy liquid and total liquid yields. The distribution of light and heavy liquids in run 85-40 suggest that distillation, and not cracking or hydropyrolysis, was the dominant process occurring.

The most significant effect of increasing the gas-to-oil ratio is on the conversion of heavy liquid. In the countercurrent flow mode, the high gas-to-oil ratio results in high downward velocity of gases, causing the droplets to impinge on the walls of the tube. These droplets were converted to coke and gases at the wall. Thus, the optimum reactor configuration will be a function of the gas/oil ratio.

The coke and gas yields also increased with increasing gas-to-oil ratio in the case of the spray nozzle with total blast. The high gas-to-oil ratio which resulted from low oil feed rates did not improve the results; on the contrary, the light fraction was gasified. This is encouraging in that a low gas-to-oil is a desirable economic objective, provided the reaction goes to completion.

Run No.	Temp(°C)	Gas/Oil	% Coke	% Gas	Lt/Hvy	% Liquid
85-89	529	0.80	1.1	6.8	80.0/12.1	92.1
85-58	530	2.10	2.1	11.6	72.2/14.1	86.3

Residence Time

Economic analysis and experimental results indicate that the hydropyrolysis process will be optimized at low residence times. Residence times as low as 2.5 sec have been recently studied, and residence times of 1 sec were previously studied.[1,2] A small reactor must be used to achieve low residence times without increasing the gas-to-oil ratios. In the final phase of the process variables study, it is expected that kinetic data will be sufficiently well-defined so that extrapolation to shorter residence times will be possible. Furthermore, this data may be used to scale-up the reactor.

Reactor Temperature

The reactor temperature has been the most difficult variable to define and control. The temperature varies considerably throughout the reactor. Three streams (2 gas and 1 liquid) are introduced into the reactor at 2 and perhaps 3 different temperatures. The gas typically enters the reactor above 600°C, while the liquid is introduced at about 400°C. The feed oil must be heated to the vaporization temperature, followed by the addition of the latent heat of vaporization in the atomization step. The hydropyrolysis reaction is exothermic; thus, the global heat of reaction is

released non-uniformly along the axis of the reactor. Heat transfer effects across the walls of the reactor influence the temperature radially. Temperature control must be achieved through adjustment of feed temperatures and flow rates, since heat transfer to and from the reaction zone is not an effective means of controlling temperature. Control of reactor temperature will almost surely be effected through the control of other important variables.

The coke, gas, and liquid yield for different reactor and nozzle configurations with respect to temperature, are summarized in Figures 26 through 28.

The following observations were drawn from the experiments. (1) As reaction temperature increased, the liquid yield decreased; and the coke and gas yield increase, but not necessarily with the same magnitude. (2) For the long tube reactor, operated in the parallel flow mode with the one-hole nozzle (curve C), coke yield was relatively insensitive to temperature but gas formation was quite sensitive. This mode of operation resulted in a shift from hydropyrolysis to distillation. (3) The counter-current flow mode (curves B and D) was found to produce less gas and more liquid product, a desirable characteristic. (4) The yields obtained with the spray nozzle operated in the parallel flow mode (curve A) were the most sensitive to temperature variations. Low coke production was achieved at temperatures below 520°C. It is apparent at high atomization efficiency and moderate temperatures that low coke and high liquid product yields can be achieved. This regime will be the focus of the next phase of study.

CONCLUSIONS

The principal reactions in hydropyrolysis were defined as cracking, dealkylation, hydrogenation, and dehydrogenation. By a model compound study the relative rates of these reactions were determined. The validity of these results was determined from application to results from a petroleum distillate.

An index of the hydrogen free radical concentration was developed and shown to be sensitive to the hydrogen-involving reactions. The generation of free radicals is a rate limiting step and is required for the generation of hydrogen radicals.

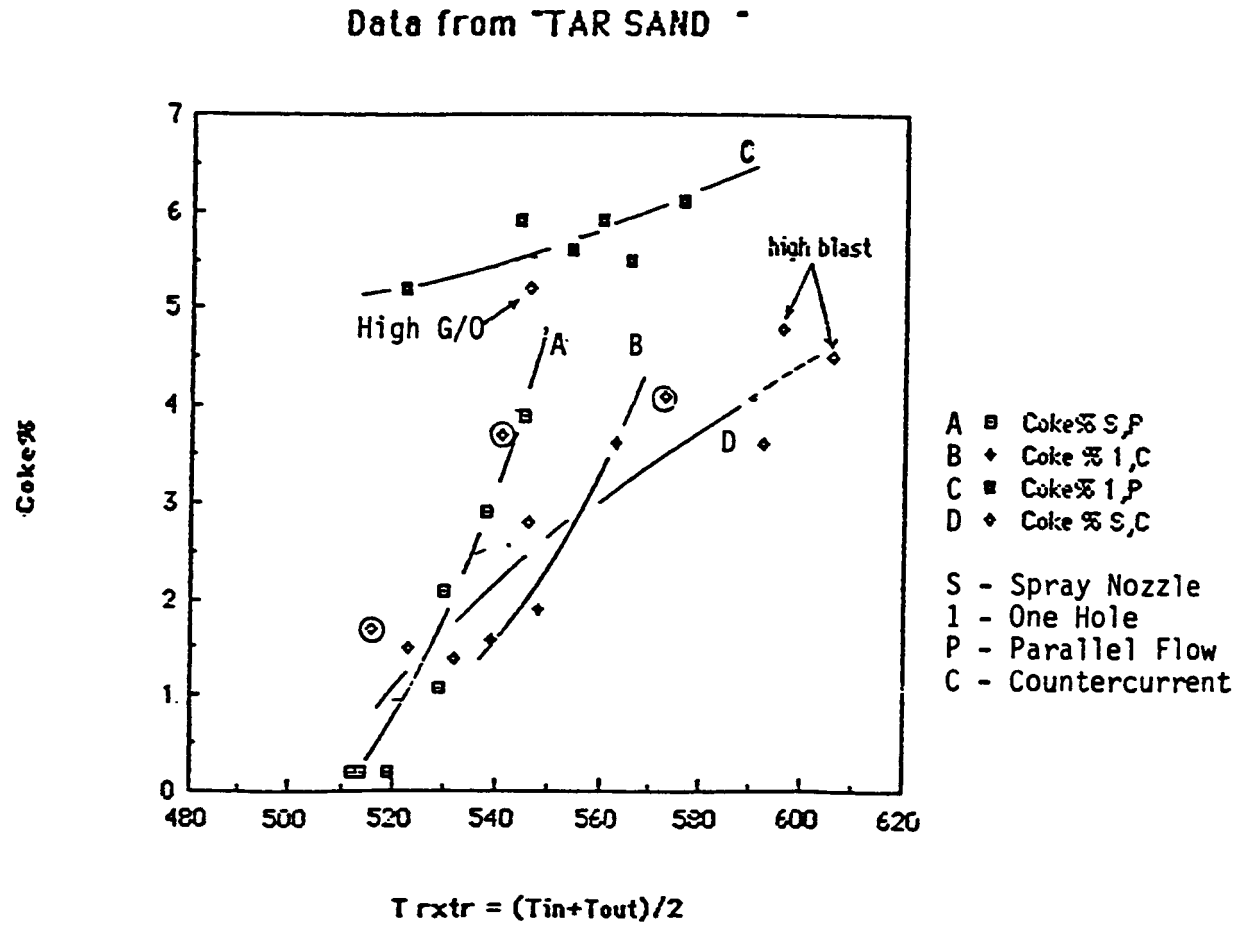

Figure 26. Coke production as a function of reactor temperature for various reactor and nozzle configurations.

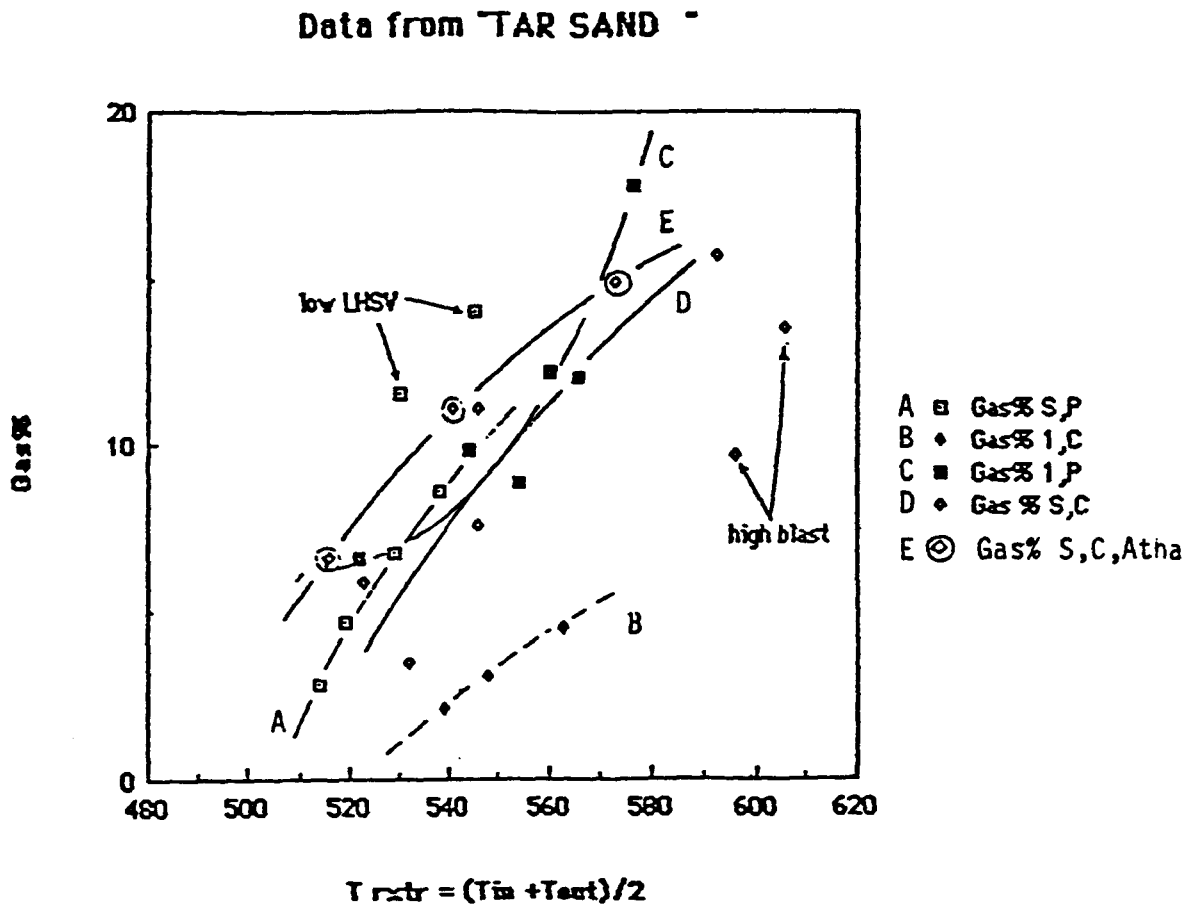

Figure 27. Gas production as a function of reactor temperature for various reactor and nozzle configurations.

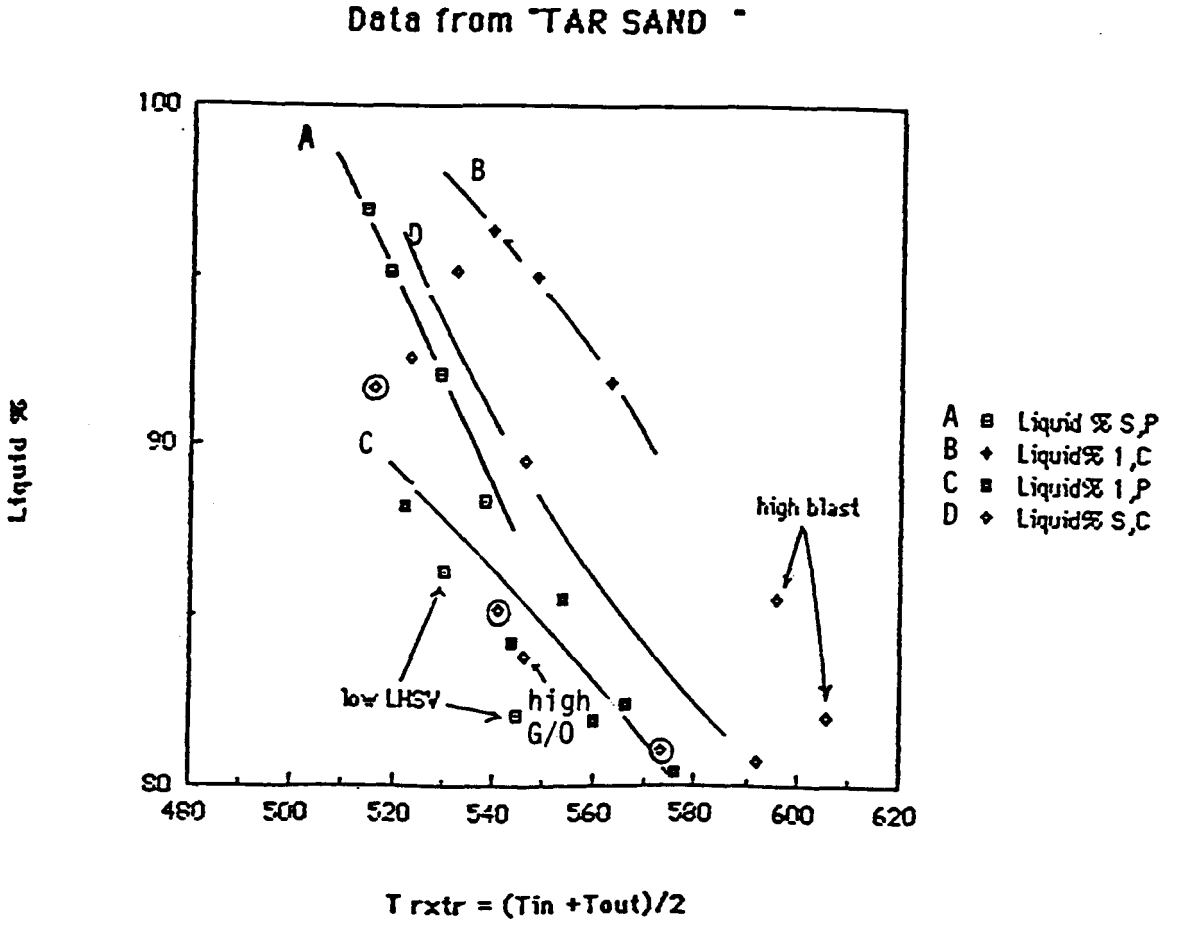

Figure 28. Liquid production as a function of reactor temperature for various reactor and nozzle configurations.

Termination reactions strongly influence hydropyrolysis. Aromatic species are shown to provide a hydrogen "sink" effect and tend to suppress the reaction. Elimination of the wall effect by using large diameter reactor tubes or developing an "inert" inner surface to assure a "clean" reactor are important areas for future development.

A hydrocarbon mixture can be classified by means of carbon types. The reaction pathways of the hydrocarbons in hydropyrolytic reaction can be traced by means of grouping the complex reactions into main reaction types and then examine the change of carbon types as a function of process variables. The magnitude of rate constants related to each reaction are obtained from a study of the kinetics of a model mixture or calculated from the kinetic model mathematically.

The results of this study have greatly extended the knowledge of the possibilities and the limitations of hydropyrolysis processing. Favorable reactions such as dealkylation, hydrogenation, and cracking are competing with dehydrogenation and "over-cracking." Hydropyrolysis clearly enhances the favorable reactions but overcracking to gas with attendant high consumption of hydrogen must be minimized to assure economic attractiveness.

Results from the 2 l/hr PDU have shown that high carbon residue feeds (>10%) can be converted in high yields (>90%) to liquid products with low coke production (<2%). Optimized results are expected to be even better with the distinct possibility in a "wall-less" reactor that no coke is produced. The next research phase will emphasize the engineering design and optimization.

SECTION B

FLUIDIZED BED PYROLYSIS OF BITUMEN-IMPREGNATED SANDSTONE

F.V. Hanson

TRIBUTE TO DR. JAY C. DORIUS
1954 - 1987

F.V. Hanson Research Advisor

The Department of Fuels Engineering at the University of Utah was deeply saddened on May 28, 1987, by the untimely death of Dr. Jay C. Dorius, one of the Department's finest graduates.

I was privileged to have known Jay Dorius as a graduate student, professional colleague, and a friend over the past ten years. Jay joined the tar sand research group in the Department of Fuels Engineering at the University of Utah in the spring of 1978. He immediately impressed faculty, staff, and fellow students with his motivation and desire to excel. These characteristics were recognized by the number of awards and honors Jay received during his years at the University of Utah.

Transcending his achievements as a student, scientist, and engineer were his courage and compassion. If courage is defined as the daily commitment by a man or woman to carry on with his or her life in the face of adversity, then J.C. Dorius must be considered one of the most courageous of men. In spite of his numerous physical difficulties, including a diabetes-related heart attack and a kidney transplant, he persevered and achieved his goal, the Doctor of Philosophy degree, with dignity and honor.

Jay's compassion for others was revealed in his work with diabetic children and in his daily interactions with other students at the University. He was always willing to help his peers in and out of the Department with their research without concern for reciprocity. He was, among his peers, a leader by example.

This section of this final report is fondly dedicated to the memory of Jay C. Dorius, Doctor of Philosophy in Fuels Engineering.

FLUIDIZED BED PYROLYSIS OF BITUMEN-IMPREGNATED SANDSTONE

F. V. Hanson	Associate Professor
J.C. Dorius	Graduate Student
L. C. Lin	Graduate Student
D. W. Shun	Graduate Student
S. H. Sung	Graduate Student
J. W. Wiser	Research Assistant

INTRODUCTION

The fluidized bed pyrolysis of the bitumen-impregnated sandstones of Utah has been investigated in a small diameter (1.5 inch) fluidized bed reactor. The deposits investigated included Sunnyside,[31] Tar Sand Triangle,[31,32] Whiterocks,[32,33] PR Spring,[33] and Circle Cliffs.[34] The small diameter reactor studies were intended to demonstrate the feasibility of the fluidized bed pyrolysis process as a method for the production of bitumen-derived hydrocarbon liquids and to determine the influence of process operating variables on the product distribution and quality.

The process operating variables investigated included pyrolysis reactor temperature, feed sand retention time in the pyrolysis zone of the reactor, and fluidizing gas velocity/residence time. The conclusions to date may be summarized as follows:

- The C_5^+ hydrocarbon liquid yield decreased with increasing pyrolysis zone temperature at constant feed sand retention time and fluidizing gas flow rate.
- The C_5^+ hydrocarbon liquid yield increased with decreasing feed sand retention time at constant pyrolysis zone temperature and fluidizing gas flow rate.
- The product distribution was insensitive to the fluidizing gas flow rate in the range of values investigated: up to 3 times the minimum fluidization gas flow rate (corresponding to 3 times the minimum fluidization velocity).
- The coke yield was independent of the process operating variables above a pyrolysis zone temperature of 723K.
- The quality of the produced hydrocarbon liquids was superior to that of the native bitumen.

- The product distribution and yields can be quantitatively correlated by the Conradson carbon residue, the atomic hydrogen-to-carbon ratio, and the asphaltene content of the native bitumen.

FLUIDIZED BED PYROLYSIS OF BITUMEN-IMPREGNATED SANDSTONE FROM THE PR SPRING TAR SAND DEPOSIT

F.V. Hanson — Associate Professor
J.C. Dorius — Graduate Student

SYNOPSIS

The fluidized bed pyrolysis of bitumen-impregnated sandstones to produce hydrocarbon liquids has been investigated using the material from the PR Spring deposit as feed-sand to the pyrolysis reactor. The PR Spring deposit is the second largest tar sand deposit in Utah, and is estimated to contain 4.0 - 4.5 billion barrels of bitumen in-place. Three distinct samples, PR Spring Rainbow I, PR Spring Rainbow II, and PR Spring South, were used in this investigation because it was found that the physical and chemical properties of the three bitumens were quite different. The process variables investigated included the pyrolysis reactor temperature and the feed sand retention time in the pyrolysis zone. Data were obtained in a continuously fed, fluidized bed reactor operating in a temperature range of 773 - 923 K, and at solids retention times that ranged from 17 to 30 minutes. The feed-sand throughput was 2.25 kilograms per hour. The particle size of the feed-sand was 300-600 microns.

The hydrocarbon liquid product yield (C_5^+ yield) generally decreased with increasing reactor temperature. Concomitant with this decline in the liquid yield, there was an increase in the light gas (C_1-C_4) yield. The liquid product yield increased slightly with decreasing feed sand retention time while the light gas yield decreased. The coke yield was insensitive to process operating variables above 798 K; however, it did appear to be a function of the origin of the feed-sand. At a fixed pyrolysis reactor temperature and sand retention time, the C_5^+ liquid product yield correlated quite well with the Conradson carbon residue and with the atomic hydrogen-to-carbon ratio of the native bitumen. That is, the liquid product yield increased with decreasing Conradson carbon residue and with increasing hydrogen-to-carbon ratio.

The quality of the bitumen-derived liquids was significantly better than that of native bitumen; that is, the viscosity was reduced by four to five orders of magnitude for the Rainbow I bitumen, and the volatility of the liquid product increased relative to the native bitumen. Similar increases were

observed for the produced liquids from the PR Spring South and Rainbow II tar sands. The Conradson carbon residue, asphaltene content, molecular weight, and heteroatom and metals content of the product liquids relative to the native bitumens were substantially reduced in the pyrolysis process.

EXPERIMENTAL APPARATUS AND PROCEDURES

Fluidized-Bed Reactor System

The reactor system utilized in this investigation was designed and constructed by Venkatesan.[31] The reactor was 3.8 centimeters in diameter, 90 centimeters in length, and was designed for a maximum throughput capacity of 2.25 kg per hour. A schematic of the reactor system is presented in Figure 29. The system consisted of the reactor assembly, a tar sand feeding system, a spent sand removal system, and a liquid product collection system.

In all experiments, nitrogen was used as the fluidizing and purge gas. The fluidizing gas, stored in cylinders (A) (refer to Figure 29), was metered through a rotameter (B_1), passed into the bottom of the reactor (D) through the gas preheater (C). The gas preheater was packed with ceramic spheres to effect uniformity of gas flow and to enhance heat transfer to the fluidizing gas. The purge gas stream was metered into the feed-sand hopper (F), through a rotameter (B_2) and eventually flowed into the top of the expansion chamber (E). The purpose of the purge gas was to prevent the flow of product vapors into the sand feeder (G). The fluidizing and purge gas also swept the product vapors from the reaction zone and into the product collection system.

Feed tar sand, stored in the feed-sand hopper (F), was fed at a constant rate into the top of the reactor by the calibrated screw feeder (G). The feed tar sand rained through the expansion chamber (E) into the reactor (D). The depth of the fluidized bed was monitored by a differential pressure cell (U) and was maintained at a predetermined level by withdrawing spent, coked sand at a constant rate through a solids flow valve (S), which was controlled by the differential pressure cell. The spent, coked sand was collected in the solids receiver (I) for subsequent analysis.

Product vapors, along with the fluidizing and purge gases, exited from the top of the expansion chamber. Entrained sand fines were removed from the vapor stream by the cyclones (J_1,J_2) and the

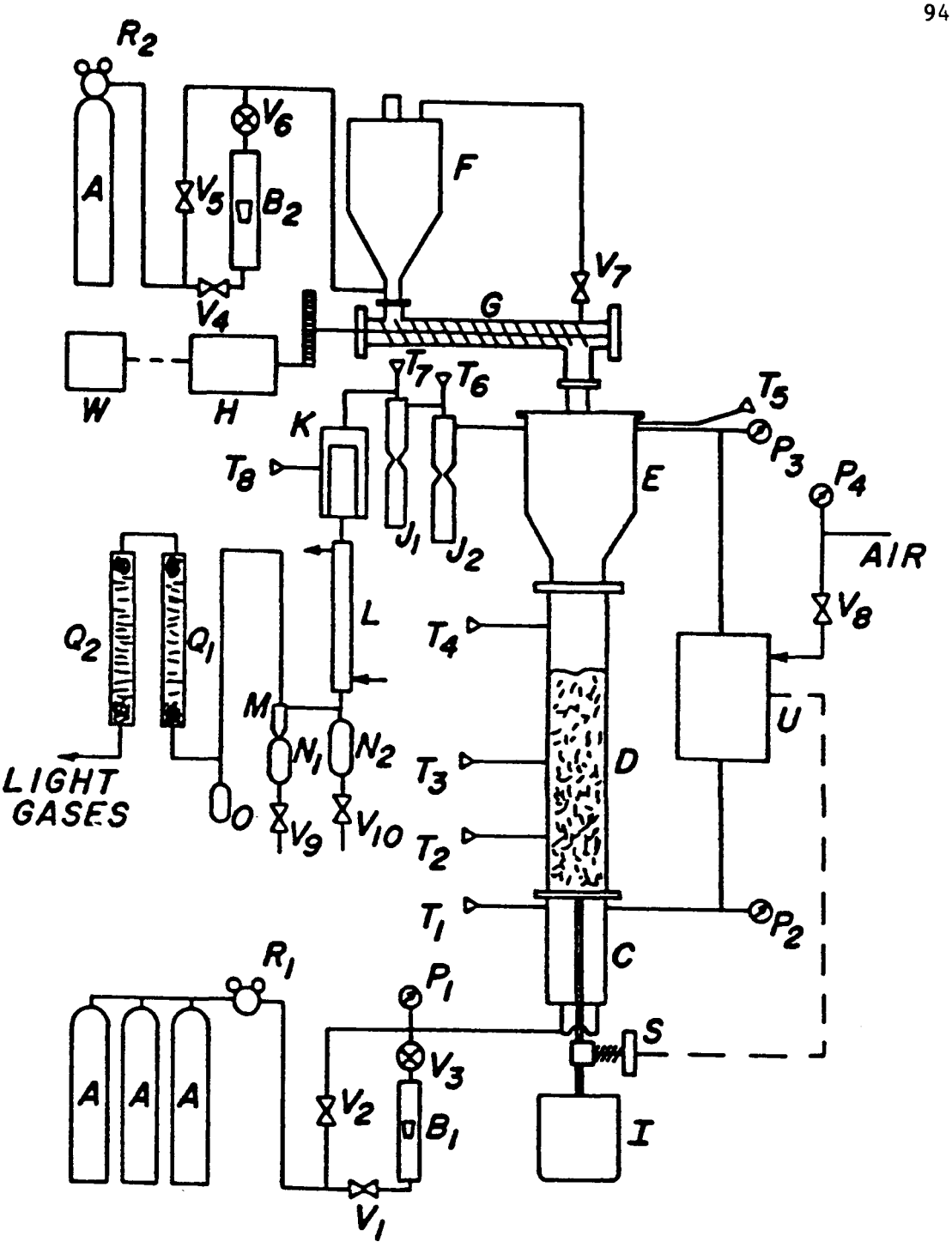

Figure 29. - See legend that follows.

Figure 29. **Schematic diagram of the bench-scale fluidized-bed pyrolysis reactor.**

A	Nitrogen Cylinder
B_1-B_2	Rotameter
C	Fluidizing Gas Preheater
D	Fluidized Bed Reactor
E	Expansion Chamber
F	Feed-Sand Hopper
G	Sand Feeder
H	Motor Drive
I	Spent Sand Receiving Vessel
J_1-J_2	Cyclones
K	Filter Housing
L	Water Condenser
M	Hydroclone
N_1-N_2	Liquid Product Receivers
O	Glass Jar
P_1-P_4	Pressure Gauges
Q_1-Q_2	Cellulose Fiber Mist Capture Tubes
R_1-R_2	Gas Regulators
S	Solids Valve
T_1-T_8	Thermocouples
U	Differential Pressure Cell
V_1-V_8	Valves
W	Motor Drive Controller

sintered stainless steel filter (K). Approximately one-third of the liquid product was condensed and collected in the liquid receivers (N_1,N_2). The major portion of the condensable vapor remained in the gas stream as an aerosol mist, which was removed by the cellulose fiber mist eliminators (Q_1,Q_2). Light product gases were vented from the system through a fume hood. During the course of each experiment, five gas samples were collected for gas chromatographic analysis. The reactor (D), gas preheater (C), expansion chamber (E), and filter (K) were heated by Kanthal resistance wires which were coiled around each vessel. The cyclones (J_1,J_2) were heated by Briskeat high temperature heating tapes. The temperature of the reactor, gas preheater, and expansion chamber were kept constant by electronic temperature controllers. The temperatures of the cyclones and filter were monitored by a temperature gauge and were controlled by manual adjustment of variable transformers. Reference should be made to Venkatesan[31] for details of the design and construction of the reactor.

Experimental Procedures

The sand feeder (G) and expansion chamber (E) were disassembled and cleaned prior to each experiment because of the buildup of solid particles on the walls of these reactor components during the previous experiment. The cyclones (J_1,J_2) and filter (K) were heated to 773 K in the presence of air to burn off any accumulated coke. The remaining sand was blown out using an air jet.

After cleaning, the reactor was reassembled and thoroughly tested for each experiment in the following sequence:

1) The solids valve (S) was cleaned by blowing of an air jet into the standpipe. The valve was also tested to assure smooth operation. The valve was then closed, and the spent sand receiving vessel (I) was placed in position.

2) Approximately 700 grams of spent, coked sand obtained from previous experiments was placed in the reactor.

3) The expansion chamber was put in place on top of the reactor. The four bolts holding the flange were tightened to 40 foot-pounds of torque to secure the expansion chamber in place.

4) The sand feeder (G) was secured in place on top of the expansion chamber by tightening the four bolts holding the flange to 30 foot-pounds of torque. In steps 3 and 4, the flange gaskets were evenly coated with high-temperature and anti-seize compound to seal the flanges.

5) The feed-sand hopper (F) was put in place on the feeder and the purge gas lines were reattached. The thermocouple (T_5) and the upper pressure line (P_3) to the differential pressure cell (U) were also reattached.

6) The heating coils around the expansion chamber were checked to make certain that they were evenly spaced. The reactor effluent tube was connected to the expansion chamber and the flange bolts were tightened to 40 foot-pounds of torque to secure the expansion chamber in place. The insulation was placed around the upper sections of the reactor assembly. All electrical connections were secured.

7) The liquid product collection system was reassembled as shown in Figure 29. The cellulose fiber mist eliminators (Q_1,Q_2) were packed and reassembled. The pyrolysis reactor was then ready for the experiment.

The following procedures were implemented to start up the reactor for each experiment.

1) The valves of the gas cylinders (A) were opened, and the delivery pressure of the regulator (R_1) was adjusted to 36 psig. The flow rate of the fluidizing gas was set at 144 liters per hour (STP) using valve (V_3) and Rotameter (B_1).

2) The set point temperatures on the controllers of the gas preheater (C) and reactor (D) were set at the required values for the experiment. The temperatures of the expansion chamber, cyclone, and filter were set at 673 K when PR Spring Rainbow I tar sand was fed. Those temperatures were set at 723 K when the other tar sands were fed. The electric power to the heating circuits was switched on and the power to the heating wires was slowly increased to the proper level. The cooling water to the condenser (L) was turned on.

3) The reactor system was allowed to equilibrate at the pre-set temperature. Usually one to two hours was required for the temperature equilibration to be established.

4) The actual pressure difference corresponding to the height of the fluidized bed was noted, and the set point of the differential pressure controller (U) was adjusted to that level. The delivery pressure of regulator (R2) was increased to 20 psig, and the flow of purge gas was adjusted to 54 liters per hour (STP) using valve (V6) and rotameter (B2).

5) Approximately 1 kilogram of spent coked sand obtained from previous experiments was charged to the feed-sand hopper (F). The sand feed rate was set at the proper level by adjusting the speed of the motor drive (H) with the controller (W). The spent, coked sand was fed to the reactor to initiate the smooth operation of the solids valve. Occasionally, it was necessary to tap the solids valve body to start the flow of solids through the valve.

6) The feed tar sand was prepared by mixing it at the proper weight ratio with spent coked sand. Small samples of the tar sand and spent coked sand were weighed, burned in a muffle furnace at 773 K for 16 to 17 hours, and then reweighed. The bitumen or coke content was determined from the weight loss of the samples.

Because the PR Spring Rainbow I tar sand agglomerated and did not flow readily, the feed mixture consisted of two parts by weight spent coked sand to one part by weight tar sand. This mixture was soaked in liquid nitrogen to improve the flow properties. In cases where the tar sand flowed readily, the ratio of the feed mixture was one part spent coked sand to one part tar sand. In those cases it was not necessary to soak the feed in liquid nitrogen. The total amount of the feed sand mixture prepared was 3 kilograms in all experiments.

7) When nearly all of the spent sand charged in step 5 had been fed to the reactor, the feed sand mixture was charged to the feed sand hopper. The feed sand was added to the hopper before the spent sand was completely fed so that the solids valve would continue to function smoothly during startup. The time was recorded, along with all temperatures, pressures, and the power levels of all heating coil transformers.

Approximately 10 minutes after the feed sand was charged, the product oil mist was observed entering the first cellulose fiber mist eliminator (Q_1). This mist was visible in the entrance to the mist

eliminator throughout the experiment. The disappearance of the mist signalled the completion of the experiment.

The first product gas sample was collected 30 minutes after the charging of the feed sand to the system. Subsequent product gas samples were collected at 20 minute intervals until the experiment was completed. Then the power to the heating coils was switched off, the solids valve was closed, the flow of purge gas was turned off, and the flow of the fluidizing gas was reduced to 25 liters per hour (STP). The reactor system was allowed to cool to room temperature overnight.

The PR Spring South tar sand presented feeding problems that had not been encountered previously, either in this study or in prior investigations.[31,32] The experiments were run at longer solids retention times because of the poor quality of fluidization at shorter solids retention times. In addition, the feed sand bridged across the top of the reactor during some experiments. Product vapors permeated this sand bridge at a slow rate, but the remaining feed sand was held up in the expansion chamber. These problems were related to the extremely asphaltic nature of the PR Spring South bitumen, as will be discussed in the following chapter. The following day, the reactor system was disassembled and cleaned according to the following sequence:

1) The fluidizing gas and condenser (L) water were turned off.

2) The liquid product captured in the receivers (N_1,N_2) was collected and weighed.

3) The liquid-product collection system was disassembled, and the components were washed thoroughly with toluene to recover the product oil. The cellulose fibers were removed from the mist eliminators and soaked in toluene for several hours.

4) The cyclones (J_1,J_2) and filter (K) were cleaned of coked sand fines. The fines were collected so that the coke and heavy oil content could be determined for the material balance.

5) The feed sand hopper (F), the sand feeder (G), and the expansion chamber (E) were removed from the system and disassembled to recover feed tar sand that was held up in these components during the experiment. The recovered sand was analyzed for bitumen, coke, and product liquid content.

6) The spent sand receiver (l) was removed from the system, and the spent coked sand remaining in the reactor bed was drained and collected. The spent sand in the receiver and that from the reactor bed were set aside for analysis.

7) The pressure lines, the standpipe, and the solids valve were cleaned with a high-pressure air jet to remove any remaining solids. This was done to prevent plugging during the subsequent experiment.

Material Balance

It was necessary to recover the product liquids from the cellulose fiber mist eliminators and walls of the product collection system in order to obtain a material balance for the experiment. The cellulose fibers from the mist eliminators, which had been soaked in toluene, were washed thoroughly with toluene to remove any remaining oil. The liquids washed from the fibers, as well as those washed from the product collection system, were separated from the toluene by stripping the solvent in a Buchi Rotovapor Model RE120 distillation apparatus. In all cases the toluene was stripped to less than 0.25 percent by weight of the liquid. The recovered product oil was weighed and added to the oil obtained from the liquid product receivers for future physical and chemical analysis.

Samples of the coked, spent sand from the spent sand receiver and reactor bed were analyzed for coke content. This was done by burning small weighed samples in a muffle furnace for 16 to 17 hours at 773 K. A temperature of 773 K was used because TGA studies indicated that carbonate decomposition did not occur at temperatures below 923 K. Therefore, at 773 K the total weight loss was attributed to the combustion of carbonaceous residue. The samples were weighed and the weight loss was equated to the coke content. The coked sand from the reactor bed was analyzed separately from the sand in the spent sand receiver, because it was discovered that the coke content of the reactor sand was significantly higher than that of the sand in the spent sand receiver. The spent sand remaining in the reactor (600-700 grams) represented approximately 25 percent of the total sand fed during the experiment. Therefore, it was important to consider the coke content of that sand in the material balance determination.

The content of organic material on the tar sand collected from the feed system (step 5) and the coked fines collected from the cyclones and filter (step 4) was determined in the same manner as the coke content of the spent sand, with the exception that the entire sand samples were analyzed rather than small samples.

The product gases that were collected during the experiment were analyzed by gas chromatography to determine the chemical composition for the material balance. The gas analysis was performed on a Hewlett-Packard model 5830A gas chromatograph with dual thermal conductivity detectors. The dual columns (0.30 cm diameter x 6.0 meters long) were packed with Chromasorb-102 column packing. Thermal response factors for the detectors were obtained from the literature.[106]

A material balance of 90 to 105 percent of bitumen fed was considered acceptable. In cases where the material balance was less than 100 percent, the data were normalized by adding the deficit to the liquid yield. The normalization accounted for liquid products lost with the cellulose fibers, liquids lost during toluene stripping, and liquids condensing in the sand feed or expansion chamber that could not be recovered. In instances where the material balance was greater than 100 percent, the results were normalized by subtracting the excess from the overall gas yield. This was done because the excess was attributed to the gas yield, which was calculated as an average yield from the gas chromatography data.

MATERIAL BALANCE CALCULATIONS

Material balance calculations for a typical pyrolysis experiment are presented in this section. The methods of determining the coke and liquid yields have been discussed in previous sections of this report. The product gas composition was determined by gas chromatography. The gas analysis included the volume fraction of fluidizing and purge gases (nitrogen) present in the product gases. The volumetric rates of production of hydrocarbon gases at STP were calculated using the known volumetric rates of fluidizing and purge gases at STP. The product gas yields are reported on a nitrogen- and hydrogen-free basis. The hydrogen composition of the product gases could not be determined accurately using the thermal conductivity detectors. The hydrogen concentration was assumed to be negligible at any rate.

Typical Material Balance Calculations

Experiment No. 20

Reactor Temperature - 823 K

Solids Retention Time - 20 minutes

Fluidizing Gas Velocity - 144 LPH (STP)

Feed Sand Composition: 1 kg PR Spring Rainbow I Tar Sand

+ 2 KG spent coked sand

Sand Feed Rate: 2.1 kg/hr.

Bitumen Content of Tar Sand: 12.71 wt.%

Coke Content of Spent Sand Diluent: 0.95 wt.%

Spent Sand Remaining in Reactor after Run: 713.18 g.

Coke Content of Sand in Reactor after Run: 1.84 wt.%

Coke Content of Sand in Bucket after Run: 0.77 wt.%

Total Liquid Products Recovered: 67.68 g.

Analysis of Sand Cleaned from Feeder Expansion Chamber

Weight of sand before burning: 184.94 g

Weight of sand after burning: 170.44 g

Weight of organic matter on sand: 14.50 g

1. Bitumen not fed to reactor:

$$170.44 \quad \left(\frac{12.71}{87.29}\right) \; 0.333 = 8.27 \text{ g}$$

2. Coke not fed to reactor:

$$170.44 \; \left(\frac{0.95}{99.05}\right) \; 0.667 = 1.09 \text{ g}$$

3. Product oil contained on sand:

$$14.50 - 8.27 - 1.09 = 5.14 \text{ g.}$$

Analysis of Fines in Cyclones and Filter

Weight of fines before burning: 42.82 g

Weight of fines after burning: 37.85 g

Weight of organic matter on fines: 4.97 g

1. Coke left in cyclones/filters:

$$37.85 \quad (\frac{1.84}{98.16}) = 0.71 \text{ g}$$

2. Product oil contained in fines:

$$4.97 - 0.71 = 4.26 \text{ g}$$

Calculation of Sand, Bitumen, and Coke Fed to Reactor

1. Total sand fed to reactor:

$$1000.00 \text{ X } 0.8729 + 2000.00 \text{ X } 0.9905 - 170.44 - 37.85 = 2645.61 \text{ g}$$

2. Total bitumen fed to reactor:

$$1000.00 \text{ X } (0.1271) - 8.27 = 118.83 \text{ g}$$

Bitumen feed rate:

$$2100 \text{ g/h X } (0.1271) \text{ X } 0.333 = 88.88 \text{ g/h}$$

3. Total coke fed to reactor:

$$2000.00 \text{ X } (0.0095) - 1.09 = 17.91 \text{ g}$$

Product Gas Composition	Mole %
CO	1.77
CO_2	6.43
H_2O	37.57
CH_4	17.86
C_2H_4	8.79
C_2H_6	4.88
C_3H_6	9.92
C_3H_8	2.50
n-C_4H_8	3.30
i-C_4H_8	0.32
n-C_4H_{10}	1.43
i-C_4H_{10}	0.07
C_5	4.93
C_6	0.03
TOTAL:	100.00

Mole % N_2 in product gases: 92.53

Volumetric rate of product gas:

$$\frac{198 \text{ LPH (STP)}}{0.9253} - 198 = 15.98 \text{ LPH (STP)}$$

Gas Yield, reported as wt.% bitumen:

$$(\text{mole \%}) \left[\frac{V_p}{V_{stp}}\right] (MW) \left[\frac{1}{F}\right] = \text{component wt.\% of bitumen fed}$$

where:

V_p = volumetric flow rate of product gas (15.98 LPH @ STP)

MW = Molecular weight of component

F = Bitumen feed rate (g/h)

V_{stp} = 22.414 ℓ/mol

e.g., for CH_4:

$$\text{Wt.\% Bitumen} = (17.86) \left\{\frac{15.98}{22.414}\right\} (16) \left\{\frac{1}{88.88}\right\} = 2.29 \text{ wt.\%}$$

Gas Yields	Wt.% of Bitumen Feed
CO	0.40
CO_2	2.27
H_2O	5.42
CH_4	2.29
C_2H_4	1.97
C_2H_6	1.17
C_3H_6	3.34
C_3H_8	0.88
n-C_4H_8	1.48
i-C_4H_8	0.14
n-C_4H_{10}	0.67
i-C_4H_{10}	0.03
C_5's	2.85
C_6's	0.00
TOTAL GAS YIELD	22.91

C_5's and C_6's were removed from gas yield and added to liquid yield.

Corrected gas yield:

22.91 - 2.85 - 0 = 20.06 wt.% Gas

Total Liquid Yield:

$$\left\{\frac{67.88 + 5.14 + 4.26}{118.83}\right\} 100 + 2.85 = 67.72 \text{ wt.\%}$$

Coke Yield:

$$713.18 \left\{\frac{1.84}{98.16}\right\} = \{2645.61 - 713.18\ (0.9816)\} \times \left\{\frac{0.77}{99.23}\right\}$$

(From Reactor) (From Spent Sand Receiver)

$$+ 0.71 - 17.91 = 11.27 \text{ g}$$

(From Cyclones/Filters) (coke fed in):

$$\frac{11.27 \text{ gm}}{118.79 \text{ gm}} \times 100 = 9.48 \text{ wt.\%}$$

Material Balance:

20.06 + 67.72 + 9.48 = 97.25 wt.% recovered

Losses: 100 - 97.26 = 2.74 wt.%

The product yields were normalized to 100% by adding the losses to the liquid yield.

Normalized product yields:

Gases	20.06 wt.%
Liquid	70.46 wt.%
Coke	9.48 wt.%

Liquid Product Analysis

Detailed chemical and physical analysis of the extracted native bitumens from the feed tar sands and the pyrolysis product liquids were performed. The methods of analysis are discussed here.

The pour points of the native bitumens and most of the products were determined according to ASTM method number D97-66. In cases where there was not a sufficient amount of liquid as specified by the ASTM method, a modified method of determination was used. Conradson carbon residue and ash content of the native bitumens and liquid products were determined using ASTM D189-65 and D482-63 methods, respectively. The simulated distillation data were obtained using a

procedure similar to the ASTM D2887-70T method. The analysis was performed on a Hewlett-Packard 5730A gas chromatograph with dual flame ionization detectors and dual 3 percent Dexsil on Anachrom q columns (0.64 cm diameter X 46 cm length).

Densities of the liquid products were measured on a Mettler/Paar Model DMA 40 digital density meter. The densities of the native bitumens were measured using a glass pycnometer. The viscosities of the native bitumens were measured on a Brookfield Model RVT viscometer with a No. 27 spindle and a Brookfield Thermosel. The product liquid viscosities were measured on Brookfield Model LVT and 5XHBT viscometers with 0.8° and 1.565° cones, respectively. Elemental analysis, molecular weight determination, and trace metals analysis were performed by Galbraith Laboratories, Knoxville, Tennessee.

Gradient elution chromatography (GEC) was performed on the native bitumens and on selected product liquid samples to determine the distribution of chemical compound types in the bitumens and in the hydrocarbon liquid products. The GEC procedure was developed by Middleton[35] and was later modified by Callen et al.[36] The GEC method was further modified by Utley[111] to fractionate tar sand bitumens and pyrolysis product liquids.

The GEC apparatus is shown schematically in Figure 30. The main column (E) was packed uniformly with activated alumina. The Alcoa F-20 alumina was activated to <5% moisture by heating it at 773 K for 16 hours in a muffle furnace. About 10 grams of oil sample were dissolved in dichloromethane ($MeCl_2$). The solution was adsorbed on 60 to 65 grams of activated alumina. After the solvent was evaporated, the oil-on-alumina was packed in the sample column (D). The apparatus was then assembled as shown in Figure 30.

Nitrogen pressure of 2-5 psig was maintained throughout the run. A series of solvents with increasing eluting power was added sequentially to the solvent reservoir. The solvent sequence used in this analysis is shown in Table 17. The mixing chamber (C) provided a gradual and continual increase in the eluting power of the solvent entering the column. The balance between the adsorption sites on the alumina and the eluting power of the solvents accomplished the separation of fractions.

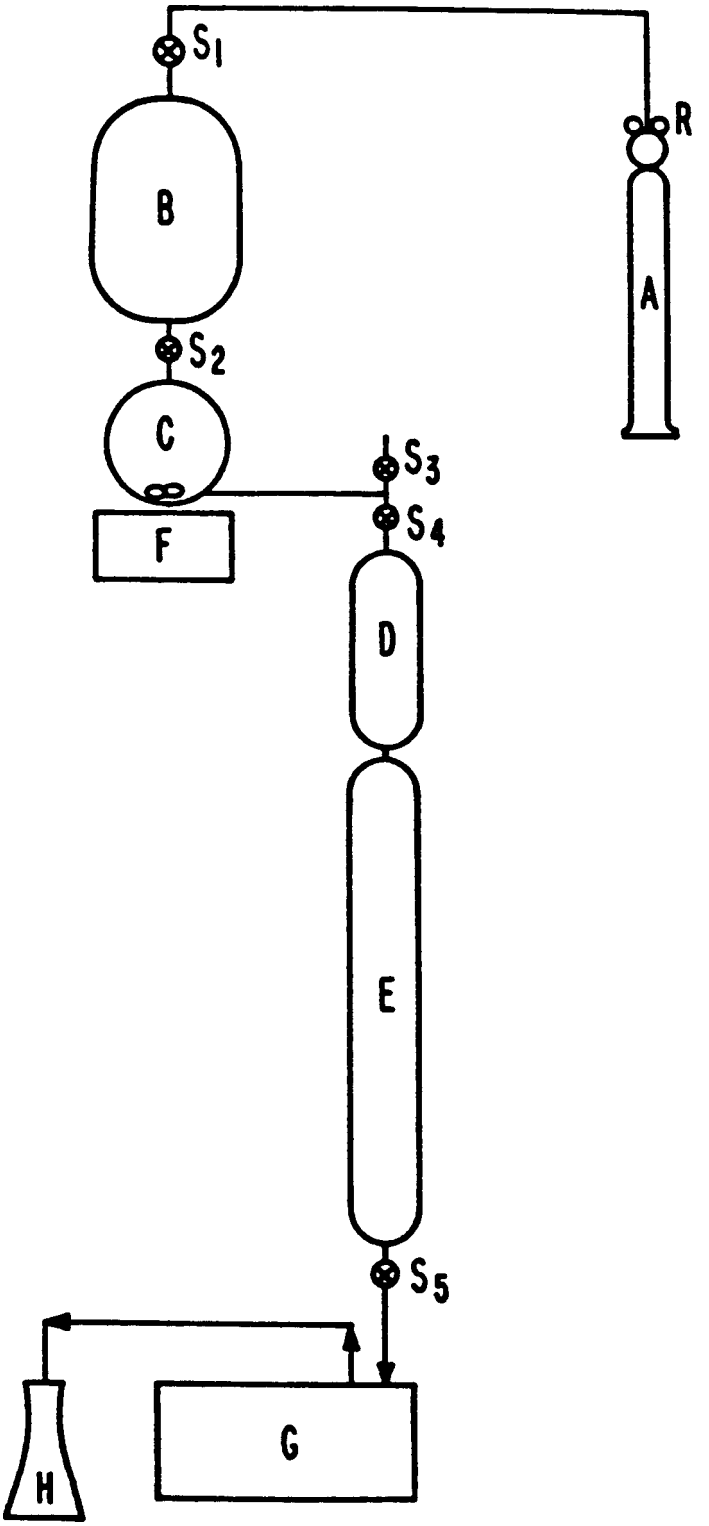

Figure 30. - See legend that follows.

Figure 30. **Schematic flow diagram of the gradient elution chromatography apparatus.**

A	Nitrogen Cylinder
B	Solvent Reservoir
C	Mixing Chamber
D	Sample Column
E	Main Column
F	Magnetic Stirring Motor
G	Ultraviolet Spectrophotometer
H	Fraction Collecting Flask
R	Nitrogen
S_1-S_5	Stopcocks

Table 17

Solvent Order for GEC
THF = Tetrahydrofuran
$MeCl_2$ = Dichloromethane
MeOH = Methanol
H_2O = Distilled Water

		Composition
1.	360 cc	n-pentane
2.	7.5 cc	$MeCl_2$ + 242.5 n-hexane
3.	15 cc	$MeCl_2$ + 235 cc n-hexane
4.	22.5 cc	$MeCl_2$ + 5 cc THF + 222.55 cc n-hexane
5.	30 cc	$MeCl_2$ + 10 cc THF + 210 cc n-hexane
6.	375 cc	$MeCl_2$ + 15 cc THF + 197.5 cc n-hexane
7.	45 cc	$MeCl_2$ + 20 cc THF + 185 cc n-hexane
8.	52.5 cc	$MeCl_2$ + 25 cc THF + 172.5 cc n-hexane
9.	62.5 cc	$MeCl_2$ + 30 cc THF + 157.5 cc n-hexane
10.	250 cc	THF
11.	37.5 cc	MeOH + 212.5 cc THF
12.	37.5 cc	MeOH + 10 cc H_2 - 202.5 cc THF

The saturates, which were weakly adsorbed on the alumina, were eluted first. The asphaltenes, which were bonded strongly to the alumina, were eluted last.

The solvent flowing from the column passed through a Varian Techtron Model 634S variable wavelength UV-VIS spectrophotometer. A typical GEC spectrogram is shown in Figure 31.

In order to obtain material balance, the solvent was evaporated from each fraction by rotovap distillation. Physical descriptions of the eluted fractions are presented in Table 18. The losses in material were attributed to noneluted asphaltenes (fraction 8). The GEC procedure provided a method of quantifying the upgrading of the pyrolysis product liquids by giving an overview of the shift from more refractive compounds in the native bitumen to more desirable compounds in the product liquids.

RESULTS AND DISCUSSION

It has been determined that the primary process variables affecting the product distribution in pyrolysis are reactor temperature and solids retention time.[32,31] Moreover, it is known that the source of the feed tar sand affects the product distribution; however, the specific relationship between physical or chemical properties of the native bitumen and the resulting product yields has not been explored previously. The effect of temperature and solids retention time in the reactor on pyrolysis product yields was investigated. In addition, the effect of bitumen properties such as Conradson carbon residue, asphaltene content, and hydrogen-to-carbon ratio on product yields was explored. Finally, detailed characterization of the native bitumens and product liquids was carried out to determine the extent of upgrading of bitumen-derived liquids during pyrolysis and to evaluate the quality of the bitumen-derived liquids as refinery feedstocks.

Nature of the Feed Bitumens

The feed tar sands used in this investigation were obtained from the PR Spring deposit in eastern Utah. The PR Spring deposit lies in the Uinta Basin near the Utah-Colorado border. The areal extent of the deposit is approximately 350 square miles,[37] and the deposit is estimated to contain four billion barrels of oil in place.[38] The PR Spring deposit outcrops high on the Roan Cliffs, which form the southeastern edge of the Uinta Basin, and dips approximately two degrees north-northwest. The

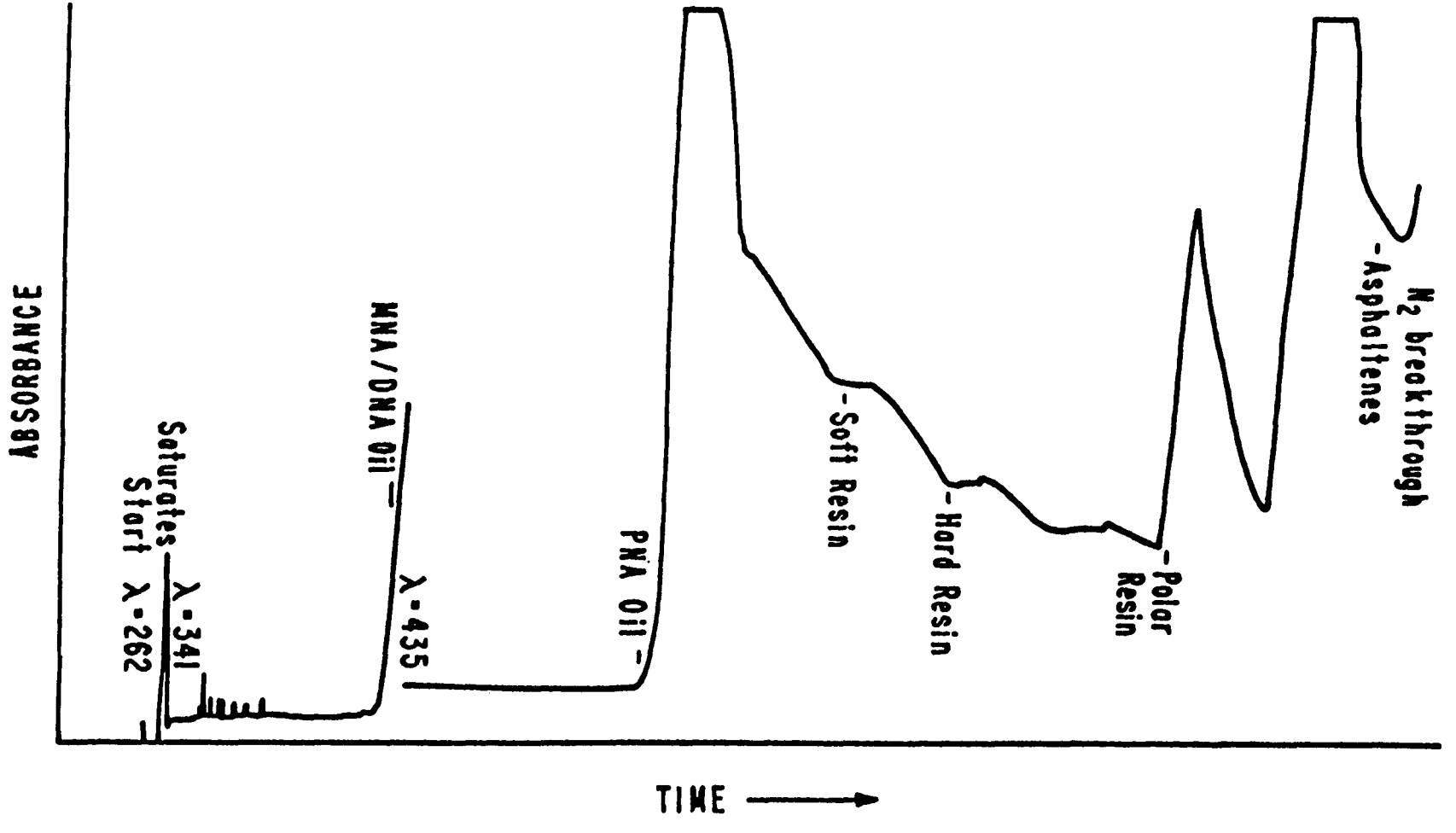

Figure 31. Typical GEC chromatogram.

Table 18

Physical Descriptions of GEC Fractions

Fraction	Description
Saturates	colorless oil
MNA/DNA oil	colorless or pale yellow oil
PNA oil	viscous, bright yellow oil
PNA soft resins	dark orange or brown semisolid
Hard Resins	dark brown solid
Polar Resins	dark brown solid
Asphaltenes	black solid
Non-eluted Asphaltenes	not recovered

poorly defined northern edge of the deposit lies under more than 500 feet of overburden.[39] The bitumen exists in five bitumen-impregnated zones varying from 27 to 97 feet in thickness,[37] indicating that the deposit is deltaic or fluvial in nature.

Three different tar sands from the PR Spring deposit were used in this investigation because it was found that the physical and chemical natures of the three bitumens varied substantially. The PR Spring Rainbow I (PRS-RI) and PR Spring Rainbow II (PRS-RII) tar sands were obtained from the northeast corner of the deposit (Township 12 South, Range 25 East, Section 32). Both of these tar sands were mined from a shallow bitumen-impregnated zone near an outcrop at the eastern edge of the deposit, as is shown in Figure 32. The PR Spring South tar sand was an outcrop sample that was obtained from the southern edge of the deposit (Township 16 South, Range 23 East, Section 19-20) as is shown in Figure 32.

Samples of the three tar sands were solvent extracted in a soxhlet apparatus to obtain bitumen samples for characterization. The extracted bitumen from the PR Spring Rainbow I tar sand appeared as a typical tar sand bitumen. That is, it was a black, semisolid tar. Conversely, both the PR Spring Rainbow II and PR Spring South bitumens were black, shiny, brittle solids resembling Gilsonite in appearance.

Physical and chemical properties of the three PR Spring bitumens are presented in Table 19. The bitumen contents of the three tar sands were quite different. The PR spring Rainbow I (PRS-RI) tar sand, which contained 14.14 percent by weight bitumen, required pretreatment with liquid nitrogen before feeding because the small particles tended to agglomerate in the feed system. Although the PRS-RI was more difficult to feed, the bitumen was of a better quality than PR Spring Rainbow II (PRS-RII) and PR Spring South (PRS-S). That is, the PRS-RI bitumen was more volatile (31.90 wt.%) than PRS-S (14.29 wt.%) or PRS-RII (22.76 wt.%). In addition, the Conradson carbon residue of the PRS-RI was lower than that of the other bitumens.

The viscosities of the three bitumens are presented in Table 20 and Figure 33. The viscosity of the PRS-RI bitumen was significantly lower than that of the other bitumens. In addition, the pour point of the PRS-RI bitumen (220°F) was much lower than that of the PRS-S (320°F) and PRS-RII

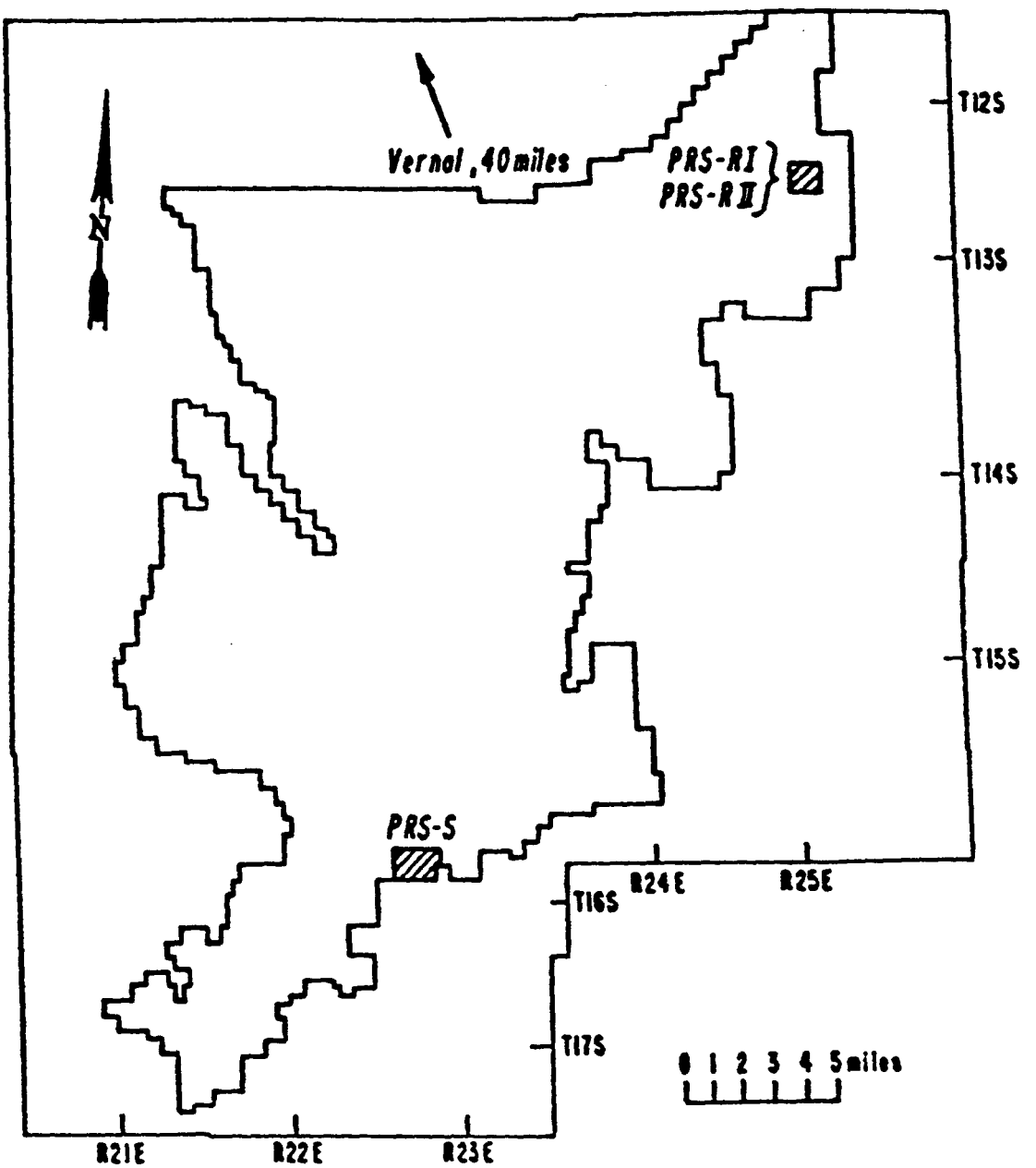

Figure 32. The PR Spring bituminous sand deposit.

Table 19

Analysis of Native Bitumens from the PR Spring Tar Sand Deposit

Source	Rainbow I	South	Rainbow II
Bitumen Content, wt.%	14.14	6.45	8.53
Specific Gravity	1.0157	1.0083	0.9872
API Gravity, ^{o}API	7.8	8.8	11.8
Conradson Carbon, wt.%	14.0	24.0	17.4
Ash, wt.%	3.3	1.9	1.4
Pour Point, K (^{o}F)	377 (220)	433 (320)	433 (320)
Simulated Distillation			
Volatility, wt.%	31.9	14.3	22.8
IBP-400^{o}F, wt.%	1.3	0.7	0.5
400-650^{o}F, wt.%	5.1	1.3	2.2
650-1000^{o}F, wt.%	25.6	12.3	20.1
1000^{o}F^{+}, wt.%	68.1	85.7	77.2
Elemental Analysis			
C, wt.%	84.66	81.73	81.44
H, wt.%	11.34	9.29	10.31
N, wt.%	1.30	1.37	1.37
S, wt.%	0.53	0.39	0.44
O, wt.%	1.75	7.22	6.27
H/C Atomic Ratio	1.61	1.36	1.52
Molecular Weight, g mol^{-1}	702.	1561.	1381.
Gradient Elution Chromatography			
Saturates, wt.%	9.5	4.1	15.8
MNA/DNA Oils, wt.%	10.2	5.3	3.5
PNA Oils, wt.%	11.4	1.0	9.0
Soft Resins, wt.%	13.9	4.0	5.8
Hard Resins, wt.%	1.1	1.8	2.3
Polar Resins, wt.%	2.0	1.1	3.6
Asphaltenes, wt.%	31.3	55.7	35.9
Noneluted Asphaltenes, wt.%	20.6	27.1	24.1
Ni, ppm	110	102	116
V, ppm	10	8	3

Table 20

Viscosities of the Native Bitumens from the PR Spring Tar Sand Deposit

Sample Temperature, (^{o}C/K)	Viscosity (cps)		
	PR Spring Rainbow I	PR Spring Rainbow II	PR Spring South
100 / 373	8.269	---	---
120 / 393	1,816	---	---
140 / 413	561	---	---
160 / 433	226	---	---
180 / 453	160	---	---
200 / 473	---	9,000	---
210 / 483	---	---	10,071
220 / 493	---	2,900	7,031
240 / 513	---	1,372	3,065
260 / 533	---	795	1,512
280 / 553	---	---	1,141
E_a for viscous flow (cal/mol)	-18.23	-20.21	-17.31
Preexponential factor, cps	1.47×10^{-7}	3.66×10^{-6}	1.4142×10^{-4}

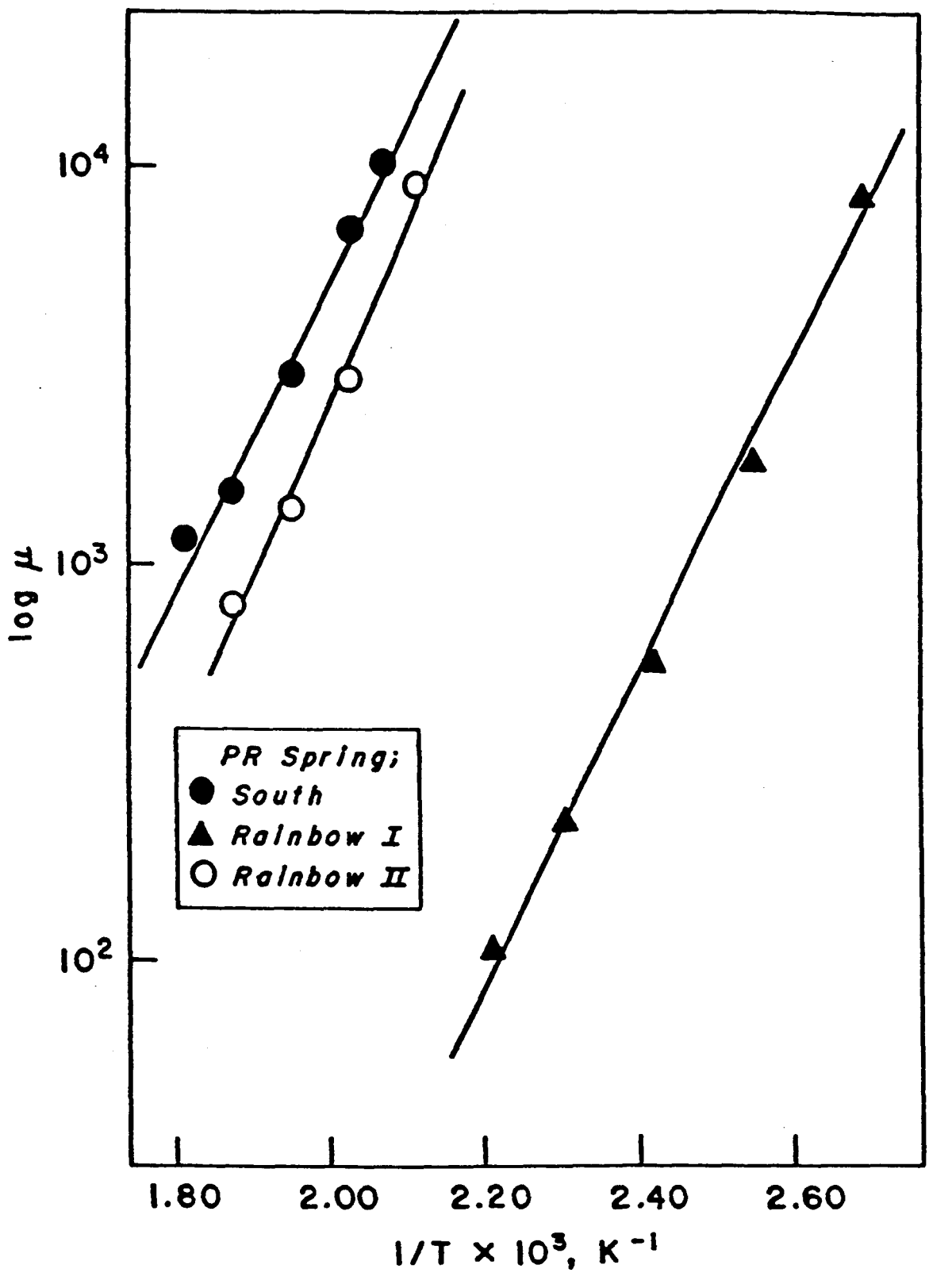

Figure 33. Viscosities of solvent extracted PR Spring tar sand bitumens with respect to temperature.

(320°F) bitumens. All three bitumens were low in sulfur content, indicating that the PR Spring bitumens were of fresh water origin.[40]

The PRS-S and PRS-RII bitumens were high in oxygen content relative to the PRS-RI sample. This difference can be explained on the basis of the origin of the samples. The PR Spring South sample was an outcrop sample which has been subjected to oxidation by exposure to the atmosphere. The PR Spring Rainbow II sample was mined; however, it was mined from a more shallow zone than the PR Spring Rainbow I sample. The bitumen was oxidized as it migrated toward the surface.[41] In addition, the atomic hydrogen-to-carbon (H/C) ratio of the PRS-RI bitumen was higher than those of the other bitumens. The gradient elution chromatography of the bitumens illustrated further the different natures of the bitumens. The PRS-RI contained more of the less refractory compound types (saturates, naphthenes, and aromatics) than the other bitumens. The PRS-RII bitumen contained fewer of the less refractory compounds than PRS-RI and more of the resins and asphaltenes. The PRS-S bitumen contained much more asphaltic material than the other bitumens and was deficient in less refractory compounds.

The low volatility and low atomic hydrogen-to-carbon ratio of the PRS-S bitumen, along with the high Conradson carbon residue, high molecular weight, asphaltene content, and oxygen content, are indicative of an outcrop sample. The differences in quality of the PRS-RI and PRS-RII bitumens can be explained on the basis of the depth of the tar sand in the deposit. According to Gwynn,[41] considerable oxidation of the bitumen occurs as it migrates toward the surface. This accounts for the difference in oxygen content between PRS-RI and PRS-RII, since the PRS-RI was mined from a greater depth than the PRS-RII. The difference in bitumen content does not appear to be related to the depth of the sample. Although the bitumen content of core samples drilled by Peterson[42] in the northern area of the deposit varied over the length of the core, the variation appeared to be random. Differences in atomic hydrogen-to-carbon ratio, molecular weight, Conradson carbon residue and volatility between the PRS-RI and PRS-RII bitumens are also related to the difference in the depth of the samples in the deposit. The PRS-RII bitumen, which was mined from a relatively shallow region, is similar in quality

to an outcrop sample such as PRS-S. Conversely, the bitumen from the deeper-mined PRS-RI sample is of a higher quality than the other bitumens.

The Effect of Reactor Temperature on Product Yields

The effect of reactor temperature on pyrolysis product yields was investigated for all three bituminous sands. A series of experiments was run for each tar sand wherein the reactor temperature was varied while the solids retention time and fluidizing gas velocity were held constant. All yield data are reported as weight percent of bitumen fed.

The results for a series of experiments using PR Spring Rainbow I tar sand as feed, wherein the reactor temperature was varied from 773 K to 873 K, while the solids retention time and fluidizing gas velocity were held constant at 20 minutes and 144 liters per hour (LPH), respectively, are shown in Table 21 and Figure 34. The liquid yield increased as reactor temperature increased from 773 K to 798 K. The maximum liquid yield decreased. The light gas yield increased as the liquid yield decreased. The coke yield was high (25.1 percent by weight) at 773 K, but decreased steadily as the temperature increased to 823 K. AT higher temperatures, the coke yield was insensitive to changes in the reactor temperature. That is, above 823 K, the coke yield was stable at 9 to 10 weight percent.

An identical series of experiments was carried out using the PR Spring Rainbow II tar sand as feed sand. That is, the reactor temperature was varied from 773 K to 873 K, while the solids retention time and fluidizing gas velocity were held constant at 20 minutes and 144 LPH, respectively. The trends in product distribution for this series of experiments, presented in Table 22 and Figure 35, were very similar to those observed for the PR Spring Rainbow I tar sand. A maximum liquid yield of 62.2 weight percent was obtained at 798 K. The liquid yield decreased with increasing temperature from 798 K to 873 K and increased with increasing temperature below 798 K. The gas yield increased as the liquid yield decreased. The coke yield was high at 773 K (31.3 weight percent), and declined to a steady value of 19 to 21 weight percent with increasing reactor temperature.

Table 21

The Effect of Reactor Temperature on Product Yields from PR Spring Rainbow I Tar Sand

Run ID No.	017-PRS (R)-JD	024-PRS (R)-JD	020-PRS (R)-JD	025-PRS (R)-JD	018-PRS (R)-JD
Reactor Temperature, K	773	798	823	848	873
Solids Retention Time, min	20	20	20	20	20
Fluidizing Gas Flow Rate, LPH	144	144	144	144	144
Product Yields[a]					
Light Gases, wt.%	9.77	13.53	20.09	20.75	23.10
C_5^+ Liquids, wt.%	65.14	71.13	70.42	68.85	67.70
Coke, wt.%	25.09	15.34	9.49	10.40	9.20

[a]Normalized to 100 percent by weight of bitumen fed.

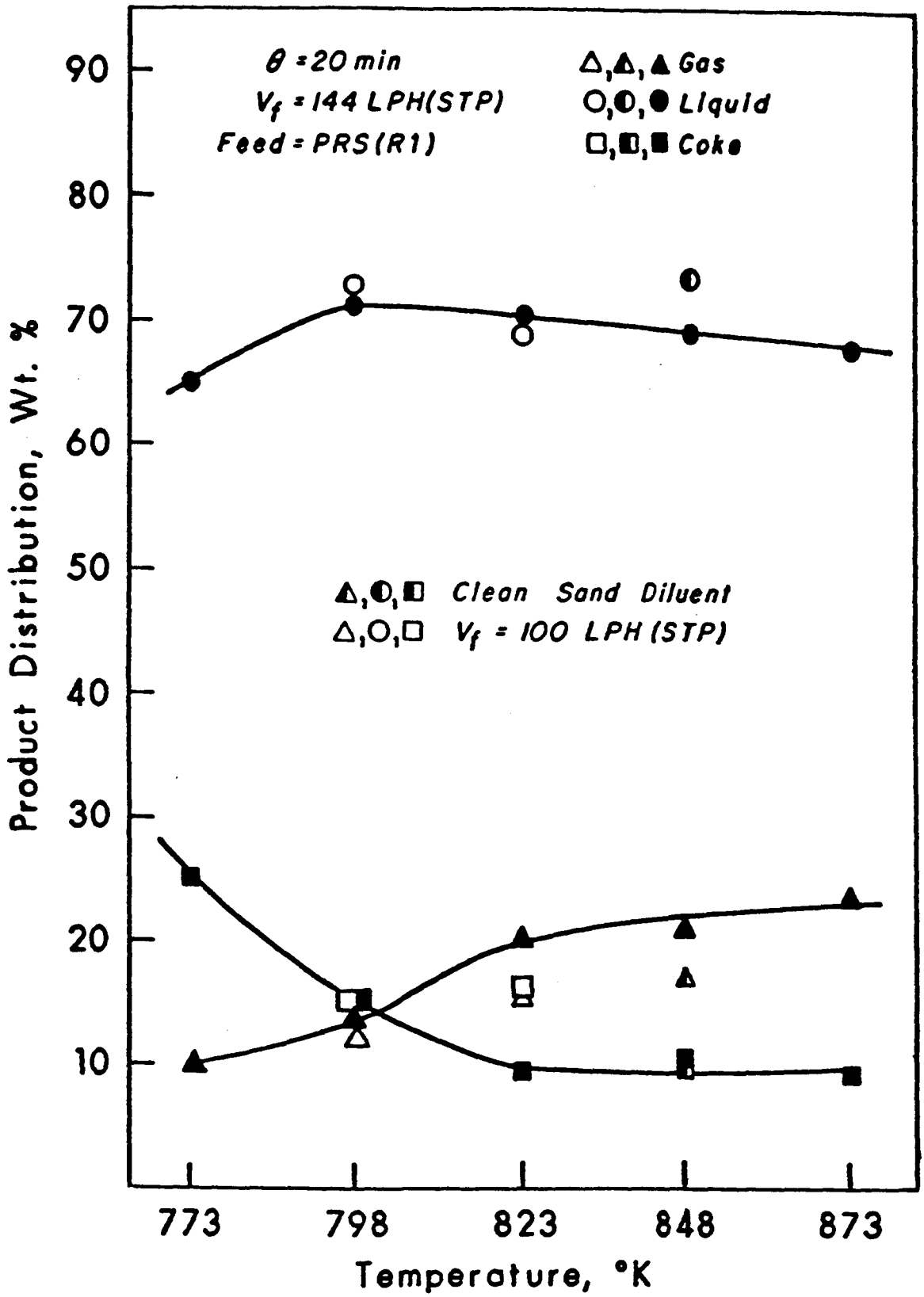

Figure 34. The effect of reactor temperature on the product distribution from the PR Spring Rainbow I tar sand.

θ = 20 minutes; V_f = 144 LPH (STP)

Table 22

The Effect of Reactor Temperature on Product Yields from PR Spring Rainbow II Tar Sand

Run ID No.	084-PRS (RII)-JD	082-PRS (RII)-JD	079-PRS (RII)-JD	081-PRS (RII-JD)
Reactor Temperature, K	773	798	823	873
Solids Retention Time, min	20	20	20	20
Fluidizing Gas Flow Rate, LPH	144	144	144	144
Product Yields[a]				
Light Gases, wt.%	14.62	18.06	20.64	18.73
C_5^+ Liquids, wt.%	54.11	62.20	60.49	60.26
Coke, wt.%	31.27	19.74	18.87	21.01

[a]Normalized to 100 percent by weight of bitumen fed.

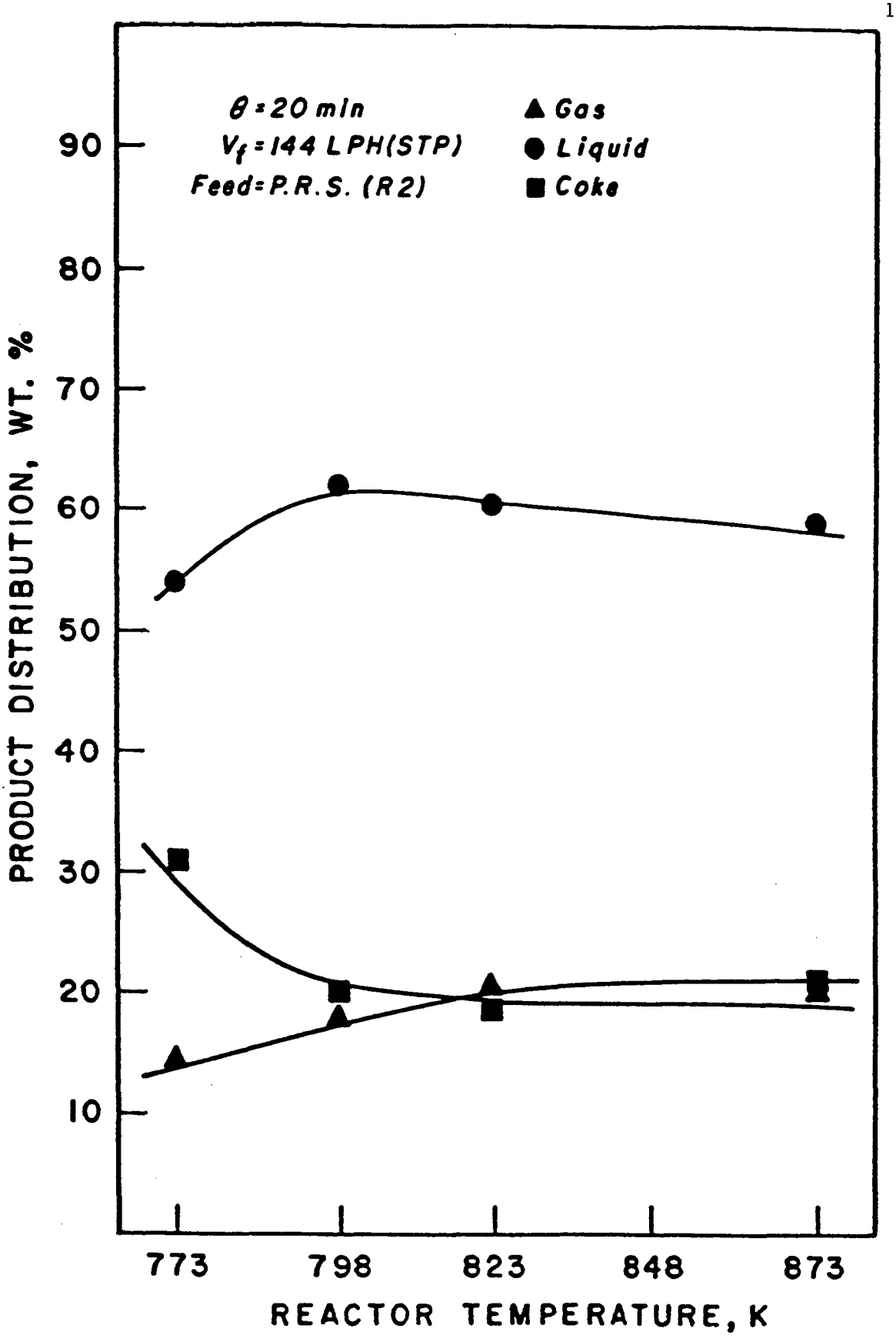

Figure 35. The effect of reactor temperature on product distribution from the PR Spring Rainbow II tar sands.

θ = 20 minutes; V_f = 144 LPH (STP)

The liquid yields from PR Spring Rainbow II were generally 9 to 10 weight percent lower than those from PR Spring Rainbow I, and the coke and light gas yields were higher. These differences in product yields were related to the differences in the native bitumens, as will be discussed later.

A series of experiments was run using the PR Spring South tar sand as feed sand wherein the reactor temperature was varied from 798 K to 923 K while the solids retention time was held constant at 27.1 minutes and the fluidizing gas velocity was held constant at 144 LPH. The results of this series of experiments are presented in Table 23 and Figure 36. The general trends in product distribution with respect to reactor temperature for PR Spring South were similar to those observed for PR Spring Rainbow I and PR Spring Rainbow II, except that the maximum liquid yield of 54.1 weight percent was obtained at 823 K rather than 798 K. The liquid yields were much lower than those from the other tar sands, and the yields of coke and light gases were higher.

The observed trends in product distribution with respect to temperature can be explained on the basis of the mechanism shown here:

$$\text{Bitumen} \longrightarrow \text{Bitumen-Derived Liquid} \longrightarrow \text{Light Gas} \qquad (22)$$

$$\text{Bitumen} \longrightarrow \text{Gas} + \text{Coke} \qquad (23)$$

The mechanism presented here is a simplified representation of a sequence of chemical and physical processes that take place during pyrolysis. As the feed sand entered the reactor and was heated, low molecular weight saturates, naphthenes, and aromatics were evaporated from the sand surface. High molecular weight naphthenes, saturates, and a portion of asphaltenes were thermally cracked on the sand surface to lower molecular weight species, which also evaporated. Concomitantly, a portion of the aromatics and asphaltenes present in the liquid phase on the sand surface undergo condensation reactions to form coke, which remained on the sand surface and light gases, which exited from the reactor with the condensable products.

The observed trends in product distribution with respect to reactor temperature are governed by the rates of the chemical and physical processes described. The rates of the cracking and reactions are much more sensitive to changes in reactor temperature than the rate of evaporation of compounds

Table 23

The Effect of Reactor Temperature on Product Yields from PR Spring South Tar Sand

Run ID No.	016-PRS (S)-JD	057-PRS (S)-JD	059-PRS (S)-JD	78-PRS (S)-JD	060-PRS (S)-JD	063-PRS (S)-JD
Reactor Temperature, K	793	823	848	873	898	923
Solids Retention Time, min	27.1	27.1	27.1	27.1	27.1	27.1
Fluidizing Gas Flow Rate, LPH	144	144	144	144	144	144
Product Yields[a]						
Light Gases, wt.%	27.22	19.40	24.53	26.89	26.35	35.77
C_5^+ Liquids, wt.%	44.95	54.06	52.46	51.65	50.03	49.00
Coke, wt.%	27.83	26.54	23.01	21.46	23.62	15.23

[a]Normalized to 100 percent by weight of bitumen fed.

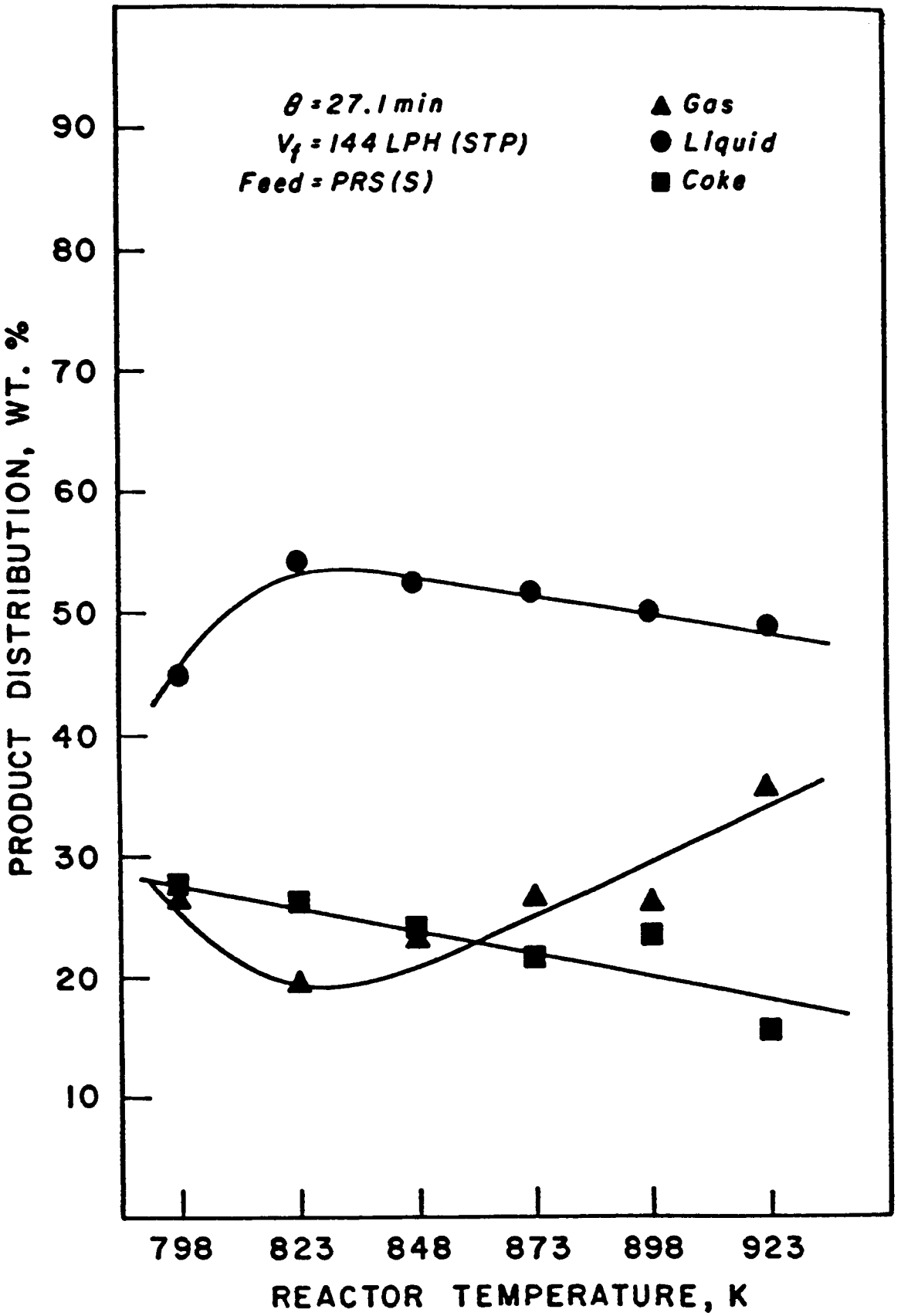

Figure 36. The effect of reactor temperature on product distribution from the PR Spring South tar sand.

θ = 20 minutes; V_f = 144 LPH (STP)

from the sand surface. In addition, the rate constants of the free-radical initiation, propagation, and termination reactions exhibit varying sensitivities to changes in reactor temperature. For instance, the activation energy for decomposition of radicals to form smaller compounds by hydrogen abstraction is 8-12 kcal/mol higher than the activation energy for b-scission of a carbon-carbon bond.[43] Consequently, the selectivity toward lighter products is increased with increases in reactor temperature, as is observed in Figures 34, 35, and 36. At reactor temperatures below 798 K (823 K for PR Spring South), the liquid yield increased with increased temperature because of an increase in the rate of cracking of heavy components on the sand surface along with an increase in the rate of evaporation. As the reactor temperature increased further, the rate of cracking continued to increase, resulting in a shift in the product selectivity toward light gases. Thus, a decrease in the liquid yield along with an increase in the light gas yield was observed.

The high coke yield at low reactor temperatures (Figures 34 and 35) actually consisted partially of unconverted high molecular weight asphaltenes which were not converted to coke. As the temperature increased, the rate of asphaltene decomposition to form coke increased. During decomposition, aliphatic side chains in the asphaltenes cracked and evaporated from the sand surface, contributing to the increase in liquid yield and concomitant decrease in observed coke yield.

The lower liquid yield, along with higher coke and gas yields, from the PR Spring South tar sand were related to the nature of the PR Spring South bitumen; that is, this bitumen is very asphaltic. It also has a high Conradson carbon residue, lower volatility and lower hydrogen-to-carbon ratio than the other feed bitumens (see Table 19). A low liquid yield and high coke yield are expected from a feed material of this nature. The slowly declining trend in coke yield and the occurrence of the maximum liquid yield are also related to the nature of the PR Spring South bitumen. This bitumen is more difficult to liberate from the sand because of the low volatility. Thus, at lower reactor temperatures, the liquid yield is low and the coke yield is high. As the reactor temperature increases, the coke yield declines because of an increased rate of decomposition of the asphaltenes, and because there is a relatively small amount of liquid product vapors present to undergo thermal cracking to form secondary coke.[44]

The Effect of Solids Retention Time on Product Yields

The retention of solids in the fluidized bed reactor (θ) is defined by the following expression:

$$\theta = \frac{W}{F} \times 60 \qquad (24)$$

where W equals the total weight of sand in the bed in grams and F equals the sand feed rate in grams per hour. Thus, the solids retention time can be varied by changing the weight of bed sand or by altering the sand feed rate. In this investigation, the solids retention time was varied by changing the sand feed rate in order to minimize the effects of variation in the height of the fluidized bed.

The effect of solids retention time on product yields was investigated for the PR Spring Rainbow I and PR Spring South tar sands. The results of a series of experiments using PR Spring Rainbow I tar sand as feed are shown in Table 24 and Figure 37. In this series of experiments, the solids retention time was varied from 17 to 30 minutes while the reactor temperature was held constant at 798 K. The liquid yield decreased with increasing solids retention time. The decrease was rapid as solids retention time increased from 17 to 20 minutes, but was less pronounced between solids retention times of 20 to 30 minutes. The gas yield increased steadily as solids retention time increased. The coke yield was essentially insensitive to changes in solids retention time.

In a second series of experiments with PR Spring south tar sand as feed sand, the solids retention time was varied from 20 to 30 minutes, while the reactor temperature was held constant at 873 K. The effect of solids retention time on product yields is presented in Table 25 and Figure 38. As with PR Spring Rainbow I, the liquid yield decreased with increasing solids retention time. The gas yield increased as the liquid yield decreased, and the coke yield declined slightly with increasing solids retention time. Once again, the liquid yield was generally much lower for PR Spring South than for PR Spring Rainbow I, while coke and gas yield were higher.

The liquid yield declined with increasing solids retention time because of the effect of solid-vapor contact time on the rate of vapor-phase thermal cracking. The aspect ratio of the reactor was about 20, and the Froude number was in the range of 2.8 to 4.0. Inhomogeneous (bubbling) fluidization

Table 24

The Effect of Reactor Temperature on Product Yields from PR Spring Rainbow I Tar Sand

Run ID No.	046-PRS (R)-JD	024-PRS (R)-JD	032-PRS (R)-JD	042-PRS (R)-JD
Reactor Temperature, K	798	798	798	798
Solids Retention Time, min	17	20	25	30
Fluidizing Gas Flow Rate, LPH	144	144	144	144
Product Yields[a]				
Light Gases, wt.%	12.34	13.53	13.99	17.30
C_5^+ Liquids, wt.%	75.94	71.13	71.14	69.21
Coke, wt.%	11.72	15.34	14.87	13.49

[a]Normalized to 100 percent by weight of bitumen fed.

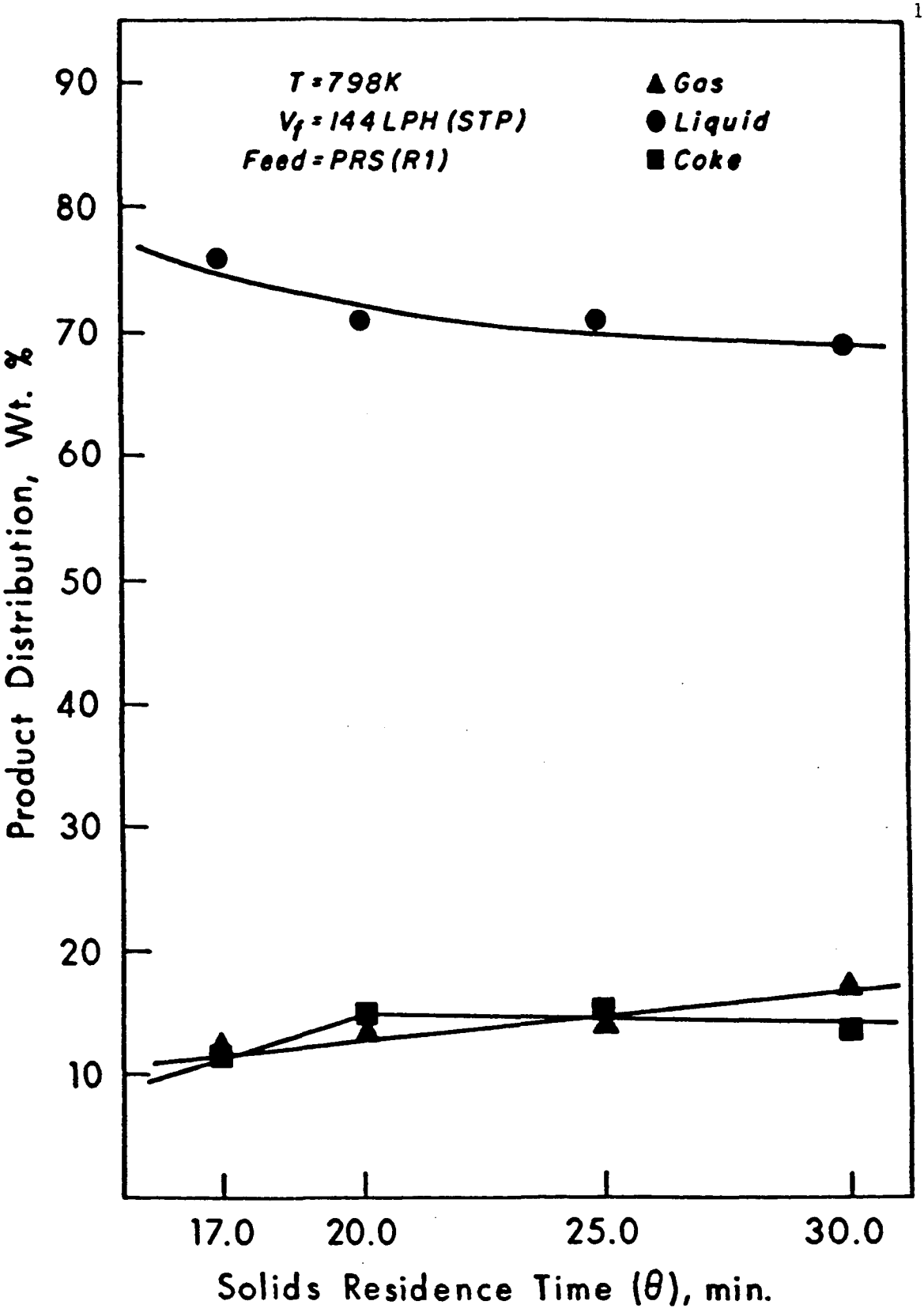

Figure 37. The effect of solids retention time on product distribution from the PR Spring Rainbow I tar sand.

T = 798 K; V_f = 144 LPH (STP)

Table 25

The Effect of Solids Retention on Product Yields from PR Spring South Tar Sand

Run ID No.	064-PRS (S)-JD	069-PRS (S)-JD	078-PRS (S)-JD	077-PRS (S)-JD
Reactor Temperature, K	873	873	873	873
Solids Retention Time, min	20	24	27.1	30.0
Fluidizing Gas Flow Rate, LPH	144	144	144	144
Product Yields[a]				
Light Gases, wt.%	23.66	32.68	26.89	43.37
C_5^+ Liquids, wt.%	55.57	45.73	51.65	38.06
Coke, wt.%	20.77	21.59	21.46	18.57

[a]Normalized to 100 percent by weight of bitumen fed.

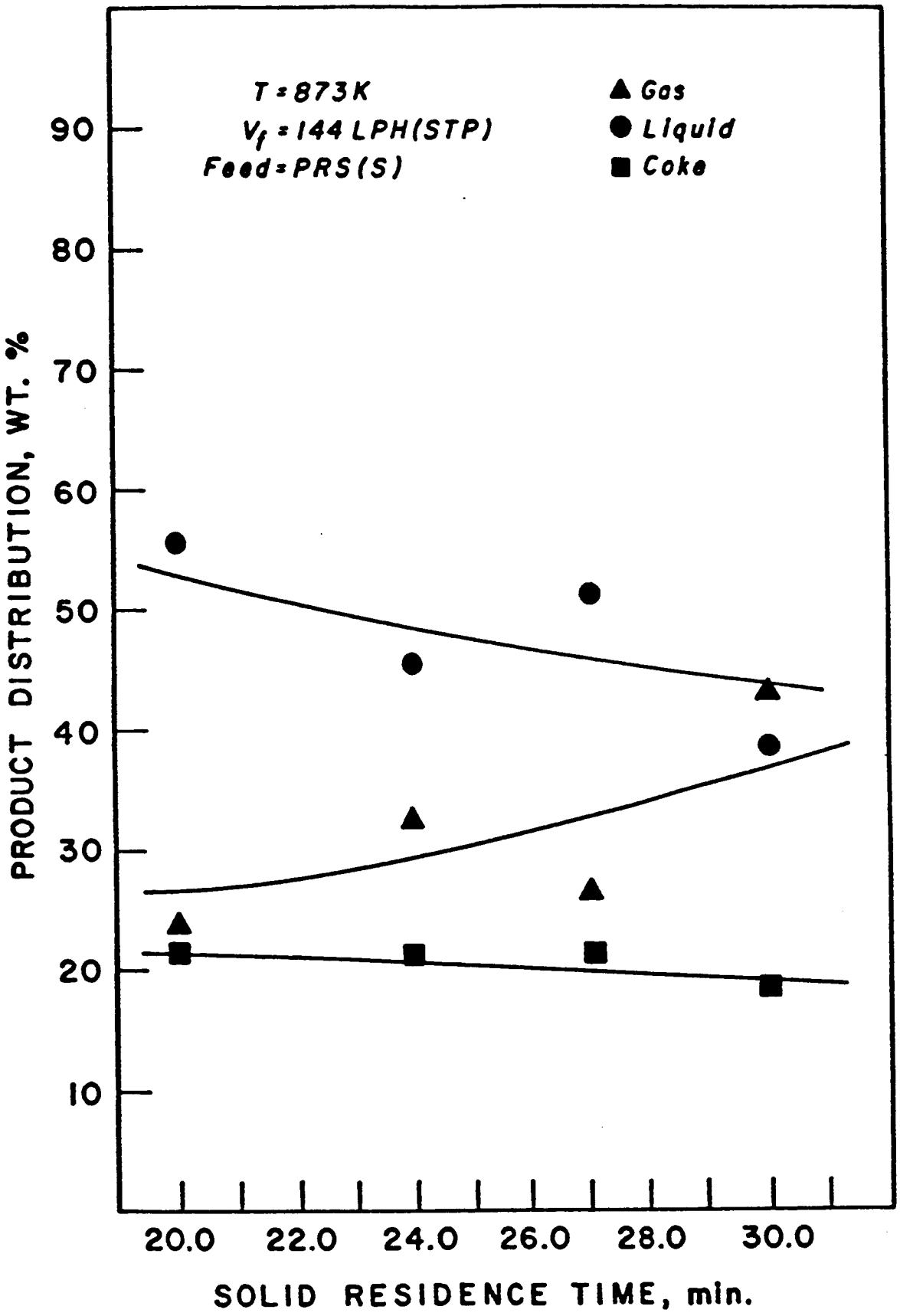

Figure 38. The effect of solids retention time on product distribution from the PR Spring South tar sand.

T = 873 K; V_f = 144 LPH (STP)

occurs in a gas-solid system under these conditions.[45] This system is closely approximated by the Kunii-Levenspiel bubbling-bed model.[106] According to the model, the fluidized bed is composed of large, solids-free bubbles surrounded by a solids-rich cloud and followed by a solids-rich wake. The bubbles, cloud, and wake rise through an emulsion that is rich in solids. Mass transfer occurs between the bubble, the cloud or wake, and the emulsion. Concurrently, chemical reaction takes place in all three phases.

The analysis of a single bubble rising through the emulsion as a multiphase batch reactor results in the following expression for the conversion, 1-X, in a fluidized bed:

$$1\text{-}X = \exp\left(-H_f \theta_b\right) \tag{25}$$

where H_f is the effective multiphase reaction-rate coefficient as defined by Carberry,[45] θ_b is the vapor-solid contact time, and X is the fraction of unconverted bitumen. It can be seen that the overall conversion decays exponentially with increases in vapor-solid contact time.

The reaction network for pyrolysis of tar sand bitumen (equation 22) is similar to the mechanism for fluid catalytic cracking.[46] Carberry[45] derived a yield-conversion relationship for the sequential reaction network represented by equations 22 and 23, which can be used to describe the pyrolysis process. It was found that at short bubble contact times, the yield of bitumen-derived liquid increased with increasing vapor-solid contact times to a maximum. The liquid yield decreased with further increases in contact time, following the trend of total conversion with respect to vapor-solid contact time.

The Effect of Fluidizing Gas Velocity on Product Yields

Wang[32] determined that the fluidizing gas velocity has no significant effect on the liquid product yield. Two experiments were run during this investigation to verify that conclusion. These experiments were run at reactor temperatures of 798 K and 823 K, solids retention time of 20 minutes, and fluidizing gas velocity of 100 liters per hour. The results of these experiments are shown as hollow points in Figure 34. The liquid yields were essentially identical to those obtained at the normal fluidizing gas velocity of 144 liters per hour, indicating that the fluidizing gas velocity had no effect on the yield of

liquid products, and that at these temperatures, secondary cracking in the bulk gas phase external to the sand particle was not significant.

The Effect of Feed Sand Diluent on Product Yields

The feed tar sand for each experiment was mixed with coked spent sand in order to improve the feeding characteristics of the tar sand. A special experiment was run in which the feed tar sand was mixed with clean spent sand. This experiment was run at a reactor temperature of 848 K, solids retention time of 20 minutes, and fluidizing gas velocity of 144 liters per hour. The results of this experiment are shown in Figure 34 as half-solid data points. It can be seen that the liquid yield for this experiment was about six weight percent higher than normal for the reactor conditions, and the gas yield was correspondingly lower. The coke yield remained unchanged.

The effect of feed sand diluent on product yields was not studied further in this investigation. It was decided that the effect of the feed sand diluent on product distribution should be investigated in the future.

The Effect of Native Bitumen Properties on Product Yields

The effect of feed sand source on product yields was investigated briefly by Venkatesan.[31] The primary purpose of that investigation was to determine the feasibility of the pyrolysis process for producing bitumen-derived liquids from lean tar sands (less than five weight percent bitumen). Differences between the product yields from Sunnyside and Tar Sand Triangle tar sands were observed, and it was speculated that the extent of aging of the feed tar sand affected the product yields. The investigation was not pursued further.

Detailed analysis of the effect of certain native bitumen properties on product yields has not been undertaken previously. The second objective of this investigation was to study the effect of certain physical and chemical properties of native bitumens on the product yields.

The effect of reactor temperature on the liquid yields from the three PR Spring tar sands is shown in Figure 39. The trends in liquid yield with respect to reactor temperature were similar for the three tar sands, although the maximum liquid yield for the PR Spring South tar sand was obtained at

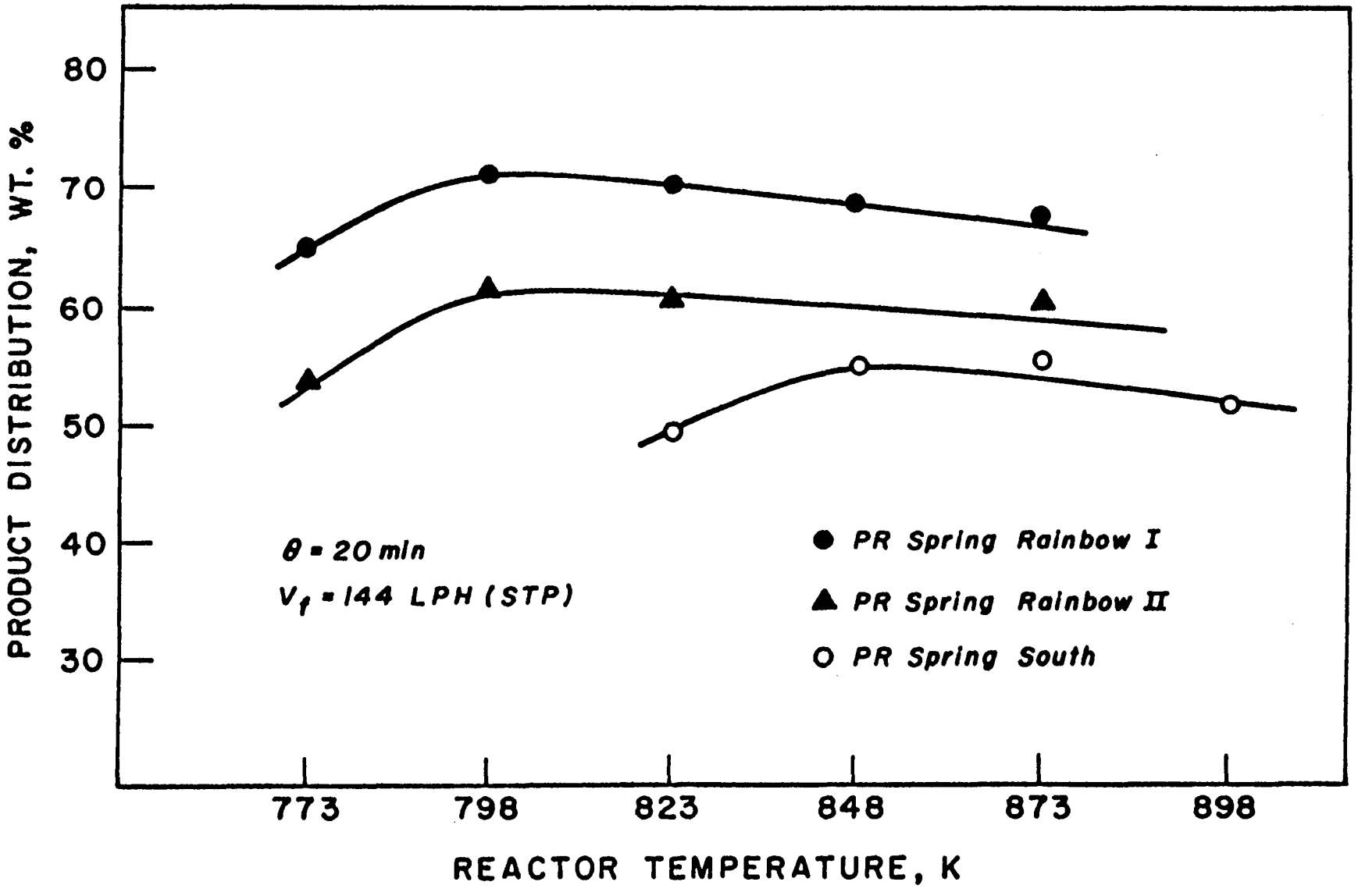

Figure 39. Liquid yields from the PR Spring tar sands with respect to reactor temperature.

848 K rather than 798 K. The liquid yields from the PR Spring Rainbow I tar sand were up to 20 weight percent higher than those from PR Spring Rainbow II. It was evident that there was a relationship between the native bitumen and the resulting product yields.

The effect of the native bitumen on product yields was studied in terms of various physical and chemical properties of the native bitumen. The product yields from the three tar sands at a single set of reactor conditions are shown in Table 26, along with three important properties of the native bitumens. The effects of the Conradson carbon residue, asphaltene content, and atomic H/C ratio of the native bitumens on product yields are shown in Figures 40, 41, and 42, respectively. It can be seen that definite trends in product yields existed with respect to the Conradson carbon residue, asphaltene content, and atomic H/C ratio of the native bitumen. As the Conradson carbon residue and asphaltene content of the native bitumen increased, the liquid yield decreased, and the gas and coke yields increased. The opposite effect was observed with respect to the atomic H/C ratio of the native bitumen. The liquid yield increased as the atomic H/C ratio increased, while the gas and coke yields decreased.

The trends in product yields with respect to the properties of the native bitumen are to be expected. The Conradson carbon residue of a hydrocarbon material is a measure of the tendency of that material to form coke during thermal processing. Thus, a feed bitumen with a high Conradson carbon residue will yield more coke and gas at the expense of liquid than a feed bitumen with a low Conradson carbon residue. Furthermore, the Conradson carbon residue of a high molecular weight hydrocarbon is directly related to the asphaltene content of that material.[41] Consequently, the effect of the asphaltene content of the native bitumen on product yields (Figure 41) is very similar to the effect of the Conradson carbon residue (Figure 40).

The effect of the atomic hydrogen-to-carbon ratio of the native bitumen on the product yields (Figure 42) can be explained on the basis of the mechanism of pyrolysis discussed previously. Thermal cracking is an important part of the pyrolysis mechanism. A higher hydrogen-to-carbon ratio is indicative of a more naphthenic bitumen. Saturated hydrocarbons are easily cracked, while aromatics tend to form coke under cracking conditions. Therefore, a bitumen with a higher hydrogen-to-carbon

Table 26

The Effect of Feed Sand Source and Native Bitumen Properties on Product Yields

Run ID No.	020-PRS(R)-JD	079-PRS(RII)-JD	083-PRS(S)-JD
Reactor Temperature, K	823	823	823
Solids Retention Time, min	20	20	20
Fluidizing Gas Flow Rate, LPH	144	144	144
Feed Tar Sand	PR Spring Rainbow I	PR Spring Rainbow II	PR Spring South
Properties of Native Bitumen			
Conradson Carbon Residue, wt.%	14.0	17.4	24.0
Asphaltene Content, wt.%	51.9	60.0	82.8
Atomic H/C Ratio	1.61	1.52	1.36
Product Yields[a]			
Light Gases, wt.%	20.09	20.64	30.55
C_5^+ Liquids, wt.%	70.42	60.49	49.30
Coke, wt.%	9.49	18.87	20.15

[a]Normalized to 100 percent by weight of bitumen fed.

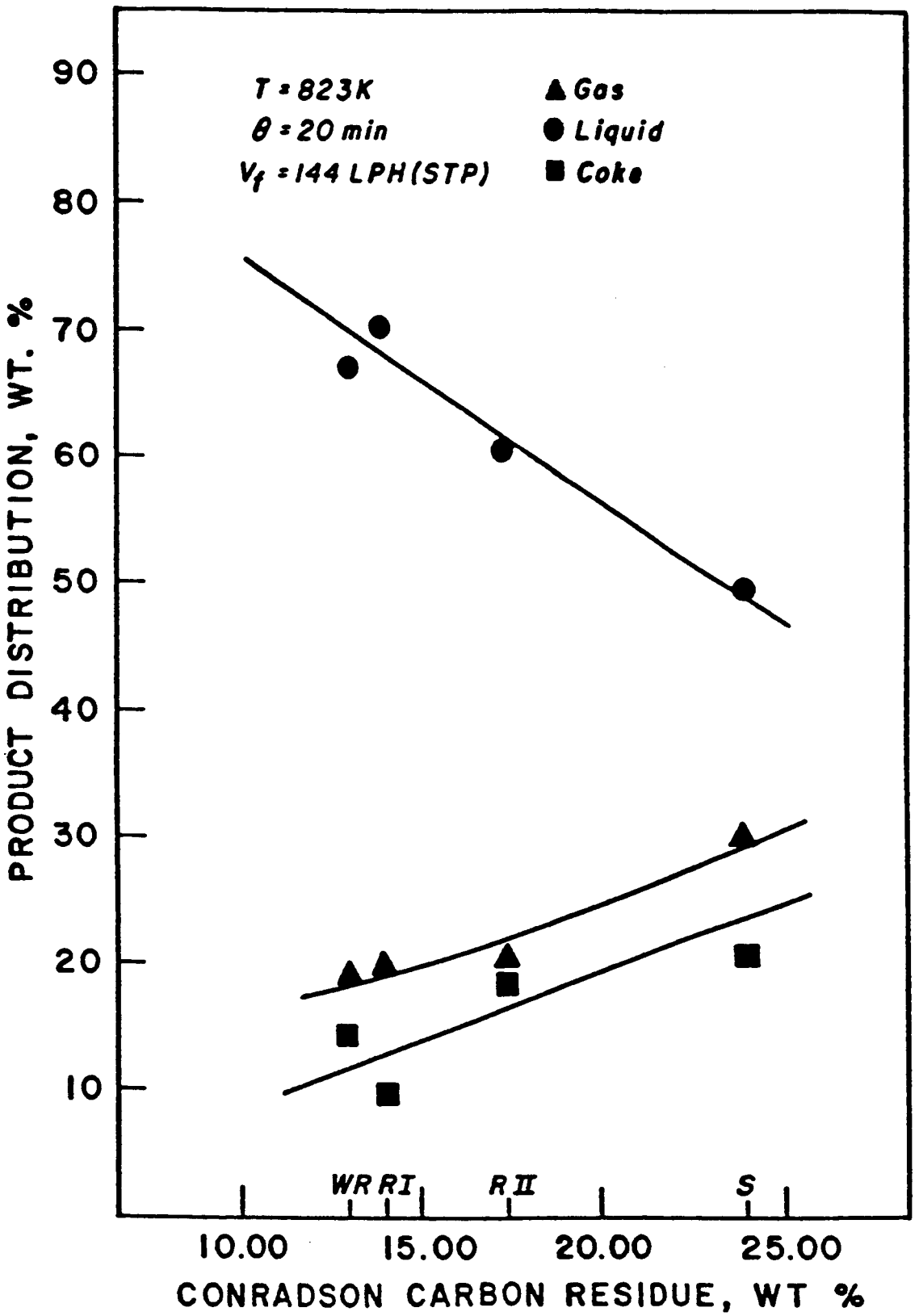

Figure 40. The effect of the Conradson carbon residue of the native bitumen on the product yields.

WR - Whiterocks; RI - PR Spring Rainbow I
RII - PR Spring Rainbow II; S - PR Spring South

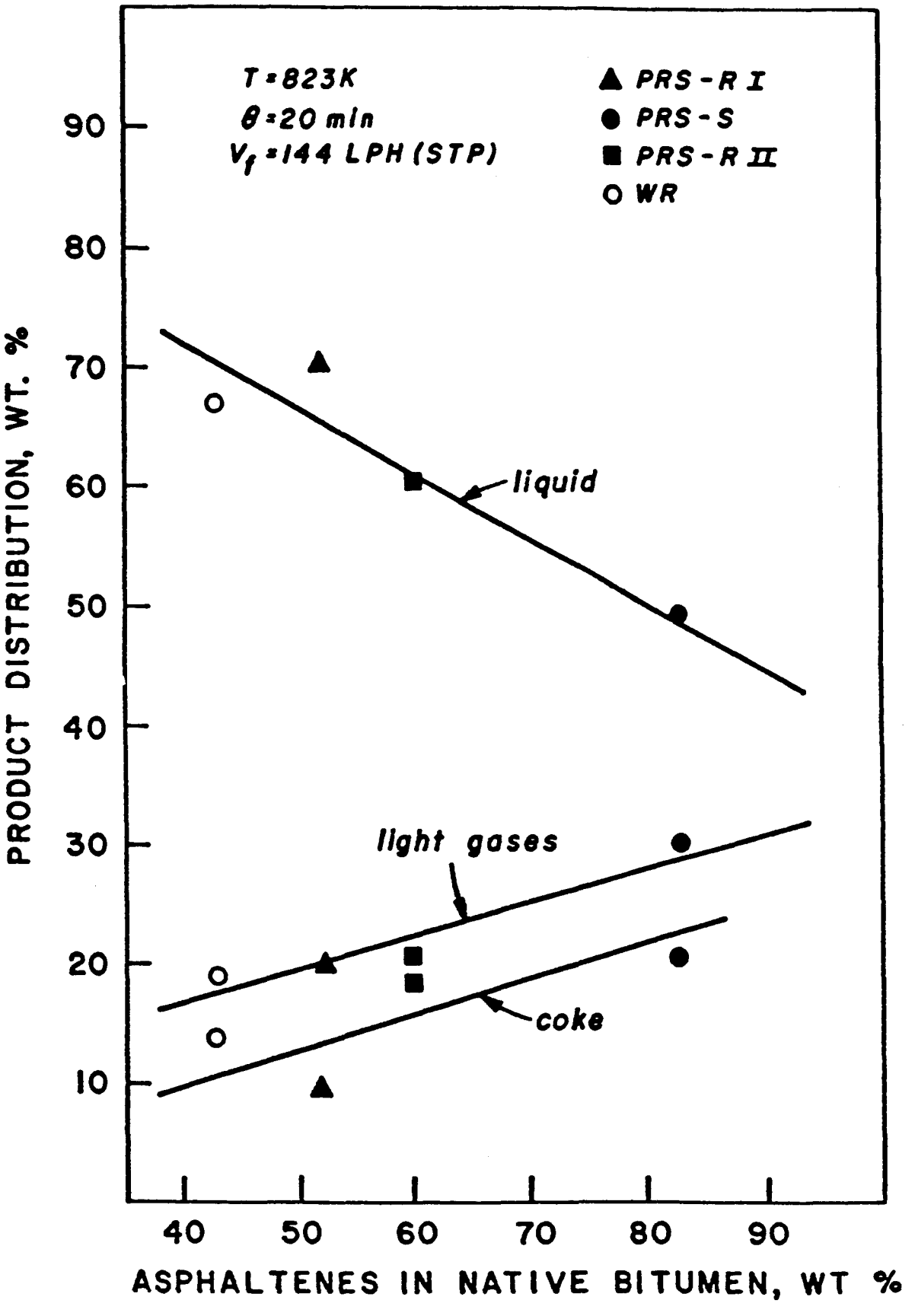

Figure 41. The effect of the asphaltene content of the native bitumen on the product yields.

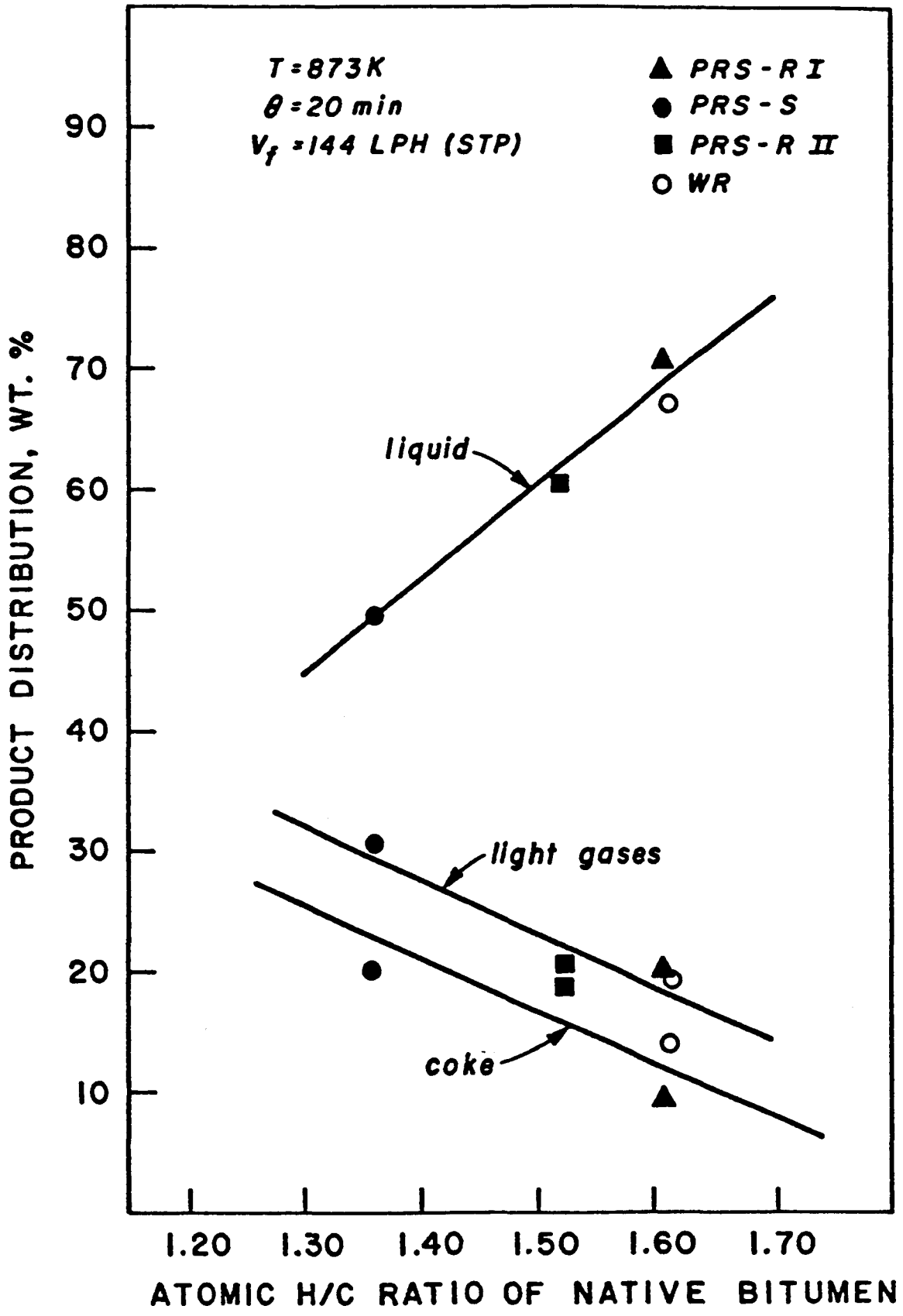

Figure 42. The effect of the atomic H/C ratio of the native bitumen on the product yields.

ratio, being more naphthenic, will yield more liquid, less coke, and less gas than a bitumen with a lower hydrogen-carbon ratio.

The definite trends in product yields with respect to these bitumen properties are significant because they indicate predictable relationships between properties of the bitumen and the resulting product yields. In the following section, correlations between these bitumen properties and the product yields will be discussed.

The Development of a Liquid Product Yield Correlation

Wang[32] developed a correlation between significant pyrolysis process variables (reactor temperature and solids retention time) and the liquid product yield. The correlation, shown here:

$$Y = 61.996 - 2.281\ X_1 - 2.556\ X_2 - 0.670\ X_1^2 + 1.636\ X_2^2 - 0.661\ X_1X_2 \quad (26)$$

where X_1 and X_2 are the coded reactor temperature and solids retention time, respectively, and Y is the liquid yield, was developed by using a Box-Wilson statistical design of experiments algorithm.[47,48] The correlation predicted accurately the yield of liquid products from the Whiterocks tar sand in the fluidized bed pyrolysis process. A maximum liquid yield of about 80 percent by weight of bitumen fed was predicted at a reactor temperature of 803 K and a solids retention time of 12 minutes.[32]

The correlation developed by Wang[32] was utilized in this investigation; however, the liquid yields from the PR Spring tar sand deposit were not predicted accurately by equation 26. Based on the trends in product yields with respect to the three properties of the native bitumens (Conradson carbon residue, asphaltene content, and atomic H/C ratio), it was decided to develop a liquid product yield correlation that would incorporate a property of the native bitumen as well as the significant process variables.

The correlations were developed by using multivariable linear regression. Separate correlations were developed for the Conradson carbon residue, asphaltene content, and atomic H/C ratio, because a single correlation including all three bitumen properties would contain too many variables to be

meaningful. The experiments in this investigation were not carried out according to the Box-Wilson algorithm; however, the ranges of process variables studied were similar to those studied by Wang.[32] Therefore, the data were analyzed using the multivariable linear regression computer program developed by Wang.[32] In all three correlations, Y, the dependent variable, is the liquid product yield in percent by weight of bitumen fed. The independent variables X_1 and X_2 are coded variables representing the reactor temperature and solids retention time, respectively. The independent variable X_3, also coded, represents the property of the native bitumen (Conradson carbon residue, asphaltene content, or atomic H/C ratio). The independent variables were coded as follows:

$$X = \frac{N_i - N_i \text{ (median)}}{N_i(\max) - N_i(\min)} \quad X\ 2 \tag{27}$$

where N is the value of the reactor temperature (i=1), solids retention time (i=2), or native bitumen property (i=3).

The liquid yield data were fitted to a second-order equation in each case because Wang[32] had determined that a first-order equation did not adequately fit the data.

The following equation describes the relationship between the Conradson carbon residue of the native bitumen and the pyrolysis liquid yield:

$$Y = 56.547 - 0.324X_1 - 2.839X_2 - 9.452X_3 - 3.525X_1^2 - 1.166X_2^2 + 3.671X_3^2 - 3.455X_1X_2 + 2.222X_1X_3 - 0.302X_2X_3 \tag{28}$$

where Y is the liquid yield in percent by weight of bitumen fed, X_1 is the reactor temperature, X_2 is the solids retention time, and X_3 is the Conradson carbon residue. The correlation between the asphaltene content of the native bitumen and the liquid yield is presented here:

$$Y = 53.857 - 0.274X_1 - 2.837X_2 - 9.467X_3 - 3.555X_1^2 - 1.183X_2^2 + 6.379X_3^2 - 3.532X_1X_2 + 2.219X_1X_3 - 0.284X_2X_3 \tag{29}$$

where Y, X_1, and X_2 are the same as in the previous correlation, and X_3 is the asphaltene content. Similarly, the correlation for the atomic H/C ratio appears as follows:

$$Y = 57.259 = 0.349X_1 - 2.748X_2 + 9.432X_3 - 3.791X_1^2 - 1.538X_2^2 + 3.053X_3^2 - 2.909X_1X_2 - 2.452X_1X_3 + 0.777X_2X_3. \quad (30)$$

Again, Y, X_1, and X_2 are the same as in the other correlations, and X_3 is the atomic H/C ratio.

Analyses of variance were performed for all three of the correlations, and are presented in Tables 27, 28, and 29. The standard F-test for goodness of fit was applied to the three correlations. In each case, the null hypothesis was accepted. That is, the three correlations were found to represent the trends in the data equally well.

The liquid yields from selected pyrolysis experiments are presented in Table 30, along with the liquid yields predicted by equations 28, 29, and 30. The predicted liquid yields from the three correlations were nearly identical in almost all cases. The trends in liquid yields with respect to reactor temperature and solid retention time are shown in Figures 43 and 44, respectively. The trends in liquid yields predicted by equation 28 are also shown. Liquid yields as determined from equations 29 and 30 are not shown because the three predictions were very similar (Table 26). The predictions of liquid yield based on the reactor temperature, solids retention time, and Conradson carbon residue of the native bitumen were accurate in most instances. The trends in liquid yield with respect to process variables were described as well by equation 28 as by the experimental data. The ability of the correlations to describe the trends in liquid yield is further illustrated in Figure 45. The data from the PR Spring tar sands were described equally well by the three correlations. However, none of the correlations predicted the liquid yield accurately for the Whiterocks tar sand.

The liquid yield from the fluidized bed pyrolysis process can be adequately predicted by any of the three correlations developed in this investigation. A detailed characterization of the native bitumen is required in order to use the correlations. Since an accurate determination of the asphaltene content of the bitumen may not be possible, it would be preferable to use the correlations based on the Conradson carbon residue or atomic hydrogen-to-carbon ratio of the native bitumen.

Table 27

Analysis of Variance of the Conradson Carbon Residue Correlation

Source	Sum of Squares	Degrees of Freedom	Mean Sum of Squares
Total Adjusted	3617.556	36	100.49
Regression	3337.962	9	370.88
Residual	279.594	27	10.35
Lack of Fit	274.322	25	10.97
Experimental Error	5.27	2	2.63

$R^2 = \frac{3337.963}{3617.556} = 0.923$; $F = \frac{10.97}{2.63} = 4.17$; $F_{crit(25,2)} = 19.45$

Since $F < F_{crit}$, the null hypothesis is accepted at the 95 percent confidence level.

Table 28

Analysis of Variance of the Asphaltene Content Correlation

Source	Sum of Squares	Degrees of Freedom	Mean Sum of Squares
Total Adjusted	3617.556	36	100.49
Regression	3337.788	9	370.86
Residual	279.768	27	10.36
Lack of Fit	274.24	25	10.97
Experimental Error	5.53	2	2.77

$R^2 = \frac{3337.788}{3617.556} = 0.923$; $F = \frac{10.97}{2.77} = 3.96$; $F_{crit(25.2)} = 19.45$

Since $F < F_{crit}$, the null hypothesis is accepted at the 95 percent confidence level.

Table 29

Analysis of Variance of the Atomic H/C Ratio Correlation

Source	Sum of Squares	Degrees of Freedom	Mean Sum of Squares
Total Adjusted	3617.556	36	100.49
Regression	3340.970	9	371.22
Residual	276.587	27	10.24
Lack of Fit	270.718	25	10.83
Experimental Error	5.868	2	2.97

$R^2 = \frac{3340.970}{3617.556} = 0.924$; $F = \frac{10.83}{2.93} = 3.70$; $F_{crit(25,2)} = 19.45$

Since $F < F_{crit}$, the null hypothesis is accepted at the 95 percent confidence level.

Table 30

Actual and Predicted Liquid Product Yields

Run ID No.	Feed Sand	Reactor Temp., K	Solids Retention Time, min.	Actual Liquid Yield, wt.%	Predicted Liquid Yields, wt.% Eq. 4-7	Eq. 4-8	Eq. 4-9
017-PRS(R)-JD	PRS-RI	773	20	65.14	67.86	67.77	67.81
024-PRS(R)-JD	PRS-RI	798	20	71.13	69.59	69.55	69.50
020-PRS(R)-JD	PRS-RI	823	20	70.42	70.53	70.54	70.35
025-PRS(R)-JD	PRS-RI	848	20	68.85	70.70	70.73	70.36
018-PRS(R)-JD	PRS-RI	873	20	67.70	70.07	70.14	69.53
032-PRS(R)-JD	PRS-RI	798	25	71.14	69.68	69.68	69.84
042-PRS(R)-JD	PRS-RI	798	30	69.21	68.40	68.40	68.35
046-PRS(R)-JD	PRS-RI	798	17	75.94	68.86	68.80	68.42
073-PRS(S)-JD	PRS-S	823	20	49.30	50.47	50.43	50.69
079-PRS(RII)-JD	PRS-RII	823	20	60.49	60.42	60.33	60.46
010-WR-JD	WR	813	20	66.90	73.93	87.06	70.63
012-WR-JD	WR	793	33.4	65.71	70.86	84.48	67.03

V_F = 144 LPH (STP) in all experiments

PR Spring Rainbow I (PRS-RI)
PR Spring Rainbow II (PRS-RII)
PR Spring South (PRS-S)
Whiterocks (WR)

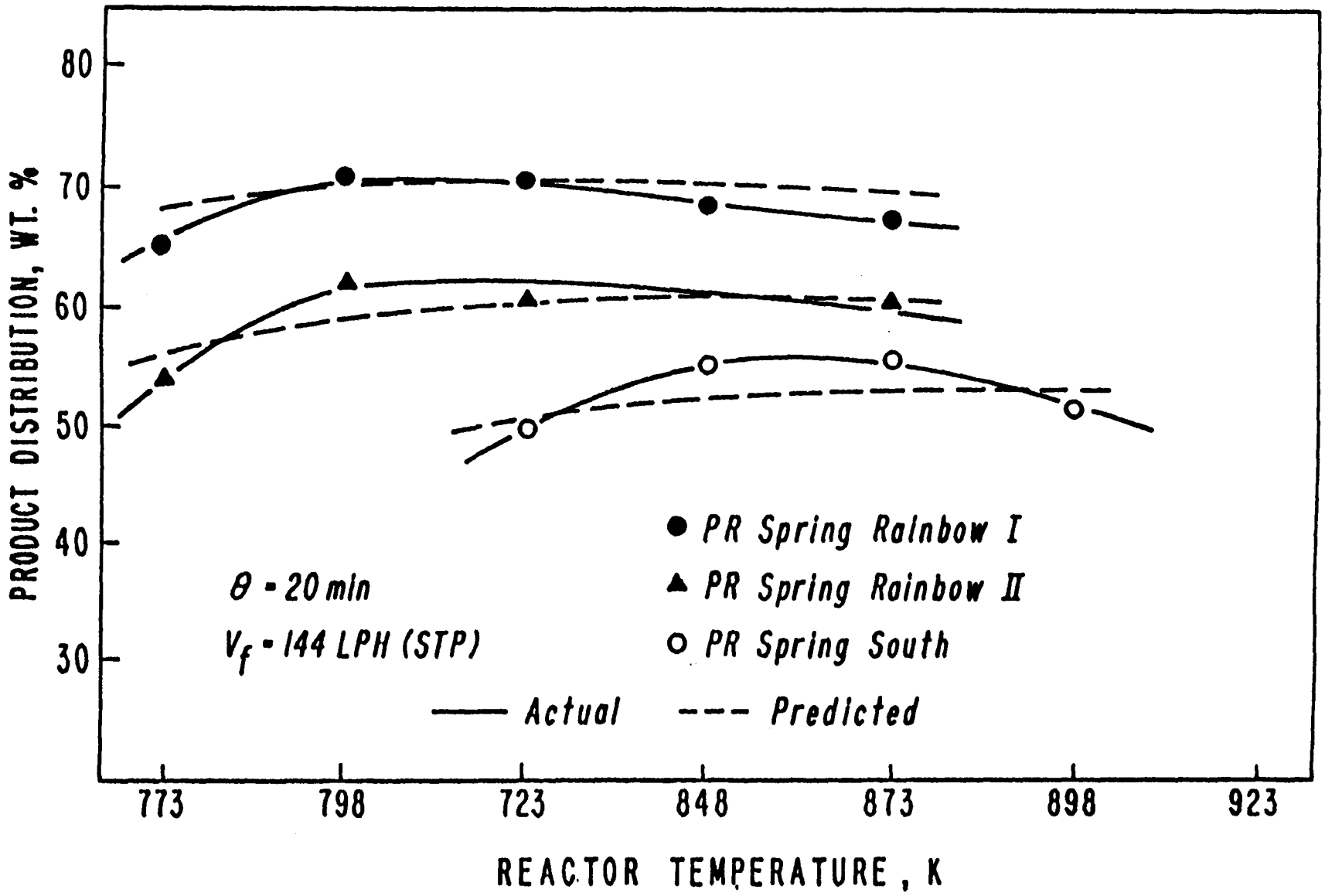

Figure 43. The effect of reactor temperature on liquid yields from the PR Spring tar sand as calculated from equation 28.

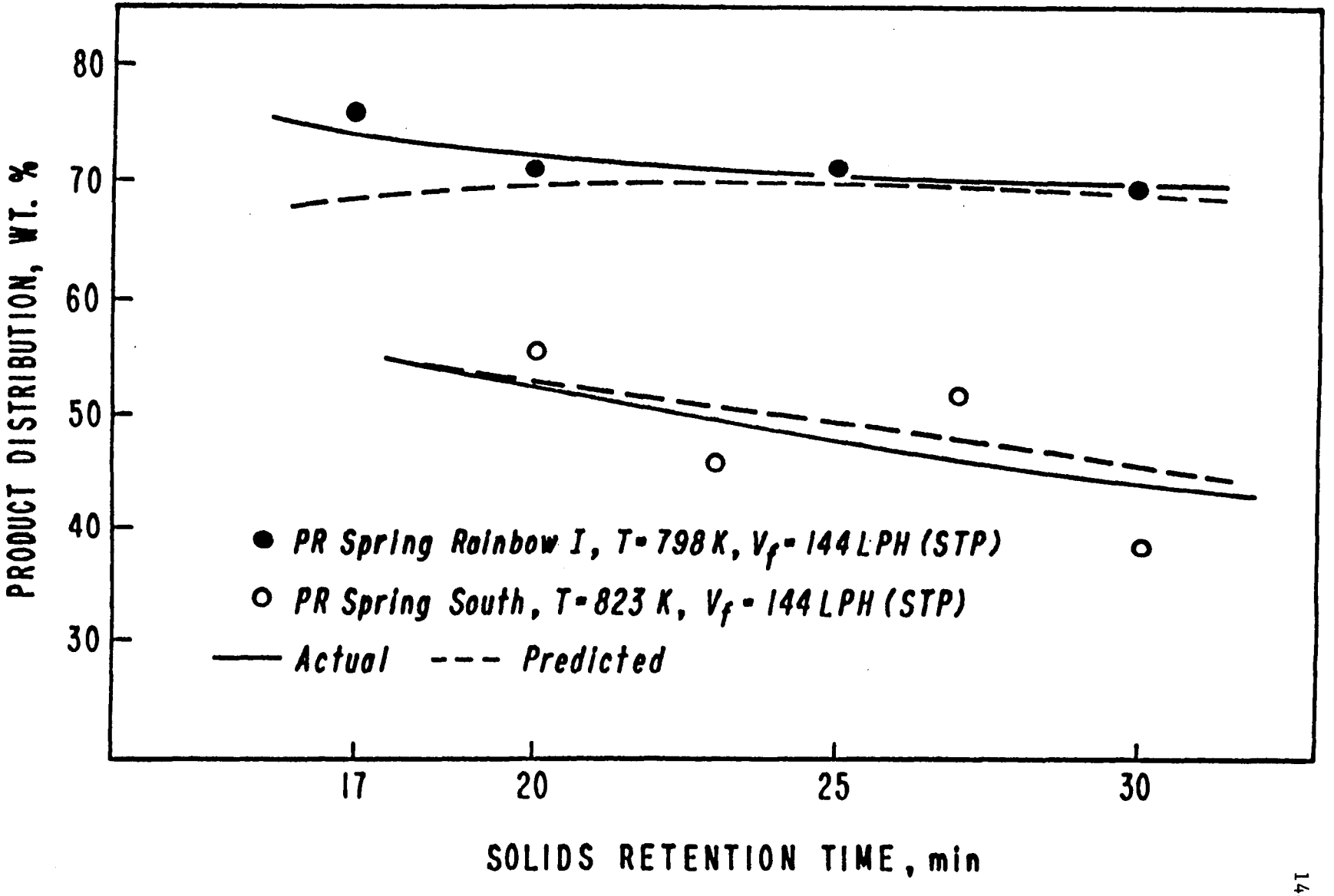

Figure 44. The effect of solids retention time on liquid yields from the PR Spring tar sand as calculated from equation 28.

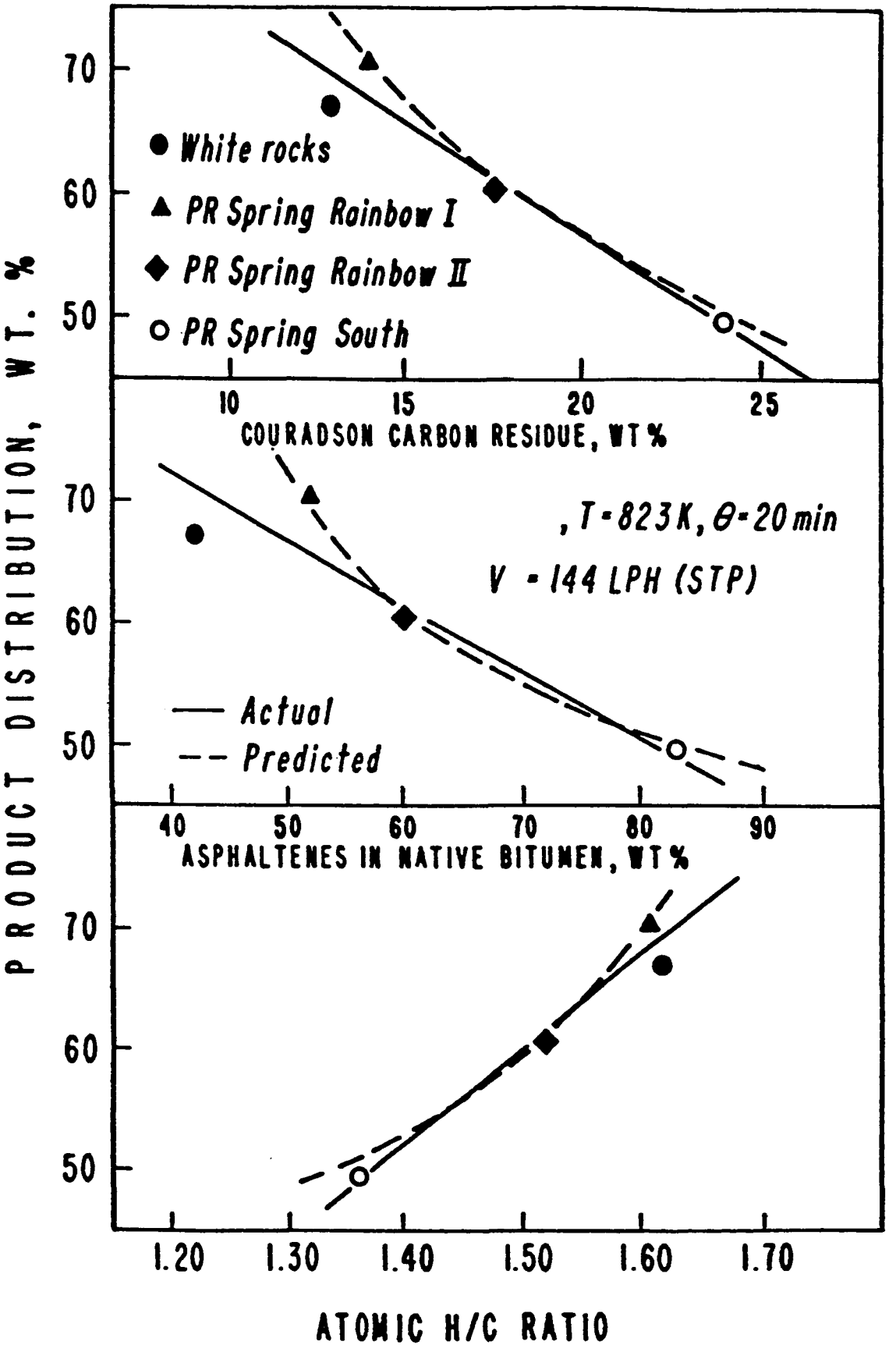

Figure 45. Trends in liquid yields with respect to native bitumen properties as calculated from equations 28, 29, and 30.

Characterization of the Liquid Products

The third objective of this investigation was to perform complete physical and chemical analyses of the liquid products. The nature of the product liquids can influence the choice of subsequent processing steps in the further upgrading or refining of the liquids. In addition, knowledge of the effect of pyrolysis process variables on the quality of liquid products could have an impact on the selection of process condition in a full-scale operation. Moreover, a comparison of the nature of the native bitumen and pyrolysis product liquids can provide an insight into the mechanism of the pyrolysis process.

The effect of process variables on liquid product properties will be discussed with respect to the mechanism of pyrolysis discussed earlier. Finally, a comparison will be made between the quality of the product liquids and the native bitumens.

The Effect of Reactor Temperature on the Quality of the Product Liquids: The effect of reactor temperature on the physical and chemical properties of the product liquids is shown in Table 31. The effect of reactor temperature on various properties is further illustrated in Figures 46 through 52. From Table 31 and Figure 46, it can be seen that the API gravity of the liquid product from the PR Spring Rainbow I (PRS-RI) tar sand did not change appreciably with changes in reactor temperature. Conversely, the API gravity of the product liquid from the PR Spring South (PRS-S) tar sand decreased with increasing reactor temperature (Figure 47), while the API gravity of the product liquid from the PR Spring Rainbow II (PRS-RII) tar sand (Figure 48) decreased slightly with increasing reactor temperature.

The decrease in API gravity with increasing temperature for PRS-S is related to the severity of thermal cracking. The PRS-S bitumen is extremely asphaltic in nature (Table 19). According to Speight,[50] asphaltenes are composed of polynuclear aromatic (PNA) structures (<6 rings/PNA) with long alkyl side chains, linked together by methylene bridges or short etheric linkages. As the reactor temperature is increased, the severity of thermal cracking is increased. Under these conditions, the alkyl side chains are cracked from the PNA groups, and the linkages between the PNA groups are broken. The alkyl groups are cracked further to smaller groups which volatilize and pass from the

Table 31

The Effect of Reactor Temperature on the Quality of Liquid Products from PR Spring Rainbow I Tar Sand

Run ID No.	017-PRS (R)-JD	024-PRS (R)-JD	020-PRS (R)-JD	025-PRS (R)-JD	018-PRS (R)-JD
Reactor Temperature, K	773	798	823	848	873
Solids Retention Time, min	20	20	20	20	20
Fluidizing Gas Flow Rate, LPH	144	144	144	144	144
Properties					
Gravity, ^{o}API @ 298 K	17.2	17.6	17.3	17.4	17.0
Viscosity, CPS @ 298 K	528.2	236.9	396.2	229.5	235.2
Pour Point, K (^{o}F)	275 (35)	272 (30)	275 (35)	275 (35)	275 (35)
Conradson Carbon Residue, wt.%	4.21	4.09	4.25	5.22	4.76
Ash, wt.%	0	0.028	0.022	0.005	
Volatility, wt.%	78.2	80.0	79.0	83.9	75.3
Elemental Analysis					
C, wt.%	86.25	86.23	86.00	84.51	86.09
H, wt.%	11.17	11.29	11.07	10.87	10.86
N, wt.%	1.33	0.98	0.99	1.35	0.99
S, wt.%	0.36	0.34	0.36	0.40	0.35
O, wt.%	1.02	1.25	1.85	3.11	1.65
Atomic H/C Ratio	1.55	1.57	1.54	1.54	1.51
Molecular wt, g mol^{-1}	321	369	335	319	308
Ni, ppm	17	12	12	16	14
V, ppm	3	< 1	< 1	2	< 1
Gradient Elution Chromatography					
Saturates, wt.%	14.81	17.11	13.87	3.18	17.38
MNA/DNA Oil, wt.%	26.81	27.79	32.91	35.26	25.73
PNA Oil, wt.%	6.34	14.44	17.68	16.63	14.37
Soft Resin, wt.%	15.16	13.35	13.67	13.89	11.94
Hard Resin, wt.%	1.88	1.19	1.56	0.85	0.97
Polar Resin, wt.%	2.94	1.58	2.25	1.51	2.23
Asphaltenes, wt.%	28.57	20.57	16.80	17.58	19.81
Noneluted Asphaltenes, wt.%	3.49	3.96	1.26	6.14	7.57

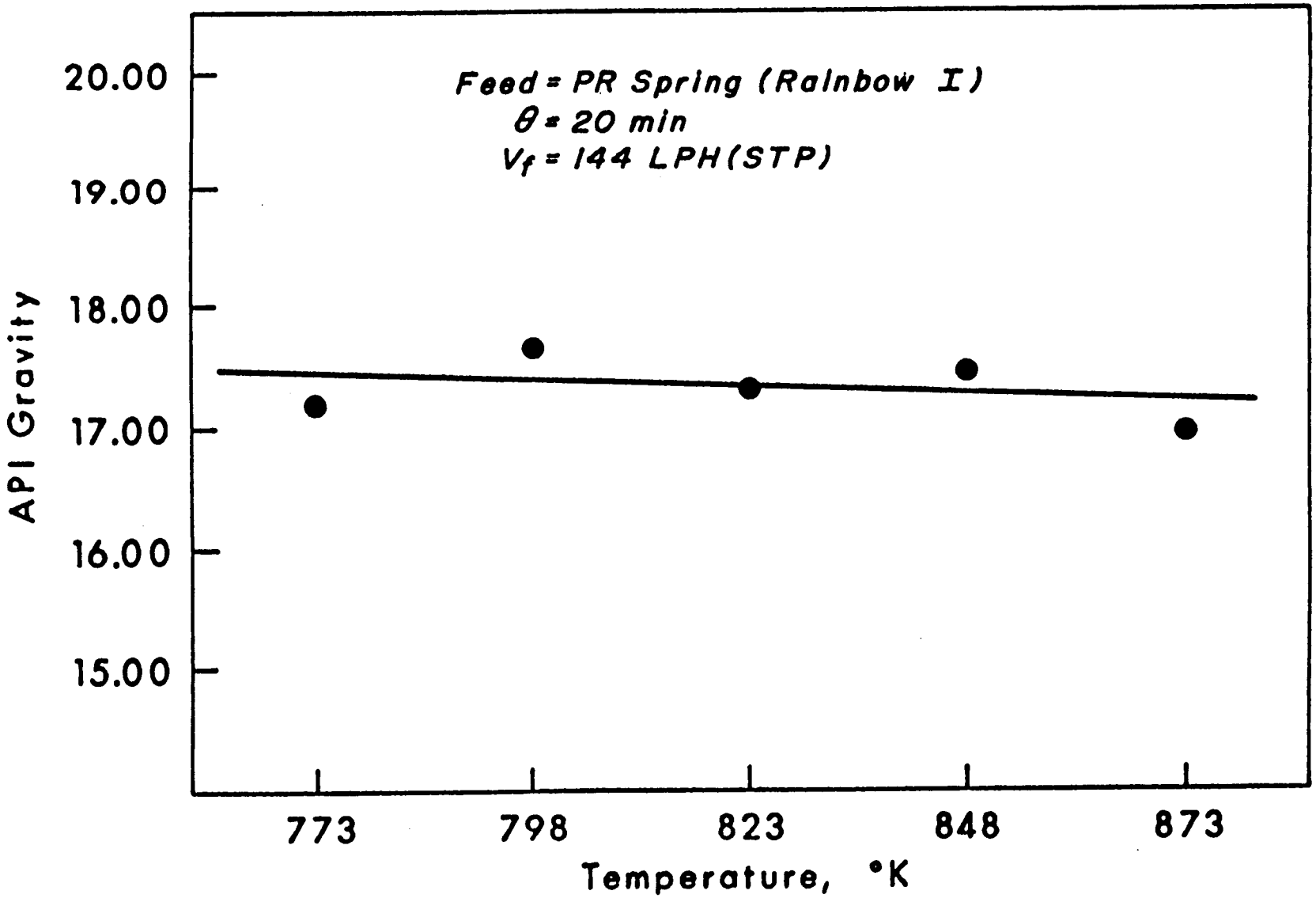

Figure 46. The effect of reactor temperature on the API gravity of product liquids from the PR Spring Rainbow I tar sand.

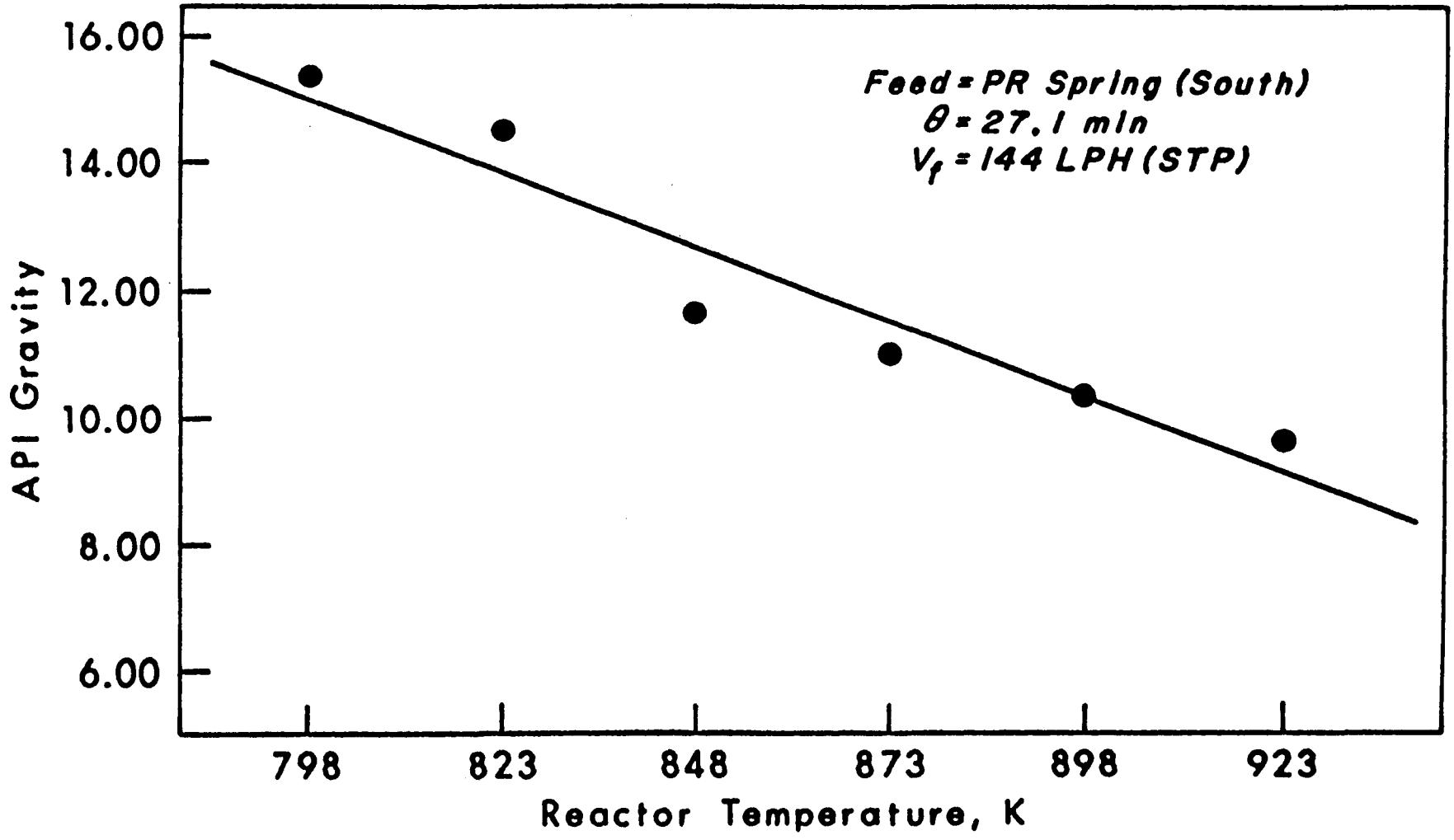

Figure 47. The effect of reactor temperature on the API gravity of product liquids from the PR Spring South tar sand.

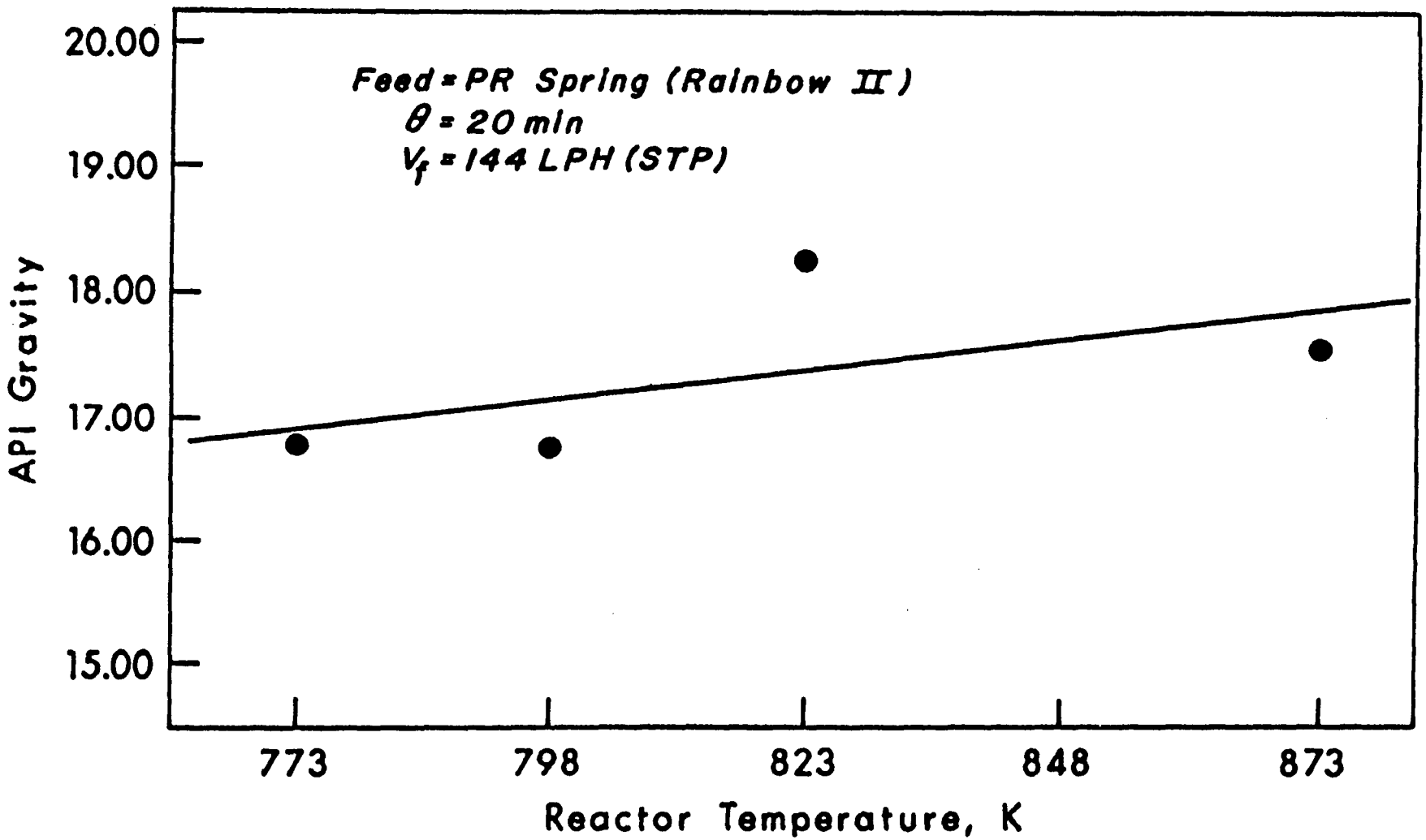

Figure 48. The effect of reactor temperature on the API gravity of product liquids from the PR Spring Rainbow II tar sand.

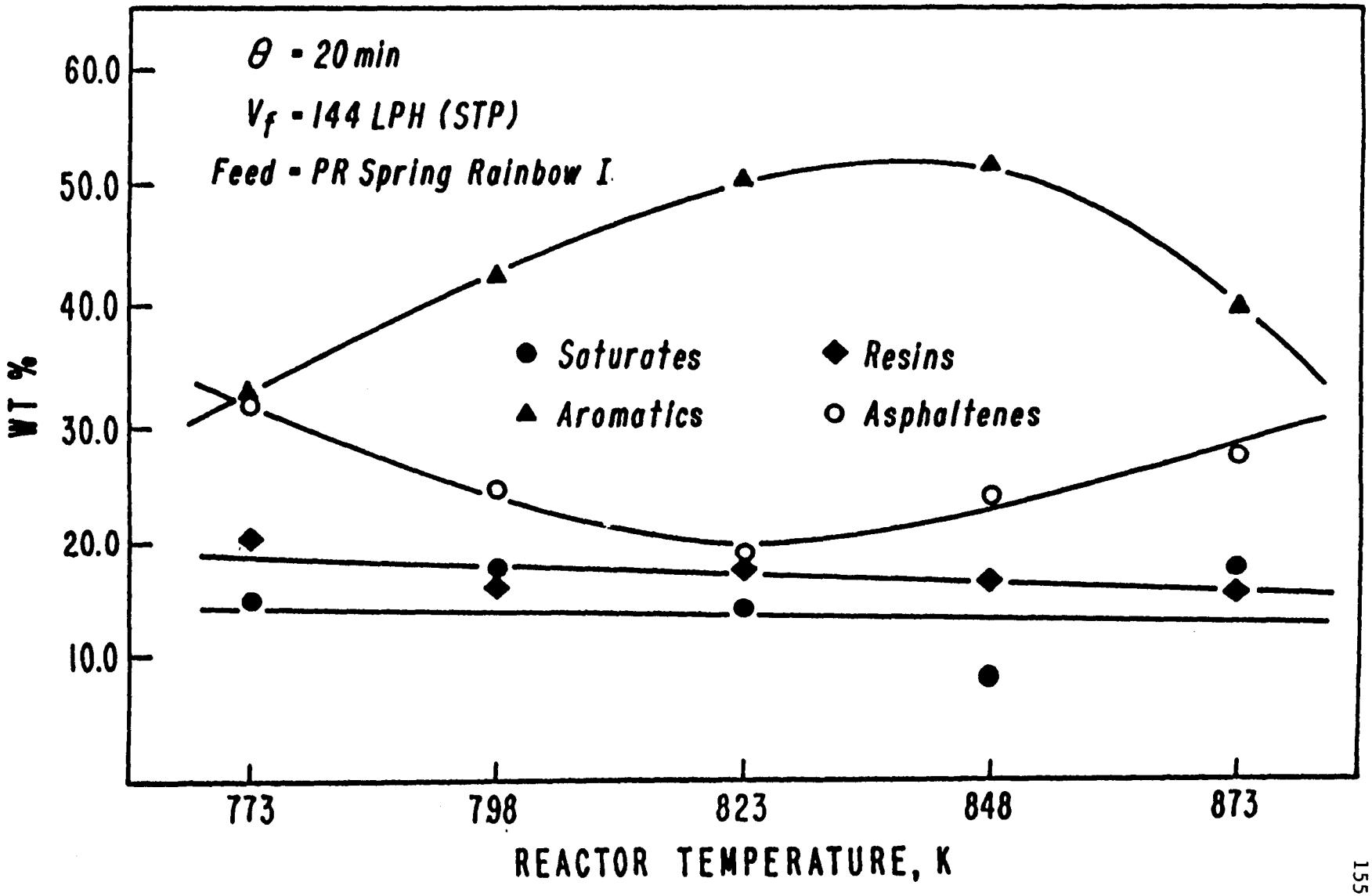

Figure 49. The effect of reactor temperature on the chemical composition of the product liquids from the PR Spring Rainbow I tar sand.

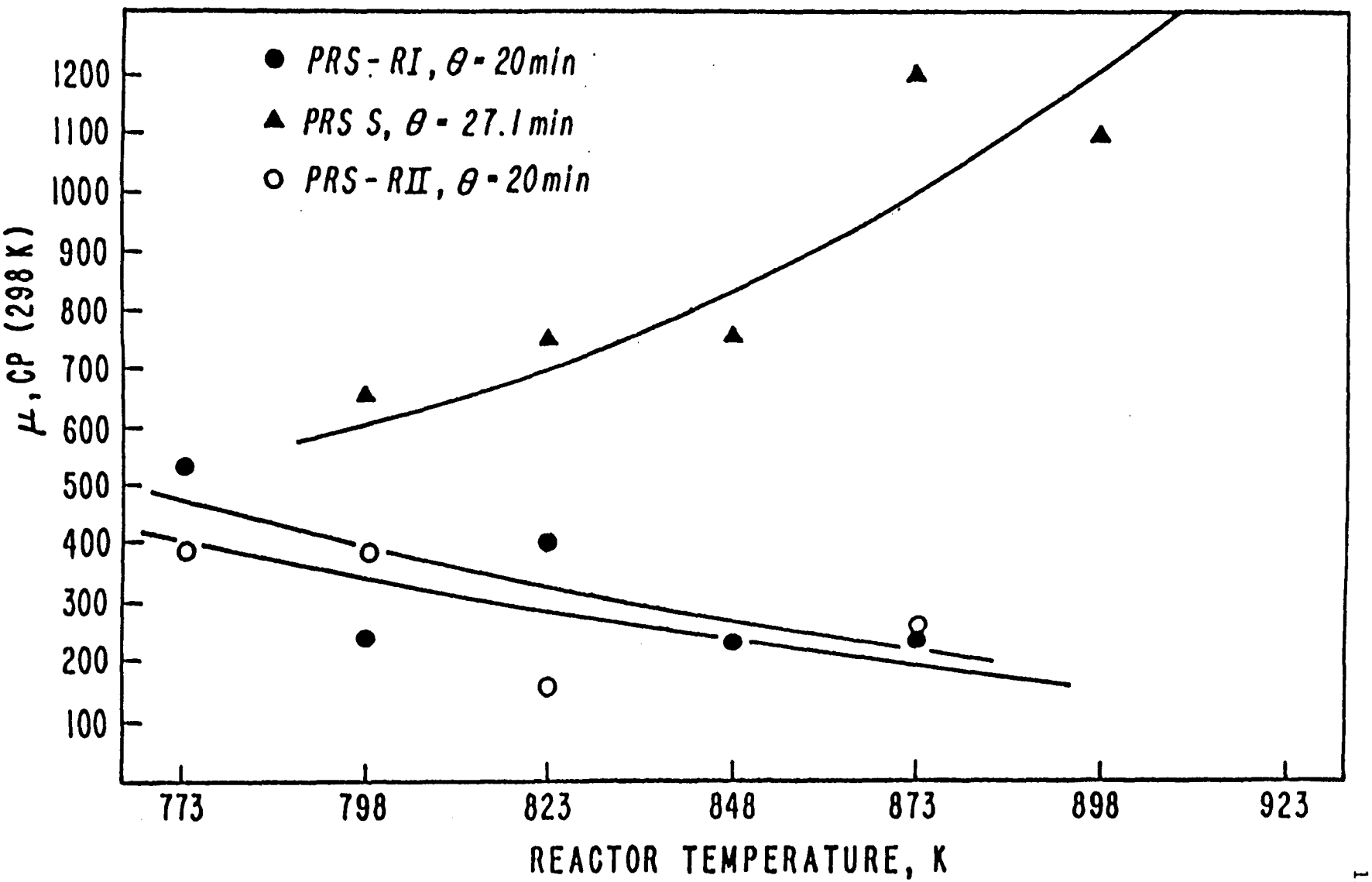

Figure 50. The effect of reactor temperature on the viscosity of the product liquids.

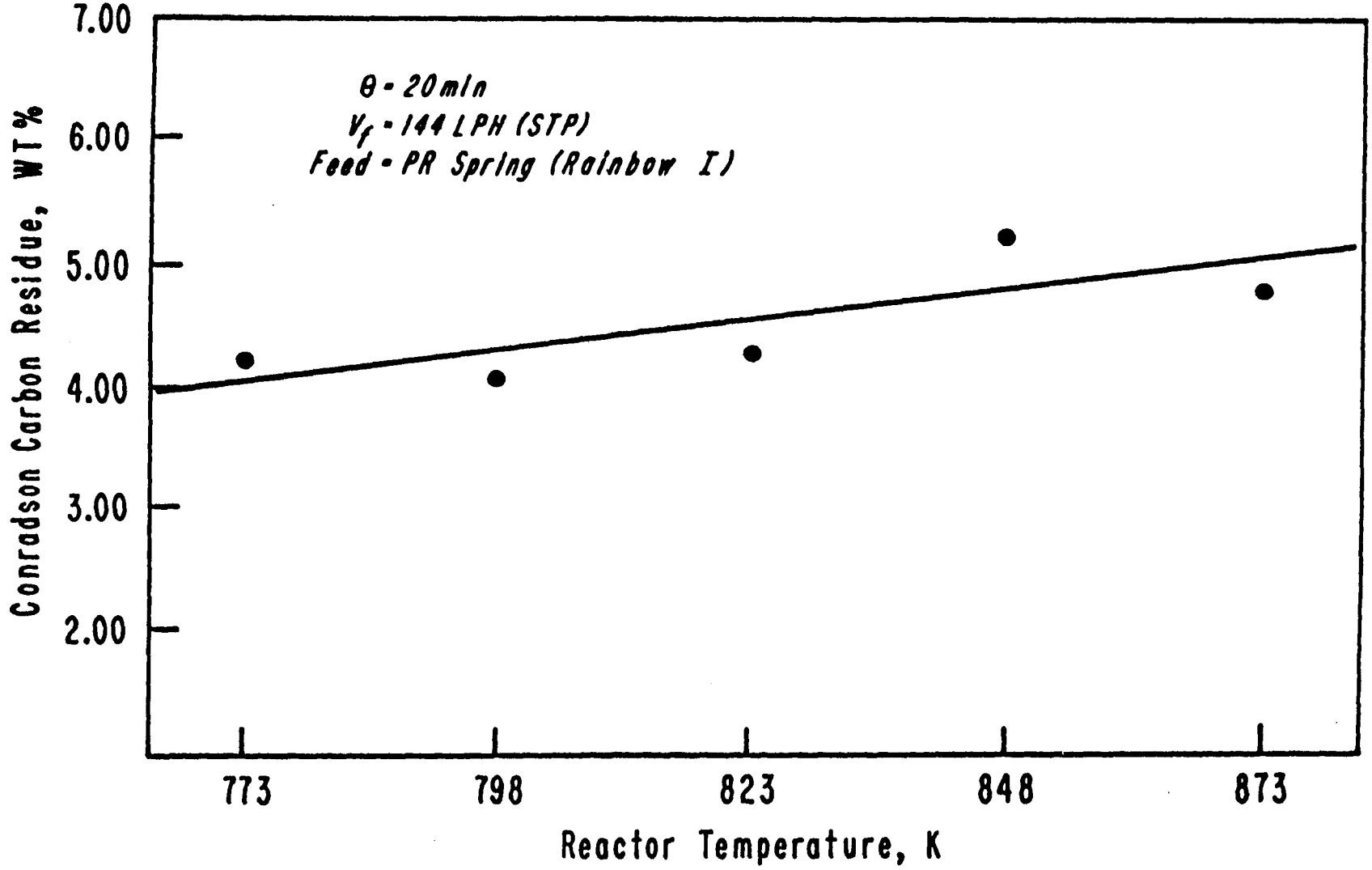

Figure 51. The effect of reactor temperature on the Conradson carbon residue of the product liquids from the PR Spring Rainbow I tar sand.

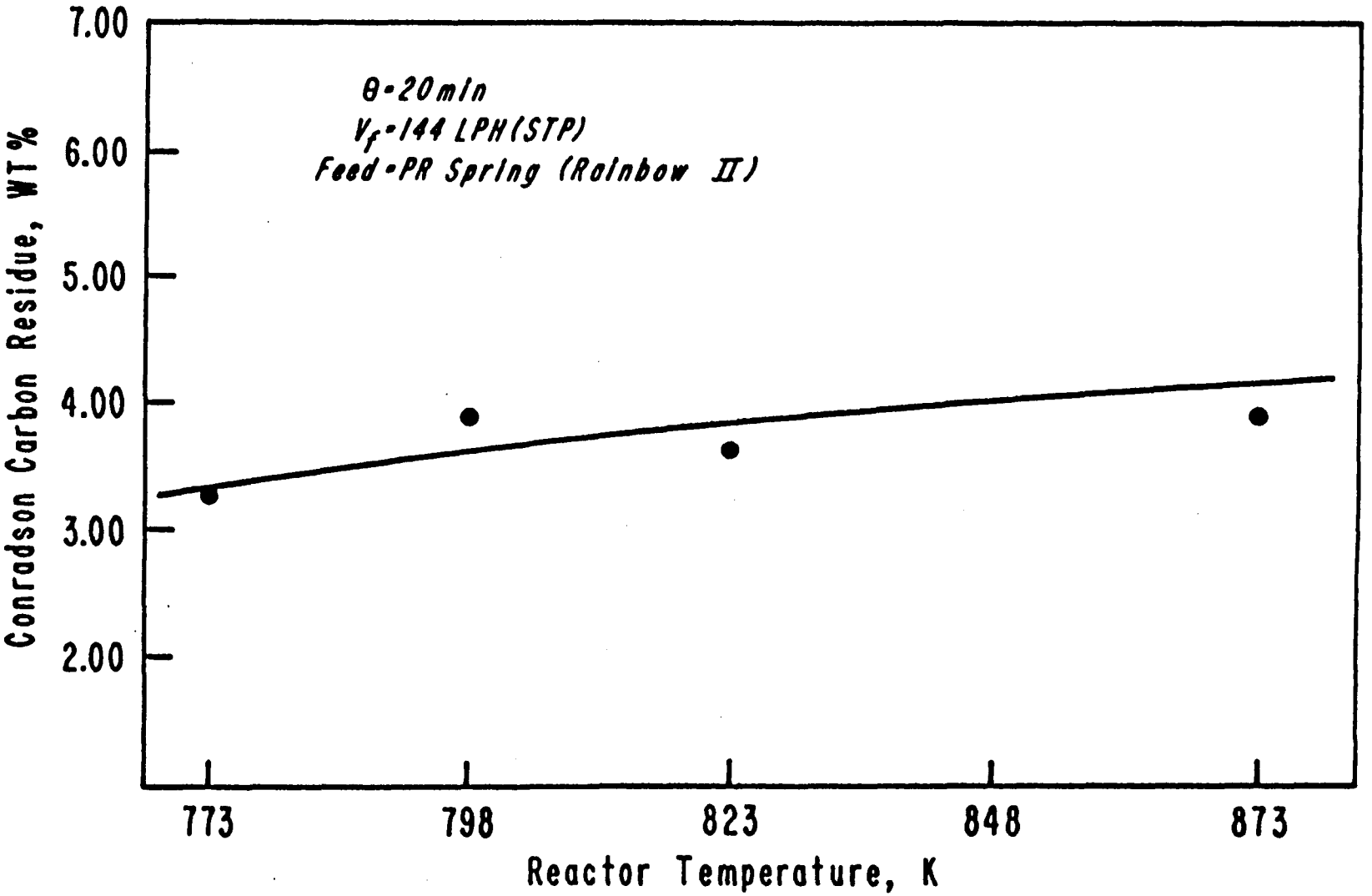

Figure 52. The effect of reactor temperature on the Conradson carbon residue of the product liquids from the PR Spring Rainbow II tar sand.

reactor in the light gas. Thus, at higher reactor temperatures, the aromaticity of the product liquids from which PRS-S is increased, and the API gravity is decreased. The opposite trend in API gravity is observed for the PRS-RII product liquid. This trend in API gravity with respect to reactor temperature is contrary to trends in the API gravity for the other product liquids, and is not consistent with trends in other liquid properties. This anomaly cannot be explained at the present time.

A breakdown of chemical compounds in the PRS-RI product liquids with respect to reactor temperature is shown in Table 31 and Figure 49. The saturates and resins remained constant over the range of reactor temperatures studied. The aromatic fraction increased initially, then decreased from 848 K to 873 K. The asphaltenes fraction exhibited an opposite trend to that of the aromatics. Because the asphaltenes consist of clustered PNA groups, the aromaticity of the liquids does not change to a great extent. Thus, the API gravity of the liquids remains essentially constant over the range of temperatures studied.

The decrease in asphaltenes from 773 K to 823 K to form aromatics (Table 31 and Figure 49) was due to the increase in the rate of thermal cracking that was discussed earlier. As the temperature increased from 848 K to 873 K, the tendency of the asphaltenes to form coke decreased.[49] A decrease in coke yield would be expected. However, the rate of condensation of aromatics to form coke also increased at the higher temperatures. Consequently, the aromatics decreased, the asphaltenes increased, and coke yields remained constant at higher reactor temperatures.

The effect of reactor temperature on the viscosity of the liquid products from the three tar sands is shown in Figure 50. The viscosity of the liquids from PRS-S was substantially higher than those of the other product liquids. Furthermore, the viscosity of the PRS-S product liquid increased with increasing temperature, while the viscosities of the PRS-RI and PRS-RII product liquids decreased slightly with increasing reactor temperature. The decrease in the viscosity of the PRS-RI product liquid is consistent with the decrease in molecular weight (Table 31). It is assumed that the decrease in the viscosity of the PRS-RII product liquids was due to a decrease in molecular weight, although the molecular weights of those liquids were not determined. The increase in the viscosity of the product liquids from PRS-S was due to the increase in the severity of thermal cracking with increasing reactor

temperature. As the severity of cracking increased, the asphaltenes condensed to form coke at a faster rate. During condensation, sticky coke precursors were formed, which increased the viscosity of the liquids. This is consistent with the sand bridging problem encountered with the PRS-S tar sand.[44]

The effects of reactor temperature on the Conradson carbon residue of the product liquids from the PRS-RI and PRS-RII tar sands are shown in Figures 51 and 52, respectively. The Conradson carbon residues of the liquids increased slightly with increasing reactor temperature. This is consistent with the trends in the other properties with respect to reactor temperature. The aromaticity of the liquids increased and the aromatics formed coke precursors as the reactor temperature increased. Therefore, the Conradson carbon residue of the liquids increased as the reactor temperature increased. The Conradson carbon residues of the product liquids from PRS-RII were lower than those of the products from PRS-RI, although the Conradson carbon residue of the PRS-RI bitumen was lower than that of the PRS-RII bitumen (Table 19). The PRS-RII bitumen contained more paraffins than the PRS-RI product liquid, while the PRS-RI product contained more aromatics and resins. The product liquids from the more aromatic bitumen would be more aromatic and, therefore, would have a higher Conradson carbon residue. The Conradson carbon residues of the product liquids from PRS-S were not determined because the product liquid sample sizes were too small to perform the test.

The simulated distillation data for the product liquids from PRS-RI, PRS-S, and PRS-RII are shown in Tables 32, 33, and 34, and Figures 53, 54, and 55, respectively. In general, the distillation curves did not change significantly with changes in reactor temperature for the product liquids from PRS-RI (Table 32 and Figure 53) and PRS-S (Table 33 and Figure 54). The volatility of the liquid from PRS-S produced at 798 K was lower than the others because the severity of thermal cracking was low at the low temperature. The result was that less volatile components in the liquid were not cracked to form more volatile compounds. The same phenomenon was observed for the products from PRS-RII (Table 34 and Figure 55). A decrease in the volatility of the PRS-RII products was also observed from 823 K to 873 K. This is consistent with the conversion of aromatics to less volatile coke precursors under more severe cracking conditions.

Table 32

The Effect of Reactor Temperature on Distillation Fractions of Product Liquids from the PR Spring Rainbow I Tar Sand

T = 773 K		T = 798 K		T = 823 K		T = 848 K		T = 873 K	
Cumulative wt.% Distilled	Boiling Temp K	Cumulative wt.% Distilled	Boiling Temp K	Cumulative wt.% Distilled	Boiling Temp K	Cumulative wt.% Distilled	Boiling Temp K	Cumulative wt.% Distilled	Boiling Temp K
IBP	371.9	IBP	346.2	IBP	366.0	IBP	355.7	IBP	354.3
5	509.2	5	504.0	5	501.1	5	493.0	5	490.1
10	545.2	10	539.3	10	535.6	10	526.8	10	523.9
20	603.2	20	597.3	20	592.1	20	580.4	20	583.3
30	560.1	30	644.3	30	639.9	30	625.2	30	628.9
40	694.9	40	688.3	40	685.4	40	669.2	40	679.5
50	730.2	50	727.2	50	719.9	50	708.2	50	720.6
60	758.1	60	754.4	60	751.5	60	737.5	60	751.5
70	795.5	70	791.1	70	788.9	70	771.3	70	797.0
78.2	838.6	80.0	838.6	79.0	838.6	80	814.6	75.3	838.6
						83.9	838.6		

Table 33

The Effect of Reactor Temperature on Distillation Fractions of Product Liquids from the PR Spring South Tar Sand

T = 798 K		T = 823 K		T = 848 K		T = 873 K		T = 898 K		T = 923 K	
Cumulative wt.% Distilled	Boiling Temp K	Cumulative wt.% Distilled	Boiling Temp K	Cumulative wt.% Distilled	Boiling Temp K	Cumulative wt.% Distilled	Boiling Temp K	Cumulative wt.% Distilled	Boiling Temp K	Cumulative wt.% Distilled	Boiling Temp K
IBP	354.2	IBP	388.8	IBP	375.5	IBP	388.0	IBP	388.0	IBP	389.5
5	502.6	5	488.6	5	483.3	5	498.9	5	487.9	5	490.1
10	533.4	10	520.9	10	513.6	10	527.5	10	520.2	10	523.1
20	591.4	20	574.5	20	563.5	20	576.0	20	573.1	20	571.6
30	643.5	30	625.9	30	608.3	30	623.0	30	622.3	30	617.8
40	693.5	40	673.6	40	651.6	40	667.0	40	668.5	40	662.6
50	733.9	50	713.3	50	693.5	50	706.7	50	713.3	50	705.9
60	775.7	60	747.8	60	728.7	60	743.4	60	752.9	60	844.1
69.6	838.6	70	783.8	70	766.9	70	783.1	70	802.1	70	787.5
		80	822.7	80	812.4	80	830.0	76.9	838.6	78.8	838.6
				85.0	838.6	81.1	838.6				

Table 34

The Effect of Reactor Temperature on Distillation Fractions of Product Liquids from the PR Spring Rainbow I Tar Sand

T = 773 K		T = 798 K		T = 823 K		T = 848 K	
Cumulative wt.% Distilled	Boiling Temp K	Cumulative wt.% Distilled	Boiling Temp K	Cumulative wt.% Distilled	Boiling Temp K	Cumulative wt.% Distilled	Boiling Temp K
IBP	358.7	IBP	366.0	IBP	360.1	IBP	347.6
5	501.8	5	487.9	5	449.7	5	476.9
10	551.0	10	525.3	10	498.2	10	520.2
20	631.1	20	583.3	20	559.1	20	584.8
30	702.3	30	637.7	30	614.2	30	645.0
40	750.7	40	684.7	40	665.6	40	700.8
50	802.9	50	722.1	50	711.1	50	744.1
65.4	838.6	60	756.6	60	739.7	60	791.9
		70	788.2	70	777.2	66.7	838.6
		80.7	838.6	82.9	838.6		

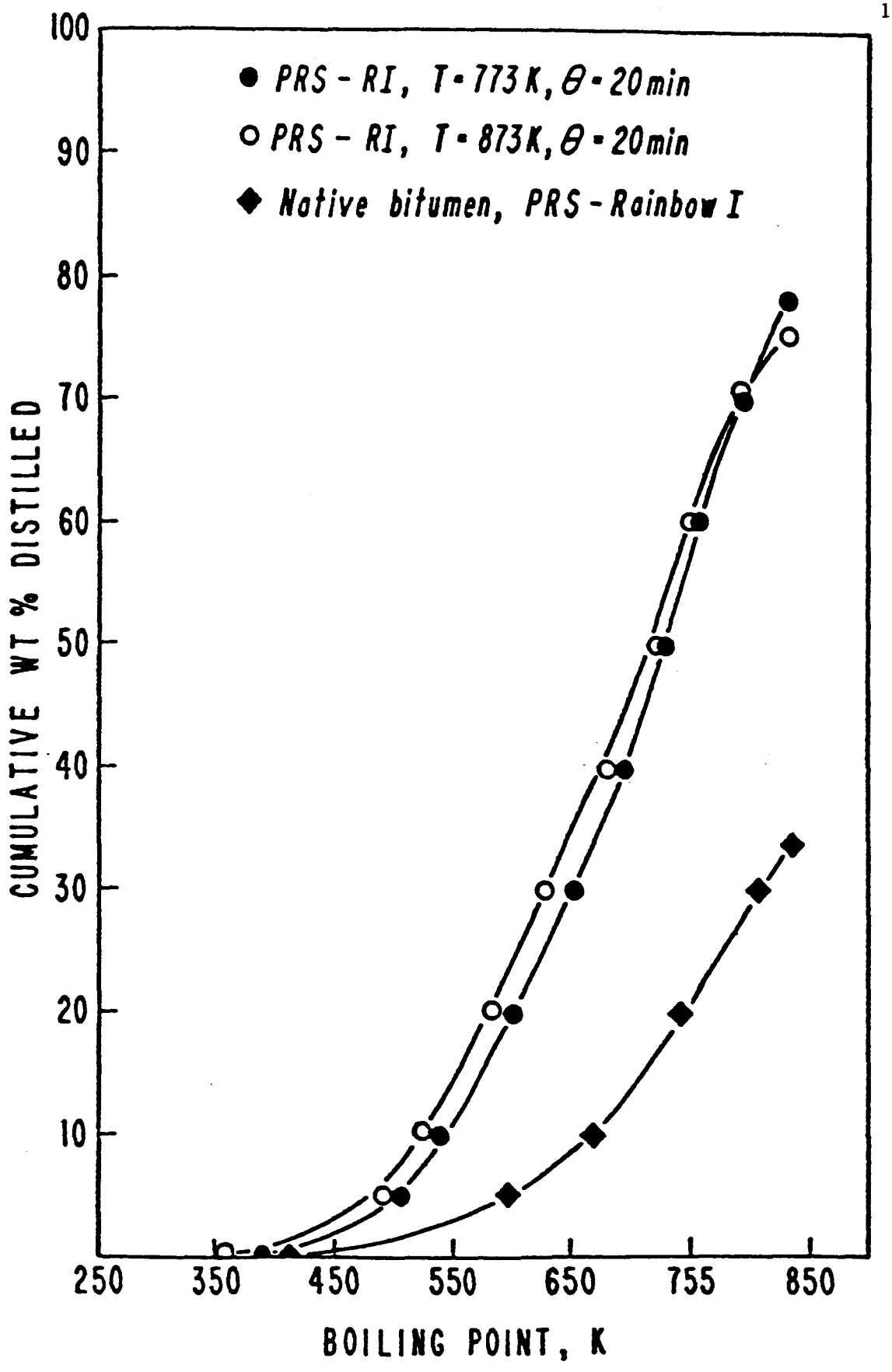

Figure 53: Distillation curves of selected product liquids from the PR Spring Rainbow I tar sand.

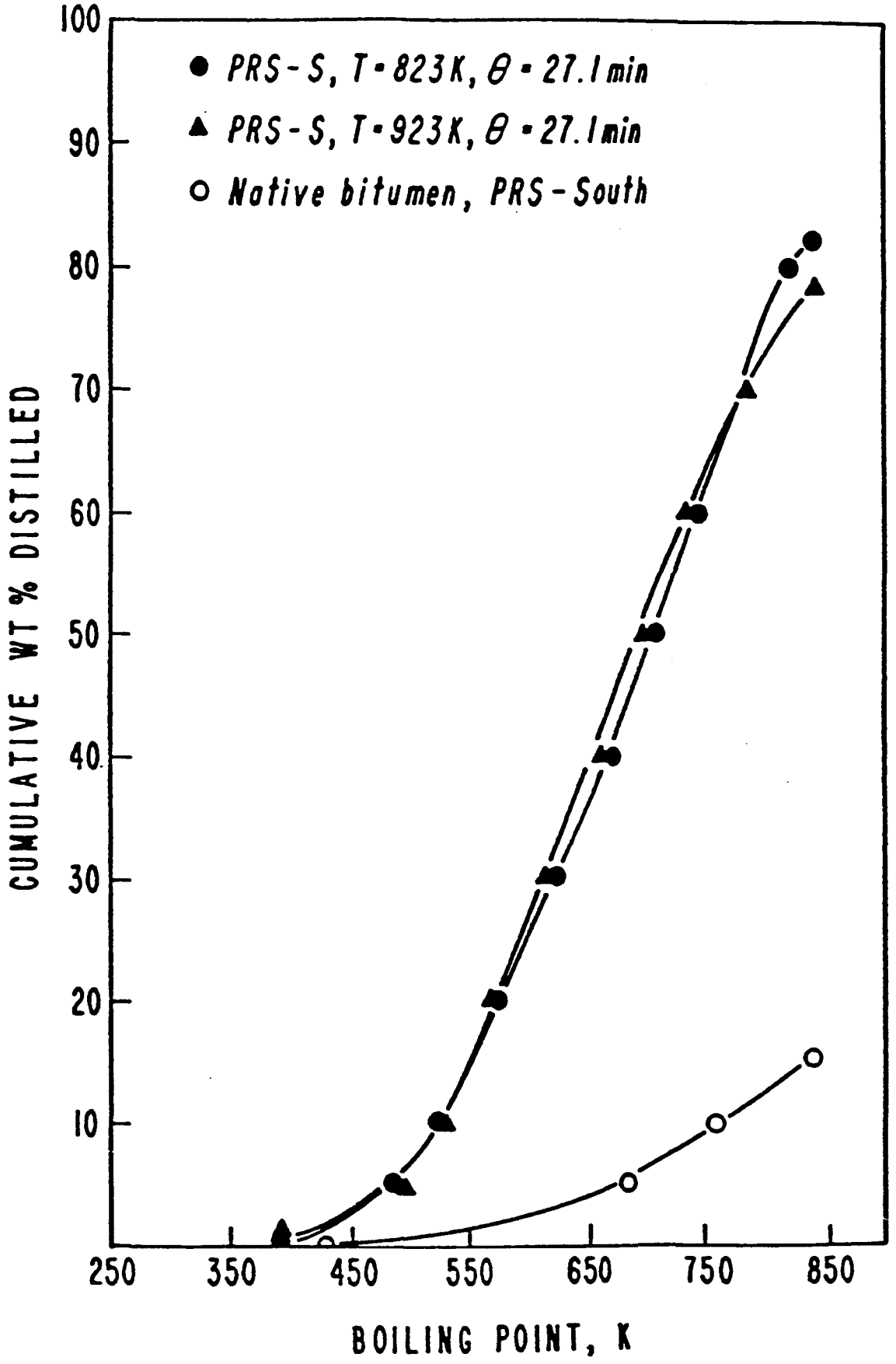

Figure 54: Distillation curves of selected product liquids from the PR Spring South tar sand.

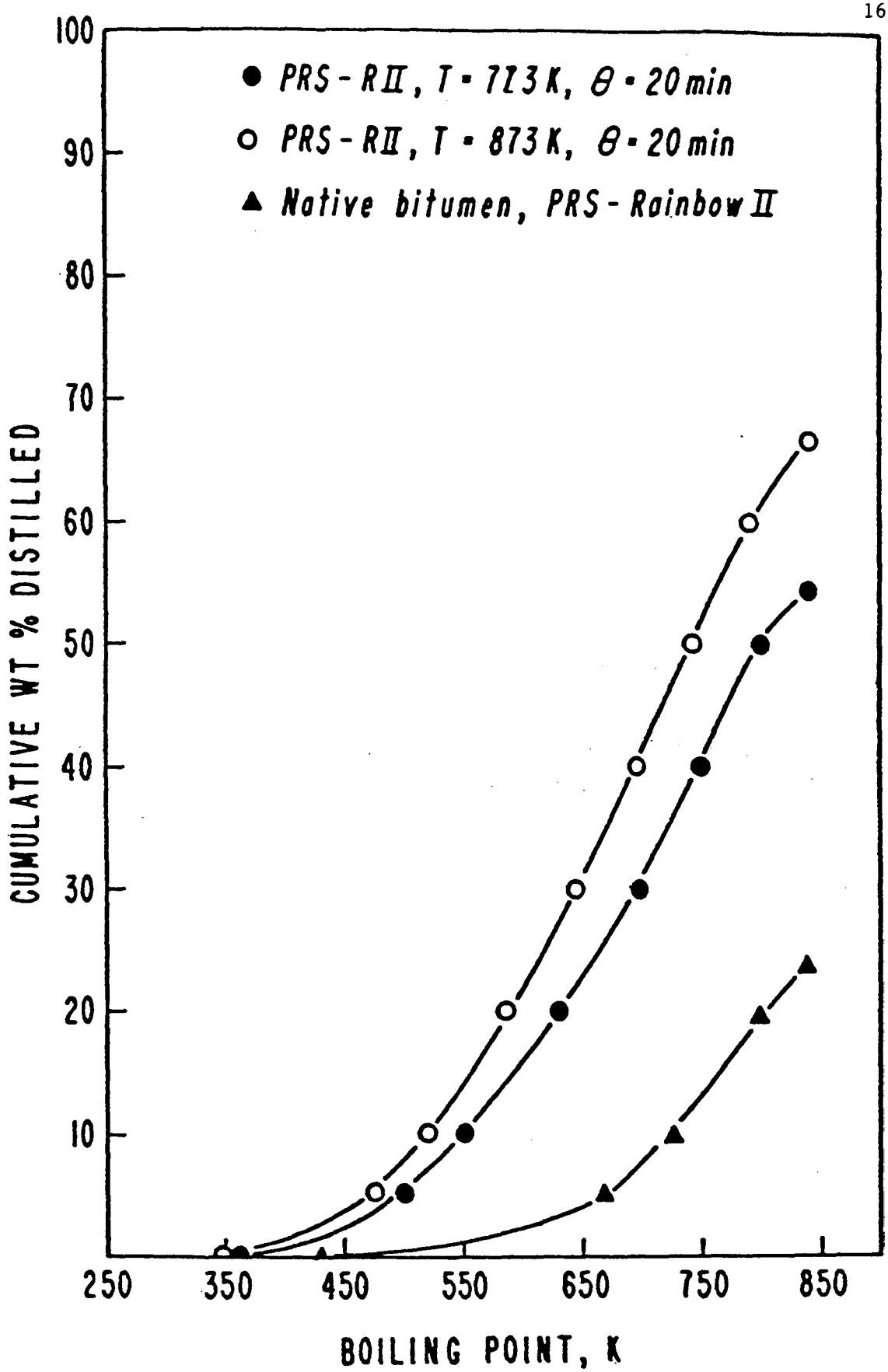

Figure 55: Distillation curves of selected product liquids from the PR Spring Rainbow II tar sand.

The effect of reactor temperature on the fractionation of the product liquids from PRS-RI is further illustrated in Figure 56. The gasoline, middle distillate, and 839 K^+ resid fractions remained essentially constant with respect to reactor temperature. The trend in the heavy ends was nearly identical to that of the total liquids. Overall, the fractionation of the product liquids remained essentially constant over the range of reactor temperatures studied. The molecular weight of the product liquids decreased with increasing reactor temperature (Table 31). This is consistent with the increased severity of thermal cracking at higher temperatures.

The Effect of Solids Retention Time on the Quality of the Product Liquids: The effect of the solids retention time on the physical and chemical properties of the product liquids from the PR Spring Rainbow I tar sand is presented in Table 35. In addition, the effect of the solids retention time on various properties of product liquids from the PR Spring Rainbow I and PR Spring South tar sands are shown in Figures 57 through 60. From Table 35 and Figures 57 and 58, it can be seen that the API gravities of the product liquids from PRS-RI and PRS-S decreased with increasing solids retention time. The thermal cracking in the reactor was enhanced by longer solids retention times, as was discussed previously. The increased severity of thermal cracking caused an increase in the aromaticity of the product liquids, resulting in increased density or decreased API gravity.

The trends in API gravity with respect to solids retention time are consistent with the trends in chemical composition of the product liquids as shown in Table 35 and Figure 59. The aromaticities in the liquids increased only slightly with increasing solids retention time, along with a similar increase in the asphaltene content. The saturates content decreased significantly from 15 percent by weight to approximately 7.5 weight percent. These trends are consistent with the decrease in API gravity of the product liquids, and are indicative of the enhancement of thermal cracking by increased solids retention times.

The Conradson carbon residue of the product liquids from PRS-RI increased with increasing solids retention time, as shown in Table 35 and Figure 60. Again, this is consistent with the trends in other properties. That is, an increase in Conradson carbon residue concurs with the increase in

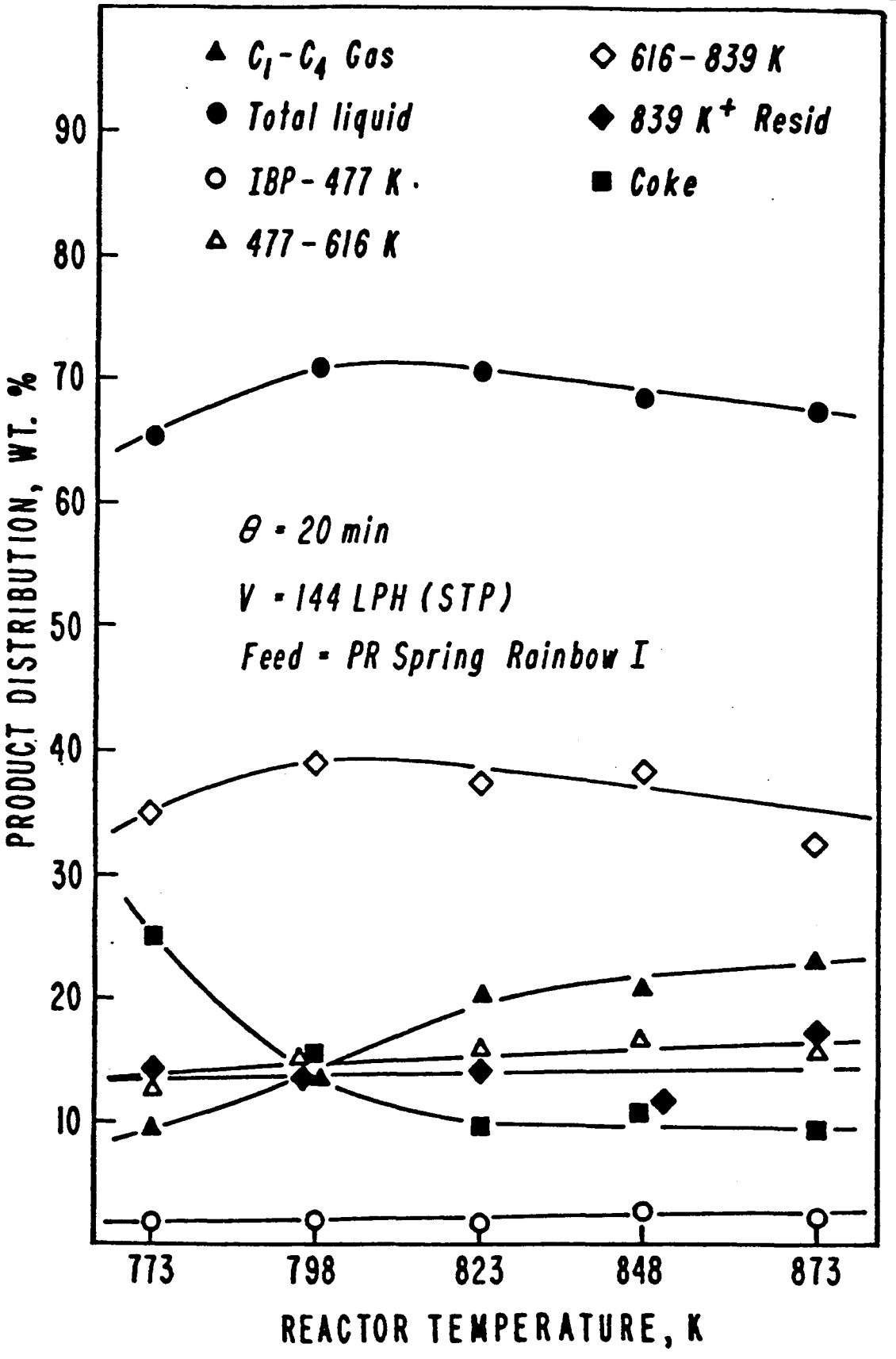

Figure 56: The effect of reactor temperature on distillation fractions of product liquids from the PR Spring Rainbow I tar sand.

Table 35

The Effect of Solids Retention Time on the Quality of Liquid Products from PR Spring Rainbow I Tar Sand

Run ID No.	046-PRS (R)-JD	024-PRS (R)-JD	032-PRS (R)-JD	042-PRS (R)-JD
Reactor Temperature, K	798	798	798	798
Solids Retention Time, min	17	20	25	30
Fluidizing Gas Flow Rate, LPH	144	144	144	144
Properties				
Gravity, ^{o}API @ 298 K	18.1	17.6	16.3	17.1
Viscosity, CPS @ 298 K	587.7	236.9	587.5	670.2
Pour Point, K (^{o}F)	272 (30)	272 (30)	272 (30)	272 (30)
Conradson Carbon Residue, wt.%	3.57	4.09	2.76	8.68
Ash, wt.%	0.0305	0.028	0.008	0.0215
Volatility, wt.%	91.6	80.0	79.2	85.65
Elemental Analysis				
C, wt.%	80.38	86.23	86.19	84.95
H, wt.%	10.49	11.29	11.33	11.39
N, wt.%	0.89	0.98	1.18	1.02
S, wt.%	0.34	0.34	0.31	0.35
O, wt.%	7.06	1.25	1.01	2.15
Atomic H/C Ratio	1.57	1.57	1.58	1.61
Molecular wt, g mol^{-1}	341	369	325	342
Ni, ppm	13	12	16	17
V, ppm	2	< 1	< 1	< 1
Gradient Elution Chromatography				
Saturates, wt.%	10.23	17.11	6.19	10.29
MNA/DNA Oil, wt.%	35.99	27.79	40.86	33.75
PNA Oil, wt.%	12.12	14.44	9.43	12.31
Soft Resin, wt.%	13.07	13.35	14.05	14.13
Hard Resin, wt.%	0.95	1.19	0.29	0.87
Polar Resin, wt.%	1.80	1.58	1.18	1.06
Asphaltenes, wt.%	20.17	20.57	21.32	18.94
Noneluted Asphaltenes, wt.%	5.68	3.96	6.68	8.65

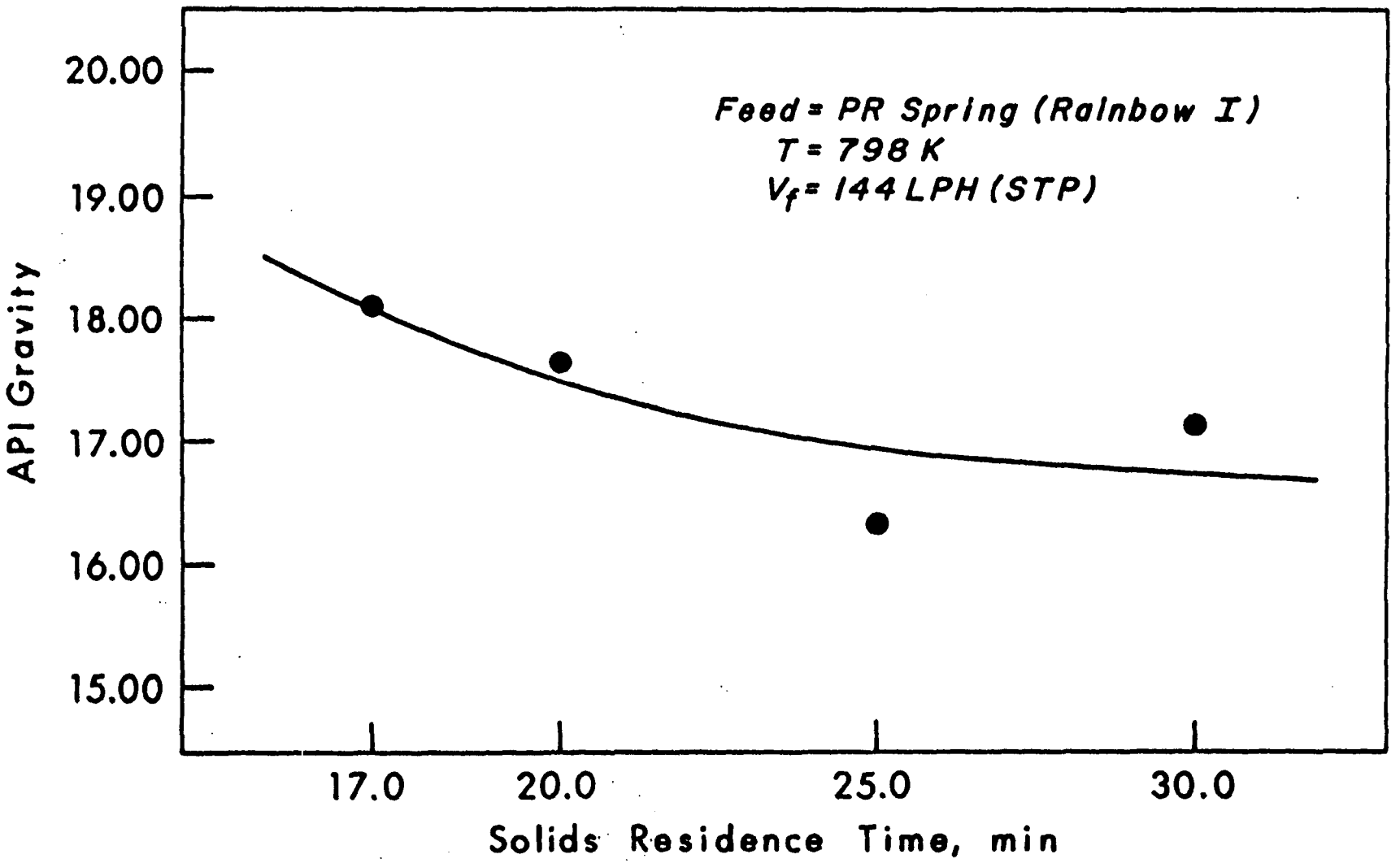

Figure 57: The effect of solids retention time on the API gravity of the product liquids from the PR Spring Rainbow I tar sand.

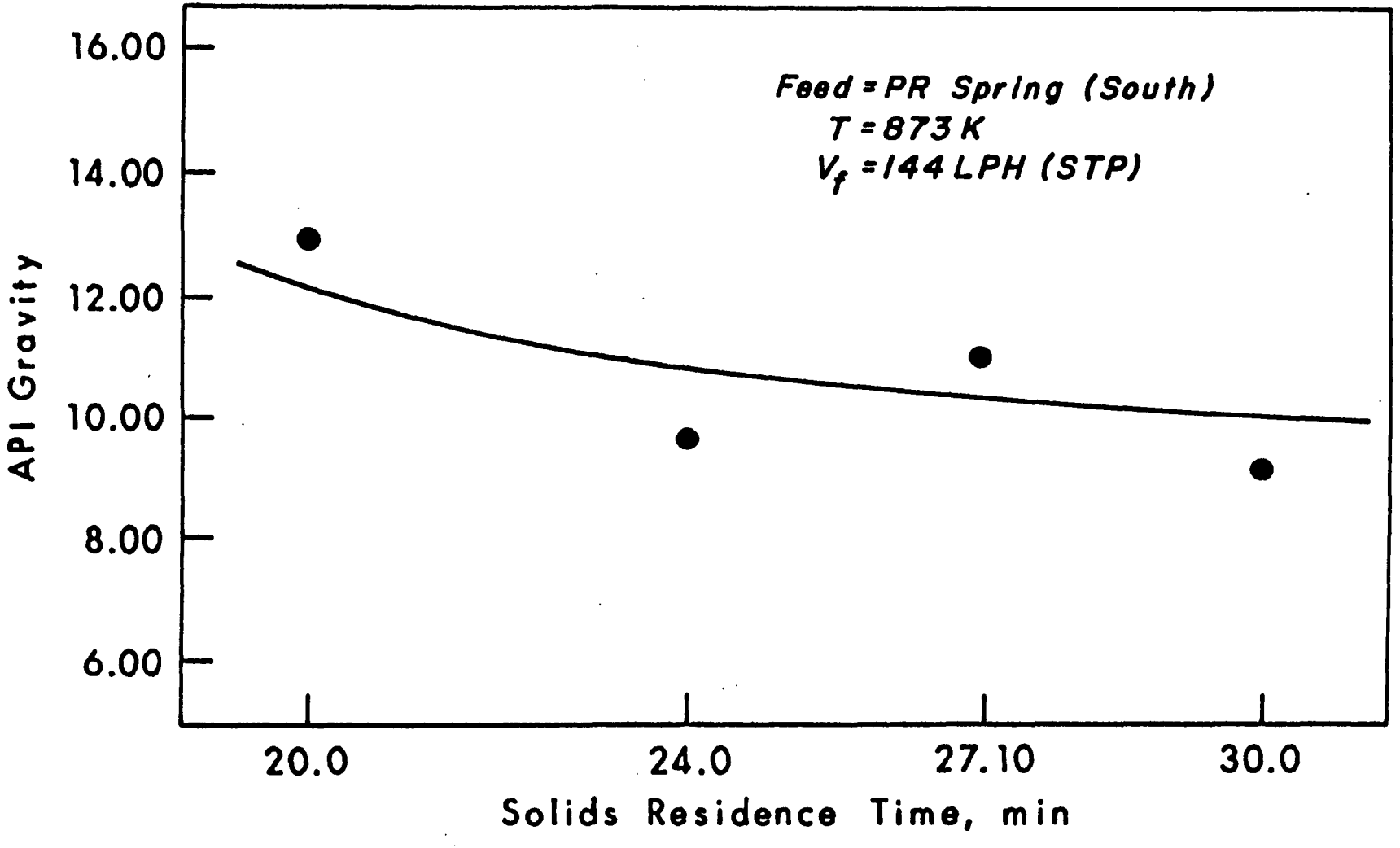

Figure 58: The effect of solids retention time on the API gravity of the product liquids from the PR Spring South tar sand.

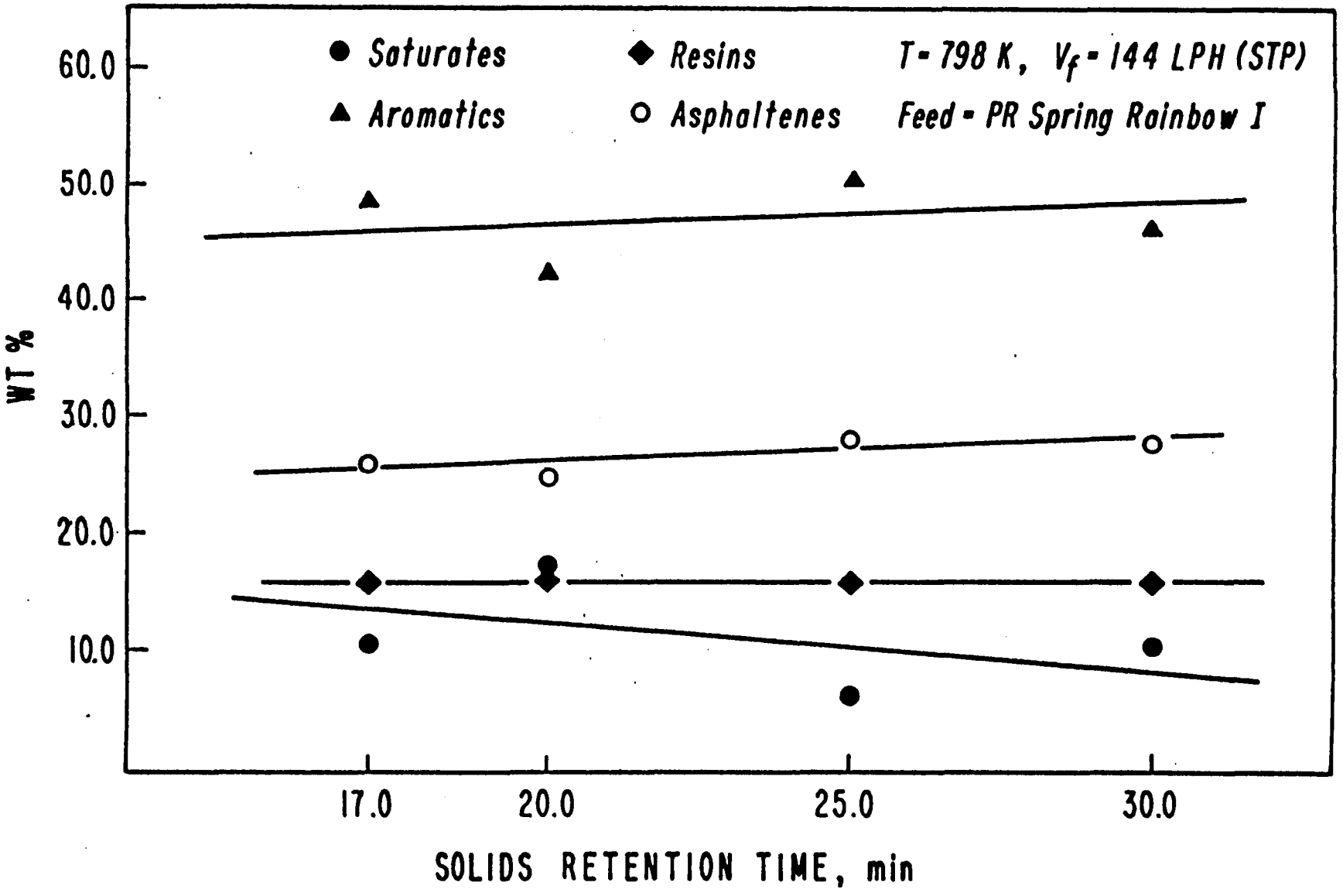

Figure 59: The effect of solids retention time on the chemical composition of the product liquids from the PR Spring Rainbow I tar sand.

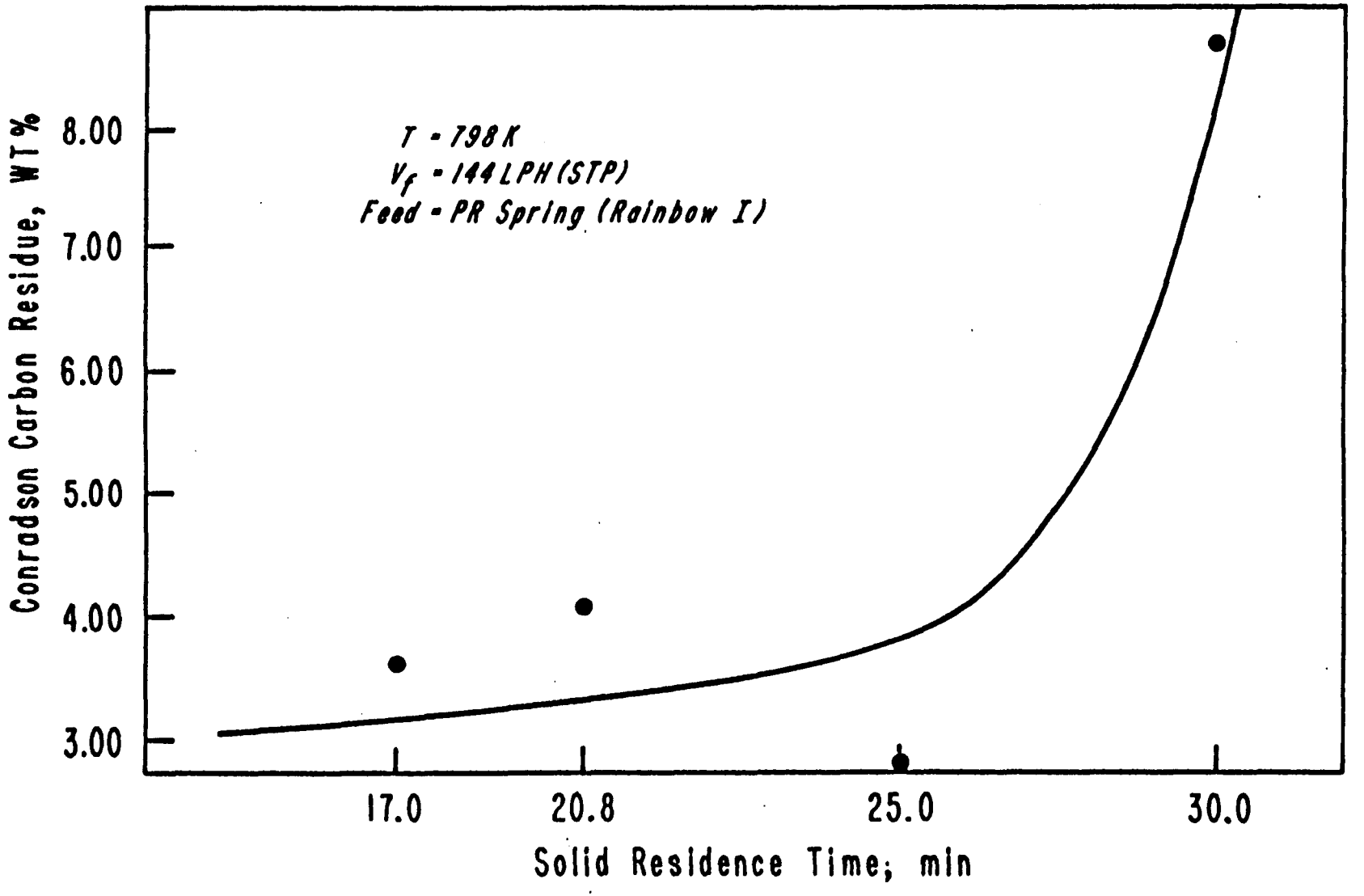

Figure 60: The effect of solids retention time on the Conradson carbon residue of the product liquids from the PR Spring Rainbow I tar sand.

other properties. That is, an increase in Conradson carbon residue concurs with the increase in aromatics and asphaltenes (Figure 59) and the decrease in saturates.

Simulated distillation data for the product liquids from PRS-RI and PRS-S with respect to solids retention time are presented in Tables 36 and 37. The volatility of the PRS-RI product liquid decreased as the residence time increased from 17 minutes to 20 minutes, and it increased as the residence time increased from 25 minutes to 30 minutes. The volatility of the PRS-S product liquids decreased steadily with the increase in solids retention time. This decrease in volatility is expected in view of the changes in API gravity and chemical composition of the liquids. The increased thermal cracking at longer solids retention times caused a decrease in more volatile components in the liquid, resulting in decreased volatility of the liquid products.

The pour point and atomic hydrogen-to-carbon ratio of the product liquids remained essentially constant with respect to solids residence time. Also, there appeared to be no clear trend in the viscosity of product liquids with respect to solids retention time.

The Extent of Upgrading of Liquid Products: It is important to discuss the extent of upgrading of liquid products that takes place during the pyrolysis process. The good quality of the liquid products is one distinct advantage of a thermal processing scheme over alternate bitumen-sand separation technologies. Hence, a comparison of the properties of the native bitumens and their product liquids is warranted.

Properties of the liquid products from the pyrolysis of the PR Spring Rainbow I, PR Spring South, and PR Spring Rainbow II tar sands are presented in Tables 38, 39, and 40, respectively, along with the properties of the native bitumens. It can be seen that in all cases the API gravity and volatility of the product liquids were increased substantially over the native bitumens, while the viscosity, Conradson carbon residue, pour point, and molecular weight were markedly decreased. In addition, the amount of preferred components (saturates, mono-, di-, and polynuclear aromatics) in the product liquids were increased at the expense of asphaltenes. Moreover, the amounts of heteroatoms were reduced in the product liquids, indicating that a portion of the heteroatoms were deposited in the coke.

Table 36

The Effect of Solids Retention Time on Distillation Fractions of Product Liquids from the PR Spring Rainbow I Tar Sand

θ = 17 min		θ = 20 min		θ = 25 min		θ = 30 min	
Cumulative wt.% Distilled	Boiling Temp K	Cumulative wt.% Distilled	Boiling Temp K	Cumulative wt.% Distilled	Boiling Temp K	Cumulative wt.% Distilled	Boiling Temp K
IBP	407.9	IBP	346.2	IBP	418.9	IBP	352.8
5	509.9	5	504.0	5	505.5	5	479.1
10	545.2	10	539.3	10	540.8	10	524.6
20	600.2	20	597.3	20	599.5	20	583.3
30	644.3	30	644.3	30	646.5	30	635.5
40	684.7	40	688.3	40	692.7	40	681.7
50	717.0	50	727.2	50	726.5	50	718.4
60	739.0	60	754.4	60	756.6	60	745.6
70	765.4	70	791.1	70	793.3	70	779.4
80	791.9	80	838.6	79.2	838.6	80	813.9
90	828.6					85.7	838.6
91.6	838.6						

Table 37

The Effect of Solids Retention Time on Distillation Fractions of Product Liquids from the PR Spring South Tar Sand

θ = 17 min		θ = 20 min		θ = 25 min		θ = 30 min	
Cumulative wt.% Distilled	Boiling Temp K	Cumulative wt.% Distilled	Boiling Temp K	Cumulative wt.% Distilled	Boiling Temp K	Cumulative wt.% Distilled	Boiling Temp K
IBP	391.0	IBP	399.0	IBP	388.0	IBP	363.1
5	484.9	5	487.9	5	498.9	5	483.5
10	511.4	10	515.1	10	527.5	10	512.1
20	553.2	20	558.4	20	576.0	20	558.4
30	592.1	30	598.0	30	623.0	30	602.4
40	628.1	40	636.9	40	667.0	40	646.5
50	665.6	50	675.9	50	706.7	50	691.3
60	697.1	60	711.1	60	743.0	60	733.9
70	728.7	70	746.3	70	783.1	70	781.6
80	758.8	80	788.9	80	830.0	79.3	838.6
90	794.8	88.9	838.6	81.1	838.6		
99.3	838.6						

Table 38

Analysis of the Liquid Product from the PR Spring Rainbow I Tar Sand

Reactor Temperature, K:	823
Solids Retention Time, min:	20
Fluidizing Gas Velocity, LPH (STP):	144
Product Yields, wt.%	
Gas	20.1
Liquid	70.4
Coke	9.5

Property	PR Spring Rainbow I	Pyrolysis Liquid Product
Gravity, ^{o}API	7.8	17.3
Viscosity, cps	8268.8 (@ 373 K)	396.2 (@ 298 K)
Pour Point, K (^{o}F)	372.1 (210)	274.7 (35)
Conradson Carbon Residue, wt.%	14.0	4.25
Ash, wt.%	3.3	0.01
Simulated Distillation		
Volatility, wt.%	31.9	79.0
IBP-400^{o}F, wt.%	1.3	2.7
400-650^{o}F, wt.%	5.1	23.1
650-1050^{o}F, wt.%	25.6	53.2
1050^{o}F^{+} Residue, wt.%	68.1	21.0
Elemental Analysis		
C, wt.%	84.66	86.23
H, wt.%	11.34	11.29
N, wt.%	1.30	0.98
S, wt.%	0.53	0.34
O, wt.%	1.75	1.25
Atomic H/C Ratio	1.61	1.57
Molecular Weight, g mol^{-1}	702	369
Ni, ppm	110	12
V, ppm	10	< 1
Gradient Elution Chromatography		
Saturates, wt.%	9.5	13.9
MNA/DNA Oil, wt.%	10.2	32.9
PNA Oil, wt.%	11.4	17.7
Soft Resin, wt.%	13.9	13.7
Hard Resin, wt.%	1.1	1.6
Polar Resin, wt.%	2.0	2.2
Asphaltenes, wt.%	31.3	16.8
Noneluted Asphaltenes, wt.%	20.6	1.2

Table 39

Analysis of the Liquid Product from the PR Spring South Tar Sand

Reactor Temperature, K:	823
Solids Retention Time, min:	20
Fluidizing Gas Velocity, LPH (STP):	144
Product Yields, wt.%	
Gas	30.6
Liquid	40.3
Coke	20.1

Property	PR Spring South	Pyrolysis Liquid Product
Gravity, ^{o}API	8.8	10.2
Viscosity, cps	10,071 (@ 483 K)	548.5 (@ 298 K)
Pour Point, K (^{o}F)	433 (320)	283 (50)
Conradson Carbon Residue, wt.%	24.0	7.2
Ash, wt.%	1.9	0.01
Simulated Distillation		
Volatility, wt.%	14.3	97.7
IBP-400^{o}F, wt.%	1.3	36.4
400-650^{o}F, wt.%	1.3	36.4
650-1050^{o}F, wt.%	13.3	56.4
1050^{o}F^{+} Residue, wt.%	85.7	2.3
Elemental Analysis		
C, wt.%	81.73	86.02
H, wt.%	9.29	10.21
N, wt.%	1.37	1.05
S, wt.%	0.39	0.31
O, wt.%	7.22	2.07
Atomic H/C Ratio	1.36	1.42
Molecular Weight, g mol^{-1}	1561	337
Ni, ppm	102	3
V, ppm	8	< 1
Gradient Elution Chromatography		
Saturates, wt.%	4.1	7.4
MNA/DNA Oil, wt.%	5.3	35.6
PNA Oil, wt.%	1.0	3.9
Soft Resin, wt.%	4.0	17.8
Hard Resin, wt.%	1.8	2.4
Polar Resin, wt.%	1.1	2.7
Asphaltenes, wt.%	55.7	26.4
Noneluted Asphaltenes, wt.%	27.1	3.8

Table 40

Analysis of the Liquid Product from the PR Spring Rainbow II Tar Sand

Reactor Temperature, K:	823
Solids Retention Time, min:	20
Fluidizing Gas Velocity, LPH (STP):	144
Product Yields, wt.%	
Gas	20.6
Liquid	60.5
Coke	18.9

Property	PR Spring Rainbow II	Pyrolysis Liquid Product
Gravity, ^{o}API	11.8	18.3
Viscosity, cps	9,000 (@ 473 K)	158.4 (@ 298 K)
Pour Point, K (^{o}F)	433 (320)	271.9 (30)
Conradson Carbon Residue, wt.%	17.4	3.6
Ash, wt.%	1.4	0.01
Simulated Distillation		
Volatility, wt.%	22.8	82.9
IBP-400^{o}F, wt.%	0.5	7.6
400-650^{o}F, wt.%	2.2	23.1
650-1050^{o}F, wt.%	20.1	52.2
1050^{o}F^{+} Residue, wt.%	77.2	17.1
Elemental Analysis		
C, wt.%	81.44	85.30
H, wt.%	10.31	11.06
N, wt.%	1.37	0.83
S, wt.%	0.44	0.24
O, wt.%	6.27	2.24
Atomic H/C Ratio	1.52	1.56
Molecular Weight, g mol^{-1}	1381	351
Ni, ppm	126	2
V, ppm	3	< 1
Gradient Elution Chromatography		
Saturates, wt.%	15.8	13.4
MNA/DNA Oil, wt.%	3.5	37.1
PNA Oil, wt.%	9.0	5.7
Soft Resin, wt.%	5.8	17.4
Hard Resin, wt.%	2.3	3.5
Polar Resin, wt.%	3.6	2.6
Asphaltenes, wt.%	35.9	15.7
Noneluted Asphaltenes, wt.%	24.1	4.6

The atomic H/C ratio of the product liquids for the PR Spring Rainbow I was lower than that of the native bitumen, which is consistent with the increase in aromaticity and loss of saturates due to thermal cracking. The atomic hydrogen-to-carbon ratios of the product liquids from the PR Spring South and PR Spring Rainbow II were increased over the native bitumens, which is indicative of the conversion of the asphaltenes to more desirable components.

The amounts of trace metals in the product liquids were substantially reduced from the amounts of trace metals in the native bitumens. With the exception of the nickel content of the PR Spring Rainbow I product, the metals contents of the product liquids are within the acceptable limits for a refinery feedstock. The nickel balance for the PR Spring Rainbow I tar sand is shown in Table 41. Approximately 93 percent of the nickel in the bitumen appears in the coke. The nickel content of the product liquid from PR Spring Rainbow I was high due to the relatively low coke formation from that tar sand. Because the coke formations from PR Spring South and PR Spring Rainbow II were higher, nearly all of the trace metals appeared in the coke.

The differences in liquid properties between the pyrolysis liquid products and the native bitumens represent a substantial improvement in liquid product quality over the native bitumens. The product liquids are amenable to transportation by pipeline because of the relatively low viscosity, pour point, and API gravity. The relatively high volatilities, along with the low asphaltene contents, Conradson carbon residues, molecular weights, heteroatom contents, and metal contents of the product liquids indicate that they could be upgraded to refinery feedstock quality by mild to moderate hydrotreating.

CONCLUSIONS AND RECOMMENDATIONS

Conclusions

After the Arab oil embargo of 1973, a great deal of emphasis was placed on the development of alternative fossil energy resources. The fluidized-bed pyrolysis process was developed as a method of producing a bitumen-derived liquid that would be compatible with existing petroleum refining technology. Recently, petroleum prices have stabilized, causing a decreased interest in the development of alternate sources of fossil fuels. Nevertheless, conventional petroleum resources are

Table 41

Nickel Balance for the PR Spring Rainbow I Tar Sand

	Native Bitumen	Product Liquid	Coke
Nickel Content, ppm	110	12	---
Amount of Material,* g	118.79	83.65	11.27
Amount of Nickel, g	0.0131	0.001	0.0121

*Bitumen, product liquid, or coke

finite, and political instabilities in the Middle East could result in an interruption in crude oil imports. Consequently, the importance of developing alternative sources of energy cannot be overlooked. Accordingly, this investigation was undertaken to determine the ability of the bench-scale fluidized-bed pyrolysis system to process bituminous sands with variable properties. Several conclusions were drawn from this investigation:

1) Fluidized-bed pyrolysis is a viable method for producing a bitumen-derived liquid from the tar sands of the PR Spring deposit of Utah. Pipeline-quality hydrocarbon liquids can be produced from a deep-mined bituminous sand, as well as a highly oxidized outcrop sample.

2) The maximum liquid yields are obtained at a reactor temperature of 798 K for the PR Spring Rainbow I and PR Spring Rainbow II tar sands. The maximum liquid yield for the PR Spring South tar sand occurs at a temperature of 823 K, because of the extremely asphaltic nature of that bitumen.

3) The liquid yield increases as solids retention time is decreased for PR Spring Rainbow I and PR Spring South tar sands. It is projected that liquid yields could be increased further with decreases in the retention time of solids below 20 minutes. Unfortunately, the design of the system and the nature of the bitumens in the PR Spring tar sands impose a limit on the throughput capacity and, therefore, the solids retention time of the reactor.

4) The coke yield is insensitive to reactor temperature above 798 K, and is relatively insensitive to changes in solids retention time. Increases in coke yield at lower reactor temperatures are due to unconverted high molecular weight asphaltic material which is not vaporized from the sand surface at the lower temperatures. The consistency of the coke yields indicates that at least a portion of the energy requirement of the process could be supplied by burning the coke in a combustion reactor.

5) There is a definite relationship between certain properties of the native bitumen and the pyrolysis product distribution. Bitumens with lower Conradson carbon residue, higher volatility, higher atomic H/C ratio, and lower asphaltene content yield more liquid, less gas, and less coke than

lesser-quality bitumens. The API gravity of the native bitumen does not appear to correlate with product distribution.

6) Substantial liquid upgrading occurs during the pyrolysis process. The product liquids are of pipeline quality due to the relatively low viscosity, low pour point, and higher API gravity. The improvement in Conradson carbon residue, chemical composition, heteroatom content, metal content, and volatility of the product liquids over the native bitumens indicate that they can be upgraded to refinery feedstock quality by mild to moderate hydrotreatment.

NOMENCLATURE

F	Feed sand rate, gm/hr.
H_f	Effective multiphase reaction rate coefficient, min^{-1}
N	In equation 27, the reactor temperature (°C), solids retention time (min), or bitumen property.
T	Reactor temperature, K
V_f	Fluidizing Gas Velocity, LPH (STP)
V_p	Volumetric flow rate of product gases, LPH (STP)
V_{STP}	Molar volume of gas at STP (22.414 liters/mole)
W	Total weight of sand in fluidized bed, gm
X	Fraction of feed bitumen remaining in the reactor
X_1	Coded reactor temperature, unitless
X_2	Coded solids retention time, unitless
X_3	Coded bitumen property Conradson carbon residue, asphaltene content, or atomic H/C ratio, unitless
Y	Liquid yield, wt.% of bitumen fed
μ	Viscosity, centipoise
θ	Solids retention time, min.
θ_b	Bubble contact time, min.

FLUIDIZED BED PYROLYSIS OF BITUMEN-IMPREGNATED SANDSTONE FROM THE CIRCLE CLIFFS TAR SAND DEPOSIT

Francis V. Hanson — Associate Professor
DoWon Shun — Graduate Student

INTRODUCTION

The Circle Cliffs tar sand deposit was selected as a candidate tar sand for the bitumen-impregnated sandstone pyrolysis studies following the completion of the small diameter fluidized bed pyrolysis studies with the material from the PR Spring[33] tar sand deposit. The Circle Cliffs tar sand, being of marine origin, was expected to be comparable to the material from the Tar Sand Triangle deposit which has been used as a feedstock in previously reported studies.[31,32]

The Circle Cliffs tar sand material was also selected for study because of the paucity of data regarding the native bitumen in the literature. Limited reservoir characteristics were available since the Circle Cliffs deposit has not been extensively cored. The only available data on the native bitumen was reported by Wood and Ritzma,[51] Campbell and Ritzma,[52] and Ritzma.[53] A gross estimate of the bitumen in place, 1.306 x 10^9 barrels, was reported by Ritzma;[53] however, it was based on a visual classification system developed by Kayser rather than on core data.[54]

The more recent publications of the Interstate Oil Compact Commission[55,56] rely almost exclusively on the referenced work of Ritzma and coworkers[51-53] for resource estimates for the Circle Cliffs deposit. A summary of the reported physical and chemical properties of the native Circle Cliffs bitumen[51-53] is presented in Table 42. Ritzma[80] has proposed that the original organic matter or hydrocarbon/bitumen precursor material was never subjected to sufficient depth of burial long enough to convert it to a bitumen of higher quality. Ordinarily the high oxygen content of outcrop samples is attributed to oxidation which has occurred over geological time. Core samples generally exhibit much lower oxygen contents due to the lack of exposure to air. The analysis of the Circle Cliffs bitumen core samples also indicated a very high oxygen content which is consistent with the speculation of Ritzma. Thus, the bitumen-derived hydrocarbon liquid produced from the Circle Cliffs tar sand may require

TABLE 42

Reported Physical and Chemical Properties
Circle Cliffs Deposit Native Bitumen

UGMS Identification	68-1A	68-6A	68-2A	68-3A	68-4A	68-12B	68-19D	68-13A
Formation Member	← Shinarump →					← Moenkopi →		
Location[1]	Muley	Muley	Stud Horse	White	White	West	West	East
Identification	Twist	Twist	Peak	Canyon	Canyon	Flank	Flank	Flank
Sample Type	Outcrop	Outcrop	Outcrop	Core	Core	Outcrop	Seep	Outcrop
Bitumen[2] Saturation, %	5.0	3.1	7.2	5.0	5.0	6.4	27.0	5.1
Specific Gravity	1.057	1.143	1.123	1.140	1.087	1.175	1.060	1.095
Gravity, °API	2.4	-7.7	-5.5	-7.4	-1.3	-11.1	-2.0	-2.2
Elemental Analysis[3]								
H_2, wt.%	8.6	8.6	7.4	9.0	8.3	7.9	3.0	9.2
C, wt.%	72.4	76.4	62.1	67.7	72.5	68.0	88.9	73.8
N_2, wt.%	0.6	0.6	0.4	0.9	0.7	0.5	0.6	0.5
S, wt.%	3.8	4.1	4.4	3.5	3.9	3.6	4.2	3.6
O_2, wt.%	14.6	10.3	25.7	18.9	14.6	20.0	3.3	12.9
Atomic H/C Ratio	1.43	1.35	1.43	1.59	1.37	1.39	0.4	1.50
Distillation[5]								
Volatility, %	34.9	21.9	24.8	41.1	44.5	29.9	37.1	53.4
Residue, %	65.1	78.1	75.2	58.9	55.5	70.1	62.9	46.6

[1]Location of samples can be pinpointed in the Circle Cliffs deposit in reference (6).
[2]Bitumen saturations are reported as percents and it would appear from the experimental procedure outlined in reference (4) that these represent weight percent saturations.
[3]The elemental analysis is presented as reported in reference (6). It was not clearly stated in reference (4) through (6) whether the hydrogen and nitrogen were being reported as dihydrogen and dinitrogen.
[4]Oxygen determined by difference.
[5]The volatility is defined as the percent overhead at 572 F and 40 mm pressure.

considerable hydrogen upgrading to remove oxygen and nitrogen as well as the sulfur which is typical (~4 wt.%) of a bitumen of marine origin.

Acquisition of Circle Cliffs Tar Sand Samples

The bitumen-impregnated sandstone used in this investigation was acquired through Kirkwood Oil and Gas Exploration and Production of Casper, Wyoming. The location of the sampling site is indicated on the map of the Circle Cliffs deposit presented in Figure 61. Initially an outcrop of the deposit was located and a section of the outcrop was dynamited to expose unweathered bitumen bearing sandstone. The impregnated sandstone was dynamited and six 55-gallon drums were filled with the more heavily saturated rock.

The entire area was cleaned, and the "mined" portion of the outcrop was restored as nearly as possible to its original appearance. The samples acquired were approximately 4-6 feet into the outcrop and may not have been exposed to excessive weathering.

The drums were sealed and transported to the University of Utah for use in the fluidized bed pyrolysis and rotary kiln studies.

Analysis of the Native Bitumen from the Circle Cliffs Tar Sand Deposit

A portion of the bitumen-impregnated sandstone from the Circle Cliffs deposit was crushed and the native bitumen was extracted from the crushed material with toluene.

The native bitumen was recovered by evaporation of the toluene in a rotary vacuum evaporator. The solvent was chromatographically analyzed to determine the amount of the native bitumen driven overhead and the native bitumen was analyzed to determine the amount of residual solvent. The weight of the bitumen-sandstone composite placed in the extractor and the weight of the recovered bitumen were used to compute the weight percent saturation of the Circle Cliffs tar sand. A second determination of the saturation was made using a pyrolysis technique. A weighed sample of the bitumen-sandstone composite was placed in a muffle furnace and the bitumen was burned at 500°C (773 K). The weight loss, corrected for water evaporation, was assumed to correspond to the original

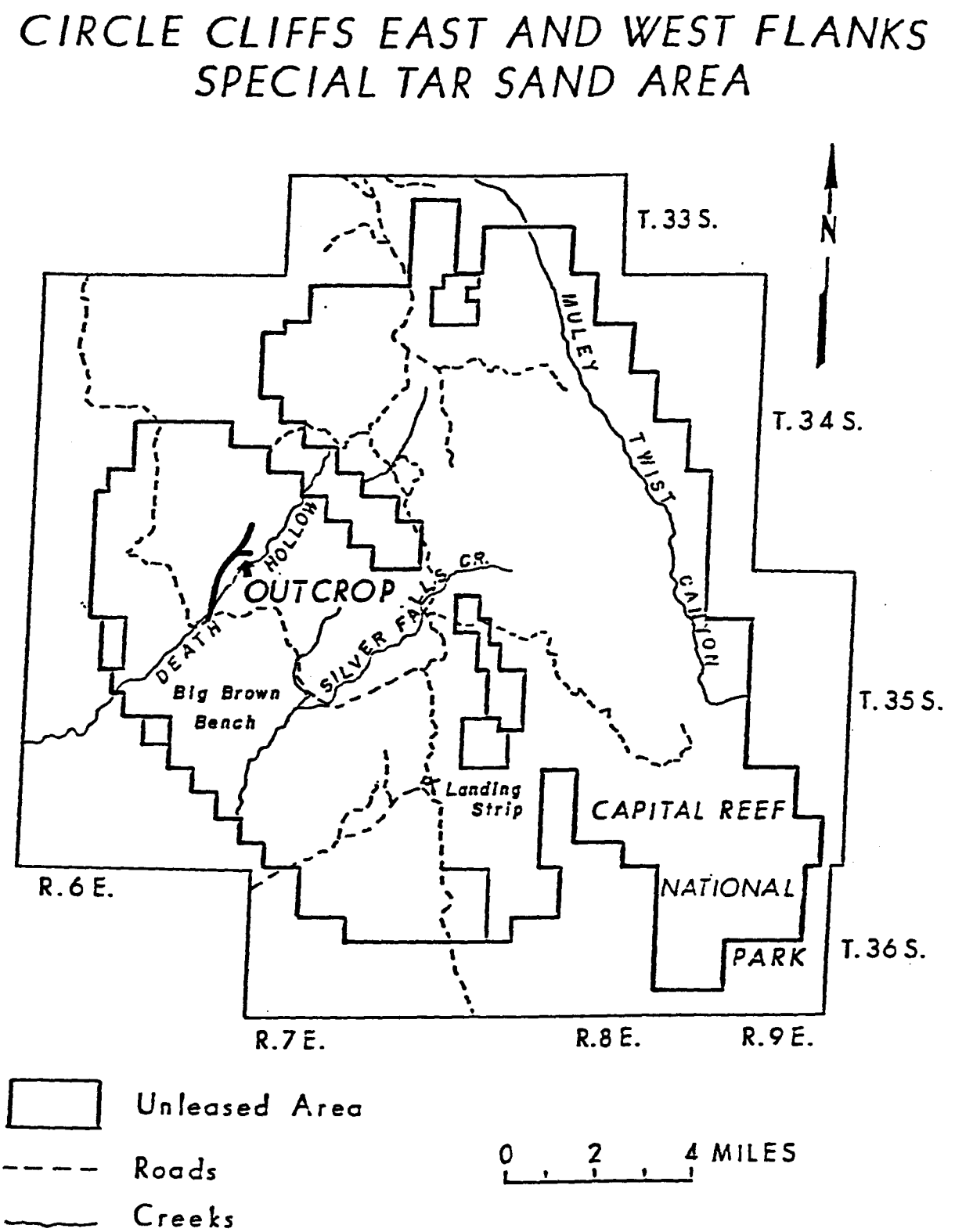

Figure 61. - Circle Cliffs east and west flanks special tar sand area.

bitumen on the sandstone. The mineral carbonates do not decompose below 650°C (923 K); therefore, the weight loss at 500°C (673 K) is not related to carbonate decomposition.

The recovered native bitumen containing less than 0.25 wt.% retained solvent (toluene) was used for the chemical, physical and spectroscopic analyses. The bitumen properties routinely determined are reported in Tables 43, 44, and 45. Only the gravity, 14.3 API, appears to differ significantly from the data reported in the literature (Table 42). The properties of the native bitumens from the Tar Sand Triangle and Circle Cliffs tar sand deposits are compared in Tables 46 and 47.

Modification of Small Diameter Reactor System

The small diameter reactor system has been relocated in the Hedco Building. The relocation provided an opportunity to revamp and repair many of the components of the system which had deteriorated with prolonged operation in the past 10 years (1976-1986). In particular, the electrical system and the temperature control systems were modernized. All the thermocontrollers were changed from on-off type controllers to proportioning controllers to reduce the gain margin of the set point temperature and more precise control of the system. The pneumatic control system was also redesigned and the control panel was separated from the electric control panel for easy operation. The obsolete parts of the system were completely replaced with new equipment and parts to provide troublefree operation.

Overall Design of the Fluidized Bed Pyrolysis Reactor

The fluidized bed tar sand pyrolysis unit is divided into three sections:

1. Fluid bed reactor assembly
2. Solids introduction and withdrawal system
3. Bitumen-derived liquid product recovery system

A schematic of the system is presented in Figure 62.

Detailed explanations of the physical specifications of the overall system are as follows:

Table 43

Characterization of Native Bitumen
Circle Cliffs Tar Sand

API Gravity, ^{o}API	14.3	--
Viscosity, cps	NA	NA
Conradson Carbon Residue, wt.%	23.4	23.3
Ash Content (Dry), wt.%	0.06	0.06
Elemental Analysis		
C, wt.%	83.32	83.27
H, wt.%	9.77	9.92
N, wt.%	0.39	0.34
S, wt.%	4.87	4.92
O, wt.%	1.93	1.58
Atomic H/C Ratio	1.4	1.42
Molecular Weight, g mol^{-1}	706	--
Metals Analysis		
Ni, ppm	66	52
V, ppm	177	152
As, ppm	--	--
Pour Point, ^{o}F	138	138

Table 44

Characterization of Native Bitumen
Circle Cliffs Tar Sand

Simulated Distillation:	
Volatility, wt.%	40.6
IBP-400°F, wt.%	0.8
400-650°F, wt.%	8.0
650-1000°F, wt.%	31.8
1000°F$^+$ Residue, wt.%	59.6

Distillation Data:

% Overhead	**Temperature (K)**
IBP, K	531
5	602
10	646
15	678
20	710
25	738
30	755
35	791
40	811

Asphaltenes,[a] wt.%	46.1
Maltenes, wt.%	53.9

[a]Pentane Insolubles

Table 45

Viscosity of the Native Bitumen from the Circle Cliffs Tar Sand Deposit

Temperature (°C)	Viscosity (cps)
90	23012.
120	1538.8
150	320.3

Table 46

Comparison of Circle Cliffs and Tar Sand Triangle Bitumens

	Circle Cliffs Bitumen	Tar Sand Triangle Bitumen
API Gravity, ^{o}API	14.3	8.6
Viscosity, cps	2301.2[a]	42,638.[b]
Conradson Carbon Residue, wt. %	23.4	16.7
Ash Content, wt. %	0.06	0.2
Elemental Analysis		
C, wt. %	83.30	84.3
H, wt. %	9.85	10.4
N, wt. %	0.37	0.4
S, wt. %	4.90	4.0
O, wt. %	1.78	1.0
Atomic H/C Ratio	1.41	1.47
Molecular Weight, g mol^{-1}	706	541
Metals Analysis		
Ni, ppm	59	--
V, ppm	165	--
Pour Point, ^{o}F	138	91
Asphaltenes, wt. %[c]	46.1	23.3
Maltenes, wt. %	53.9	76.7

[a] measured at 194^{o}F
[b] measured at 113^{o}F
[c] pentane insolubles

Table 47

Comparison of Circle Cliffs and Tar Sand Triangle Bitumens

	Circle Cliffs Bitumen	Tar Sand Triangle Bitumen
Simulated Distillation:		
Volatility, wt. %	40.6	34.4
IBP-400°F, wt. %	0.8	0.7
400-650°F, wt. %	8.0	7.6
650-1000°F, wt. %	32.8	26.2
1000°F+ Residue, wt. %	59.4	65.6

Distillation Data:

% Overhead	Temperature (K)	
	CCB	TSTB
IBP,K	531	473
5	602	--
10	646	660
15	678	--
20	710	708
25	738	--
30	755	756
35	791	--
40	811	798
42.8	--	811

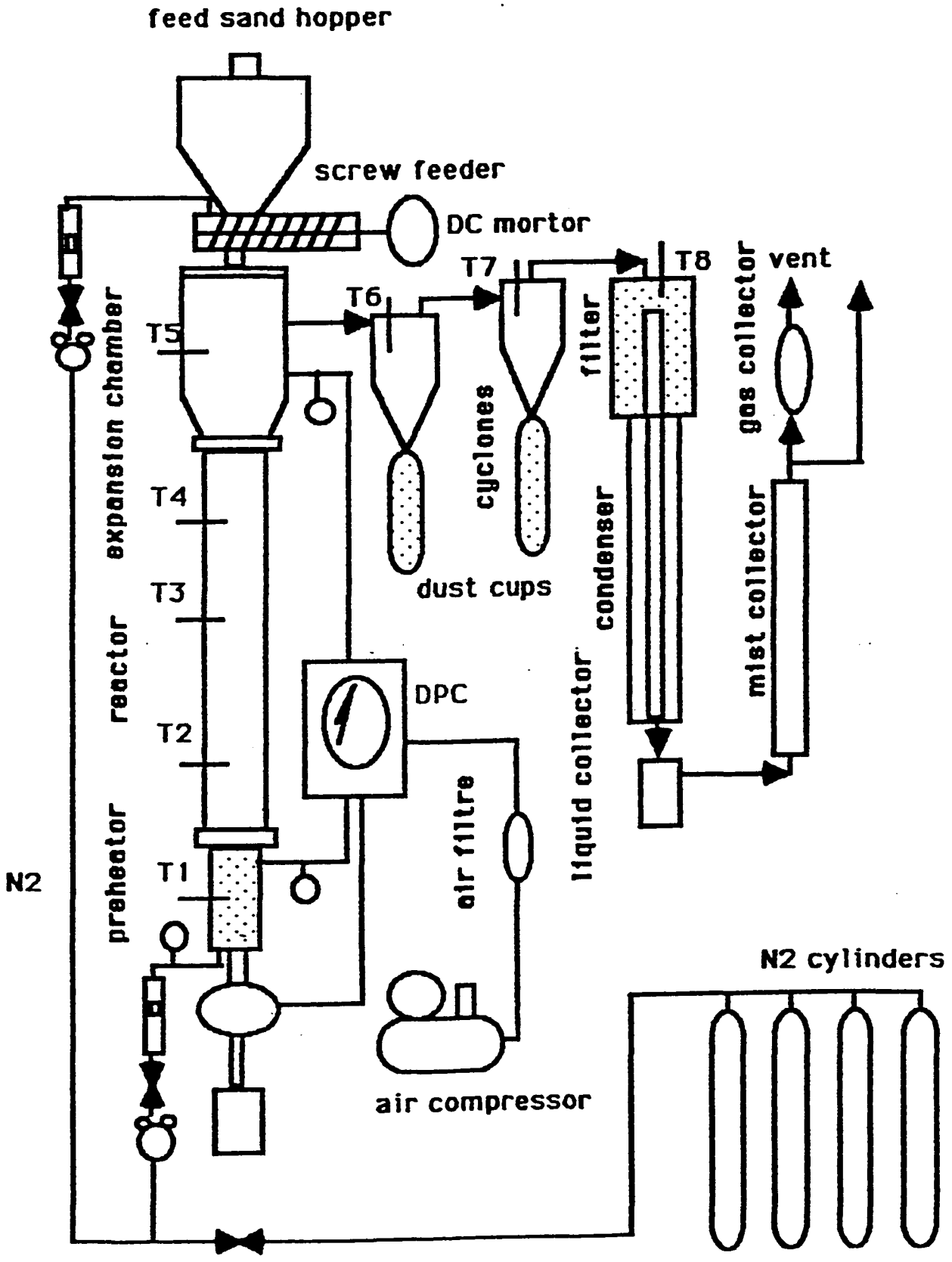

Figure 62. - Diagram of reactor arrangement.

Fluid Bed Reactor Assembly:

Preheater: The purpose of the preheater is to provide sensible heat to the fluidizing gas. The preheater is a 3.13 cm nominal diameter 316 stainless steel schedule 10 pipe (3.6 cm inside diameter and 4.15 cm outside diameter) 25 cm in length (Figure 63). A standard 150 lb flange (304 stainless steel) was welded to one end of the pipe. The other end was closed with provisions for introducing the fluidization gas and for withdrawing solids through a stand pipe.

Gas Distributor and Gas Seal: The gas distributor is located between the upper flange of the preheater and the lower flange of the reactor (the tar sand coking bed). The gas distributer screen is cut from a Tyler 325 mesh stainless steel cloth and is held in place between two stainless steel rings which were welded together. At the center, the gas distributor had a 1 cm orifice through which the sand discharge is passed. For this and all the other pyrolysis sections, standard 150 lb Flexitallic metal gaskets (supplied by Elastomer Products, Utah) are used for gas seals between each set of flanges (Figure 64).

Fluid Bed Reactor: The reactor is a 3.13 cm nominal diameter 304 stainless steel schedule 10 pipe with standard 150 lb flanges welded at each end to give a total length of 90 cm between the flange faces. Four taps are provided along the length of the reactor and are used to monitor the bed temperature. The bottom tap is used for monitoring the bed height.

Expansion Chamber: The expansion chamber is used to decrease the velocity of the effluent gas from the reactor and to permit the separation of the entrained solids from the gas, decreasing the entrainment of the solids from the reactor. The fresh tar sand is fed to the reactor by allowing it to rain through the expansion chamber.

The expansion chamber is a 7.5 cm nominal diameter 304 stainless steel schedule 10 pipe 22.5 cm in length and a 3.13 cm nominal diameter 304 stainless steel schedule 10 pipe 8.75 cm in length. The two pieces are connected to each other by a conical section. A standard 150 lb flange is welded to the 3.13 cm nominal diameter pipe at the lower end of the expansion chamber. Another flange,

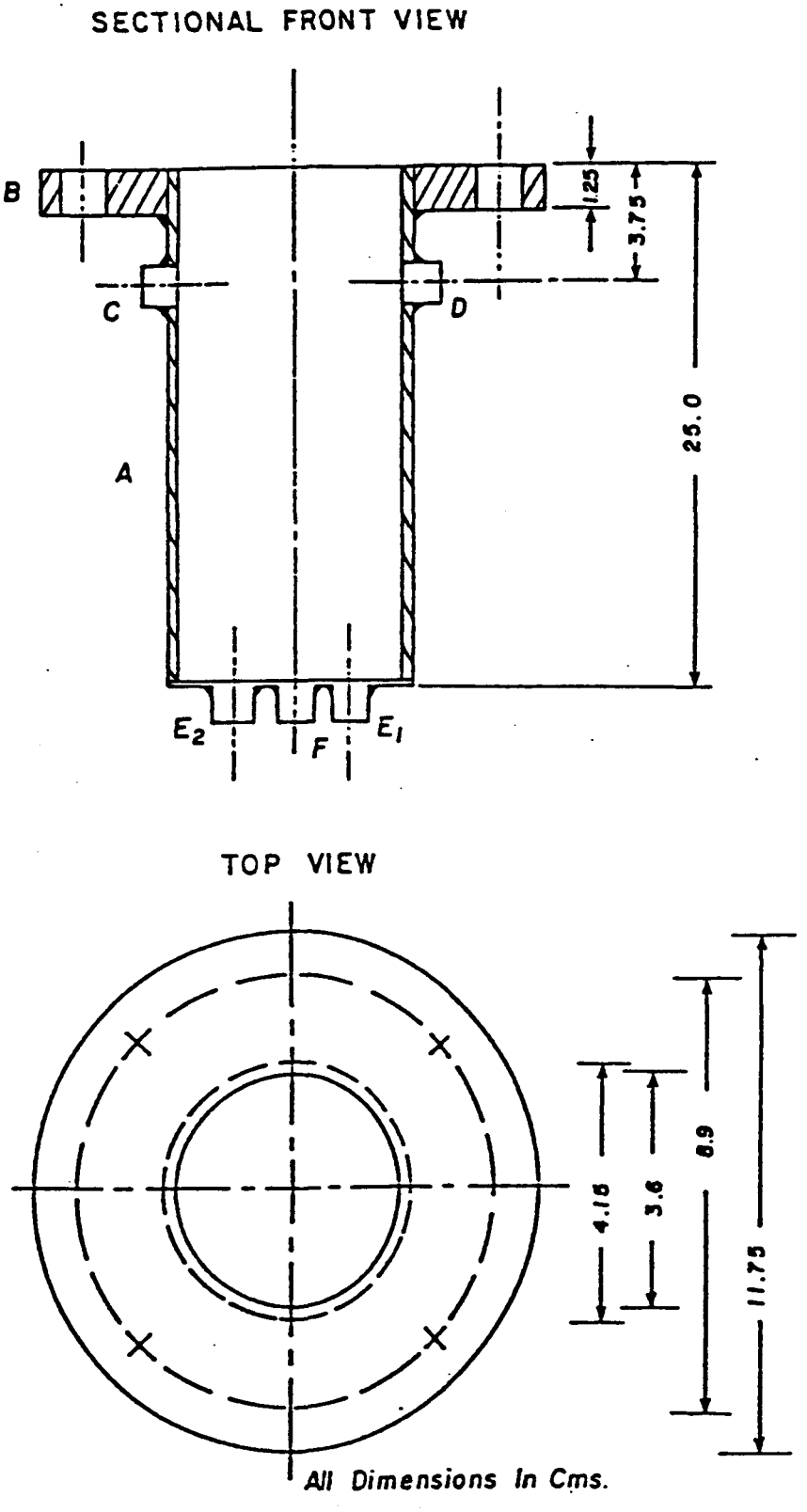

Figure 63. - Diagram of the fluidizing gas pre-heater.

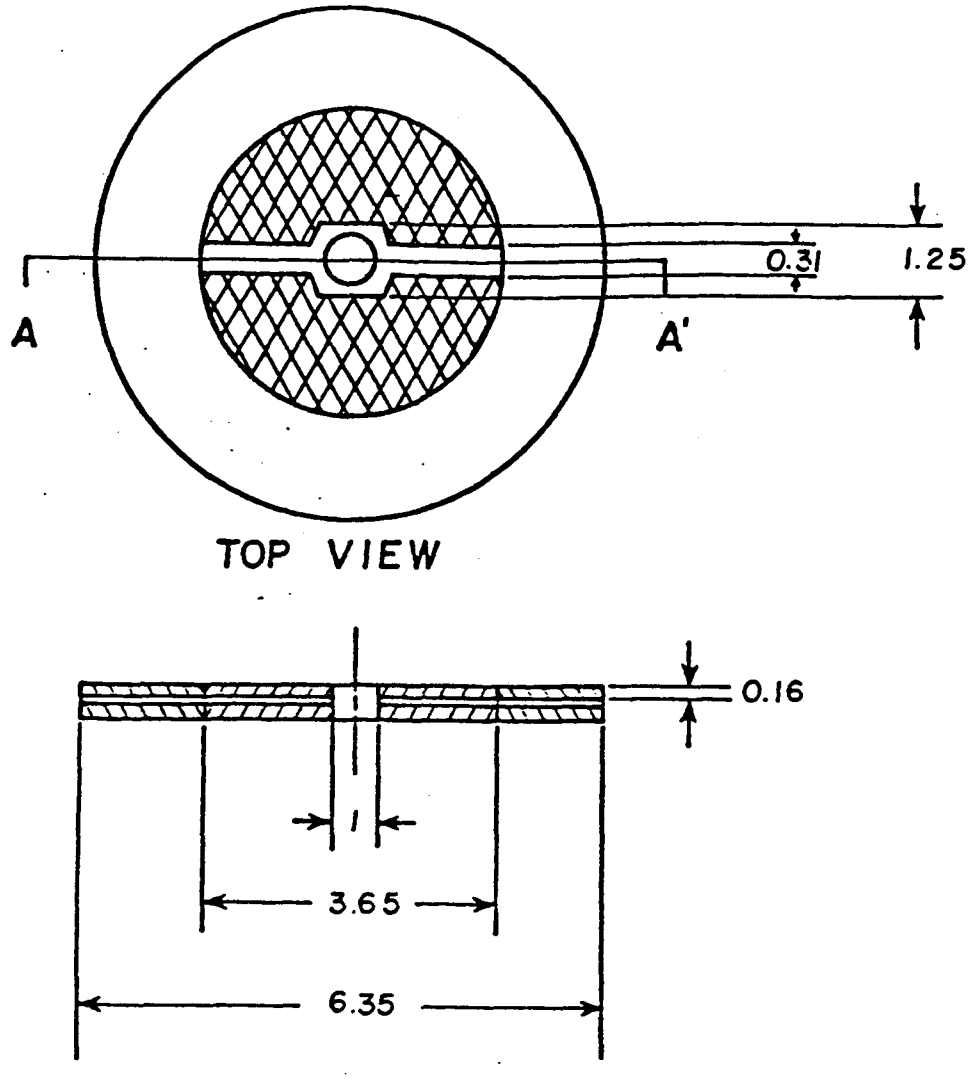

Figure 64. - Detail of the Gas Distributor

made from an 0.625 cm thick 304 stainless steel plate, was welded to the 7.5 cm nominal diameter pipe at the upper end of the expansion chamber (Figure 65).

Solids Introduction and Withdrawal System

Feed Hopper: The feed hopper is a 0.31 cm thick mild steel plate, rolled to form a cylindrical section of 27.5 cm diameter and 25.4 cm in length. The cylindrical section of the hopper and one end of the outlet tube (2.54 cm O.D. and 2.54 cm in length) were connected by a conical section. A flange of 10.8 cm outside diameter and 1.25 cm thick was welded to the other end of the outlet tube (Figure 66). The hopper was bolted to the inlet of the screw feeder.

Screw Feeder: The crushed and sized tar sands are fed to the reactor by a screw feeder attached to the feed hopper. A variable speed of 0.5 hp D.C. mortar, with a Speed-A-Matic VP-150 controller (manufactured by U.S. Electric Motors, Connecticut), and a speed reduction gear is used to drive the screw (Figure 67).

Solid Control Valve: The coked sand is removed through a solid control valve attached below the fluidizing gas preheater. The solid control valve is made of a brass body with an inlet port and outlet port. The inlet and outlet port are connected through an 0.93 cm valve opening (Figure 68).

Synthetic Crude Product Recovery System

Cyclone: Two cyclones connect ed in series are used for fine sands removal (Figure 69). The cyclones are connected between the gas outlet of the expansion chamber and the fine sand filter.

Filter: A filter with a filtering element of a MCS 1001 PE sintered stainless steel cartridge (supplied by Pall Trinity Micro Corporation, New York) is used to remove the remaining fine particles from the second cyclone. The filter element housing is a 12.5 cm O.D. 304 steel schedule 40 pipe and 37 cm in length. The filter cartridge is a 2.5 cm thick stainless steel disc.

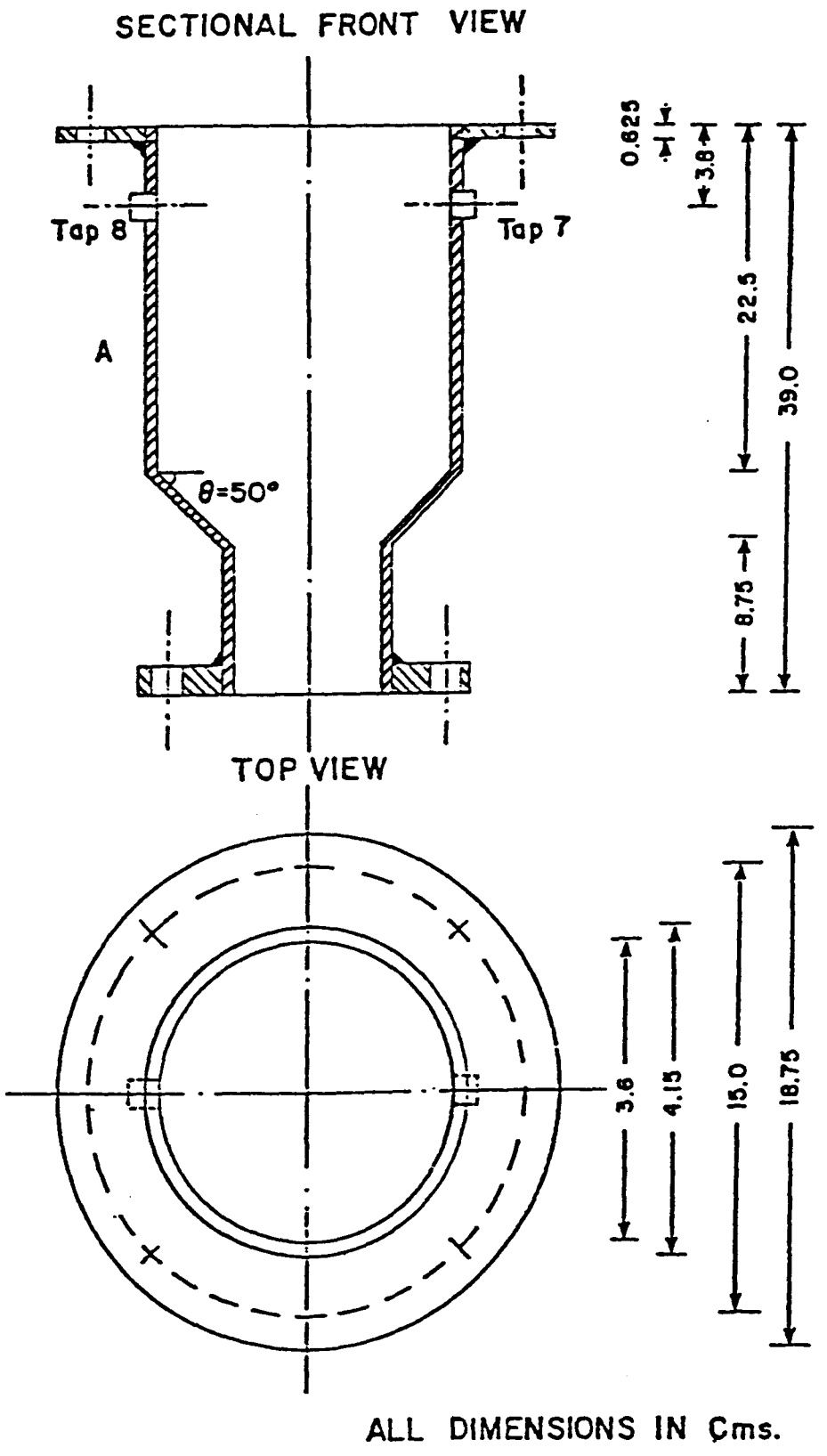

Figure 65. - Diagram of the expansion chamber.

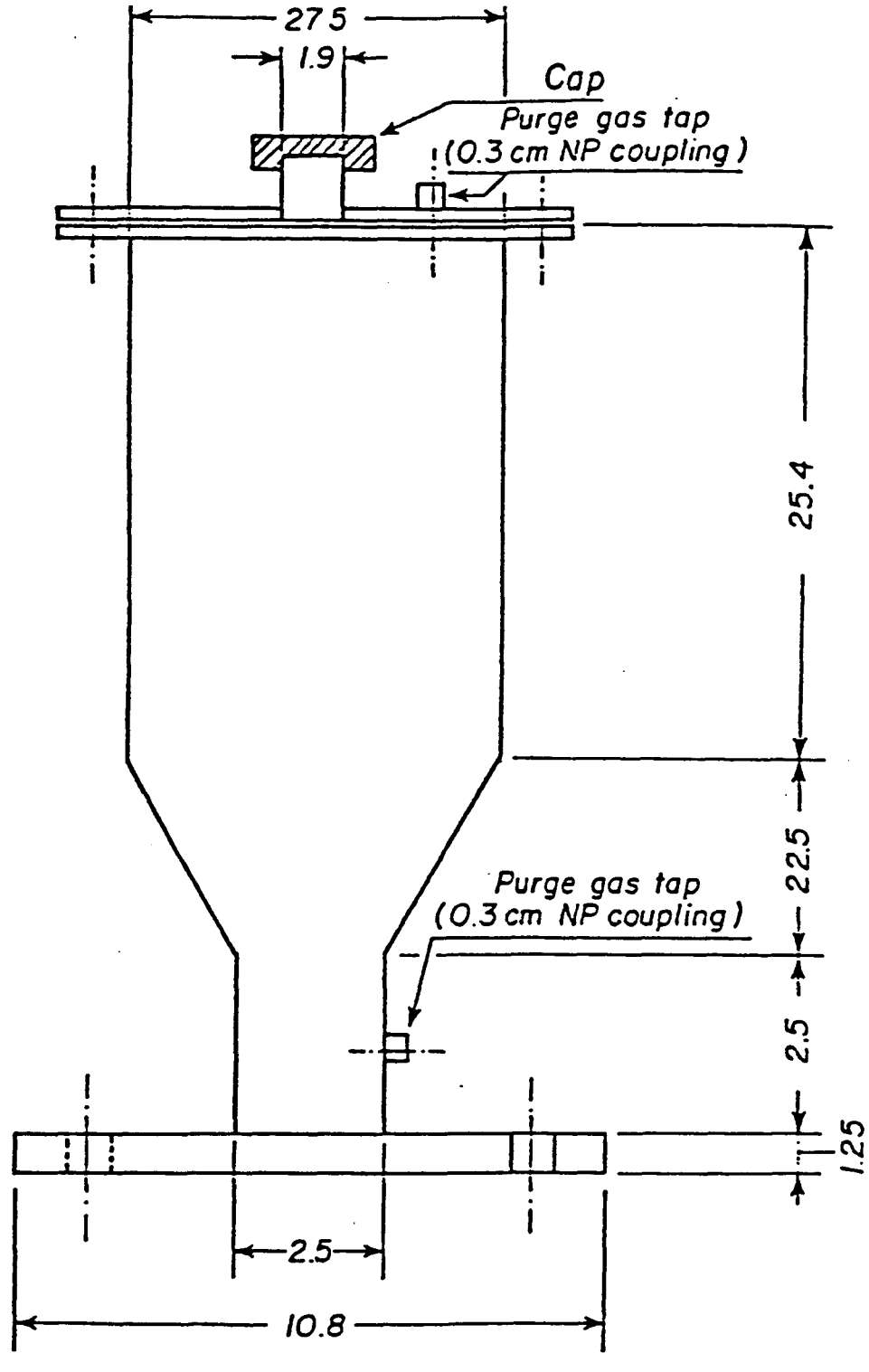

Figure 66. - Feed sand hopper.

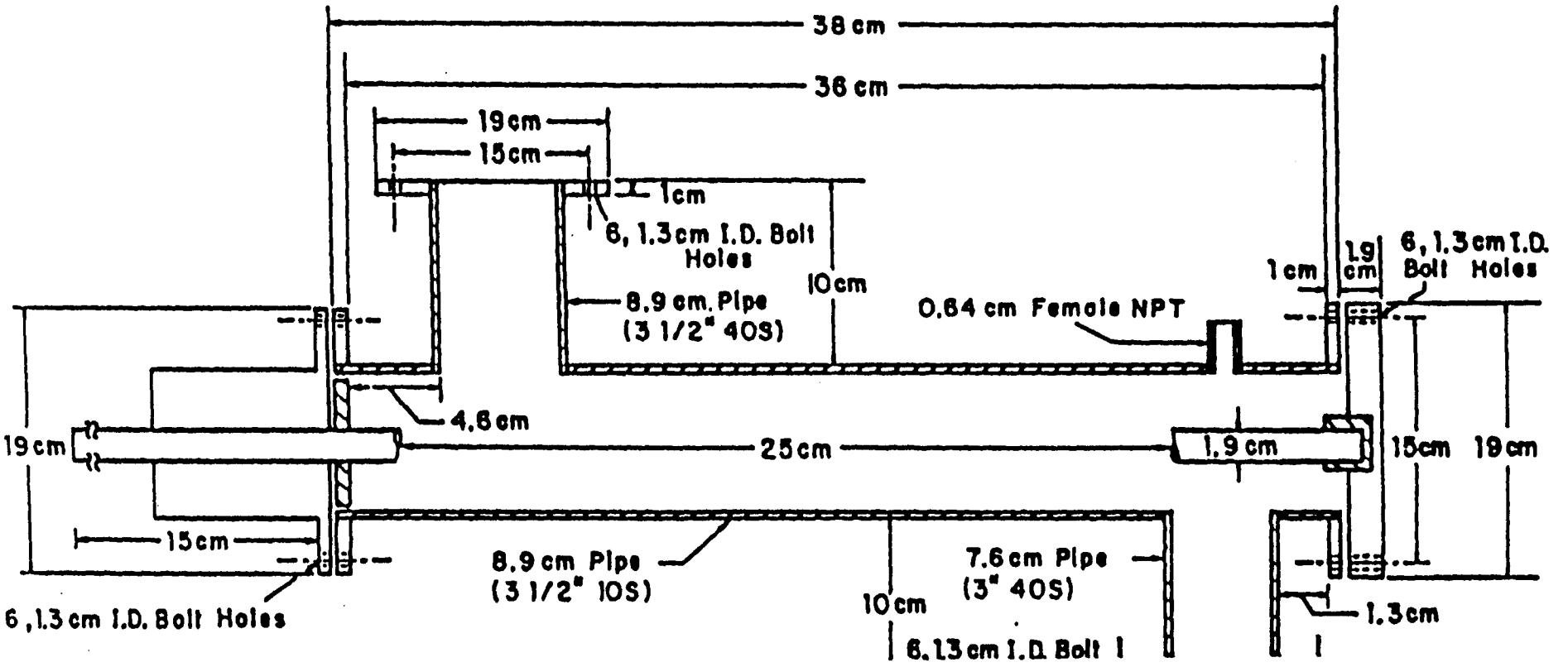

Figure 67 . - Screw feeder. Stainless steel 304.

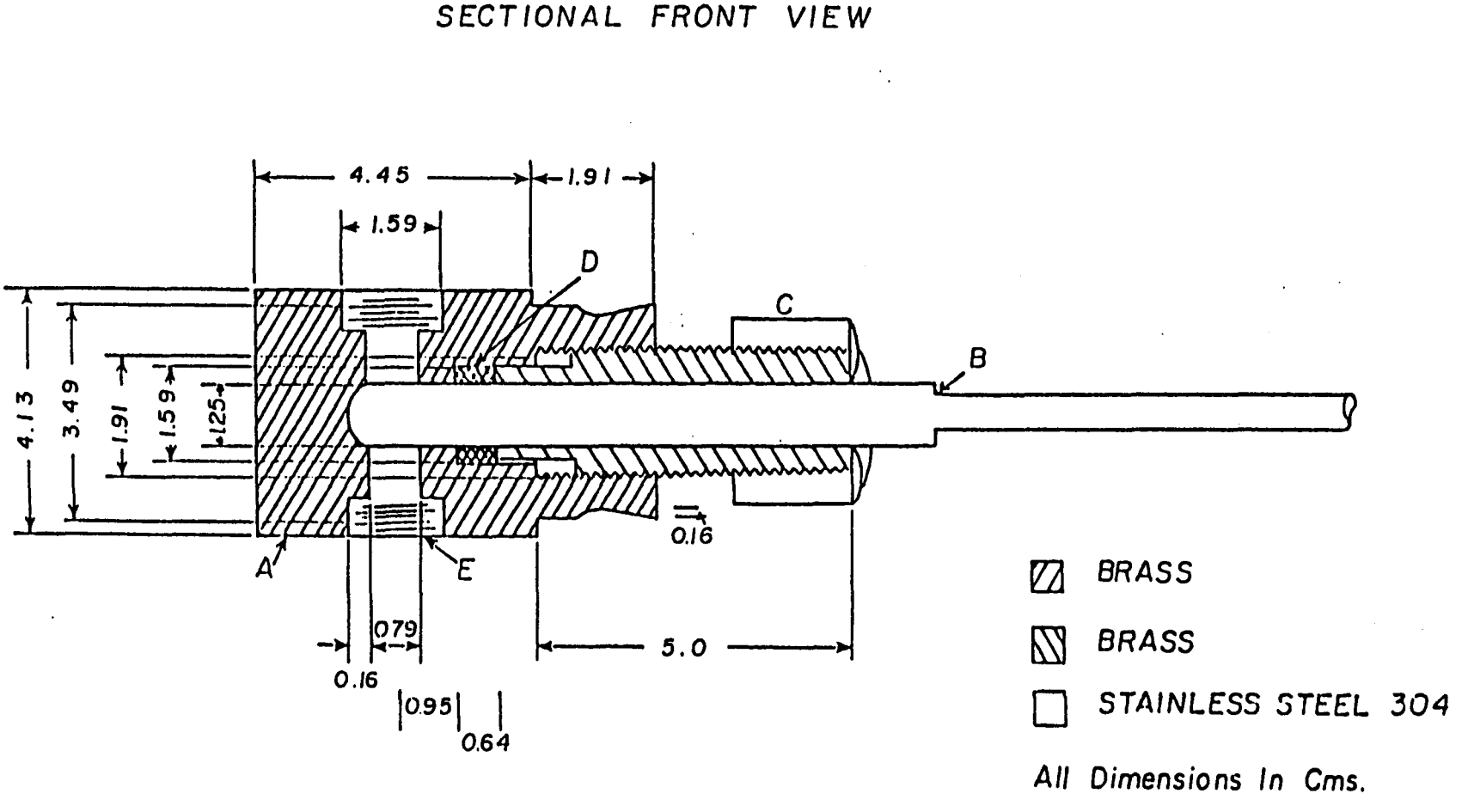

Figure 68. - **Diagram of the solid control valve.**

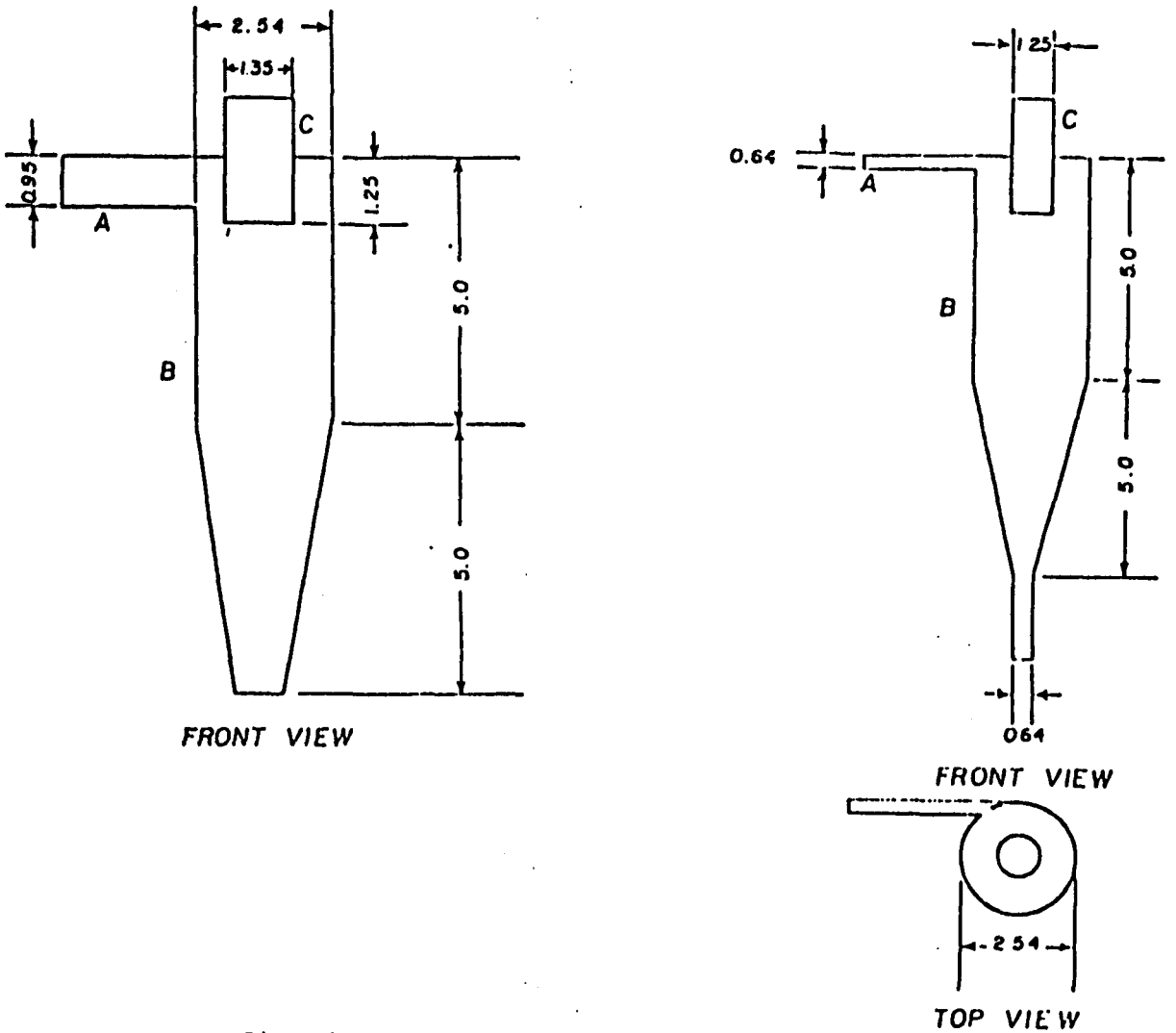

Figure 69. - Diagram of the cyclones.

Temperature Control Unit Design

The control panel diagram is presented in Figure 70. Six sections are reserved for the temperature control system and two sections are reserved for the reactor. Love proportioning #49 thermocontrollers (manufactured by Love Controls Corporation, Illinois) are used to control the system. The electric current necessary for each section is as follows:

No.	Section	Current
#1	preheater	12A
#2	reactor 1	5A
#3	reactor 2	5A
#4	expansion chamber	12A
#5	cyclones	8-10A
#6	filter	8-10A

The six controllers consume totally 1A of the current, and the screw feeder mortar will consume 1A of the current. Total electricity necessary will be around 60A.

Nicrom heating wire is used to heat all sections of the pyrolysis unit, and all sections are insulated by two or more layers of insulation cloth (manufactured by Carborundum Co.). The temperatures in the bed of solids are measured by the type K thermocouples (manufactured by Barber-Colman Co.) introduced through taps on the reactor which were designed thermowells.

Pressure Control Unit Design

Since the system is to be operated as a continuous process, where the bituminous sand is continuously added to the expansion chamber and coked sand is continuously withdrawn from the bottom of the preheater, the solid bed height should be maintained constant to prevent accumulation of solids within the bed.

The differential pressure controller in combination with a pneumatically operated solid discharge valve are used to control the bed height. The specifications for the ITT Barton Model 338 pressure recording pneumatic controller (manufactured by Barton Instruments, California) are presented below.

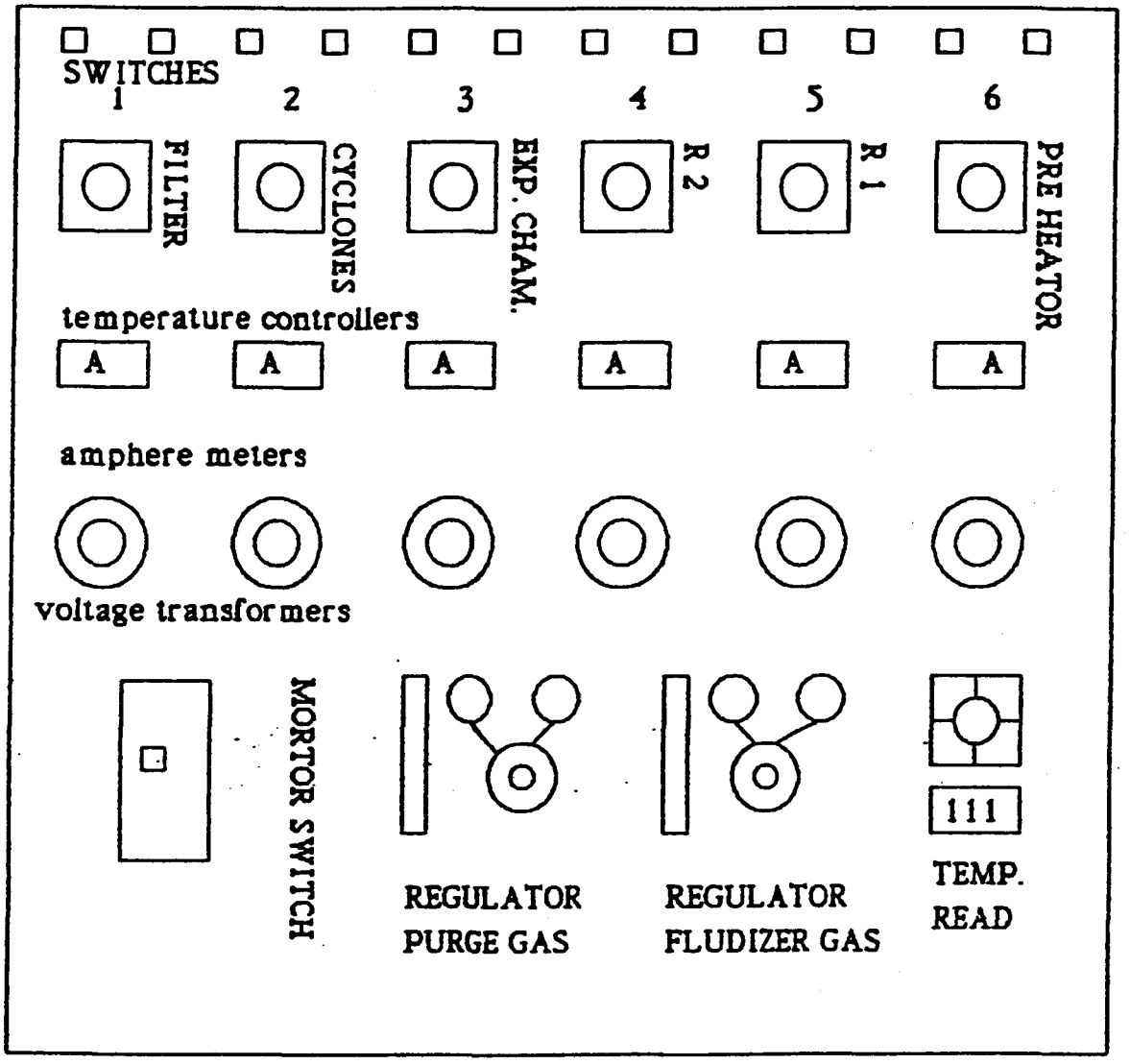

Figure 70. - Diagram of the control panel.

Actuator	Model 199 Differential Pressure Unit
Instrument Air	20.7-103.5 kPa
Output Air	20.7-103.5 kPa
Temperature Limits	222 K to 367 K
Differential Pressure	
(DP) Range	0-125 cm water column
Accuracy of DP Recording	0.5% of full scale error
Safe Working Pressure	6890 kPa
Bellow Material of	
Construction	316 stainless steel
Operating Fluid of the	
Bellows	Mineral oil, Grade 1005

The pressure differential is measured between the expansion chamber and the upper part of the preheater by connecting both pressure taps to a 0-35 psi pressure gauge (manufactured by Marshalltown Manufacturing Co., Iowa) (Figure 71). The pneumatic controller (DPC) panel is separated from the electric control panel (main control section) and mounted on the lower level for convenience. The sand feeder will be at the upper level and the burnt sand exhaust line will be at the lower level to protect the main control section (second level) from the dust.

Fluidization Gas Velocity Studies at High Temperatures

The experimental program to be carried out after completion of the modifications to the reactor system will include an investigation of feed sand particle size. The minimum fluidizing gas velocity may be computed as follows.

According to Richardson, et al.,[57] the pressure drop across the fluidized bed is:

$$\Delta P_B = (\rho_s - \rho_g)\ (1-E)\ H^* g$$

where ρ_s is particle density, g cm^{-3};

ρ_g is the fluidizing gas density, g cm^{-3};

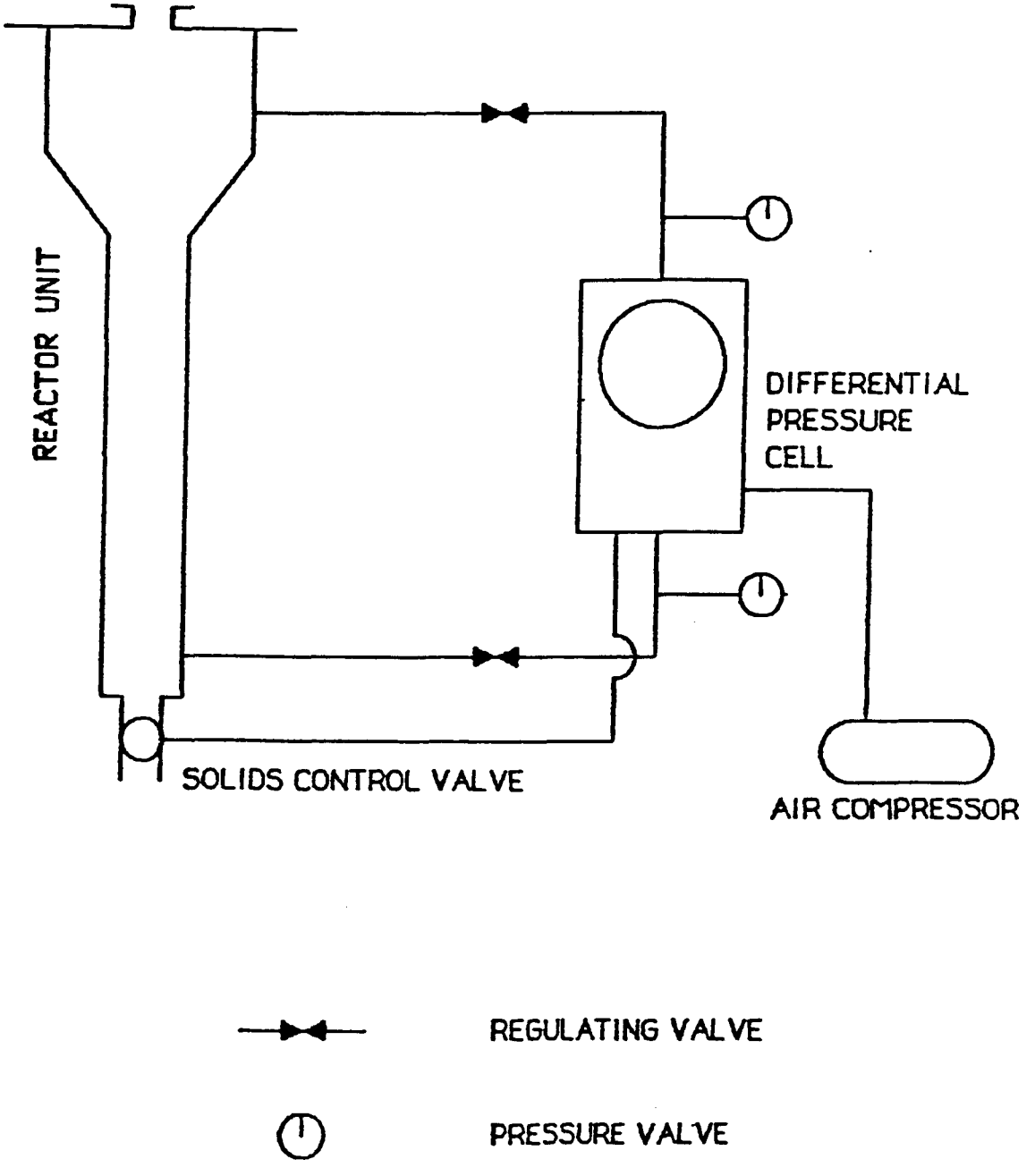

Figure 71. - **Differential pressure controller--piping diagram.**

H is the bed height, cm;

g is 980 cm/s^2.

The steady state sand inventory in the reactor is 700 g, the pressure drop is approximately:

$$\Delta P = w/Ac = 700/ 9.65 = 72.54 \text{ (cm } H_2O)$$

where Ac is cross sectional area of the reactor, cm^2

W is buoyant weight of the bed.

The theoretical minimum fluidizing gas velocity is calculated from the following equation.

$$N_{Re} = \frac{d_p U_m \rho_g}{Mg} = [(33.7)^2 + 0.048 * d_p (\rho_s - \rho_g) g]^{0.5} - 33.7$$

$$Q = U_m A_c$$

where N_{Re} is the Reynolds number

d_p is the average sand particle size, cm

U_m is the minimum fluidization velocity, cm s^{-1}

Q is the minimum fluidization gas flow rate, cm^3 s^{-1}

The tar sand sample identities and the operating conditions are as follows:

Solid Sand	Circle Cliff Tar Sand
Sample Sizes #1	14 tyler mesh (0.119 cm sieve opening)
#2	24 tyler mesh (0.0707 cm sieve opening)
#3	42 tyler mesh (0.0354 cm sieve opening)
Reactor Temperature	823°K
Fluidization Gas (N_2)	μ = 0.00037 g/cm sec
	ρ_s = 0.000475 g/cm^3
	ρ_g = 2.0 g/cm^3

Reactor Dimensions	I.D.	1.380 in (3.505 cm)
	O.D.	1.660 in (4.216 cm)
	Length	35.4 in (90 cm)
	Area	1.49 in^2 (9.65 cm^2)

The calculated results are as follows:

Sizes	U_m(cm/s)	Q_m(l h^{-1})	N_{Re}	Q(at stp l h^{-1})
14	41.50	1441.71	6.34	478.82
24	15.70	549.42	1.43	182.47
42	4.01	139.22	0.18	46.18

The above equations were intended for spherical particles; therefore, this calculation must be corrected by means of an appropriate shape factor to account for the irregular shape of the sand particles. The operating fluidization gas velocity will be 1.5-2 times larger than the minimum fluidization velocity. The preliminary fluidization studies also included an investigation of the influence of reactor temperature on the minimum fluidization velocity. The fluidization tests at 473, 573, and 763°K using the 24-42 Tyler mesh cut of Mason sand are presented in Figures 72 through 74. A comparison of the experimentally determined and the theoretically computed minimum fluidization velocities at various reactor temperatures are presented in Table 48.

Fluidized Bed Pyrolysis Experiments

The small diameter system has been used to process the sized material from the Circle Cliffs tar sand deposit (west flank). The particle size of the feed sand was 707-354 microns. Average retention time was 30 minutes. The pyrolysis products were distilled and the produced water was separated and weighed. Gas samples were collected during the reaction at the proper intervals and analyzed by GC. Total material balance including gas, produced liquids, and coke were calculated based on bitumen flow rate. The product distribution from the fluidized bed pyrolysis of this material was unusual in that large quantities of water were produced (Table 49). Furthermore, the yield of water

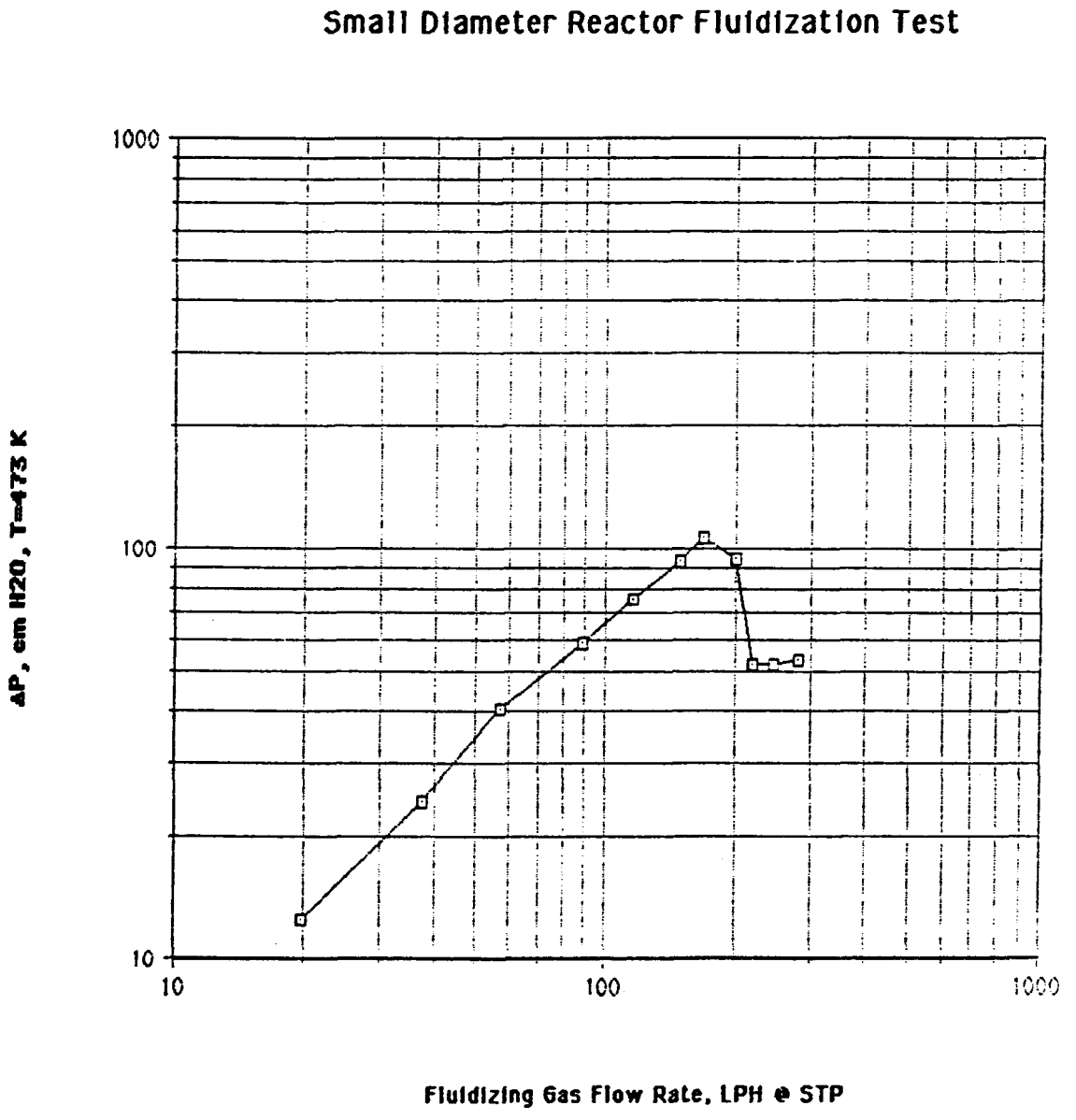

Figure 72. - Small diameter reactor fluidization test.

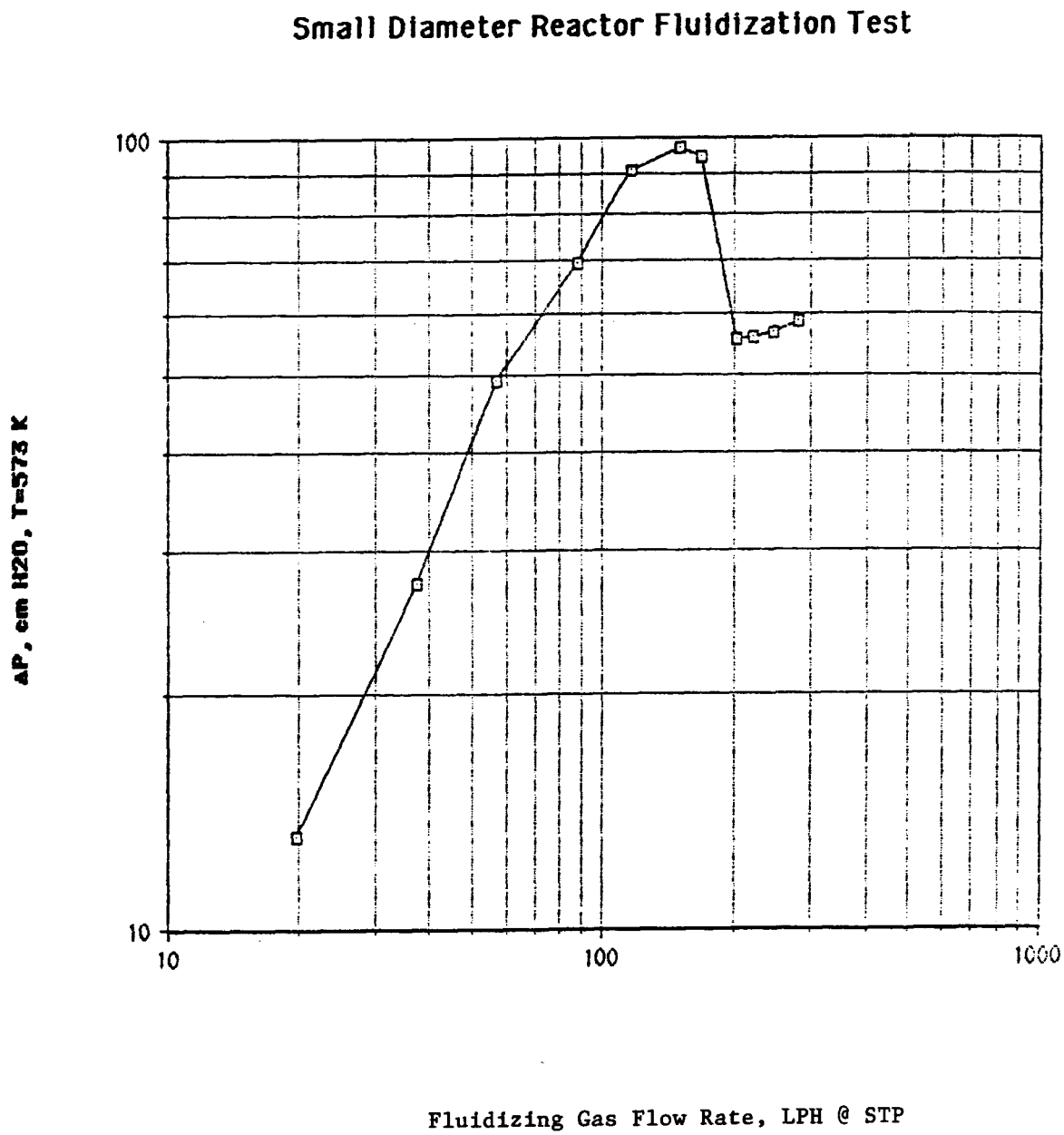

Figure 73. - Small diameter reactor fluidization test.

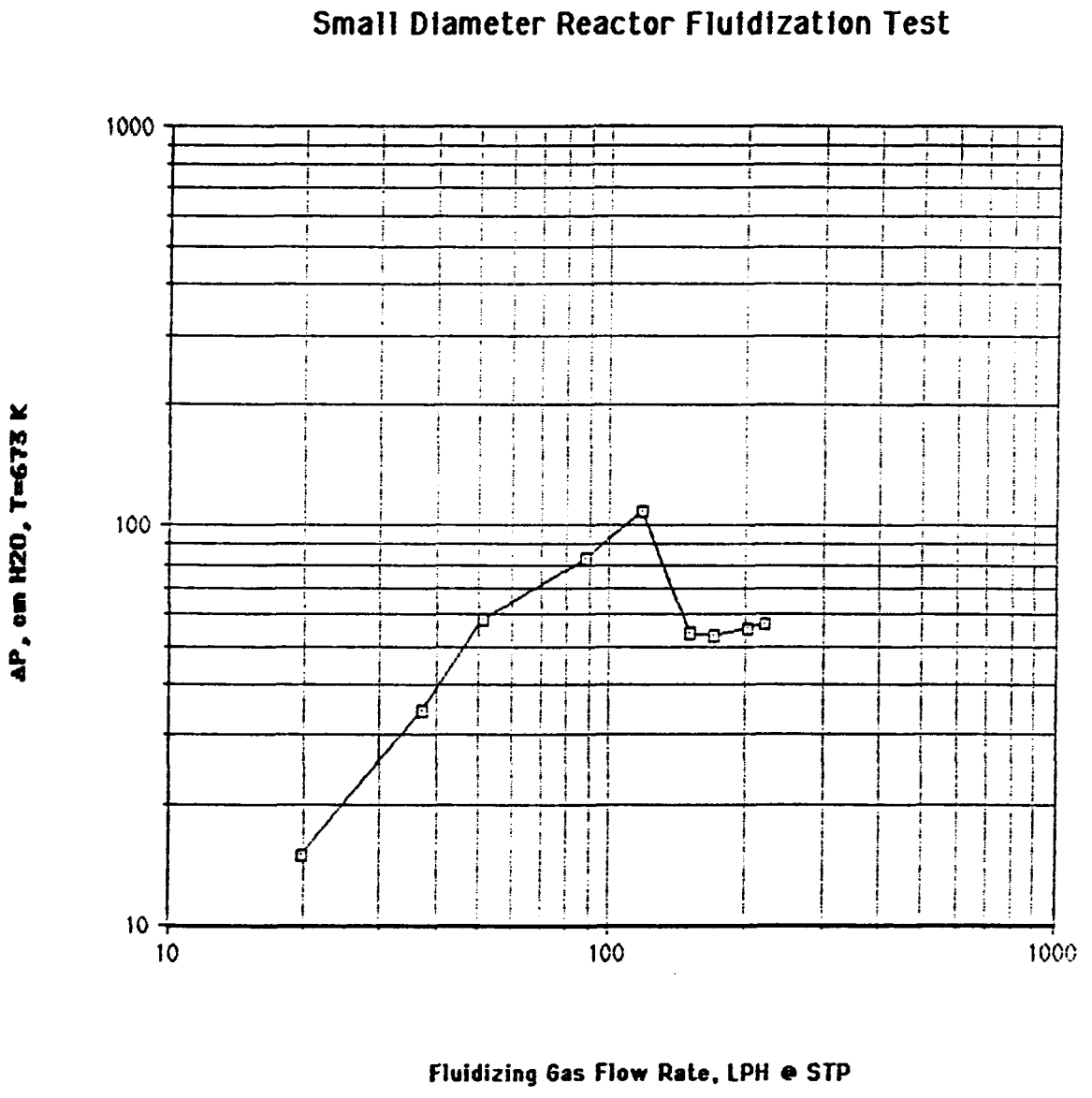

Figure 74. - Small diameter reactor fluidization test.

Table 48

Comparison of Experimental and Theoretical Values of Minimum Fluidization Velocity

	Minimum Fluidization Velocity U_{mf} (cm s^{-1})	
Temperature (K)	Theoretical[a]	Experimental
640.3	2.01	2.96
723.9	1.68	1.71
782.8	1.47	1.68
882.7	1.24	1.46

(a) Theoretical Values computed from following equation:

$$\frac{d\, U_{mf}\, \rho_g}{\mu_g} = (33.7^2 + 0.0408\, d^3\, \rho_g\, (\rho_s - \rho_g)\, g/\mu^2)^{1/2} - 33.7$$

where U_{mf} is minimum fluidization velocity; cm s^{-1}

d is equivalent diameter of particles; cm

μ is viscosity of fluid; g $cm^{-1}s^{-1}$

ρ_g is density of fluid; g cm^{-3}

ρ_s is density of solid particle; g cm^{-3} (grain density)

Table 49

Small Diameter Reactor Yields
Circle Cliffs Tar Sands

Run Id. No.	Temperature (^{O}K)	Product Yields (wt%)	
		Produced Water	Bitumen-Derived Hydrocarbon Liquid
PY-#26	798	10.9	13.6
PY-#23	823	13.7	21.6
PY-#24	853	22.3	16.6
PY-#25	873	26.3	11.4

Table 50

Analysis of Circle Cliffs Tar Sand

	A	B
Bitumen Saturation		
Pyrolysis at 773K, wt. %	5.96	5.98
Solvent Extraction (Toluene), wt. %	3.3	3.4
Dean Stark Water Analysis, wt. %	0.18	0.17
Karl Fisher Water Analysis, wt. %	0.28	--
Solvent Extraction (Toluene), wt.% loss	3.25	3.40
Pyrolysis of Spent Sand, wt. % loss	2.58	2.59
Total Weight Loss, wt. %	5.83	5.99
Bound Water, wt. %	2.58	2.59
Bitumen Saturation (Confirmed), wt. %	3.35	

increased with increasing pyrolysis reactor temperature at constant sand retention time and constant fluidizing gas flow rate or velocity. The yield of produced water did not correspond to the water recovered from the Dean Stark analysis of the native tar sand ore. Concomitant with this increase in produced water there was a decrease in the hydrocarbon liquid (C_5^+) yield and an increase in the light hydrocarbon gas (C_1-C_4) yield at temperatures above 820°K. The source of the produced water was not immediately apparent; however, a detailed analysis of the Circle Cliffs tar sand (Table 50) revealed that it was probably chemically bound water to the non-sand constituents of the solid substrate. We speculate the water was produced by mineral hydrate and/or clay decomposition at the pyrolysis temperature.

Two methods have generally been applied for the determination of the bitumen saturation: solvent extraction and combustion of the bitumen. The combustion is usually conducted at 773°K (500°C) to avoid decomposition of mineral carbonates present in the solid substrate. The initial combustion determination indicated a bitumen saturation of 5.97 weight percent. Subsequently, the bitumen saturation was determined by solvent extraction using toluene. The bitumen saturation was 3.4 weight percent. The connate water was determined by both Dean-Stark and Karl Fisher analysis and was less than 0.3 weight percent. Thus it was concluded that the Circle Cliffs tar sand contained 2.6 weight percent chemically bound water in the solid substrate.

The sand-mineral substrate was analyzed at the United States Bureau of Mines Laboratory in Salt Lake City. The sand-mineral substrate consisted of silicon dioxide (α-quartz), kaolinite, and feldspar (Table 51). It was concluded that the source of the produced water was the kaolinite clay. Furthermore, the decrease in produced hydrocarbon liquids with increasing pyrolysis reactor temperature may be related to the catalytic activity of the kaolinite (note: kaolinite was one of the original catalytic cracking catalysts), that is, the greater the amount of water, the larger the potential catalytically active surface area. The larger the catalytically active surface area, the higher the yield of hydrocarbon gases and the lower the yield of hydrocarbon liquids.

Table 51

Analysis of Circle Cliffs Sand Substrate

Elemental Analysis			
Element	**wt.%**	**Probable Compound**	**Maximum Possible Concentration (wt.%)**
Calcium	8.3	$CaCO_3$	20.7
Magnesium	1.5	$MgCO_3$	5.3
Iron	1.2	Fe_2O_3, FeO	--
Potassium	0.94	$KalSi_3O_3$	6.7
Aluminum	3.66	$Al_2Si_2O_s(OH)_4$	14.4

Identified Components in Sand Substrate

- Silicon Dioxide (α-quartz)
- Kaolinite
- Feldspar

PYROLYSIS OF BITUMEN-IMPREGNATED SANDSTONE IN A LARGE DIAMETER (4.5 INCH) REACTOR

Francis V. Hanson	Associate Professor
L.C. Lin	Graduate Student
S.H. Sung	Graduate Student
J.W. Wiser	Research Associate

SUMMARY

The pilot plant constructed during the period of this contract is a scaled-up version of the fluid bed thermal process equipment designed by Venkatesan.[31] Venkatesan's equipment was a continuous bench-scale, fluidized bed reactor, designed for a maximum throughput capacity of 2.25 kilograms of feed sand per hour. In his investigation, Venkatesan studied the effects of reactor temperature, solids retention time, and feed sand particle size using a reactor that was 1.38 inches in diameter and 35 inches long. An extrapolation of the results of this study predicted that a retention time of 16 minutes would yield 80 percent liquid product, 8 percent light hydrocarbon gas, and 12 percent coke. Extrapolations of the data in both the retention time and particle size indicate the need for a larger reactor. Dorius[33] studied the effects of the same process variables on three distinctly different feed stocks, PR Spring Rainbow I, PR Spring Rainbow II, and PR Spring South. The amount of coke left on the sand was a function of the feed properties, but the data from all three samples also pointed to shorter residence times and larger particle size in order to maximize liquid yield and minimize the gas produced.

INTRODUCTION

The fluidized bed technique represents a unique method for thermal processing of tar sands to obtain a bitumen-derived hydrocarbon liquid which can serve as a hydrogen refinery feedstock. The influence of process operating variables on the product distribution and the yields have been investigated in a small scale (1.5 inch diameter) fluidized bed reactor. These exploratory process variable studies indicated that the feed sand retention time in the pyrolysis zone significantly influenced the C_5^+ hydrocarbon liquid yield; that is, the C_5^+ liquid yield increased with decreasing feed sand

retention time. Unfortunately, the feed sand throughput for the small scale reactor is limited by the quality of fluidization at short residence times; that is, excessive slugging of the bed occurs at feed sand retention time below 16-20 minutes. Further development of this type of process requires the design and construction of a larger scale laboratory apparatus (4-6 inch diameter) than the small scale apparatus presently in use. The larger diameter reactor will permit an expansion of the range of feed sand retention times to better define the influence of this variable on the product distribution and product yields from the fluidized bed.

Successful operation of the large diameter reactor should provide scale-up data for engineering design purposes. The large diameter reactor must be capable of meeting the following conditions:

- operate continuously for 48 hours or longer;
- accept feed sand particle size ranges from 0.032 inches (20 mesh) to 0.25 inches; and
- produce bitumen-derived hydrocarbon liquids at a rate of at least 300 gh^{-1}.

Phase I (Figure 75) is a once-through operation for the fluidizing nitrogen gas. A bank of high pressure cylinders supplies the nitrogen to the fluid bed, which is later separated from the solid particles and the condensable products, and then is vented. Operation variables are set manually and data will be logged on an IBM microcomputer. Phase II (Figure 76) will add a recycle blower and process control to the computer functions. The off gases will be burned in a combustion furnace and all of the equipment will be capable of on-line maintenance for continuous operation of the plant.

It was assumed in all calculations that the product distribution and yields obtained with the small diameter reactor would also be obtained with the large diameter reactor for feed sands of the same particle size.

A number of scale-up techniques were employed in these calculations; however, a complete review of all derivations and computations is beyond the scope of this report. The following relations were used to sale the dimensions of the reactor:

$$D(2) / D(1) = 2.92$$

$$A(2) / A(1) = 8.51$$

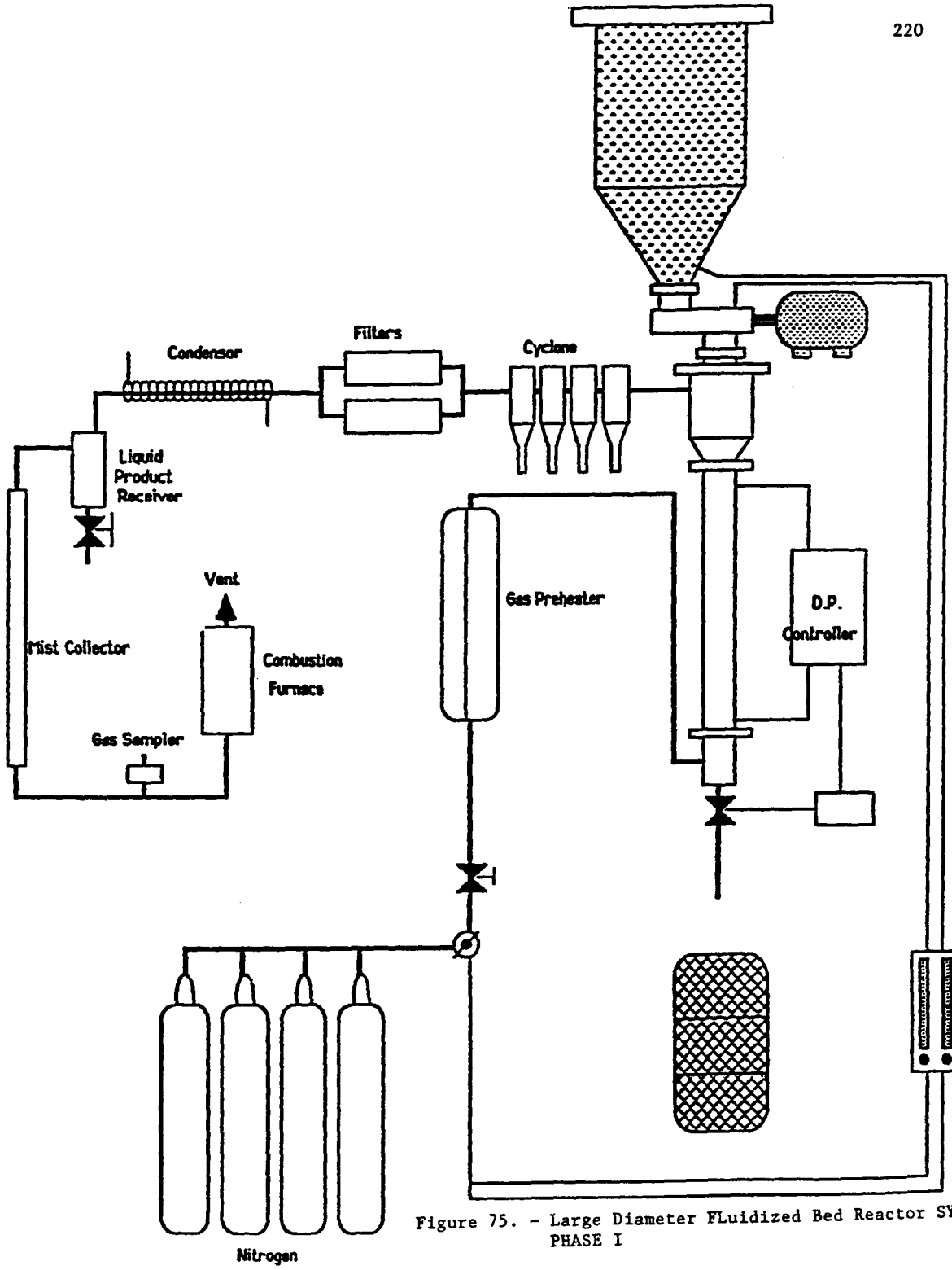

Figure 75. - Large Diameter FLuidized Bed Reactor SYstem
PHASE I

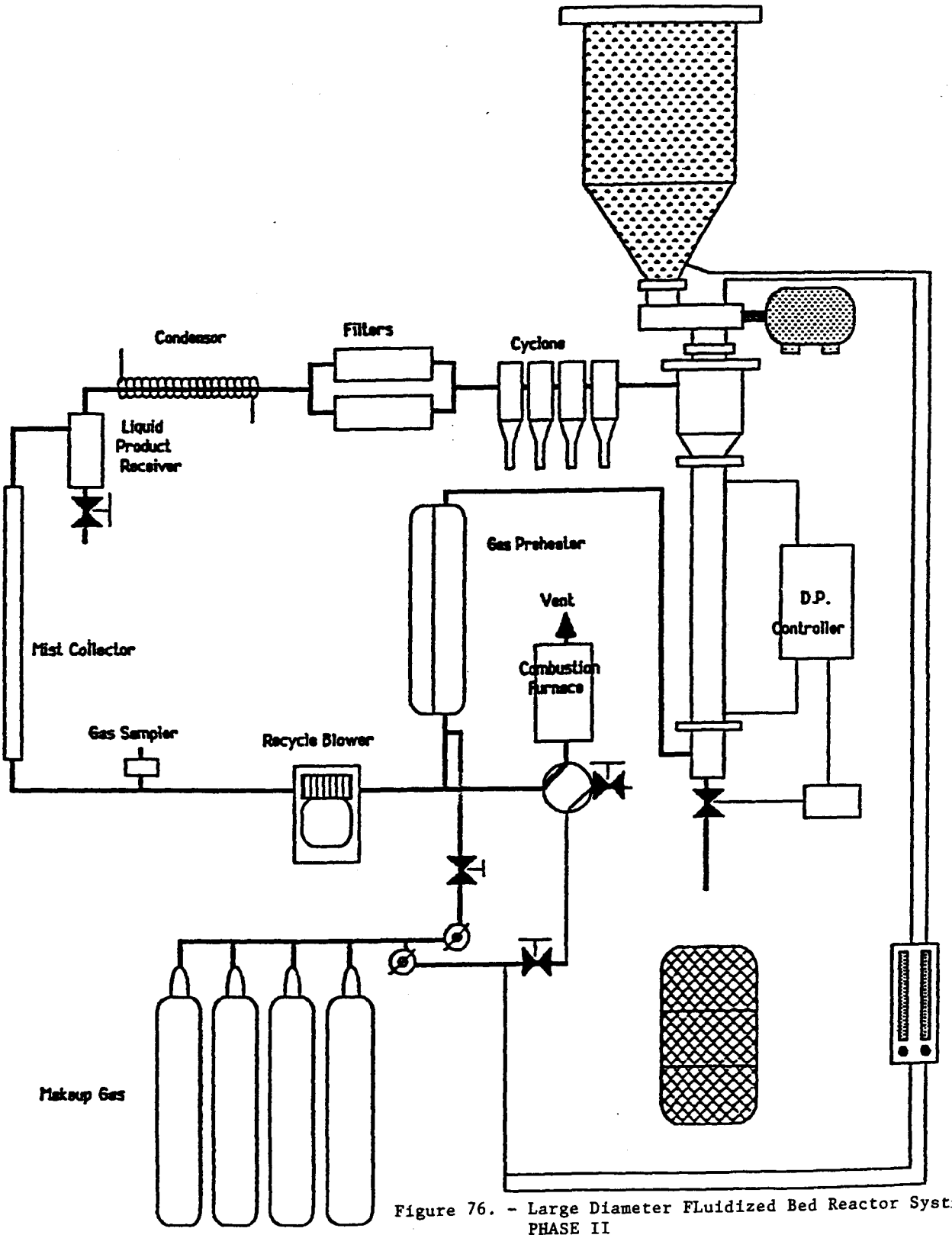

Figure 76. - Large Diameter FLuidized Bed Reactor System
PHASE II

$$V(2) / V(1) = 12.55$$

Where A is the cross sectional area of the reactor:

V is the volume of the reactor;

D is the inside diameter of the reactor;

2 indicates the large diameter reactor;

1 indicates the small diameter reactor.

Using the data accumulated by Venkatesan[31] and Dorius,[33] the following design considerations have been used for the design of the pilot plant:

- Fluidize up to 1/4 inch particle size;
- Solids retention time of 4 to 25 minutes;
- Capable of continuous operation;
- Computer control.

The first two specifications fix most of the design parameters, and the last two are to accomplish the usual objectives of building a pilot plant. The graphs in Figure 77 are TGA data compiled by L.C. Lin for two different particle sizes. The axis labeled "conversion" in these charts reflects the weight loss of removable bitumen from the tar sands.

This data demonstrates that high conversions can be reached in just a few minutes, further supporting the trends observed in data from the small reactor. The higher temperatures produce higher conversions; however, this data does not determine the amount of gas vs. liquid produced. It also does not consider the coke which is formed.

The following specifications were calculated from the above design considerations and will be addressed further in the Design section of this report:

Reactor Diameter	4 inches
Reactor Length	4 feet
Tar Sand Feed Rate (max/min)	231/16 (lbs./hr.)
Gas Flow Rate (max)	60 scfm
Operating Temperature (max)	550°C

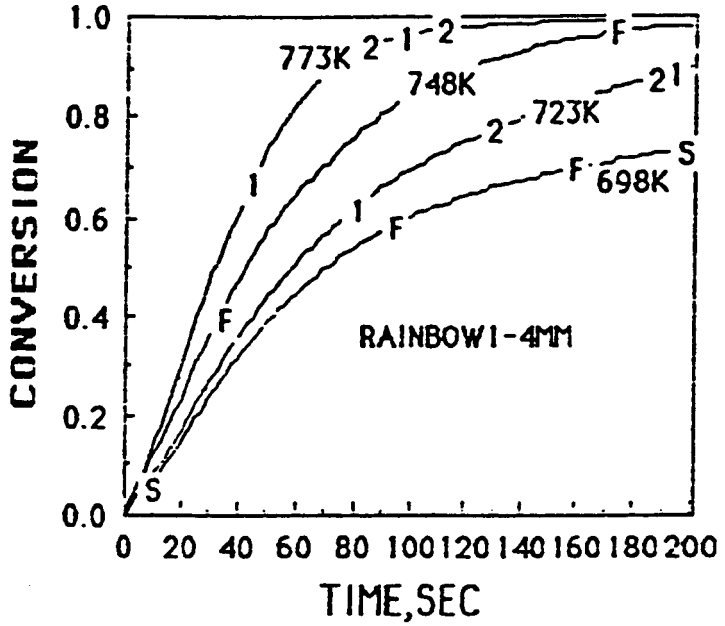

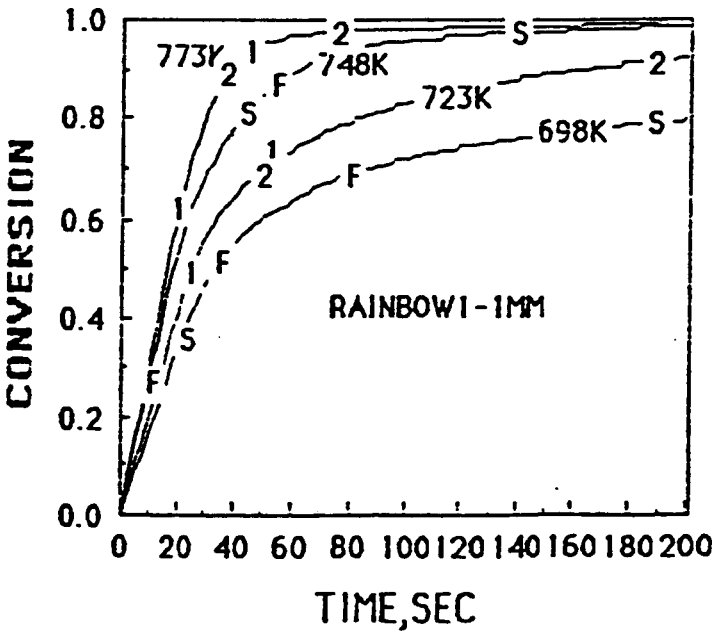

Figure 77. - Bitumen conversion curves.

Operating Pressure	Atmospheric
Run Time	Continuous

Reactor Sizing

The reactor dimension of initial interest is the diameter. Fluid bed characteristics limit the diameter of particle which can comprise a bed in a given diameter reactor without experiencing an appreciable wall effect. Particles 0.25 inches in diameter give a reactor diameter/particle diameter ratio of 16. A minimum ratio of 10 has been suggested before channeling is observed in stationery beds. The limiting factor for increasing the reactor diameter is gas flow rates. Bed fluidization is a function of the linear velocity of the gas through the bed. The volumetric flow rate of the gas needed to maintain a minimum fluidization velocity increases with the square of reactor diameter. Difficult gas handling problems could arise by sizing the reactor too large.

Once the diameter has been determined, the length can be determined as a function of material hold-up in the reactor. This is determined by the bulk density of the bed and retention time which is limited by achievable flow rates of solids from the reactor.

Reactor Configuration

- Small Reactor Tube

  1.25" 40S Pipe, S.S. 304

  I.D. = 1.380 in. = 3.505 cm

  O.D. = 1.660 in. = 4.216 cm

  Length = 35.4 in. = 90 cm

  Cross Sectional Area = 1.49 in^2 = 9.65 cm^2

- Large Reactor Tube

  4" 40S Pipe, S.S. 304

  I.D. = 4.026 in. = 10.116 cm

  O.D. = 4.5 in. = 11.430 cm

Length = 52.25 in. = 132.7 cm

Cross Sectional Area = 12.73 in^2 = 83.13 cm^2

Solids Handling System

Feed Sand Hopper and Screw Feeder: The fluidized bed reactor solids inventory was assumed to be 7 kg at the standard operating conditions. At a feed sand retention time of 10 minutes, the feed sand feed rate would be 42 kg per hour. Under ordinary circumstances, an experiment would be expected to last for 6-8 hours; thus, the mass of feed sand required would be 250 to 350 kg. If the bulk density of the feed sand is 1.4 g/cm^3 (1400 kg/m^3) the volume of feed sand required would be 0.2 to 0.25 cubic meters. Thus the hopper was sized to hold 0.2 cubic meters of feed sand.

Volume of hopper designed is 195,340 cm^3

Assume the feedstock bulk is 1.4 g/cm^3

then the hopper contains feedstock 273.5 kg

If the amount of feedstock inventory in the fluidized bed is 7 kg and the residence time is 10 min, then the feed rate is

7 kg / F(kg/hr) = 10 / 60 hr

F = 42 kg/hr

The hopper will last 6.5 hr.

A schematic of the hopper and hopper cover assembly is presented in Figure 78. The feed sand screw feeder is presented in Figure 78.

Feed System: The fluidized bed height and weight were maintained at constant values by a solid flow valve controlled by a differential pressure cell which monitored the pressure drop across the bed. The weight of solids in the bed has a direct influence on the retention time of the solids.

At the onset of fluidization, the pressure drop across the bed is directly related to the weight of solids (W) in the bed as given by

Pressure Drop = W/A

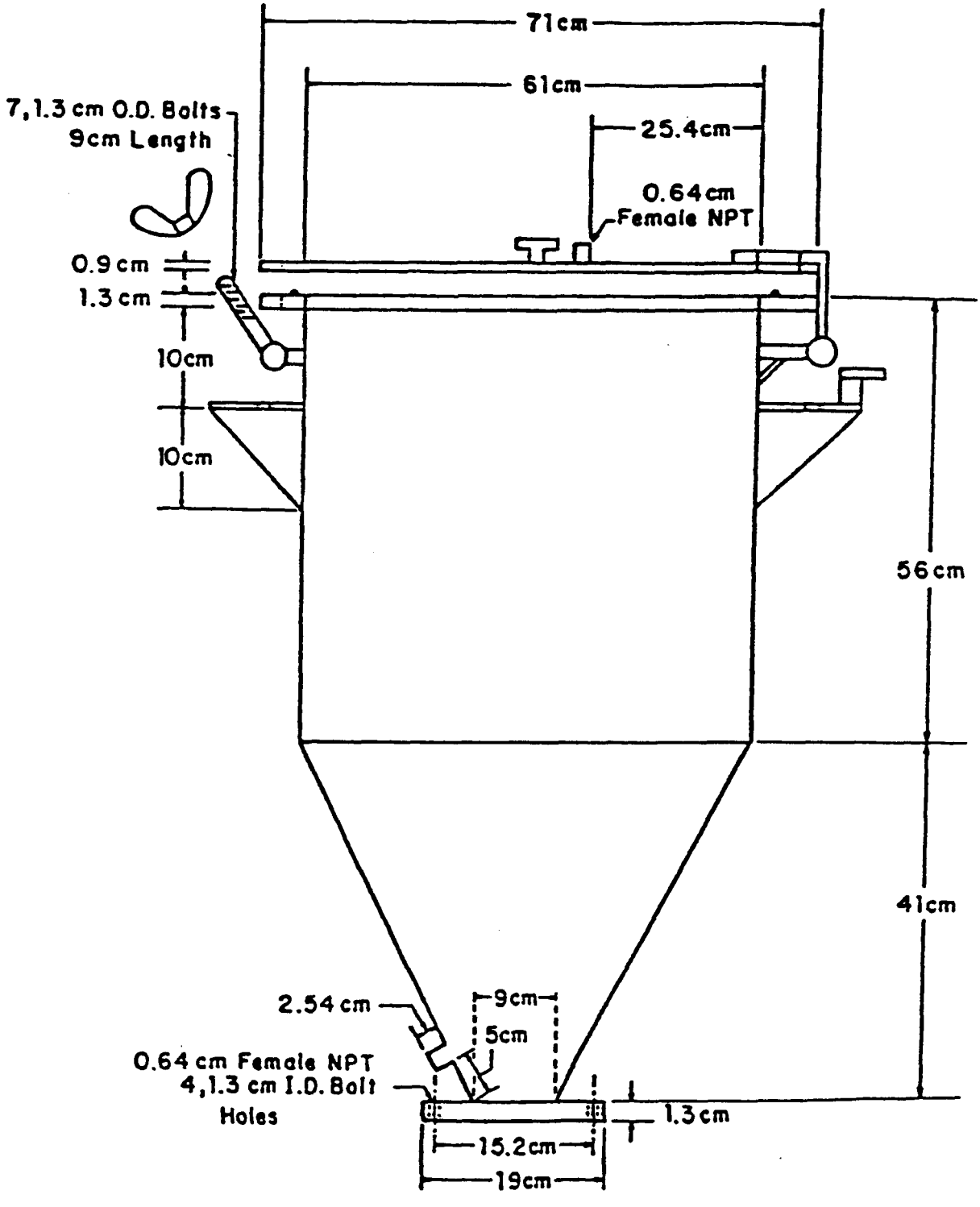

Figure 78. - Diagram of the feed sand hopper.

where W is a mass of particles and A is cross sectional area of the fluidized bed reactor. The bituminous sand feed rate influences the average holding time of solids in the reactor for a given bed height of solids. The sand feed rate can be varied by changing the speed at which the screw turns. During the calibration of the screw, the feeder and the drive assembly were arranged such that the sand coming from the outlet could be collected in a bucket.

The feed system consists of a feed hopper capable of holding about 500 pounds of tar sands and a screw feeder which is operated by a three-phase motor powered by a frequency controller. The frequency controller has an output range of 8 to 80 Hz, giving the motor an operating range of 225 to 2250 rpm. The motor is connected to the screw feeder through a reducing drive that has a gear ratio of 210/1, giving the screw feeder a range of 10.7 to 1.1 rpm. The speed of the A.C. motor that drives the screw can be varied by a frequency controller. Ten to twelve kilograms of sand were loaded into the hopper. The dial on the frequency was set from 20 to 80 Hz and the flow rate of solids from the feeder outlet was established. The flow rate per minute of solids was obtained by collecting the sand for 10 minutes and weighing it.

These are four different particle sizes which were tested.

1. 7 mesh (2.794 mm)----14 mesh (1.168 mm)
2. 14 mesh (1.168 mm)----24 mesh (0.701 mm)
3. 24 mesh (0.701 mm)----42 mesh (0.351 mm)
4. below the 42 mesh (<0.351 mm)

* average interval in each size: 0.8 mm

The results of the sand feed rate calibration for different particle sizes are presented in Figure 79. The value of maximum and minimum residence time can be obtained from this calibration curve.

The reactor maintains: 7 kg

Smallest feed rate: 0.5 kg/min

Largest feed rate: 2.25 kg/min

Max. residence time: 7/0.5 = 14 (min)

Min. residence time: 7/2.25 = 3.11 (min)

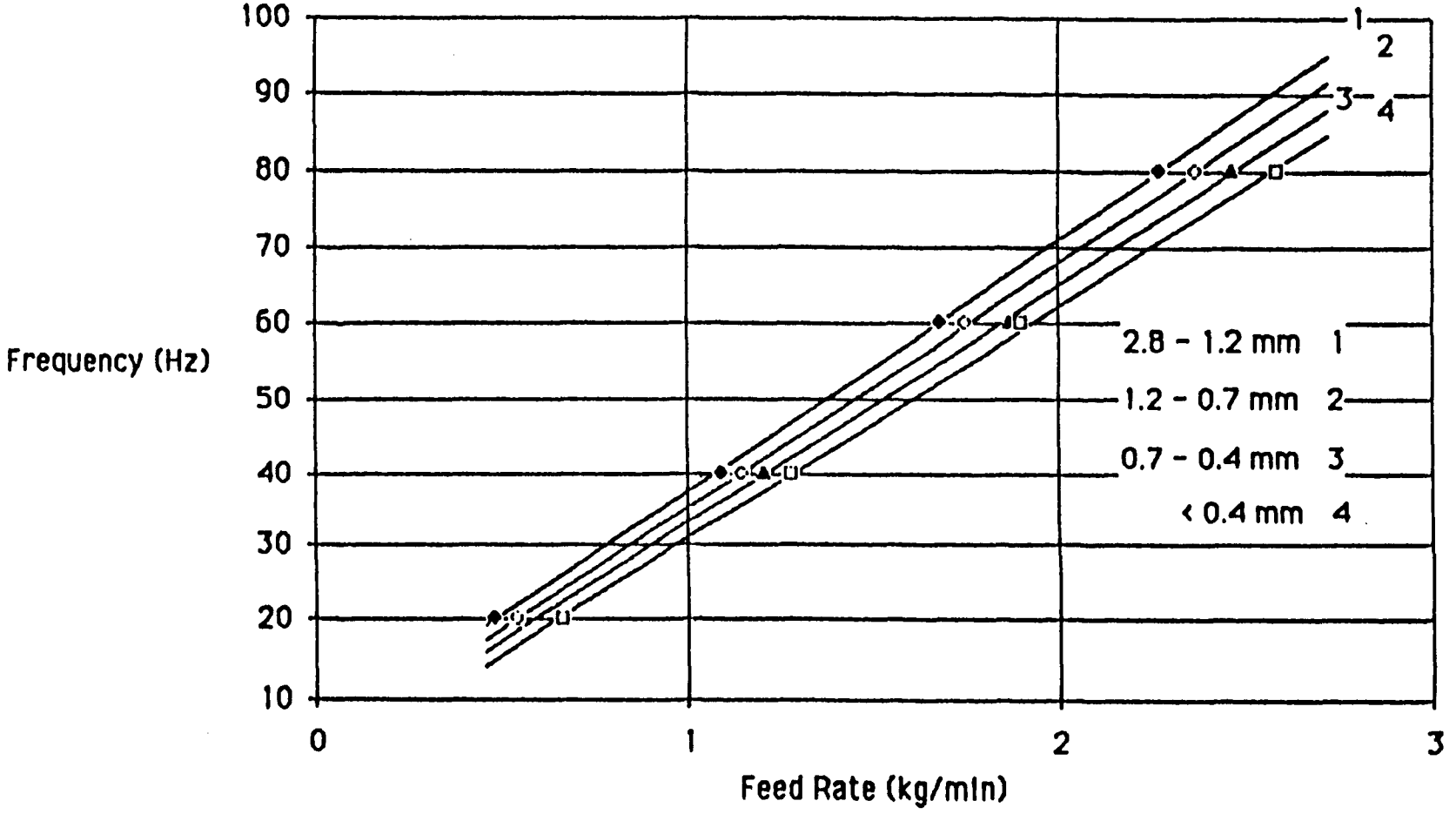

* Correlation Coefficient (R^2)

1. R^2=0.9999 2. R^2=1.0000 3. R^2=0.9990 4. R^2=0.9994

Figure 79. - Pilot plant feed rate test for the Circle Cliff tar sands.

In the work of Venkatesan,[31] the standard residence time was 27.2 minutes. Residence times of 20 to 30 minutes can be obtained on the large unit by winding a spacer on the screw feeder augur.

There are four sizes which will be used for pilot plant ranging from 1/8 inch to 1/4 inch.

a. 0.25 (1/4 inch)---0.221 inch (No 3.5)

6.4 mm---5.6 mm

b. 0.221 inch (No 3.5)---0.187 inch (no 4)

5.6 mm---4.8 mm

c. 0.187 inch (No 4)---0.157 inch (No 5)

4-8 mm---4.0 mm

d. 0.157 inch (No 5)---0.11 inch (No 7)

4.0 mm---2.8 mm

* average interval in each size: 0.9 mm

The average interval in each size which was tested is 0.8 mm and the other size which will be used for pilot plant is 0.9 mm. Therefore, it is possible to predict the feed rates for larger sizes by use of these curves in Figure 80.

For the larger particle size,

max. predicted residence time: 7/0.5 = 14 (min)

min. predicted residence time: 7/1.9 = 3.68 (min)

If the frequency is set at 60 Hz, the feed rate of 1/4 inch particle size will be 1.35 (kg/min) and the residence time will be 5.19 min.

Bed Height Control: Tar sand is continuously added to the reactor, making it necessary to also continuously remove spent coked sand at the same rate. A Differential Pressure (DP) controller operates the valve which allows the spent sand to flow from the reactor. One of the characteristics of a fluidized bed is that the pressure drop across the bed is equal to its static head. A differential pressure controller will accurately control the pressure drop across the bed by keeping the height constant by allowing the sand to flow out of the reactor. This maintains a constant solids loading inside the reactor. The retention time then is set by the feed rate.

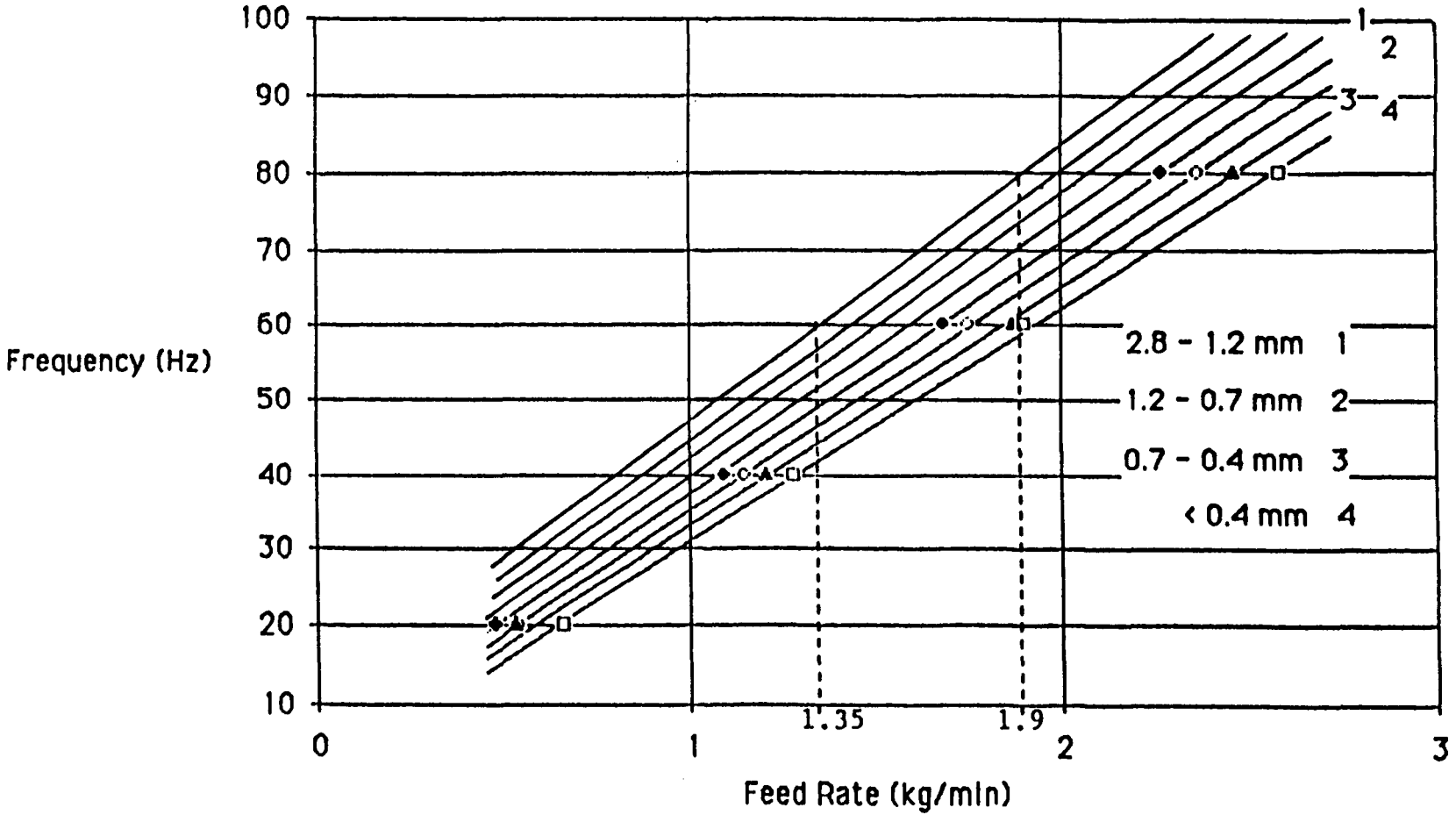

Figure 80. - Pilot plant feed rate test for the Circle Cliff tar sands.

Solids Control Valve: There have been several different techniques devised to continuously remove solids from a reactor system. The system used for this pilot plant is a simple cone valve design which is shown in Figure 81. This design was decided on because of its ability to function at very high temperatures and because of the simplicity of its construction and control. The valve seat is located approximately one inch below the level of the distributor plate and has an opening of 0.88 inches. The stem is controlled by a pneumatic actuator which has a stroke of 1.5 inches, long enough to completely remove the cone from the valve seat providing an unobstructed opening for sand to flow.

Dust Removal: As the gas leaves the bed, a certain amount of fine particles are entrained in the gases rising from the surface at the fluidized bed. The removal of this dust is accomplished by the following sequence: a disengager section, a series of cyclones, and filters.

The disengager is the first in the series. It operates by simply increasing the cross-sectional area, thus decreasing the fluid velocity allowing the largest of the entrained particles to fall back into the bed. The gas enters the cyclones through pipe in the side of the disengager. These cyclones were designed for maximum efficiency using the data from the fluidization test.[38] Because of the wide variation in possible flow rates, the three cyclones are different sizes, each designed for maximum efficiency over a different flow range. If the second cyclone is designed as a standard, the length of the first cyclone can be calculated by multiplying 1.3 times the length of the standard cyclone. Also the length of the third cyclone can be calculated by dividing the length of the standard cyclone by 1.3. The specifications of the cyclones are presented in Figures 82 through 84.

Any particles still remaining in the gas stream after the cyclones will be filtered out using two cintered stainless steel filters (Figure 85). These filters have an estimated nominal pore size of 10 microns.

Product Separation: Once the solid particles are removed from the gas stream, it is cooled to allow the hydrocarbon products to condense and be collected in the liquid product receiver.

Experience with the operation of the small reactor shows that a fine mist forms which contains droplets that approach sub-micron size. The technique used to remove this mist in the small reactor is a fiber mist eliminator. This same technique has been used in Phase I of the big reactor. In Phase

Figure 81. - **Solids flow control valve.**

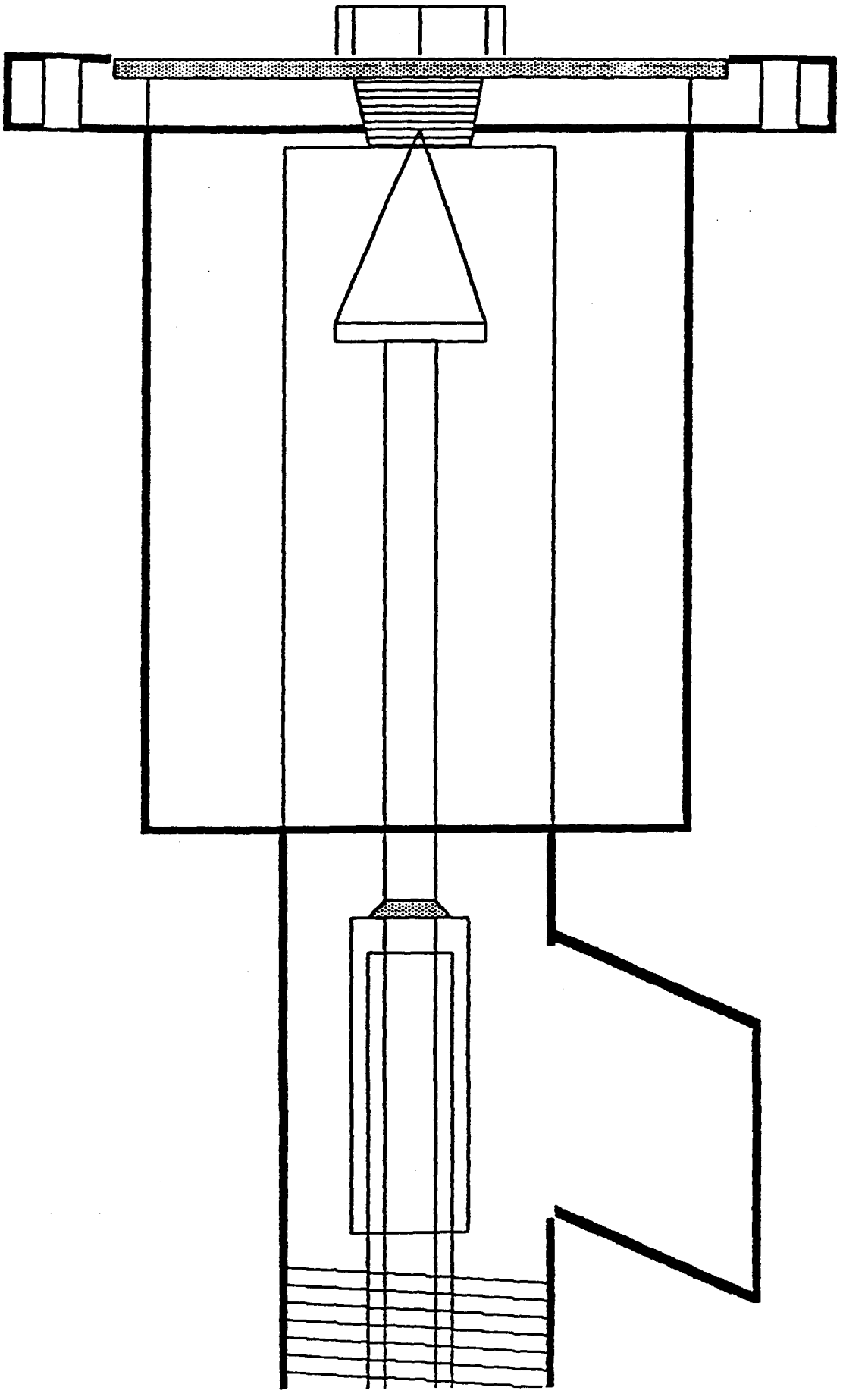

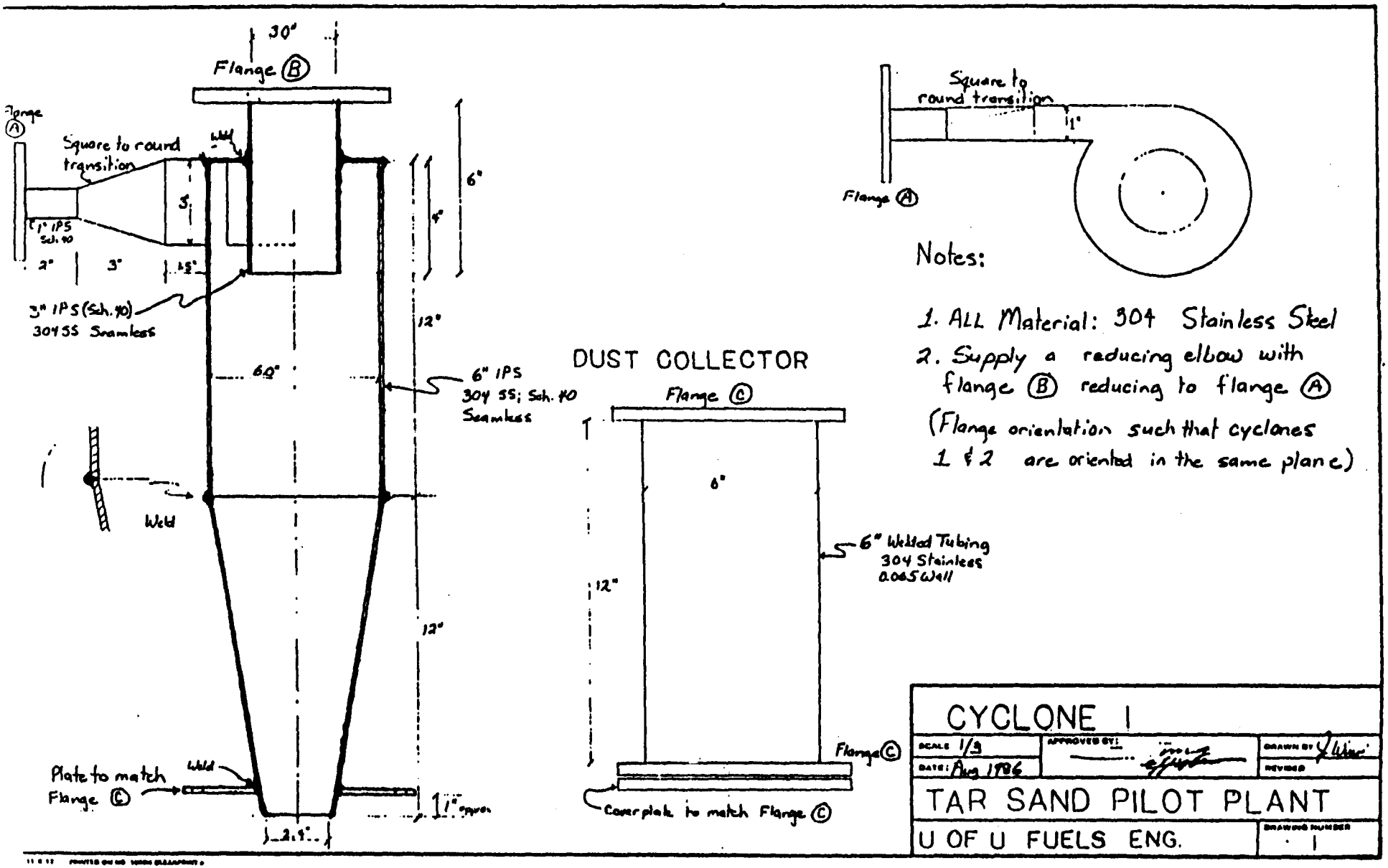

Figure 82. - Cyclone 1 schematic.

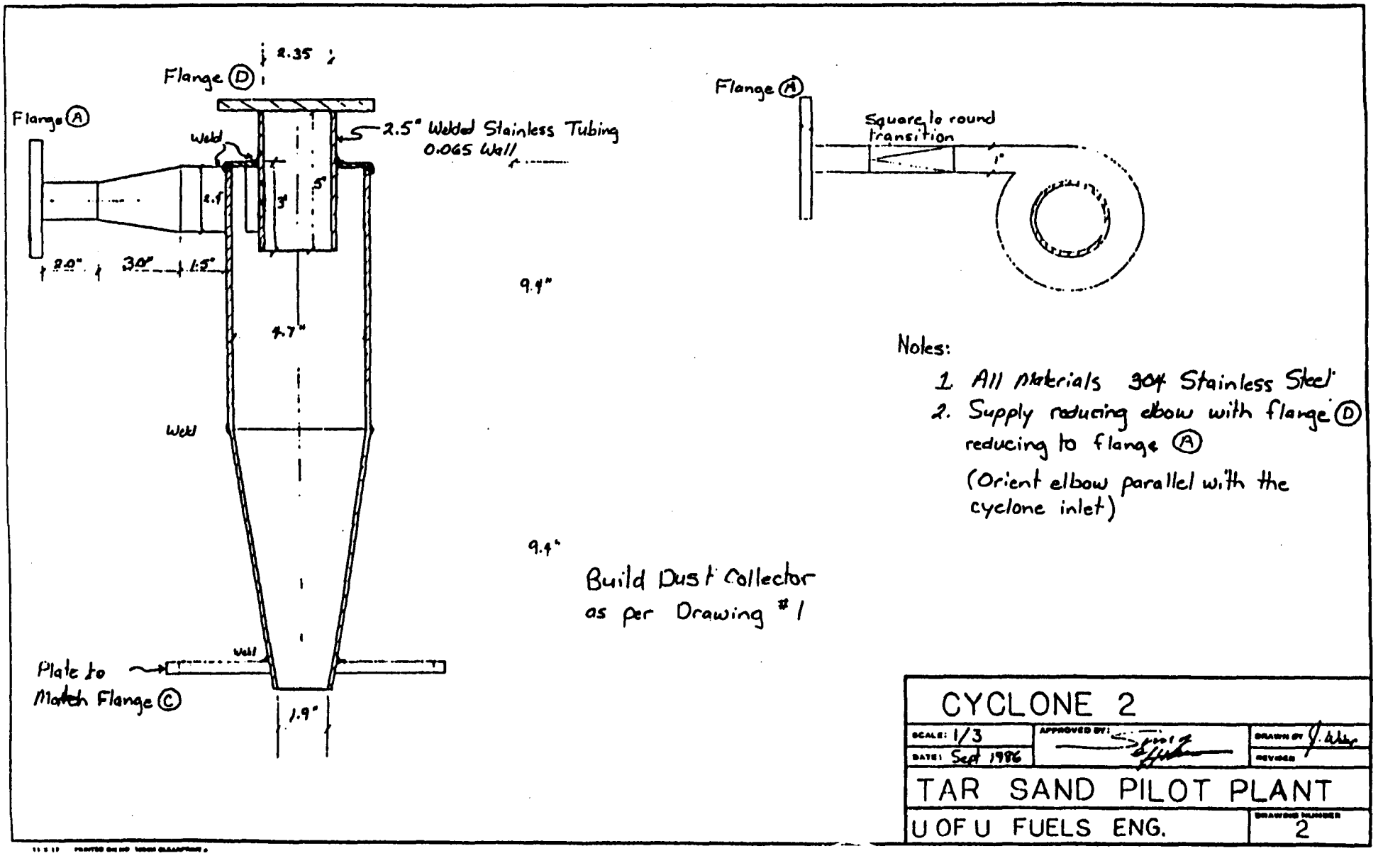

Figure 83. - Cyclone 2 schematic.

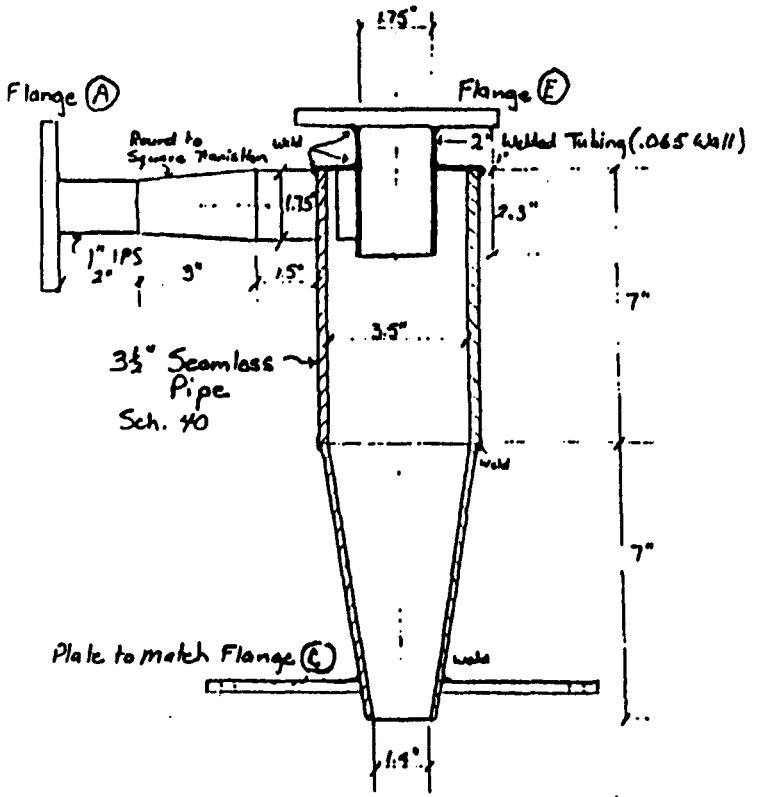

Flange Schedule

Sym	O.D.	I.D.	Number of Bolts	Bolt Hole Diameter	Bolt Pattern Diameter (°/c)	Flange Thickness
(A)	4¼"	To fit 1" IPS	4	⅜"	3"	⅜"
(B)	6½"	To fit 3" IPS	6	⅜"	5¼"	⅜"
(C)	9¾"	To fit 6" O.D. Tubing	5	½"	8¼	¼"
(D)	5½"	To fit 2½" O.D. Tubing	6	⅜"	4½"	⅜"
(E)	4⅞"	To fit 2" O.D. Tubing	6	⅜"	3¾"	⅜"

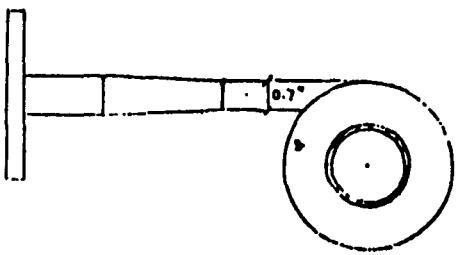

Build Dust Collector as per drawing 1

Notes:

1. ALL Material 304 Stainless Steel
2. Supply a reducing elbow with flange (E) reducing to flange (A) (orientation such that elbow can be parallel with inlet)

CYCLONE 3		
SCALE: 1/3	APPROVED BY:	DRAWN BY:
DATE: Sept. 1986		REVISED
TAR SAND PILOT PLANT		
U OF U FUELS ENG.		DRAWING NUMBER 3

Figure 84. - Cyclone 3 schematic.

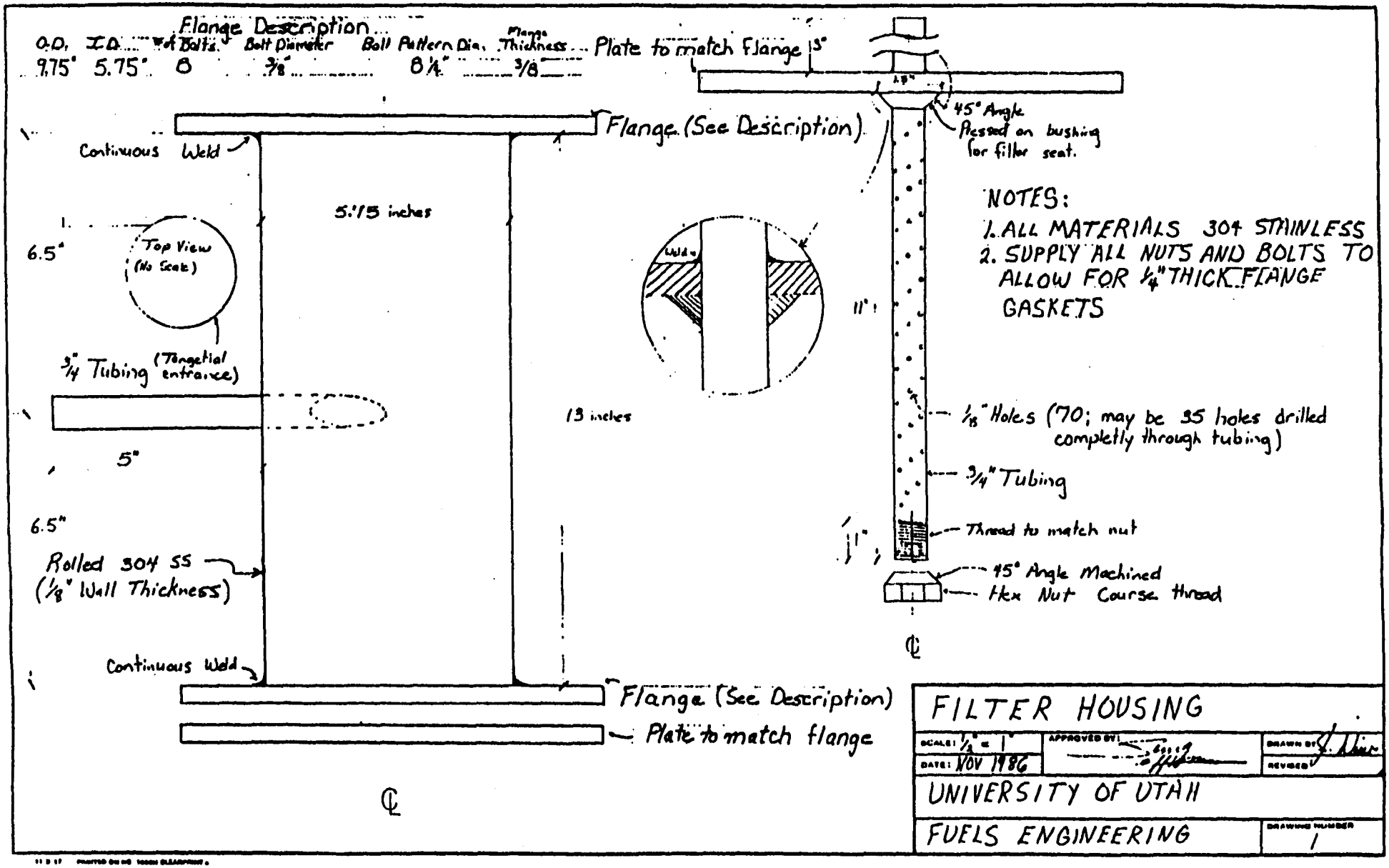

Figure 85. - Fine particle filter schematic.

II, the effectiveness of commercially available equipment will be explored. The schematic of the mist collector is presented in Figure 86.

Temperature Control Systems

Reactor Furnace: Heat will be supplied to the reactor by a 14,000 watt electric furnace. The reactor furnace will be controlled in four different zones using four temperature controllers. Each controller operates a solid state switch which allows current to flow through the resistance heater inside the furnace. Following is an estimate for the heat duty required for the reactor furnace.

Sand feed rate (@25°C) 42 kg/hr

Gas flow rate (@200°C) 100,000 g/hr

(42,000 g/hr)(0.21 cal/g°C) (450°C) +

(100,000 g/hr) (.26 cal/g°C) (275°C) = 11,100 kcal/hr

11,100 kcal/hr = 13,000 Watts

This simple calculation does not consider heat transfer inefficiencies and the location of the heater elements. The top zone of the furnace is located in the freeboard space of the reactor and thus unable to transfer heat to the bed. Therefore, it will be necessary to use additional or supplemental heating units when operating at high flow rates.

Nitrogen Preheat: The fluidizing nitrogen will be preheated using a 5,500 watt Lindburg Furnace. This furnace will not be able to supply the heat necessary to heat the nitrogen to reaction temperatures at higher flow rate needed to fluidize larger particles sizes; therefore, an auxiliary preheater will also be necessary. However, the availability of the furnace at no cost was a key consideration in its incorporation into the unit. Calculations are as follows:

Heater capacity: 5,500 Watts = Joules/sec = 4,730 kcal/hr

$$\frac{(4,730,000 \text{ cal/hr})}{(0.26 \text{ cal/g C})\ (100,000 \text{ g/hr})} = (182+25)^{\circ}C = 207^{\circ}C$$

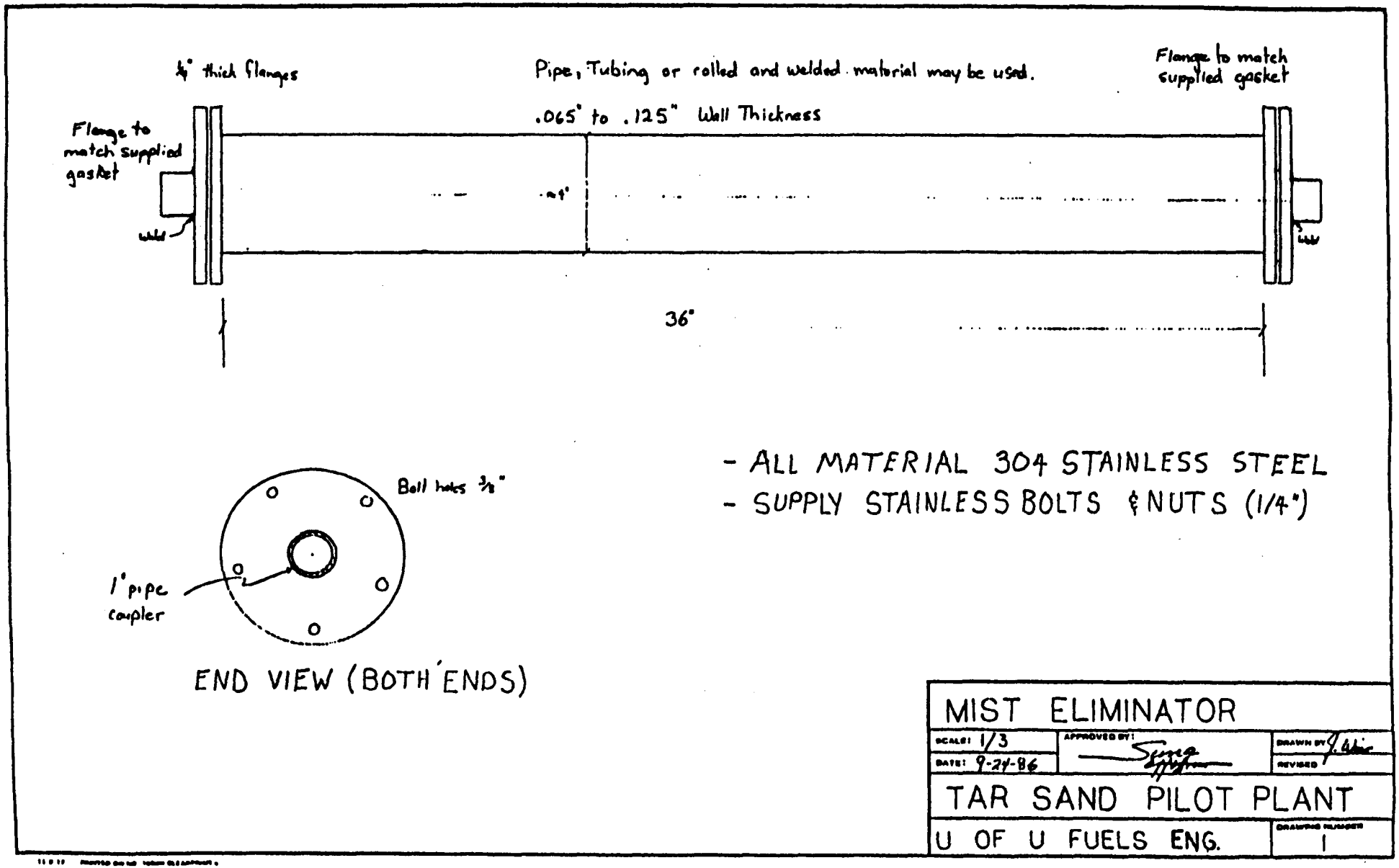

Figure 86. - **Mist eliminator housing.**

Gas Handling System

Cyclones and Filter Heat: It will be important to maintain the temperature of the cyclones and the filter close to reactor temperature to prevent any condensation of the produced bitumen-derived hydrocarbon liquid that might cause plugging. The gas entering the cyclones and filter will still be close to reactor temperature; therefore, the only heat input required will be to offset losses through the insulation. This can be accomplished using heating tapes. The schematic of the gas handling system is shown in Figure 87.

Condenser: The condenser is a simple tube and shell heat exchanger using cold water as the cooling fluid. Calculations for the condenser heat duty:

Maximum gas flow rate (1.5* Min.)	100,000 g/hr
Nitrogen heat capacity	0.26 cal/g°C
ΔH vap of C_5^+	80 cal/g°C
Maximum Bitumen condensation rate	3,000 g/hr

(100,000) (0.26) (475-25°C) + (3,000) (0.80) (475-25°C) = 12,800 kcal/hr

Heat transfer calculations indicated that the required surface area can be achieved using a 20 ft long tube and shell heat exchanger. This was built in four sections.

Screw Feeder Cooling: The tendencies for the feed sand to agglomerate during the feeding process is a function of temperature. The temperature of the disengager will be close to reaction temperature, thus making it necessary to cool the screw feeder. There are three ways that screw feeder heating will be prevented. First, the flange gasket between the disengager and the screw feeder is comprised of three 300-pound asbestos felt gaskets. This should give maximum insulation at the flange face. Second, a nitrogen bleed is connected to the screw feeder and the hopper. This will keep a flow of cool nitrogen moving down through the screw feeder and enter the top of the disengager carrying with it some heat. Third, a copper tube carrying cold water will be wrapped around the screw feeder housing to maintain the appropriate feed sand temperature.

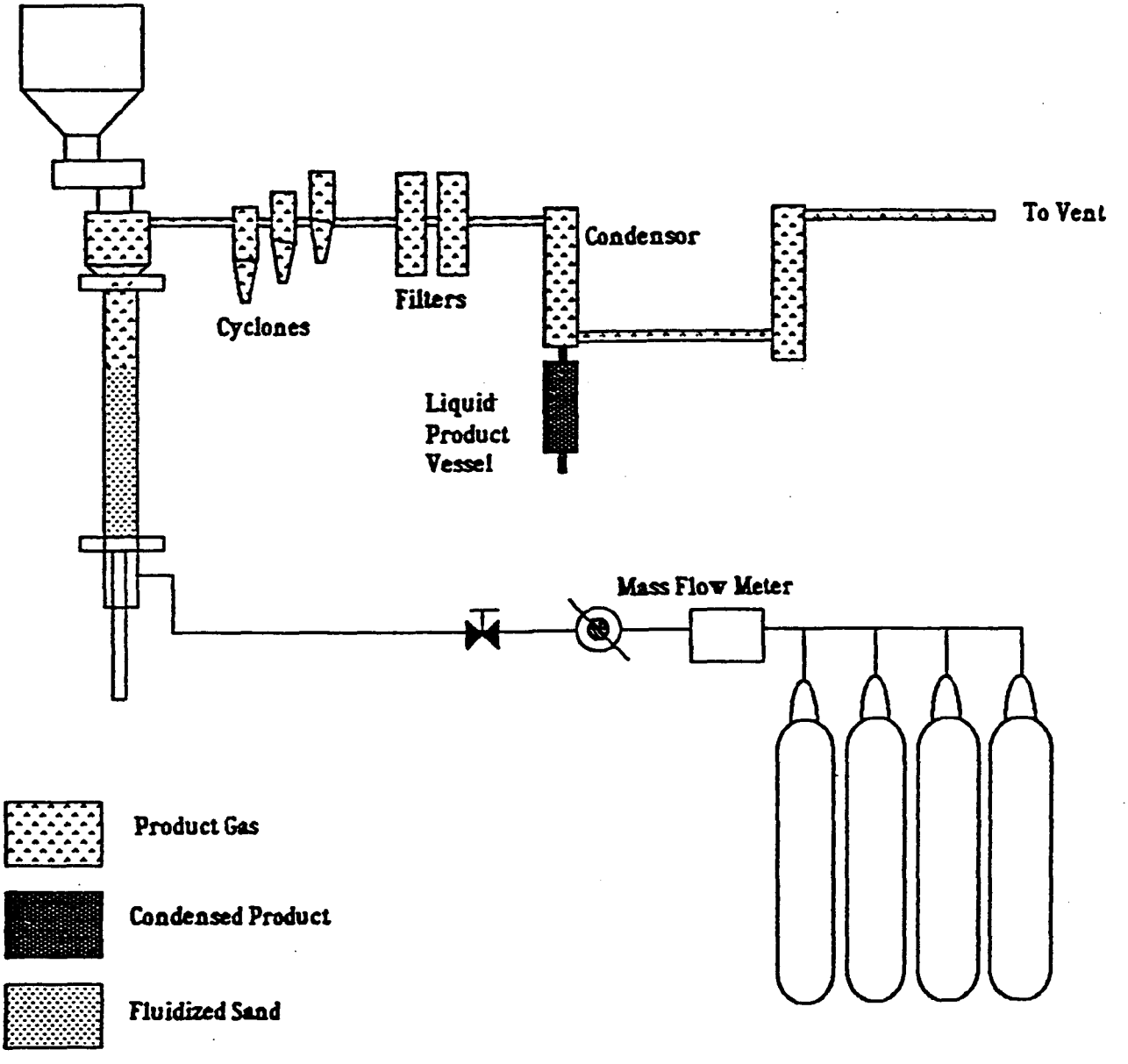

Figure 87. - Gas handling system.

Instrumentation

Temperature Measurement: The temperatures being measured in this pilot plant will range from 25°C to 550°C. This system has been designed using K-type thermocouples and standard digital temperature readout with built-in cold junction compensation.

Reactor and gas stream temperatures are measured directly by using the appropriate tube fittings such that the thermocouple can be inserted directly into the process stream. Control thermocouples are placed on the outside close to the heater element, which for this high current demand system provides the safest and most effective control.

Pressure Measurement: Several types of pressure measurement will be used in this system: pressure transducers, differential pressure meters, and gauges. The data from the pressure measurement is used to control bed height and to monitor any plugging of the cyclones and filters.

Flow Rates: A differential pressure transducer will be used to determine the gas flow rate in place of the mass flow meter which created an unacceptable pressure drop.

Computer Control and Data Logging: The data logging for Phase I and the process control for Phase II will be done using an IBM PC-XT. This micro computer has a 20 megabyte fixed disk drive which is capable of storing data from runs lasting several weeks. Also present is a single floppy disk drive and a printer with a fifteen inch wide carriage for the purpose of printing reports after each run. Interface hardware is readily available for the IBM; Metrabyte products have been chosen for this system.

Each of the components purchased for the pilot plant was done so with the Metrabyte specifications in mind. Data logging in Phase I will consist of the following:

16 Thermocouples

3 Pressure Transducers

1 Turbine Type Flow Indicator

Preliminary Testing Program: The large diameter reactor system is at a point where pre-operation calibration and fluidization experiments have been completed. Several preliminary test runs have been completed using the Circle Cliffs tar sand. The experiments were carried out at a reactor temperature of 723 K and a sand retention time of 24 minutes. While the experiments were not entirely satisfactory in terms of equipment performance, the produced liquid product recovery was good. The produced hydrocarbon liquid analyses from runs CC-4 and CC-5 are reported in Table 52. The data indicate the produced liquid had a much higher volatility, 88 wt.% versus 41 wt.%, than the native Circle Cliffs bitumen; however, the gravity of the liquid product was little different from that of the native bitumen.

Table 52

Product Qualities from Circle Cliffs Tar Sand
Large Diameter Reactor

Hydrocarbon Liquid Product Analyses	Run #4	Run #5
Reactor Temperature, K	723	723
Sand Retention Time, min.	24	24
Density, g cm^3 (288.7 K)	0.962	0.970
Specific Gravity	0.963	0.972
^oAPI	15.4	14.1
Viscosity, cps (228.7 K)		
Simulated Distillation		
Volatility, wt.%	84.8	88.7
IBP - 125°F, wt.%	--	--
125 - 400°F, wt.%	0.5	2.1
400 - 650°F, wt.%	16.0	23.3
650 - 1050°F, wt.%	68.3	63.3
1050^oF^+ Residue, wt.%	15.2	11.3

MATHEMATICAL MODEL OF THE PYROLYSIS OF BITUMEN-IMPREGNATED SANDSTONE PARTICLES

F.V. Hanson — Associate Professor
Liang C. Lin — Graduate Student

ABSTRACT

A mathematical model of the pyrolysis of bitumen-impregnated sandstone particles has been developed. The governing equations describing diffusion and chemical reaction within the tar sand particles were solved analytically using a finite integral transform technique. The analysis gave not only the final distribution of products in the bulk fluid phase but also the transient intraparticle concentration profiles for the various products as a function of time.

INTRODUCTION

Bitumen-impregnated sandstone, or tar sand, represents a significant hydrocarbon resource. The world's identified tar sand resources are estimated to be approximately 2,265 billion barrels, of which about 944 billion barrels are located in Canada, 692 billion barrels in Venezuela, and 604 billion barrels in the Soviet Union.[58] The United States has an identified resource of about 28 billion barrels, much of which is located in seven major deposits in the eastern and southeastern regions of the State of Utah.[59]

It has been estimated that approximately 25 percent of the Utah tar sand resource is amenable to surface mining.[60] Several mining-surface recovery methods have been developed to recover the bitumen or a bitumen-derived hydrocarbon liquid from the bitumen-wet tar sands of Utah. Among the processes are the high temperature water separation,[61] solvent assisted modified high temperature water separation,[62] low temperature water separation,[63] fluidized bed pyrolysis,[31-33,64] and rotary kiln pyrolysis.[65,66] An excellent overview of the aqueous separation/recovery processes has been reported by Miller and Misra.[67] The retorting processes have an advantage over the separation processes in that the produced hydrocarbon liquid may be directly integrated into a hydrogen refinery feed slate without additional coking.

Fluidized bed pyrolysis is an effective method for the surface recovery of bitumen-derived hydrocarbon liquids from tar sands. In the retort, the tar sand rapidly is heated to the pyrolysis temperature. A sequence of physical and chemical events takes place as the bitumen-impregnated sand grains are heated from the ambient, inlet temperature to the final fluidized bed pyrolysis temperature. The initial physical process involves the vaporization of low molecular weight volatiles in the absence of coking or thermal cracking. This phase takes place up to 598 K and may involve upwards of 65 percent (by weight) of the original bitumen within the particle. Above 598 K temperatures are attained at which the bitumen decomposes to lower molecular weight hydrocarbon species in the liquid phase. These produced hydrocarbon species are vaporized, transported to the outer surface of the sand particle, and swept out of the retort by the fluidizing gas which may be an inert gas such as nitrogen or steam or by the produced gas from the combustion of the carbonaceous residue on the spent sand. In order to optimize the retorting process, several physical and chemical variables must be controlled. The analysis of the pyrolysis reaction for bitumen-impregnated sandstone particles requires consideration of heat transfer from the gas phase to the sand particles and to the bitumen, the non-equilibrium vaporization of the volatile components of the bitumen, the transport of these volatile species from the interior regions of the particle to the external surface,the decomposition of the bitumen to lower molecular weight species and the transport of the vapor phase bitumen-derived hydrocarbon species from the interior of the porous sand particle to the bulk fluid phase at the external surface of the particle. In this analysis, the pyrolysis reaction accompanied by the diffusive transport of the vapor phase bitumen-derived hydrocarbon products formed the basis for the model while the effect of the vaporization of volatile components accompanied by bulk flow of these species to the external surface has been assumed to be negligible above 598 K to a first approximation.

A preliminary mathematical model for the isothermal pyrolysis of a single bitumen-wet tar sand particle has been reported in which the product distribution and yields of hydrocarbon fractions from a single particle were calculated as a function of particle temperature and size for a simple reaction network.[68] A subsequent model will treat the vaporization-bulk flow transport model.

PROBLEM FORMATION

The bitumen pyrolysis reaction network for bitumen which remains in contact with the sand matrix in its natural state is extremely complex. The following reaction network is now proposed as a more realistic and yet amenable model of the system for temperatures above 598 K:

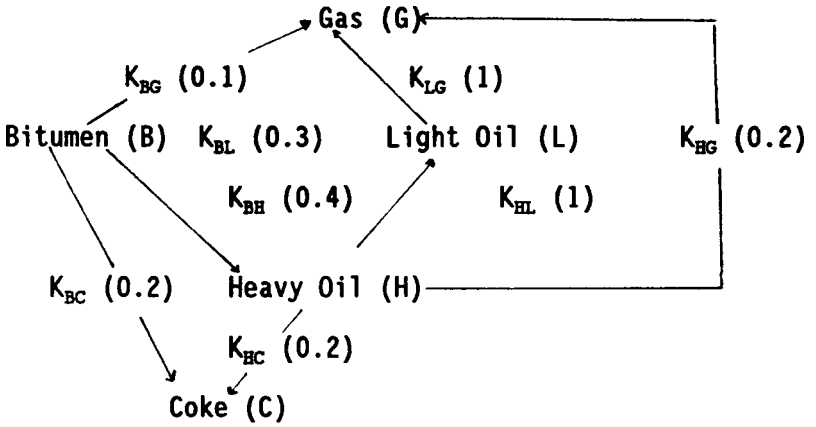

Four "classes" of hydrocarbon species are assumed to comprise the products of the pyrolysis reactions: light gas (G), light oil (L), heavy oil (H), and coke (C). Coke is the carbonaceous residue on the surface of the sand, and light gases are the C_1-C_4 hydrocarbons. There is no defined distinction between light oil and heavy oil, since any convenient boiling ranges could be designated as the light and heavy oil fractions. The condensible hydrocarbon liquid with a boiling range from C_5^+ to 650°F is classified as light oil, and that boiling above 650°F is classified as heavy oil for the purpose of this study.

As a first approximation, all reactions are assumed to be first order. Spherical coordinates were used due to the assumption that the sand particles are spherical in shape. The variables were assumed symmetric in both the θ and ϕ dimensions. The differential material balance equation for the five classes of species are given by the following equations:

$$\partial C_B/\partial t = -(k_{BG} + k_{BL} + k_{BH} + k_{BC})\, C_B; \tag{31}$$

$$\partial C_H/\partial t = D_H\, \nabla^2 C_H + k_{BH} C_B - (k_{HL} + k_{HG} + k_{HC})\, C_H; \tag{32}$$

$$\partial C_L/\partial t = D_L \nabla^2 C_L + k_{BL} C_B + k_{HL} C_H - k_{LG} C_L; \quad (33)$$

$$\partial C_G/\partial t = D_G \nabla^2 C_G + k_{BG} C_B + k_{LG} C_L + k_{HG} C_H; \text{ and} \quad (34)$$

$$\partial C_C/\partial t = k_{BC} C_B + k_{HC} C_H. \quad (35)$$

The initial conditions are as follows:

$$@ \quad t = 0; \; C_B = C_{BO}, \; C_H = C_L = C_G = C_C = 0; \quad (36)$$

and the boundary conditions are

$$@ \quad r = 0; \; \partial C_H/\partial r = \partial C_L/\partial r = \partial C_G/\partial r = 0; \quad (37)$$

$$@ \quad r = R; \; C_H = C_L = C_G = 0. \quad (38)$$

The first term on the right-hand side of equations 32 through 34 is the molar flux of the class of species. The driving force in these expressions is identical to Fick's law of diffusion. The conductances of these driving forces, or more specifically, the "modified effective diffusivities," D_G, D_L, and D_H, are defined (based on total cross-section area) in such a way that they encompass the overall effects due to molecular diffusion, eddy diffusion, and convective flow. Only when convective flow predominates does the consideration of the pressure gradient within the particle become important.[69] The bitumen undergoing pyrolysis is assumed to be in the plastic state and is considered immobile on the surface of the sand. The film resistance at the solid-fluid interface has been assumed to be negligible because of the high sweep velocity of the bulk fluid flowing past the particle. The present model assumes that the particle size remains constant throughout the course of the pyrolysis reaction and that the heat of reaction is negligible. This second assumption is reasonable since the bitumen content is relatively low for consolidated tar sand particles and the bulk of the particle (88 to 95%) is the sand matrix. Isothermal conditions were assumed for relatively small particles and the intraparticle temperature was assumed to be the surface temperature of the particle. In the fluidized bed, isothermal conditions were

usually assumed because of the small amount of feed tar sand fed to the reactor per unit time compared to the hot sand inventory in the reactor.

The analysis was simplified by defining the following dimensionless variables:

$$k_1 = k_{BG} + k_{BL} + k_{BH} + k_{BC} \quad (39)$$

$$\tau = k_1 t \quad (40)$$

$$U_j = C_j/C_{BO} \ (j = B, H, L, G, C) \quad (41)$$

$$x = r/R \quad (42)$$

$$\phi_j^2 = R^2 k_1/D_j \ (j = H, L, G) \quad (43)$$

$$f_1 = k_{BH}/k_1 \quad (44)$$

$$f_2 = (k_{HL} + k_{HG} + k_{HC})/k_1 \quad (45)$$

$$f_3 = k_{BL}/k_1 \quad (46)$$

$$f_4 = k_{HL}/k_1 \quad (47)$$

$$f_5 = k_{LG}/k_1 \quad (48)$$

$$f_6 = k_{BG}/k_1 \quad (49)$$

$$f_7 = k_{HG}/k_1 \quad (50)$$

$$f_8 = k_{BC}/k_1 \quad (51)$$

$$f_9 = k_{HC}/k_1 \quad (52)$$

In terms of the dimensionless variables and parameters, equations 31 through 35 become:

$$\partial U_B/\partial \tau = -U_B; \quad (53)$$

$$\partial U_H/\partial \tau = (1/\phi_H^2)\ \nabla^2 U_H + f_1 U_B - f_2 U_H; \quad (54)$$

$$\partial U_L/\partial \tau = (1/\phi_L^2)\ \nabla^2 U_L + f_3 U_B + f_4 U_H - f_5 U_L; \quad (55)$$

$$\partial U_G/\partial \tau = (1/\phi_G^2)\ \nabla^2 U_G + f_6 U_B + f_5 U_L + f_7 U_H; \text{ and} \quad (56)$$

$$\partial U_C/\partial \tau = f_8 U_B + f_9 U_H; \quad (57)$$

where

$$\nabla^2 = (1/x^2)\ \partial/\partial x\ (x^2/\partial x). \quad (58)$$

The dimensionless initial conditions are

$$@\ \tau = 0;\ U_B = 1,\ U_H = U_L = U_G = U_C = 0; \tag{59}$$

and the dimensionless boundary conditions are

$$@\ x = 0;\ \partial U_H/\partial x = \partial U_L/\partial x = \partial U_G/\partial x = 0; \tag{60}$$

and

$$@\ x = 1;\ U_H = U_L = U_G = 0. \tag{61}$$

It is pointed out that $'_j$ (j = H, L, G) served as a Thiele-type modulus for a spherical particle.[70]

SOLUTIONS TO THE PARTIAL DIFFERENTIAL EQUATIONS

The differential material balance equation for diffusion and chemical reaction inside a porous particle is given by the following equation:[71]

$$D_{eff}\ \nabla^2 C(r,t) + R(r,t) = \partial C(r,t)/\partial t. \tag{62}$$

The homogeneous part of the above equation can be separated to obtain the following eigenvalue problem in the spacial coordinate alone:

$$\nabla^2\ \psi(r) + \lambda^2\ \psi(r) = 0 \quad \text{in region V} \tag{63}$$

This equation has solutions for specific values of λ ($\lambda = \lambda_m$, m = 1, 2, 3, ...,); and the corresponding functions $\psi(\lambda_m,r)$ are the eigenfunctions. The eigenfunctions $\psi(\lambda_m,r)$ of this eigenvalue problem satisfy the following orthogonality condition:

$$\int_V \psi(\lambda_m r)\psi(\lambda_n,r)dv = \begin{cases} 0 \text{ for } m \neq n \\ N(\lambda_m) \text{ for } m = n \end{cases} \tag{64}$$

where the normalization integral $N(\lambda_m)$ is defined as

$$N(\lambda_m) = \int_V [\psi(\lambda_m,r]^2 \, dv \ . \tag{65}$$

The representation of a function C(r,t) defined in the finite region V, in terms of the eigenfunctions $\psi(\lambda_m,r)$ is given by

$$C(r,t) = \sum_{m=1}^{\infty} C_m(t)\psi(\lambda_m,r) \quad \text{in region V} \tag{66}$$

where the summation is taken over the entire discrete spectrum of eigenvalues λ_m. The coefficient $C_m(t)$ can be determined if we multiply both sides of the equation by $\psi(\lambda_m,r)$ and integrate over the region V, utilizing the orthogonality relation to obtain:

$$C_m(t) = [1/N(\lambda_m)] \int_V \psi(\lambda_m,r)C(r,t) \, dv. \tag{67}$$

This expression is introduced into equation 66 and the resulting representation is split into two components which define the integral-transform pair in the space variable r for the function C(r,t):

$$\text{Inversion formula:} \quad C(r,t) = [\psi(\lambda_m,r)/N(\lambda_m)] \, C(\lambda_m,t) \tag{68}$$

$$\text{Integral formula:} \quad C(\lambda_m,t) = \int_V \psi(\lambda_m,r) \, C(r,t) \, dv \tag{69}$$

where $C(\lambda_m,t)$ is called the integral transform of the function C(r,t) with respect to the space variable r, and $\psi(\lambda_m,r)$ is the kernel of the integral transformation. The spacial coordinate r in the function C(r,t) is removed through the integral transformation.

The integral transform of $\nabla^2 C(r,t)$ can be evaluated by making use of Green's theorem:

$$\int_V \psi(\lambda_m,r) \, \nabla^2 C(r,t) dv = \int_V C(r,t)\nabla^2\psi(\lambda_m,r) \, dv$$

$$+ \sum_{i=1}^{s} \int_{S_i} [\psi(\lambda_m,r)\ \partial C(r,t)/\partial n_i - C(r,t)\partial\psi(\lambda_m,r)/\partial n_i]\ ds_i \qquad (70)$$

where i = 1, 2, 3, ...,s and s is the number of continuous boundary surfaces in the region V. If the surface concentration is equal to zero, then the summation term in equation 70 is eliminated. The homogenous part of the original equation (33) provides the following relationship:

$$\nabla^2\ \psi(\lambda_m,r) = -\lambda_m^{\ 2}\ \psi(\lambda_m,r)\ . \qquad (71)$$

If we multiply both sides of equation 71 by C(r,t) and integrate over the region V, we obtain:

$$\int_V \nabla^2\psi(\lambda_m,r)C(r,t)dv = -\lambda_m^{\ 2} \int_V \psi(\lambda_m,r)C(r,t)dv = -\lambda_m^{\ 2}\ C(\lambda_m,t)\ . \qquad (72)$$

When the surface concentration is zero, it is obvious from equations 70 and 71 that the integral transform of $\nabla^2 C(r,t)$ is:

$$\int_V \psi(\lambda_m,r)\ \nabla^2 C(r,t)\ dv = -\lambda_m^{\ 2}\ C(\lambda_m,t)\ . \qquad (73)$$

It is to be noted that in the above representation, the integral is a volume, surface, or line integral for the three-, two-, or one-dimensional regions, respectively. Furthermore, the Sturm-Liouville weighting function must be included for non-rectangular coordinate systems.[72-74]

The solution for the dimensionless bitumen concentration is given by:

$$U_B = \exp(-\tau). \qquad (74)$$

The concentration distribution for the heavy oil, light oil, and the hydrocarbon gas fractions were obtained by means a of finite integral transformation. The transform of U_j is given by:

$$U_j = \int_0^1 x^2 U_j k_n(x)\ dx \qquad (75)$$

where x^2 is the weighting function for the spherical coordinate system. The kernel of the transformation, $k_n(x)$, is given by:

$$k_n(x) = \sin(\lambda_n x)/x. \tag{76}$$

The parameter λ_n is the eigenvalue corresponding to the function $k_n(x)$ and is given by:

$$\lambda_n = n\pi;\ (n = 1, 2, 3, \ldots, \infty). \tag{77}$$

When the integral transform is applied to equation 54, we obtain:

$$dU_H/d\tau + [\lambda_n^2/\phi_H^2 + f_1 \exp(-\tau)]\mathbf{1} \tag{78}$$

where **1** is the transform of unity and is given by:

$$1 = \int_0^1 x^2(1)k_n(x)\,dx = -\cos\lambda_n/\lambda_n\ . \tag{79}$$

The transformed equation (equation 78) is of the form of an ordinary differential equation and was solved by applying the initial condition:

$$\tau = 0\ ;\ U_H = 0 \tag{80}$$

The solution to this equation is given by:

$$U_H = \frac{1f_1}{(H-1)}\ [(\exp(-\tau) - \exp(-H\tau)] \tag{81}$$

where

$$H = \lambda_n^2/\phi_H^2 + f_2. \tag{82}$$

If we apply the inverse formula (equation 68) and the normalization relationship (equation 65), we obtain the dimensionless concentration of the heavy oil fraction, U_H, as a function of τ and x as follows:

$$U_H = \sum_{n=1}^{\infty} \frac{1 f_1 k_n(x)}{k_n(H-1)} [(\exp(-\tau) - \exp(-H\tau)] \tag{83}$$

where

$$k_n = \int_0^1 x^2 \, k_n^2 \, dx = 1/2 \, . \tag{84}$$

The dimensionless material balance equations for the light gases and the light oil (equations 55 and 56) were solved by the same procedure. The dimensionless concentration of light oil is given by:

$$U_L = \sum_{n=1}^{\infty} \frac{1 k_n(x)}{k_n} \{\frac{f_1 f_4}{H-1}[\frac{\exp(-\tau)-\exp(-L\tau)}{L-1} - \frac{\exp(-H\tau)-\exp(-L\tau)}{L-H}]$$

$$+ \frac{f_3 f_4}{L-1} [\exp(-\tau)-\exp(-L\tau)]\} \tag{85}$$

where

$$L = \lambda_n^2/\phi_L^2 + f_5. \tag{86}$$

The dimensionless concentration of light gas is given by:

$$U_G = \sum_{n=1}^{\infty} \frac{1 k_n(x)}{k_n} \{ \frac{f_1 f_7}{H-1}[\frac{\exp(-\tau)-\exp(-G\tau)}{G-1} - \frac{\exp(-H\tau)-\exp(-G\tau)}{G-H}]$$

$$+ \frac{f_1 f_4 f_5}{(H-1)(L-1)}[\frac{\exp(-\tau)-\exp(-G\tau)}{G-1} - \frac{\exp(-L\tau)-\exp(-G\tau)}{G-L}]$$

$$+ \frac{f_1 f_4 f_5}{(H-1)(L-H)}[\frac{\exp(-L\tau)-\exp(-G\tau)}{G-L} - \frac{\exp(-H\tau)-\exp(-G\tau)}{G-H}]$$

$$+ \frac{f_3 f_4 f_5}{L-1}[\frac{\exp(-\tau)-\exp(-G\tau)}{G-1} - \frac{\exp(-L\tau)-\exp(-G\tau)}{G-L}]$$

$$+ \frac{f_6}{G-1} [\exp(-\tau)-\exp(-G\tau)]\} \tag{87}$$

where

$$G = \lambda_n^2/\phi_G^2. \tag{88}$$

Substitution of the bitumen concentration (equation 74) and the dimensionless heavy oil fraction concentration (equation 83) into the dimensionless material balance differential equation for the coke (equation 57) permits solution of the equations for the dimensionless concentration of coke. The dimensionless coke concentration is given by:

$$U_c = \sum_{n=1}^{\infty} \frac{1 f_1 f_9 k_n(x)}{k_n(H-1)} \left[1-\exp(-\tau) - \frac{1-\exp(-H\tau)}{H}\right] + f_8[1-\exp(-\tau)] . \tag{89}$$

PRODUCTION RATE

The production rates of the heavy oil, light oil, and light gas fractions were calculated from the concentration profiles as determined by equations 83, 85, and 87, respectively. The mass production rate (mass per unit time) of each species (j = H, L, G) is:

$$-4\pi R^2 p_p D_j (\partial C_j/\partial r)\,|_R \tag{90}$$

where p_p is the tar sand matrix particle density, that is, mass of the sand matrix (bitumen excluded) per unit total volume. Therefore, the mass production rate of species j (j = H, L, G) per unit mass of tar sand matrix is:

$$M_j = \frac{-4\pi R^2 p_p D_j (\partial C_j/\partial r|_R)}{4/3\ \pi R^3 p_p} = -(3/R) D_j (\partial C_j/\partial r)|_R . \tag{91}$$

The mass of the j th species transported across the exterior surface of the particle is given by:

$$w_j = \int_0^t M_j dt = (3/R) D_j \int_0^t (\partial C_j/\partial r)|_R dt . \tag{92}$$

In terms of dimensionless variables and parameters, the mass of species j produced per initial mass of bitumen is given by:

$$W_j = w_j/C_{BO} = (3/\phi_j^2) \int_0^\tau (-\partial U_j/\partial x)|_1 d\tau \ . \tag{93}$$

The masses of heavy oil, light oil, and light gas per unit mass of native bitumen are obtained by differentiation of the concentrations of heavy oil, light oil, and light gas (equations 53, 55, and 57, respectively) with respect to x, evaluation of the derivative at x = 1, followed by substitution into equation 93. The final results are given by:

$$W_H = (6/\phi_H^2) \sum_{n=1}^{\infty} \frac{f_1}{H-1} \{1-\exp(-\tau) \quad \frac{1-\exp(-H\tau)}{H} \} \tag{94}$$

$$W_L = (6/\phi_L^2) \sum_{n=1}^{\infty} \{\frac{f_1 f_4}{(H-1)(L-1)} \{1-\exp(-\tau) - \frac{1-\exp(-L\tau)}{L}]$$

$$- \frac{f_1 f_4}{(H-1)(L-H)} [\frac{1-\exp(-H\tau)}{H} - \frac{1-\exp(-L\tau)}{L}]$$

$$+ \frac{f_3 f_4}{L-1} [1-\exp(-\tau) - \frac{1-\exp(-L\tau)}{L}]\} \ . \tag{95}$$

$$W_G = (6/\phi_G^2) \sum_{n=1}^{\infty} \{\frac{f_1 f_7}{(H-1)(G-1)} [1-\exp(-\tau) - \frac{1-\exp(-G\tau)}{G}]$$

$$- \frac{f_1 f_7}{(H-1)(G-H)} [\frac{1-\exp(-H\tau)}{H} - \frac{1-\exp(-G\tau)}{G}]$$

$$+ \frac{f_1 f_4 f_5}{(H-1)(L-1)(G-1)} [1-\exp(-\tau) - \frac{1-\exp(-G\tau)}{G}]$$

$$- \frac{f_1 f_4 f_5}{(H-1)(L-1)(G-L)}\left[\frac{1-\exp(-L\tau)}{L} - \frac{1-\exp(-G\tau)}{G}\right]$$

$$+ \frac{f_1 f_4 f_5}{(H-1)(L-1)(G-L)}\left[\frac{1-\exp(-L\tau)}{L} - \frac{1-\exp(-G\tau)}{G}\right]$$

$$- \frac{f_1 f_4 f_5}{(H-1)(L-H)(G-H)}\left[\frac{1-\exp(-H\tau)}{H} - \frac{1-\exp(-G\tau)}{G}\right]$$

$$+ \frac{f_3 f_4 f_5}{(L-1)(G-1)}\left[1-\exp(-\tau) - \frac{1-\exp(-G\tau)}{G}\right]$$

$$- \frac{f_3 f_4 f_5}{(L-1)(G-L)}\left[\frac{1-\exp(-L\tau)}{L} - \frac{1-\exp(-G\tau)}{G}\right]$$

$$+ \frac{f_6}{G-1}\left[1-\exp(-\tau) - \frac{1-\exp(-G\tau)}{G}\right]\Big\} . \qquad (96)$$

The overall mass balance can be obtained by adding all the dimensionless material balance equations (equations 53 through 57) to eliminate the kinetic reaction terms. The final result is:

$$\sum_{j=1}^{5} \partial U_j/\partial\tau = (1/\phi_H^{\,2})\nabla^2 U_H + (1/\phi_L^{\,2})\nabla^2 U_L + (1/\phi_G^{\,2})\nabla^2 U_G \qquad (97)$$

where j = 1, 5 represents heavy oil, light oil, gas, bitumen, and coke, respectively. Multiplying this expression by x^2dx and integrating with respect to x yields:

$$\partial/\partial\tau \sum_{j=1}^{5} \int_0^1 x^2 U_j dx = \sum_{j=1}^{3} (1/\phi_j^{\,2})(-\partial U_j/\partial x)\big|_1 . \qquad (98)$$

If we multiply equation 98 by $3d\tau$ and integrate with respect to τ, we obtain:

$$3 \sum_{j=1}^{5} \int_0^1 x^2 U_j dx + \sum_{j=1}^{3} (3/\phi_j^{\,2}) \int_0^{\tau} (-\partial U_j/\partial x)\big|_1 \, d\tau = 1 . \qquad (99)$$

Finally, substitution of equation 93 into equation 99 gives the overall material balance:

$$3 \sum_{j=1}^{5} \int_{0}^{1} x^2 U_j dx + W_H + W_L + W_G = 1 \ . \qquad (100)$$

This expression indicates that the amount of all five species within the particle plus the amount of heavy oil, light oil, and light gas evolved at any time must be equal to the initial amount of bitumen, which is unity in the dimensionless form.

The amount of coke accumulated inside the particle on the surface of the sand grains per unit mass of bitumen is obtained as:

$$3 \int_{0}^{1} x^2 U_c dx = \sum_{n=1}^{\infty} \frac{6 f_1 f_9}{(\lambda_n)^2 (H-1)} \left[1-\exp(-\tau)- \frac{1-\exp(-H\tau)}{EH}\right]$$

$$+ f_8(1-\exp(-\tau)) \ . \qquad (101)$$

DISCUSSION

The model presented in this paper assumes the pyrolysis takes place isothermally and that all reactions are first order. The isothermal assumption is valid for small particles. The average temperature of a spherical particle with a uniform initial temperature T_i can be calculated by the following equation when its surface temperature is suddenly changed from T_i to T_s:[68]

$$(T_s-T_{ave})/(T_s-T_i) = 0.068 \exp(-9.87\ N_{FO}) + 0.152 \exp(-39.5\ N_{FO}) + 0.676 \exp(-88.8\ N_{FO}) + \ldots \qquad (102)$$

where T_{ave} is the average particle temperature at time t and N_{FO} is the Fourier number. The Fourier number is given by[77]

$$N_{FO} = \alpha t/R^2 \qquad (103)$$

where α is the thermal diffusivity of the particle, and R is the radius of the particle. The thermal diffusivity is given by[78]

$$\alpha = k_p/\rho_p C_p \tag{104}$$

where k_p is the thermal conductivity; C_p is the specific heat or thermal capacity; and ρ_p is the tar sand particle density. The application of equation 102 to a particle having an initial temperature of 298 K whose surface temperature is suddenly changed to 773 K is illustrated in Figure 88. The particle properties used in this calculation were k_p = 0.003 cal $cm^{-1}s^{-1}K^{-1}$;[71] ρ_p = 2.3 g cm^{-3};[72] C_p = 0.3 cal $g^{-1}K^{-1}$.[73] Thus the isothermal assumption appears to be reasonable for particle sizes smaller than 1 centimeter as compared to the time required to complete the pyrolysis (conversion vs. time is presented in Figures 88 through 90 for particle sizes of 1 and 4 millimeter).

Thermogravimetric analysis of the pyrolysis of tar sand bitumen in contact with the sand matrix indicated an overall reaction order between one and two. However, first order kinetics fit the conversion data over wider ranges of the data and only breaks down at low pyrolysis temperatures. Thus first order kinetics was assumed to be a reasonable first approximation for all the pyrolysis reactions in the reaction network.

The overall rate constant k_1 determined for the pyrolysis of 1 millimeter particles of the Whiterocks tar sand was used as a starting point in this study; the other rate constants were assumed to be arbitrary ratios of k_1 in this model since kinetic parameters for the individual steps for this complex reaction scheme was not available at this stage of the development of the model. The overall rate constant was

$$k_1 = (3.22 \times 10^6\ s^{-1}) \exp(-26.68\ \text{kcal mol}^{-1}/RT) \tag{105}$$

and agreed well with the value reported by Barbour and Dorrence;[82] that is,

$$k_1 = A \exp(-E/RT) \tag{106}$$

where A, the pre-exponential factor, was $3.2 \times 10^{+7}$ sec^{-1} and the activation energy was 34 kcal mol^{-1}. The ratios of the rate constants to k_1 used in this calculation were shown in the reaction network and the values of f_1 to f_9 were listed in the Appendix.

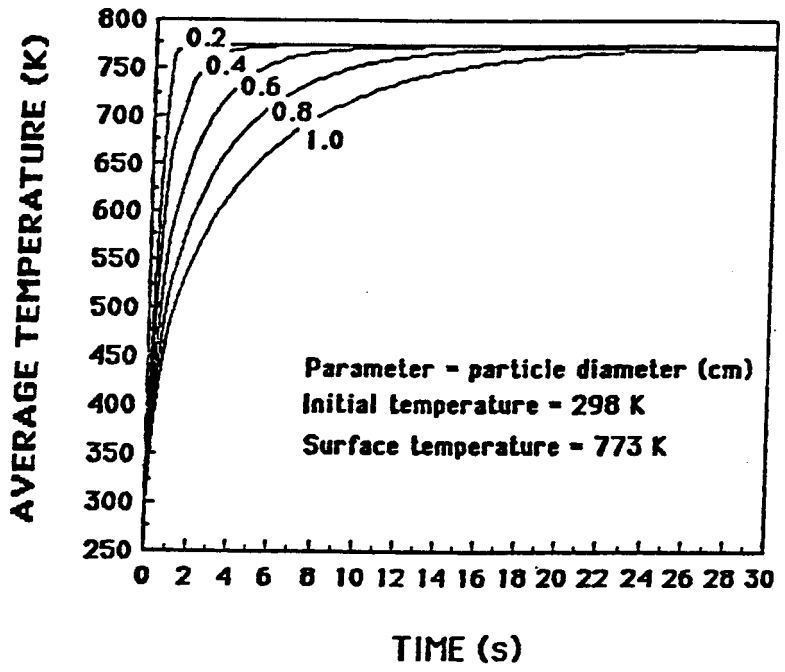

Figure 88. - Average particle temperature versus time for various particle diameters.
Initial temperature = 298 K; surface temperature = 773 K.

The empty pores or channels in a typical Whiterocks tar sand sample after bitumen combustion in air at 773 K are generally larger than 30 microns and possibly as large as 100 microns. The transport of oil vapor and gas produced by the bitumen pyrolysis reactions in such large pores could occur by convective flow and/or bulk diffusion. As a first approximation, a "modified effective diffusivity" was assumed to represent the transport of the vapor phase hydrocarbons from the interior region of the particle to the external surface. Molecular weights of 44 (C_3H_8), 198 ($C_{14}H_{30}$), and 394 ($C_{28}H_{58}$) g/mol were assigned as representative of the average molecular weights of gas, light oil, and heavy oil fractions, respectively.

The Lennard-Jones expression for the intermolecular force potential was used to estimate the binary bulk diffusion coefficient D_{12}. The diffusion coefficient for a single species in a ternary mixture, D_{1m}, was then related to D_{12} by assuming that the vapor mixture contained 20 percent light gas, 40 percent light oil vapor, and 40 percent heavy oil vapor. The effective bulk diffusion coefficient $D_{1m,eff}$ was computed from D_{1m} by the relationship $D_{1m,eff} = D_{1m}\varepsilon/\tau$, where ε is the porosity of the particle, and τ is the tortuosity factor. The porosity was assumed to be 30 percent (by volume) and the tortuosity factor was assumed to be 3.[70] The values of $D_{1m,eff}$ were used as the "modified effective diffusivity" in these calculations.

The production (g/g bitumen) curves for heavy oil, light oil, gas, and coke (calculated from equations 94-96 and equation 101) for pyrolysis temperatures of 723 and 773K and a particle size of 0.4 cm are presented in Figure 89. The comparison of the evolution of heavy oil and gas as a function of time is presented in Figure 90 for particle sizes of 0.4 and 0.8 cm in diameter. The ultimate yields of heavy oil, light oil, gas, and coke are presented in Figure 91.

The model predicts an increased heavy oil yield accompanied by a decrease in gas yield at lower pyrolysis temperatures and an increase in the gas yield with increasing pyrolysis temperature accompanied by a decrease in heavy oil yield. The gas yield is increased with increasing pyrolysis temperature; the light oil yield is relatively unchanged by increases or decreases in the reaction temperature (Figure 91). At the higher temperature the cracking reaction is accelerated, thus the amount of gas increased with a decrease in the heavy oil; while the amount of light oil remains

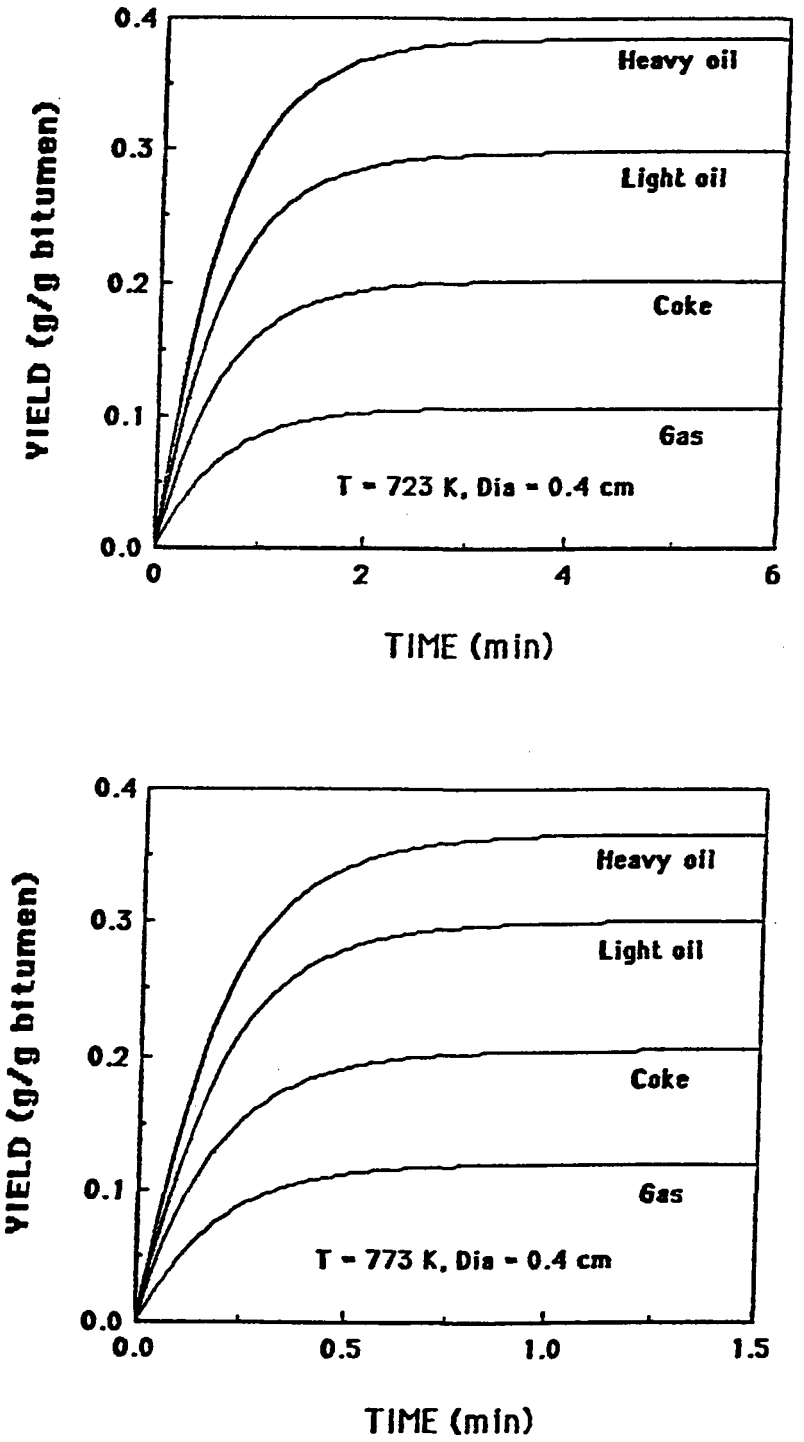

Figure 89. - Product distribution and yields versus time for the bitumen pyrolysis in a 0.4 cm tar sand particle predicted by the model.

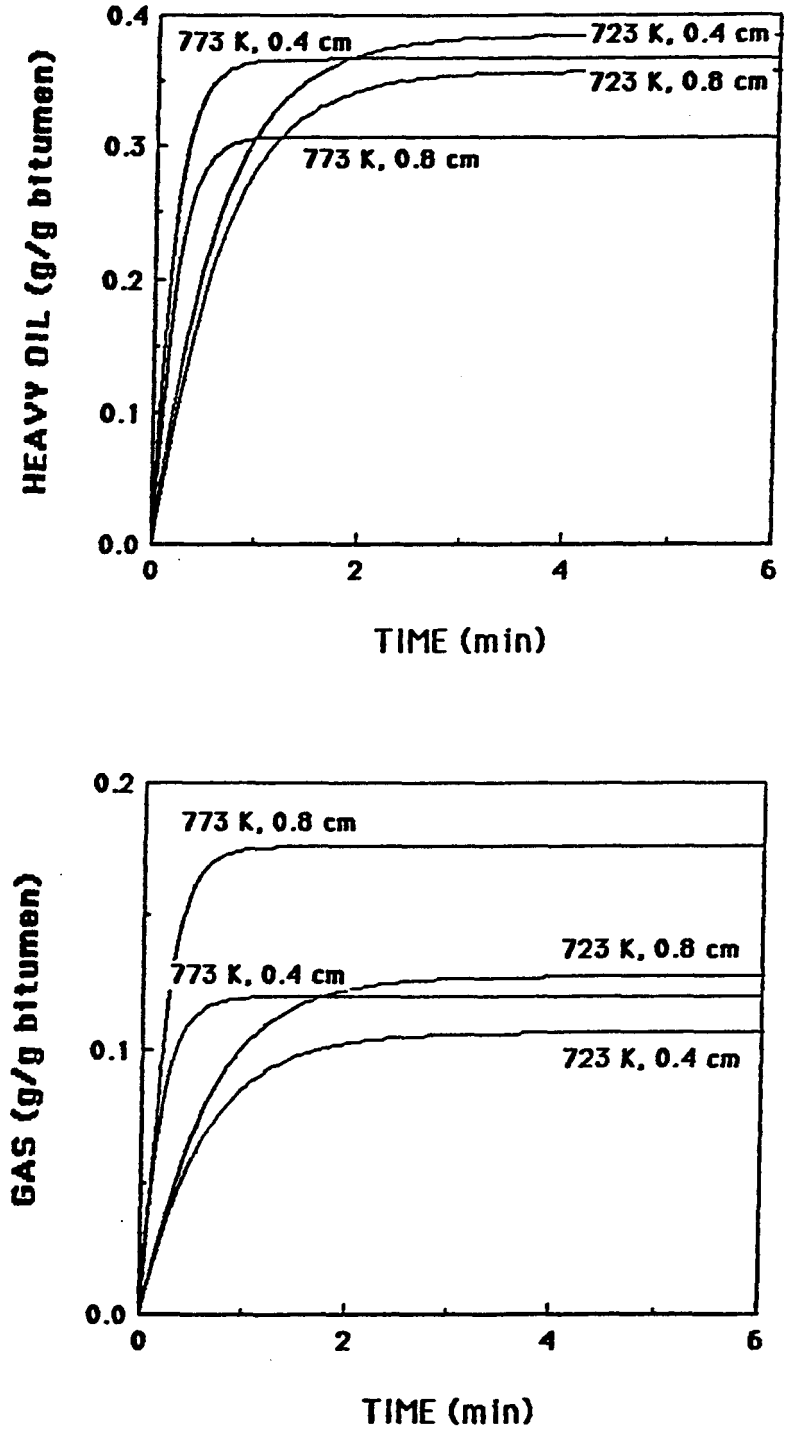

Figure 90. - Evolution of heavy oil fraction and gas versus time for various particle sizes and temperatures.

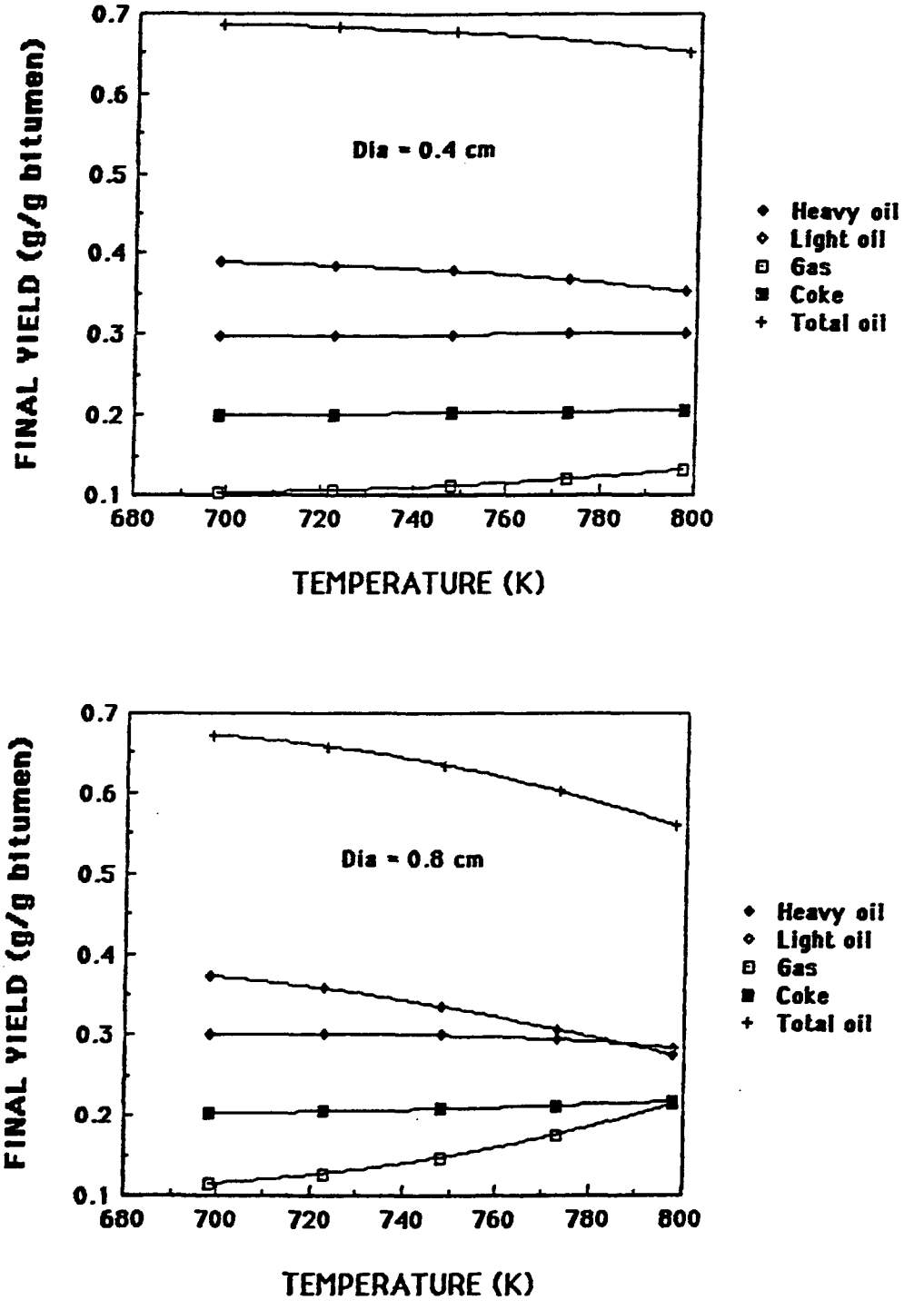

Figure 91. - Final product distribution and yields versus temperature for tar sand particle sizes of 0.4 cm and 0.8 cm.

unchanged since light gas produced from light oil pyrolysis is balanced by the light oil produced from heavy oil pyrolysis. At a given temperature, a small particle results in a higher yield of heavy oil (total oil) and a lower yield of gas while the amount of light oil is little changed. This is because of the shorter retention time of the vaporized hydrocarbons which remained inside smaller particle, thus the time for cracking is shorter. It is observed (Figure 90) that the rate of production of heavy oil and gas is higher at high temperatures, and it takes less time to complete the reaction. This is expected, since higher temperatures result in higher reaction rates and the transport of oil and gas from inside the particle to the surface is fast.

The intraparticle concentration profiles of heavy oil and light oil at various values of time for temperatures of 773K and particle diameter of 0.4 cm are shown in Figure 92. The plots of concentration at radial position 0.0 (center of the sphere) and 0.5 vs. time are presented in Figure 93. The concentration profiles rise from zero to a maximum value and then decrease to zero as the degree of advancement of the bitumen pyrolysis reaction approaches unity. The concentration of heavy oil as well as light oil reaches its maximum in about 3 seconds and then decreases slowly to zero. It is noted that before the concentration profile reaches its maximum, it flattens and then bends sharply to match the surface boundary condition; after the maximum, it decreases smoothly along the particle radial coordinate.

The preexponential factor and activation energy obtained from the isothermal first order kinetics for the pyrolysis of a 1 millimeter Whiterocks tar sand particle was used in this calculation. The analytical solutions for the yields of heavy oil, light oil, gas, and coke for various pyrolysis temperatures and particle sizes are listed in reference 83.

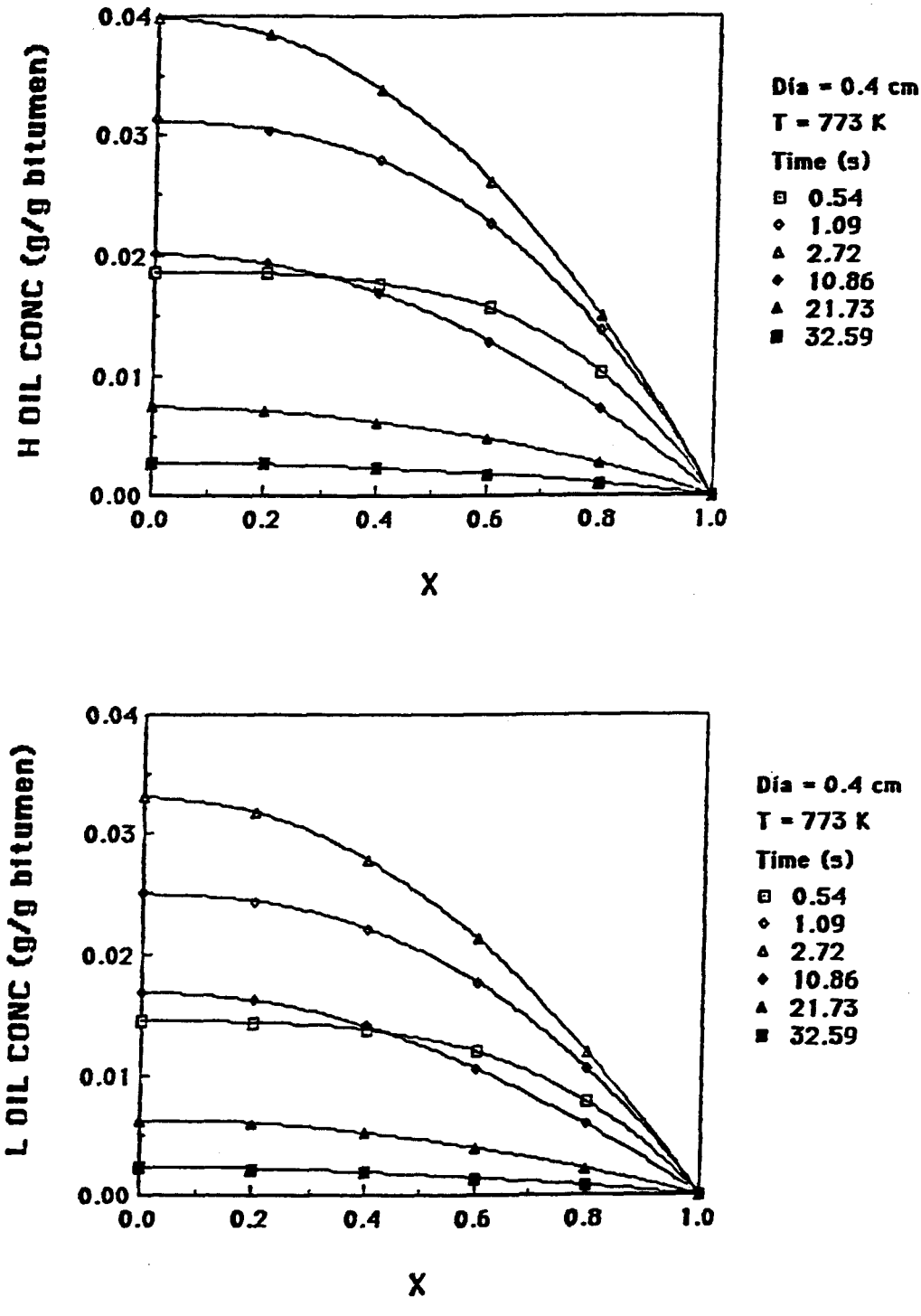

Figure 92. - Predicted intraparticle concentration distribution of heavy oil and light oil at various times.
Temperature = 773K; particle diameter = 0.4 cm.

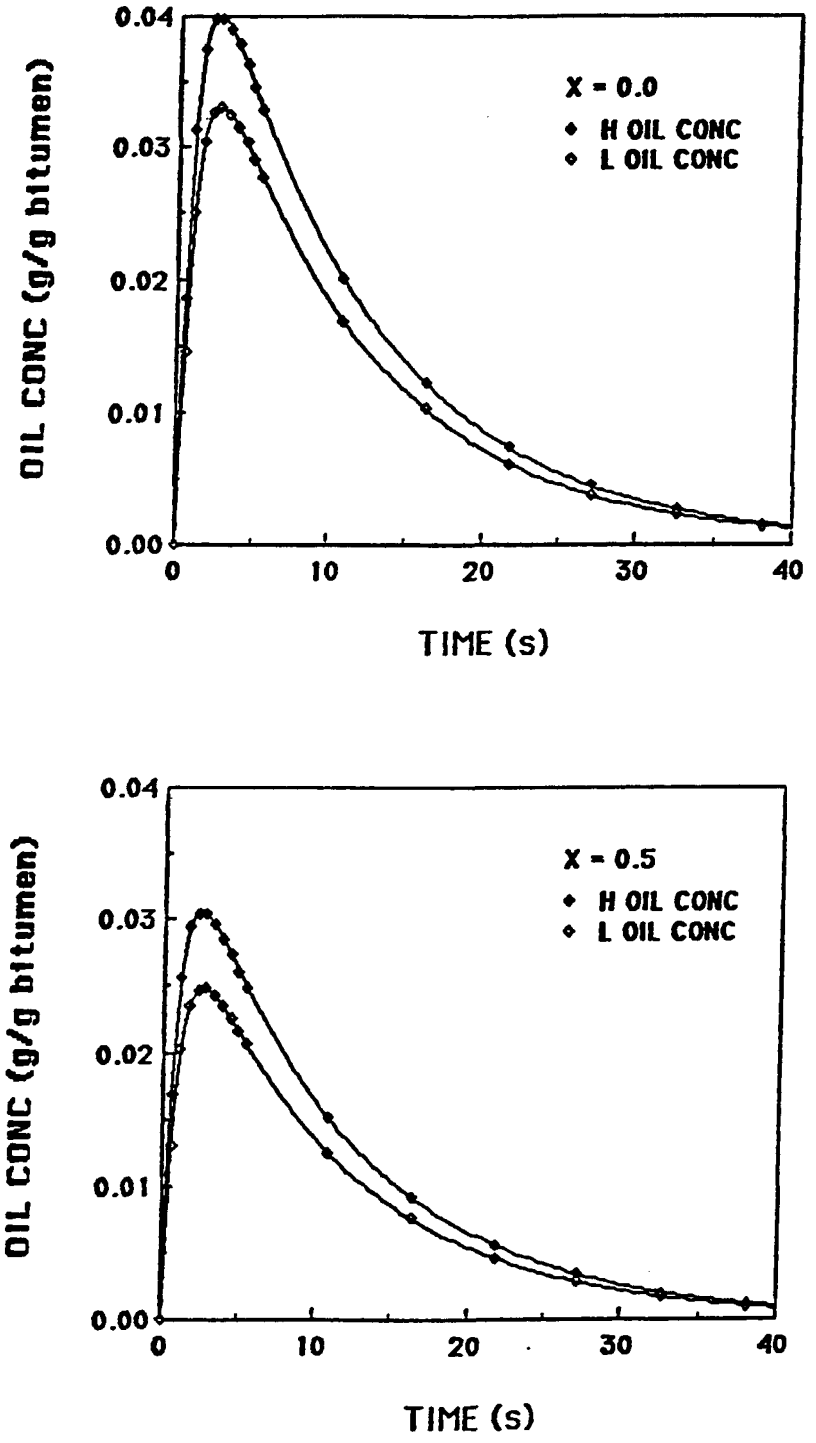

Figure 93. - Predicted intraparticle concentration distribution of heavy oil and light oil at the radial position 0.0 and 0.5 versus times.
Temperature = 773 K; particle diameter = 0.4 cm.

NOMENCLATURE

A	preexponential factor, 3.22×10^6 s^{-1}
C_B, C_G, C_H, C_L	concentration of bitumen, gas, heavy oil, and light oil; g/g bitumen
C_{BO}	initial concentration of bitumen; g/g bitumen
C_p	thermal capacity; cal g^{-1} K^{-1}
D_{eff}	effective diffusivity for a porous solid; cm^2 s^{-1}
D_G, D_H, C_L	modified effective diffusivity of gas, heavy oil, and light oil; cm^2 s^{-1}
D_{12}	diffusivity for bulk diffusion of species 1 in a mixture of species 1 and 2; cm^2s^{-1}
D_{1m}	diffusivity for bulk diffusion of species 1 in a multicomponent mixture, cm^2s^{-1}
$d_{1m,eff}$	effective diffusivity for a porous solid under condition of bulk diffusion for species 1 in a multicomponent mixture; cm^2s^{-1}
E	activation energy; 26.68 kcal/mol
G, H, L	defined in equations 88, 86, and 82
k_1	rate constant for bitumen decomposition, defined in equation 39
k_{BG}, k_{BL}, k_{BH}, k_{BC}, k_{HC}, k_{HL}, k_{HG}, k_{LG}	rate constants for the pyrolysis scheme
K_n	integral transform kernel, defined in equation 76
k_p	thermal conductivity; cal $cm^{-1}s^{-1}K^{-1}$
M_j	mass production rate of species j, defined in equation 91
r	radial coordinate
R	particle radius; reaction term defined in equation 62
t	clock time; s
T_i	initial particle temperature; K
T_s	particle surface temperature; K
T_{ave}	average temperature; K
U_j	non-dimensional concentration of species j
$\bar{U}_j$	integral transform of U_j, defined in equation 75

w_j	mass of species j evolved, defined in equation 92
W_j	non-dimensional mass of species j evolved, defined in equation 93
X	non-dimensional radial coordinate defined in equation 42
$f_1 \sim f_9$	parameter defined in equations 44 through 52
α	thermal diffusivity; cm^2s^{-1}
ε	porosity
θ_j	Thiele-type modulus for species j, defined in equation 43
λ, λ_m, λ_n	eigenvalue
ρ_p	particle density; g/cm^3
τ	non-dimensional time, defined in equation 40; tortuosity factor

PYROLYSIS OF BITUMEN-IMPREGNATED SANDSTONE IN A CYCLONE REACTOR

F.V. Hanson — Associate Professor
Liang C. Lin — Graduate Student

SUMMARY

The concept of a short contact time, cyclone reactor has been evaluated for the pyrolysis of tar sands from the Whiterocks and PR Spring deposits. Thermal analysis data (TGA) was obtained as a function of particle size to determine the extent of bitumen conversion to products: hydrocarbon liquids and gases and a carbonaceous residue on the sand. The extent of the pyrolysis reaction (conversion) decreased with increased sand particle size at a fixed pyrolysis temperature and reaction time. Approximately 18 seconds was found to be required for a 0.025 cm diameter bitumen-impregnated sand particle to achieve 90% conversion of the bitumen to hydrocarbon products.

A 400-cm diameter cyclone reactor would provide adequate residence time at pyrolysis temperatures to achieve greater than 90% conversion of the bitumen to hydrocarbon liquids and to C_1-C_4 hydrocarbon gases for sand particles having a diameter less than 0.03 cm. The cyclone reactor does not provide adequate retention time for sand particles having a diameter in excess of 0.1 cm; however, a riser-cyclone reactor would permit the processing of larger diameter particles.

INTRODUCTION

The influence of process variables on the hydrocarbon product distribution and yields for the pyrolysis of bitumen-impregnated sandstone in a fluidized bed reactor has been investigated for a number of domestic tar sand deposits.[31-34] The process variables investigated included pyrolysis reactor temperature, sand retention time in the pyrolysis zone of the reactor, and the fluidization gas velocity. The ranges of the variables were as follows: temperatures of 673-973 K (752-1291°F) feed sand retention times of 15-35 minutes and fluidizing gas velocities 1-4 times the minimum fluidization

velocity. The Utah tar sand deposits investigated included Sunnyside,[31] Whiterocks,[32,33] PR Spring,[33] Tar Sand Triangle,[31,32] and Circle Cliffs.[34]

The yield of C_5^+ bitumen-derived hydrocarbon liquid decreased with increased pyrolysis temperature at fixed sand retention time and increased with decreased sand retention time at fixed reactor temperature. The hydrocarbon product distribution and yields appeared to be insensitive to the fluidization as velocity in the range of velocities investigated. The coke yields were independent of process operating variables; however, they were dependent upon the source of the feed sand. The most important operating variables were determined to be the pyrolysis reactor temperature and the sand retention time in the pyrolysis zone.[32] In general, the most significant variable affecting the product distribution and quality appeared to be the sand retention time at a fixed pyrolysis zone temperature.

The increase in liquid hydrocarbon yield as the feed sand retention time decreased led to the conclusion that short contact or residence time reactors would produce the highest yields of C_5^+ bitumen-derived hydrocarbon liquids and the lowest yields of C_4^- hydrocarbon gases. Reactor options would include tubular transport reactors, spiral transport reactors, cyclone reactors and/or transport-cyclone reactor combinations. A schematic of a tar sand pyrolysis scheme in which cyclones are employed as the pyrolysis and combustion reactors is presented in Figure 94. T_a is the inlet bitumen-impregnated sandstone temperature, and T_s is the surface temperature of the sandstone particle within the cyclone. The operating parameters for the cyclone pyrolysis reactor-spent sand combustor scheme are presented in Table 53.

THEORY

The optimum residence time for each reactor type would, of course, be dependent upon the rate of heat transfer to the bitumen-impregnated sandstone particles and consequently upon the average particle diameter.

The factors that dominated the analysis of the pyrolysis cyclone reactor problem included the following:

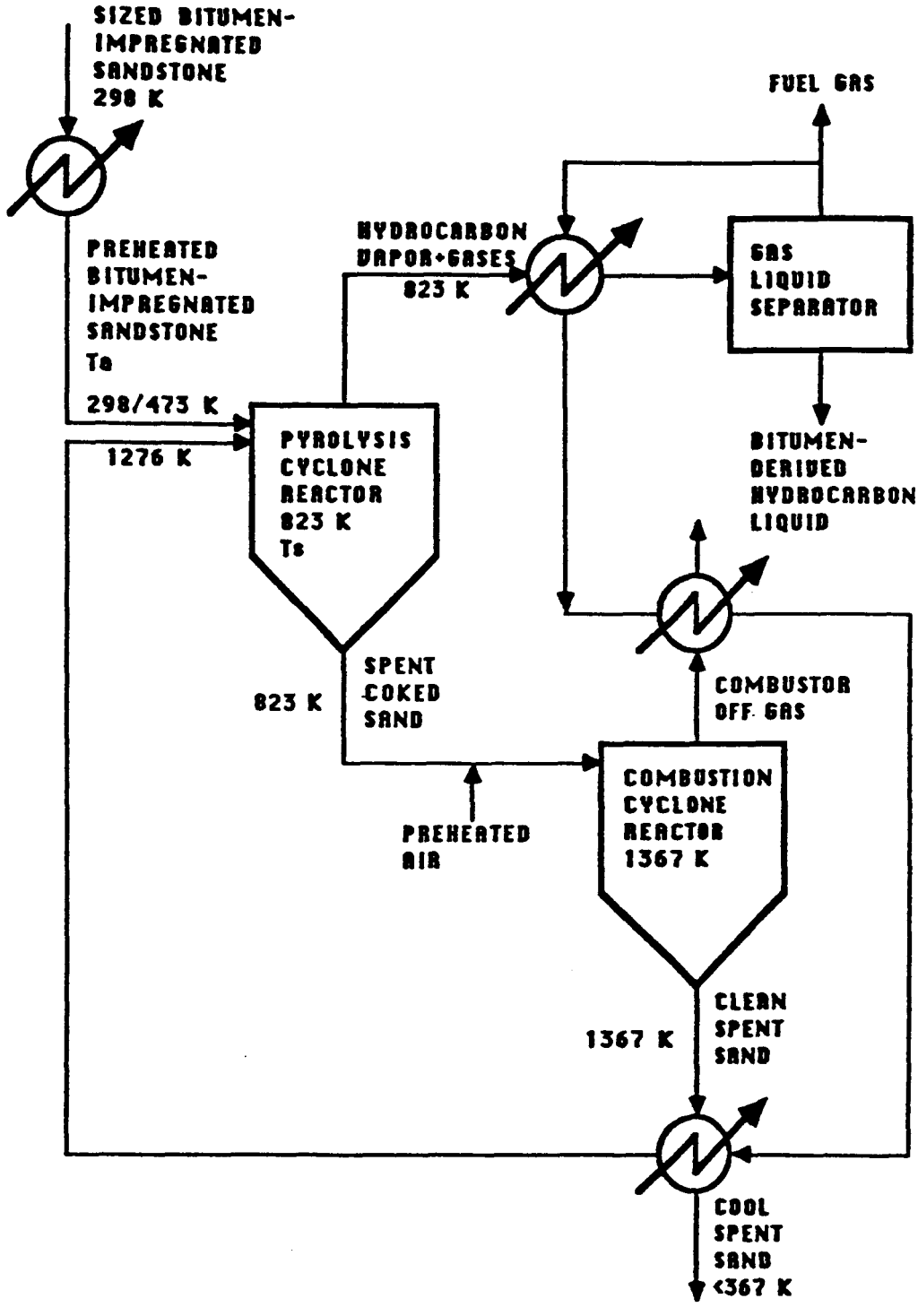

Figure 94. - Schematic of cyclone pyrolysis reactor.

Table 53

Operating Parameters for Cyclone Pyrolysis Reactor

Reactor Temperatures, K	
Pyrolysis Cyclone	823
Combustion Cyclone	1,367
Inlet Gas Temperatures, K	
Pyrolysis Cyclone	1,276
Combustion Cyclone	1,292
Reactor Pressures, psig	
Pyrolysis Cyclone	Ambient
Combustion Cyclone	Ambient
Hydrocarbon Liquid Production Rate, BBL/D	3,000
Bitumen Saturation, wt.%	
PR Spring Rainbow I	14.1
Whiterocks	8.0
Fuel Gas Production Rate, SCFH	100,000
Fuel Gas Heating Value, Btu/SCF	825
Tar Sand Feed Rates, TPH	
PR Spring Rainbow I	210
Whiterocks	370
Tar Sand Feed Temperatures, K	
Case I	298
Case II	473

- heat transfer from the gas phase to the sand particle
- bitumen conversion to hydrocarbon liquids and gases as a function of time;
- sand particle entrainment from the cyclone; and
- sand particle residence time in the pyrolysis zone.

The sand particles were assumed to be spherical in shape and composed of cemented sand grains as would be expected for the consolidated sandstones that form the solid matrix in the Utah tar sand deposits. The sand grains were assumed to be wetted by the bitumen as is the case for the oil wet sands of Utah. A representation of a bitumen-impregnated, oil-wet, spherical sandstone particle is presented in Figure 95.

The pyrolysis reactor was assumed to operate at 823 K (1022°F) and the inlet gas temperature was assumed to be 1276 K (1837°F). In the analysis, two cases were considered: the tar sand fed to the pyrolysis reactor was at the ambient temperature in Case I, and it was preheated to 473 K (392°F) in Case II. The ambient temperature was assumed to be 298 K (77°F).

The surface temperature of the sand particles in the pyrolysis reactor was assumed to be 823 K (1022°F), the cyclone operating temperature. Film resistance to heat transfer at the surface of the sand particles was assumed to be negligible.

TRANSFER OF HEAT TO THE SAND PARTICLES

The average temperature of a spherical sand particle in the pyrolysis zone of the reactor as a function of time in the pyrolysis zone may be determined by applying the energy balance equation for reacting systems to the particle:[71]

$$\rho_p \hat{C}_{p,p} \frac{\partial T}{\partial t} = - (\vec{\nabla} \cdot \vec{q}_c) + q_r \qquad (107)$$

where $(\vec{\nabla} \cdot \vec{q}_c)$ is the rate of energy input to the particle per unit volume by conduction, cal s^{-1} cm^{-3};

q_r is the rate of thermal energy generation or consumption per unit volume within the sand particle due to chemical reaction, cal s^{-1} cm^{-3};

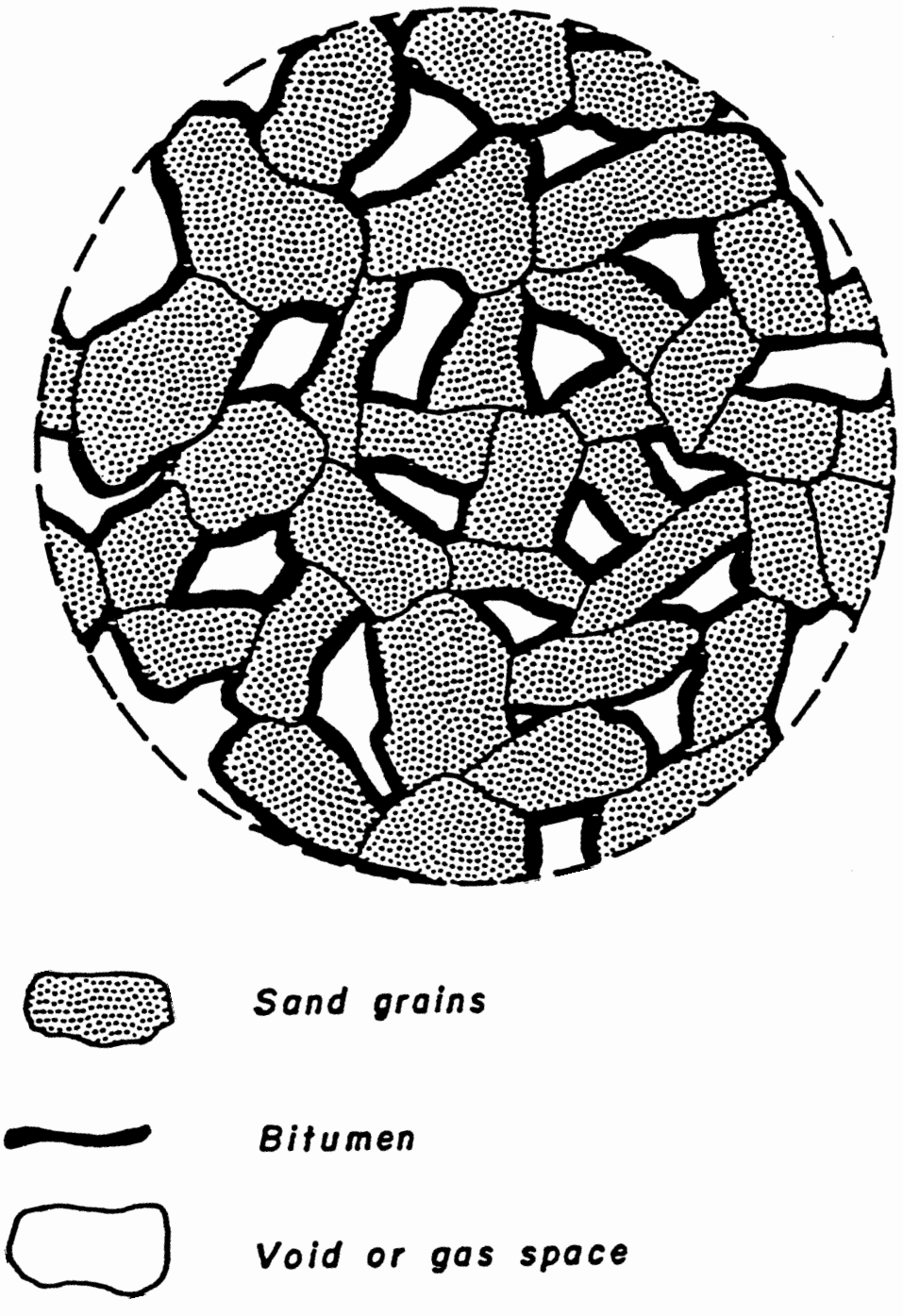

Figure 95. - Bitumen-impregnated sandstone particle.

ρ_p is the density of the spherical sand particle, g cm^{-3}; and

$\hat{C}_{p,p}$ is the heat capacity of the sand particle, cal $g^{-1}K^{-1}$.

The convective energy term and the work terms within the particle have been neglected. The bitumen saturations for the tar sand deposits investigated in the fluidized-bed pyrolysis studies ranged from 4% by weight for Tar Sand Triangle[31,32] and Circle Cliffs[34] samples to 14% by weight for PR Spring Rainbow I sample.[33] Therefore, it was assumed that the energy consumption term, due to the bitumen pyrolysis reaction, was negligible relative to the energy required to heat the particle (i.e., bitumen-sand matrix) to the pyrolysis temperature. Thus, the energy balance equation can be reduced to:

$$\rho_p \hat{C}_{p,p} \frac{\partial T}{\partial t} = - (\vec{\nabla} \cdot \vec{q}_c) . \tag{108}$$

The heat conduction term is expressed in terms of Fourier's Law of Heat Conduction:[70]

$$\vec{q}_c = -\vec{\nabla}(k_p T) \tag{109}$$

where k_p is the thermal conductivity of the sand particle, cal s^{-1} cm^{-1} K^{-1}. Upon substitution the energy balance equation is written

$$\rho_p \hat{C}_{p,p} \frac{\partial T}{\partial T} = -[\vec{\nabla} \cdot \vec{\nabla}(k_p T)]. \tag{110}$$

If the thermal conductivity of the sand particle is assumed to be independent of temperature and position in the temperature range of interest, then the energy balance equation for the sand particle reduces to:

$$\rho_p \hat{C}_{p,p} \frac{\partial T}{\partial T} = k_p \nabla^2 T; \tag{111}$$

or

$$\frac{\partial T}{\partial T} = \alpha \nabla^2 T; \tag{112}$$

where α is the thermal diffusivity of the sand particle, $cm^2\ s^{-1}$. The thermal diffusivity is given by:

$$\alpha = k_p/\rho_p \hat{C}_{p,p} . \tag{113}$$

The solution to the energy balance equation may be cast in the following form:[78]

$$\frac{T_s - T_p}{T_s - T_a} = \phi\ (N_{Fo}) \tag{114}$$

where:

T_s is the constant average temperature at the surface of the sand particles in the cyclone, K;

T_a is the initial, cyclone inlet temperature of the sand particle, K;

T_p is the average temperature of the sand particle at time t in the cyclone, K; and

N_{Fo} is the Fourier number.

The Fourier number is the ratio of the heat transferred by conduction to the rate of energy storage in the system and is given by:[77]

$$N_{Fo} = \alpha t/R_p^2 \tag{115}$$

where

t is the time the sand particle spends in the pyrolysis zone, s; and

R_p is the radius of the sand particle, cm.

The function $\phi(N_{Fo})$ for spherical geometry is given by:[76]

$$\phi(N_{Fo}) = 0.608 \exp(-9.87\ N_{Fo}) + 0.152 \exp(-39.5\ N_{Fo}) + 0.0676 \exp(-88.8\ N_{Fo}) + ..., \tag{116}$$

and the sand particle temperature can be computed from the following equation:

$$\frac{T_s - T_p}{T_s - T_a} = 0.608 \exp(-9.87\ N_{Fo}) + 0.152 \exp(-39.5\ N_{Fo}) + 0.676 \exp(-88.8\ N_{Fo}) + \ldots. \quad (117)$$

The calculation of the thermal diffusivity and the Fourier number required specification of the thermal conductivity, density, and heat capacity of the sand particles. The density of the sand particle (ρ_p) was computed from the sand grain density and the estimated void volume of the particle. The grain density was measured for a number of tar sand core samples and an average value of 2.7 g cm^{-3} was used.[80] The void fraction for the sand particle was assumed to be 0.3. Although porosity data were available from Tar Sand Triangle core samples, the wide range of values dictated that a reasonable estimate of the void fraction would provide sufficient accuracy in the calculations. The heat capacity of a quartzitic sandstone[84] was used as an approximation to the heat capacity of the sand grain matrix that comprised the particle. The reported heat capacity of the quartzitic sandstone, $\hat{C}_{p,ss}$, was adjusted to account for the presence of the bitumen on the surface of the sand grains, $\hat{C}_{p,p}$. A similar approximate value for the heat capacity was obtained when the heat capacity of α-quartz[81] was used for the heat capacity of the sand grains comprising the particle and allowance was made for the void volume of the particle. The thermal conductivity of the quartzitic sandstone, k_{ss}, adjusted for the presence of the bitumen, was used as an approximation for the thermal conductivity of the bitumen-impregnated sand particle, k_p. The particle properties used in the calculations were:

$k_p = 4X10^{-3}$cal $cm^{-1}s^{-1}K^{-1}$;

$\rho_p = 2.0$ g cm^{-3}; and

$\hat{C}_{p,p} = 0.3$ cal $g^{-1}K^{-1}$

Thus the thermal diffusivity was calculated to be $\alpha = 6.67 \times 10^{-3} cm^2 s^{-1}$ and the Fourier number was

$$N_{Fo} = (6.67 \times 10^{-3} cm^2 s^{-1})\ t/R_p^2 \quad (118)$$

The final equation relating the sand particle temperature to the sand particle radius, R_p, and the time the particle spends in the pyrolysis zone of the reactor, t, is given by:

$$\frac{T_s - T_p}{T_s - T_a} = 0.608 \exp(-6.58 \times 10^{-2} t/R^2_p) \quad (119)$$

$$+ 0.152 \exp(-2.64\times10^{-1}t/R_p^2)$$

$$+ 0.676 \exp(-5.92\times10^{-1}t/R_p^2) + \ldots$$

This equation was used to determine the time required for a typical bitumen-impregnated sandstone particle of a given diameter to reach the pyrolysis reactor temperature, 823 K (1022°F).

CONVERSION OF BITUMEN TO HYDROCARBON PRODUCTS AS A FUNCTION OF TIME

The conversion of bitumen is defined as the fraction or percentage of the original native bitumen present on the feed sand that is not converted to a carbonaceous residue or "coke" on the sand grains during pyrolysis, that is, the sum of the fractions or percentages of the native bitumen converted to a condensable bitumen-derived hydrocarbon liquid and to non-condensable hydrocarbon gases. If f_C is the fraction of the native bitumen feed to the reactor which is converted to residual coke on the sand, then $1-f_C$ is the fractional conversion or selectivity to recoverable hydrocarbon products, f_{HC}:

$$f_{HC} = 1-f_C \tag{120}$$

The influence of bitumen saturation on the conversion of bitumen to hydrocarbon products was investigated by using bitumen-impregnated sandstone from the Whiterocks and PR Spring tar sand deposits. The bitumen saturations of the Whiterocks and the PR Spring Rainbow I samples were 8% and 14.1% by weight, respectively. The physical and chemical properties of the native Whiterocks and PR Spring Rainbow I bitumens are presented in Tables 54, 55, and 56.[32,33]

The conversion, f_{HC}, as a function of time was determined by thermogravimetric analysis in an isothermal operating mode. In each experiment, approximately 80% of the native bitumen on the sand particles was converted to recoverable hydrocarbon liquids and gases, whereas 20% was converted to a carbonaceous residue on the spent sand.

Table 54

Native Bitumen Properties

	PR Spring Rainbow I	Whiterocks
Bitumen Saturation, wt.%	14.1	8.0
API Gravity, API	7.8	10.3
Viscosity, cps	160 (453 K)	29,250 (347 K)
Conradson Carbon Residue, wt.%	14.0	13.0
Ash Content, wt.%	3.3	0.8
Simulated Distillation		
Volatility, wt.%	31.9	22.1
IBP-400^{o}F, wt.%	1.3	0.9
400-650^{o}F, wt.%	5.1	3.3
650-1000^{o}F, wt.%	25.6	18.8
1000^{o}F^{+}, wt.%	68.1	77.2
Pour Point, ^{o}F	220	--

Table 55

Native Bitumen Properties

	PR Spring Rainbow I	Whiterocks
Elemental Analysis		
Carbon, wt.%	84.7	85.0
Hydrogen, wt.%	11.3	11.4
Nitrogen, wt.%	1.3	1.3
Sulfur, wt.%	0.5	0.4
Oxygen, wt.%	1.8	1.6
Atomic H/C Ratio	1.61	1.61
Molecular Weight, g mol^{-1}	702	NA
Nickel, wt.%	110	84
Vanadium, wt.%	10	< 200

Table 56

Native Bitumen Properties

Gradient Elution Chromatographic Analysis

	PR Spring Rainbow I	Whiterocks
Saturates, wt.%	9.5	15.3
MNA-DNA Oils, wt.%	10.2	8.5
PNA Oils, wt.%	11.4	11.9
PNA Soft Resins, wt.%	13.9	16.7
Hard Resins, wt.%	1.1	2.6
Polar Resins, wt.%	2.0	2.7
Asphaltenes, wt.%	31.3	31.2
Non-Eluted Asphaltenes, wt.%	20.6	11.1
	100.0	100.0

PARTICLE ENTRAINMENT AND CYCLONE RESIDENCE TIME

A solid particle will be entrained from the reactor when the particle terminal velocity is less than the fluid velocity leaving the reactor. The terminal velocity of a spherical particle depends upon the magnitude of the particle Reynolds number and is given by one of the following equations:[85]

$$U_t = \left\{ \frac{4(\rho_p - \rho_g)^2 g^2}{225 \rho_g \mu_g} \right\}^{1/3} d_p \quad , \quad 0.4 < Re_p < 500; \text{ or;} \tag{121}$$

$$U_t = 1.75 \left\{ \frac{g d_p (\rho_p - \rho_g)}{\rho_g} \right\}^{1/2}, \quad 500 < Re_p < 200{,}000; \tag{122}$$

where

U_t is the terminal velocity for the spherical sand particle, cm s^{-1};

ρ_p is the solid particle density, g cm^{-3};

ρ_g is the carrier gas density, g cm^{-3}, [8.6 x 10^{-4} g cm^{-3} for nitrogen at 823 K(1022°F)];

μ_g is the carrier gas viscosity, g $cm^{-1}s^{-1}$ [160 x 10^{-6} g $cm^{-1}s^{-1}$ for nitrogen at 823 K(1022°F];

g is the acceleration due to gravity, cm s^{-2};

d_p is the particle diameter, cm; and

Re_p is the particle Reynolds number.

The particle Reynolds number is given by

$$Re_p = \frac{d_p U_t \rho_g}{\mu_g} \quad . \tag{123}$$

The maximum size particle which would be transported into the cyclone, $(d_p)_{max}$, was calculated using equations 121 and 122.

The particle residence time inside a cyclone is determined by the size of the cyclone and the gas inlet velocity.[85] Two values for the cyclone diameter were used in these calculations, that is, 200

cm and 400 cm. The number of turns made by the gas stream in the cyclone was assumed to be five, which corresponds to the standard cyclone design. It was assumed that at the stationary state for an operating cyclone, the maximum residence time of a sand particle collected by the cyclone was the same as the gas residence time in the cyclone. The maximum particle residence time in the cyclone was then estimated from the following equation:[45]

$$\theta = \frac{\pi D_c N_t}{U_o} \tag{124}$$

where

D_c is the cyclone diameter, cm;

N_t is the number of turns the gas stream makes in the cyclone; and

U_o is the inlet gas stream velocity, cm s^{-1}.

The minimum diameter of a particle which can be completely collected by a cyclone of standard design is given by:[45]

$$(d_p)_{min.} = \left[\frac{9\mu_g B_c}{\pi N_t U_o(\rho_p - \rho_g)}\right]1/2 \tag{125}$$

where

(d_p)min. is the minimum diameter of particle which is completely collected by the cyclone, cm;

U_o is the cyclone inlet gas velocity, cm s^{-1};

N_t is the number of turns made by the gas stream in the cyclone (N_t = 5);

B_c is the width of the rectangular cyclone inlet duct, cm, (1/4 of the cyclone diameter);

ρ_p is the density of the sand particle, g cm^{-3}, and

ρ_g is the density of the gas, g cm^{-3}.

Thus, we can establish a relationship between the time required for conversion of the bitumen to recoverable hydrocarbon products and the residential time of an average sand particle in the cyclone pyrolysis reactor.

EXPERIMENTAL

The physical and chemical properties of the native bitumens were determined according to standard ASTM procedures. The gradient elution chromatographic analysis was performed according to the procedure developed by Middleton[35] and modified by Callen and co-workers.[36] The elemental and metals analyses were done by Galbraith Laboratories, Inc., Knoxville, Tennessee.

The thermogravimetric experiments (TGA) were conducted in a DuPont 990 Thermal Analysis system. Prepurified nitrogen was used as the carrier gas in all TGA experiments. The carrier gas flow rate was 100 cm^3 min^{-1}. The pyrolysis temperatures for the TGA experiments were well below the mineral carbonate decomposition temperature (~617 K) of the sand-mineral substrate.

The consolidated Whiterocks and PR Spring Rainbow I tar sand samples were crushed and sized to obtain narrow size range fractions. The bitumen conversion was determined for four different average particle reactors; 0.025 cm, 0.12 cm, 0.2 cm, and 0.4 cm.

RESULTS AND DISCUSSION

The average sand particle temperatures, as a function of time in the pyrolysis zone of the reactor, are presented in Figures 96 through 99. The final temperature of the sand particle and the time required to approach or attain the final temperature appeared to be independent of the inlet, feed sand temperature for sand particles of diameter less than 1 cm. Sand particles having a diameter greater than 1 cm required a longer time to approach or attain the final temperature at the lower inlet, feed sand temperature. Sand particles of 0.2 cm diameter attained the final temperature in less than one second whereas the sand particles of 3 cm diameter required more than 180 seconds to achieve the final temperature.

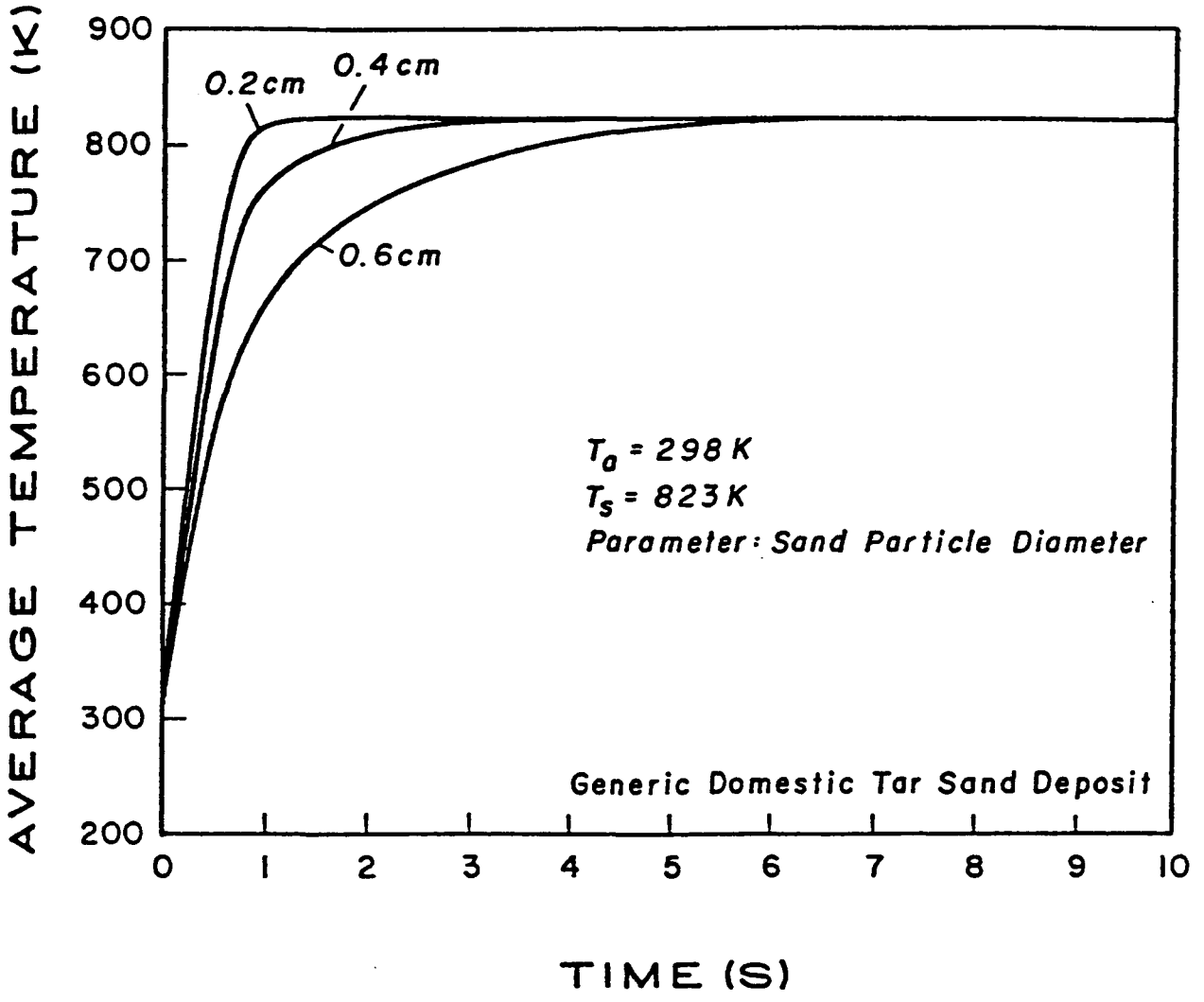

Figure 96. - Average sand particle temperature as a function of time. Sand particle diameter range 0.2-0.6 cm; inlet sand temperature 298 K.

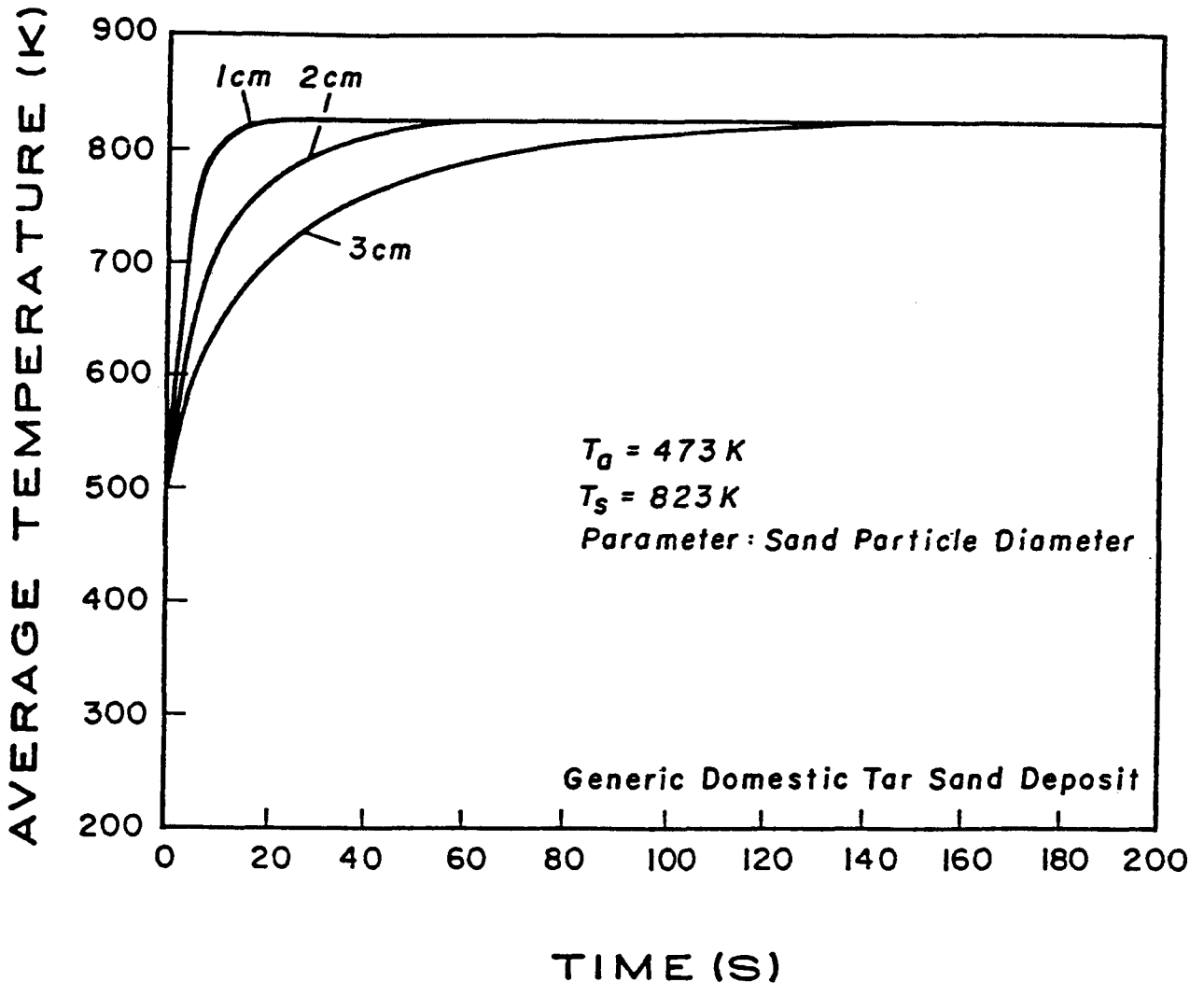

Figure 97. - Average sand particle temperature as a function of time. Sand particle diameter range 1-3 cm; inlet sand temperature 298 K.

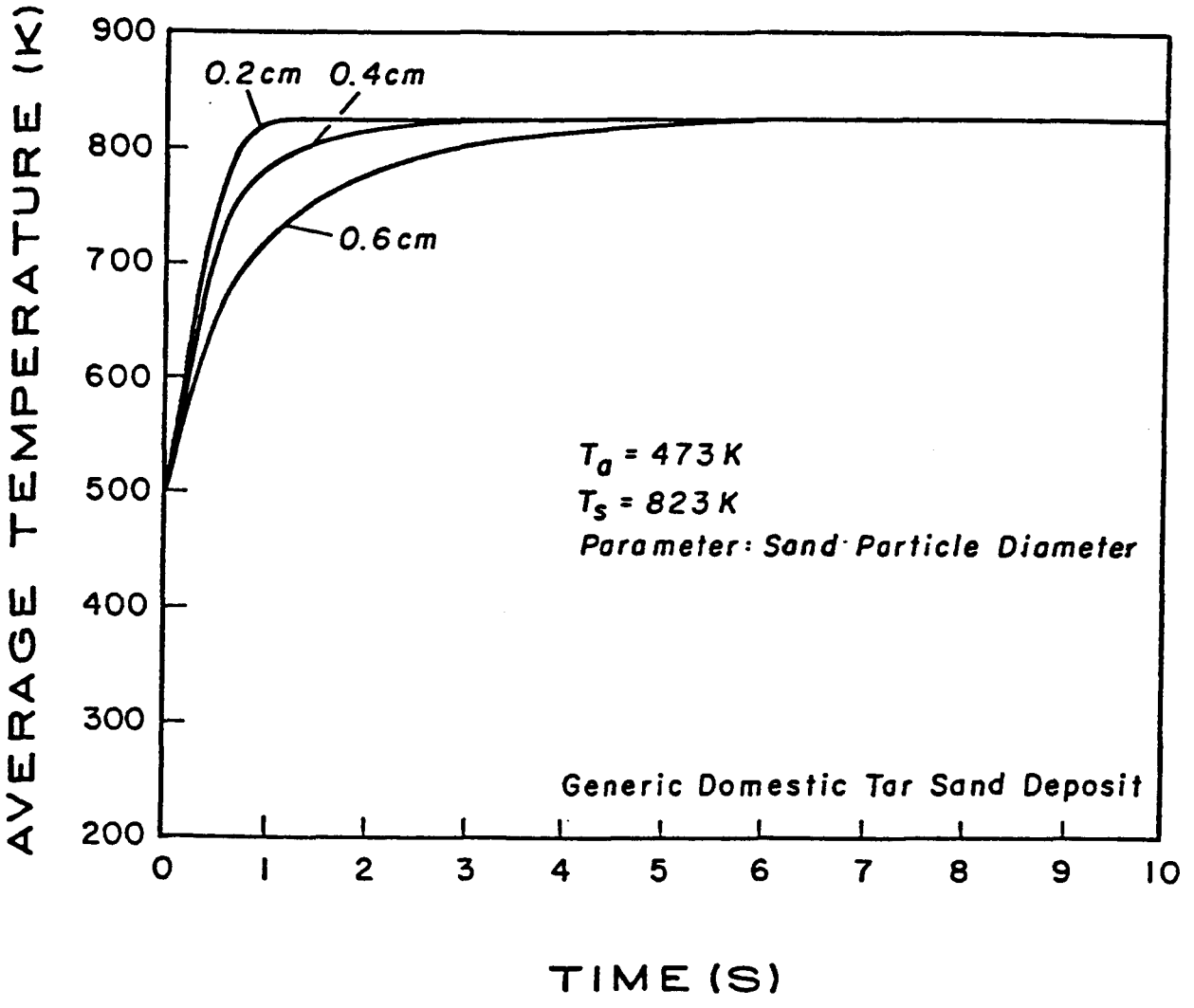

Figure 98. - Average sand particle temperature as a function of time. Sand particle diameter range 0.2-0.6 cm; Inlet sand temperature 473 K.

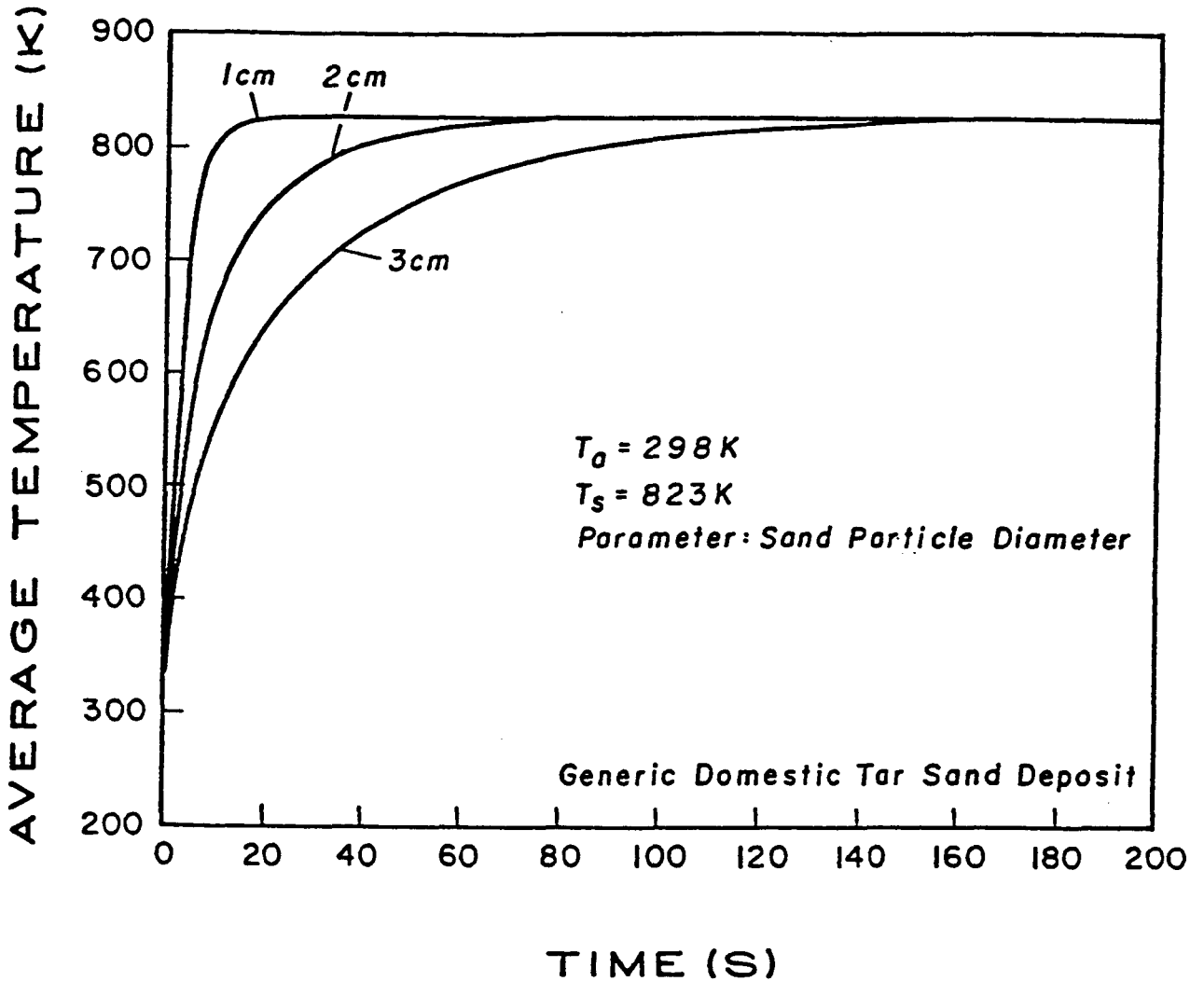

Figure 99. - Average sand particle temperature as a function of time. Sand particle diameter range 1-3 cm; Inlet sand temperature 473 K.

The bitumen conversion to bitumen-derived hydrocarbon liquids and gases (normalized to a coke-free basis) as a function of time for the PR Spring Rainbow I and Whiterocks samples are presented in Figures 100 and 101, respectively. The selection of the PR Spring Rainbow I and Whiterocks tar sand samples for this investigation was based on the comparative analysis of the chemical and physical properties of the native bitumens and upon the difference in bitumen saturations. The physical properties of the two bitumens appear to be somewhat different as reflected by the gravity, viscosity, and distillation data; however, the chemical properties such as elemental analysis, Conradson carbon residue, and compound type analysis are quite similar (see Tables 54, 55, and 56). Since the bitumen pyrolysis reaction is probably more dependent upon the chemical nature of the bitumen rather than upon its physical properties, it was presumed that the two samples would behave similarly with regard to bitumen conversion in this instance and that any significant differences could be attributable to the difference in bitumen saturation. Furthermore, in a previous investigation[33] of the fluidized bed pyrolysis of bitumen-impregnated sandstone from the PR Spring and Whiterocks deposits, the product distribution correlated well with the Conradson carbon residue, the atomic H/C ratio and the asphaltene content of the native bitumen, whereas there was no correlation between the product distribution and the gravity, viscosity or distillation data.

The bitumen conversion (on a coke-free basis) as a function of time, as determined by TGA analysis, for the two tar sand samples was similar for the three smaller sand particle diameters (0.025 cm, 0.12 cm, 0.2 cm) in all isothermal TGA experiments; however, in several instances the 0.4 cm diameter Whiterocks sample required longer times (49 versus 41 s) to attain the same level of conversion as the 0.4 cm diameter PR Spring Rainbow I samples. However, careful selection of samples for TGA analysis was made for all experiments. The 0.4 cm diameter particles appeared to be uniformly impregnated with bitumen and were of the same color in all regions on the surface of the particle. Therefore, the difference in time required to achieve 90% conversion may be related to the higher molecular weight species present in the Whiterocks sample as indicated by the lower volatility of the native bitumen or to the difference in the total asphaltene contents of the Whiterocks and PR Spring Rainbow I bitumens. The asphaltene species are assumed to react to form a carbonaceous

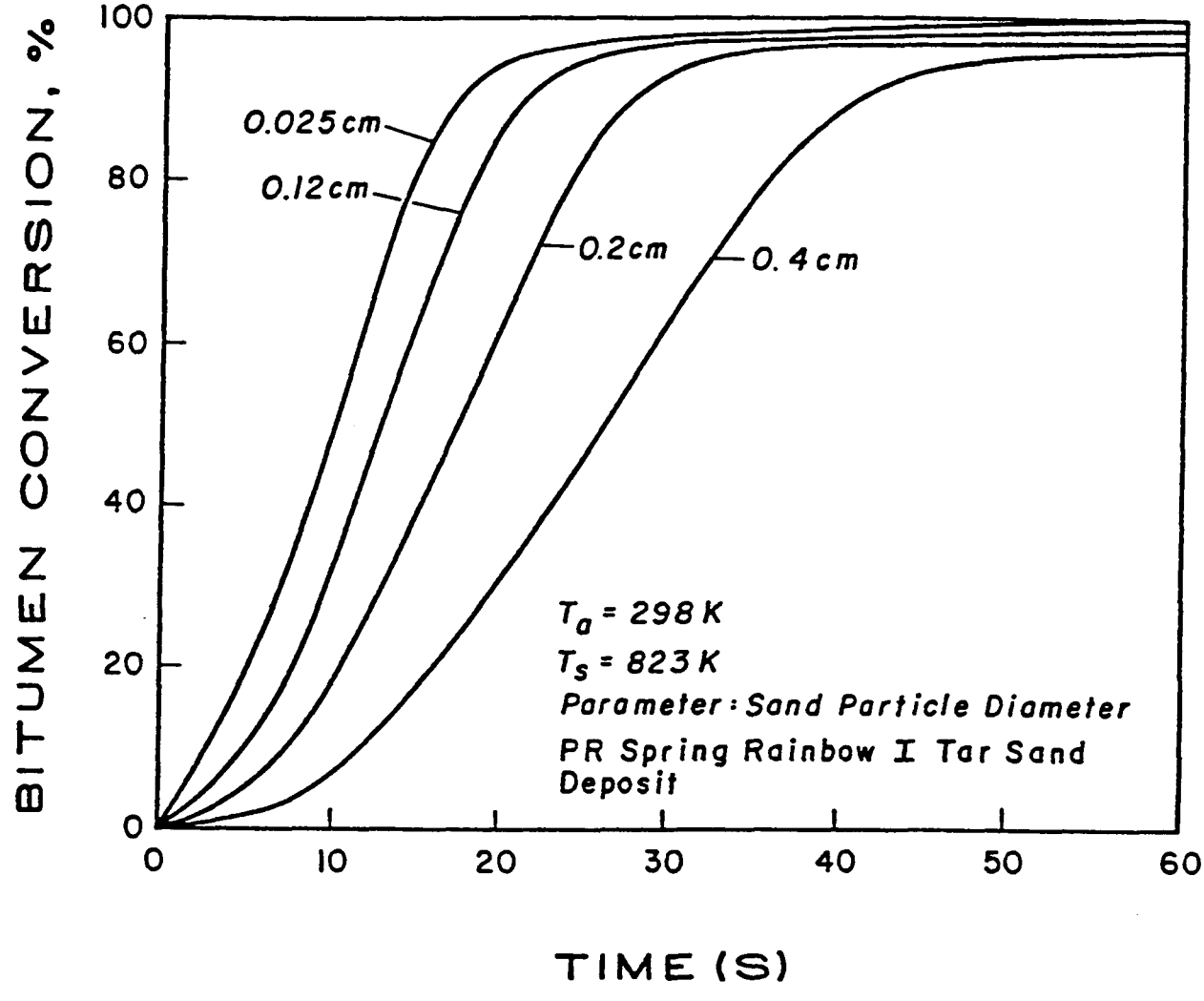

Figure 100. - Bitumen conversion as a function of time, PR Spring Rainbow I bitumen-impregnated sandstone.

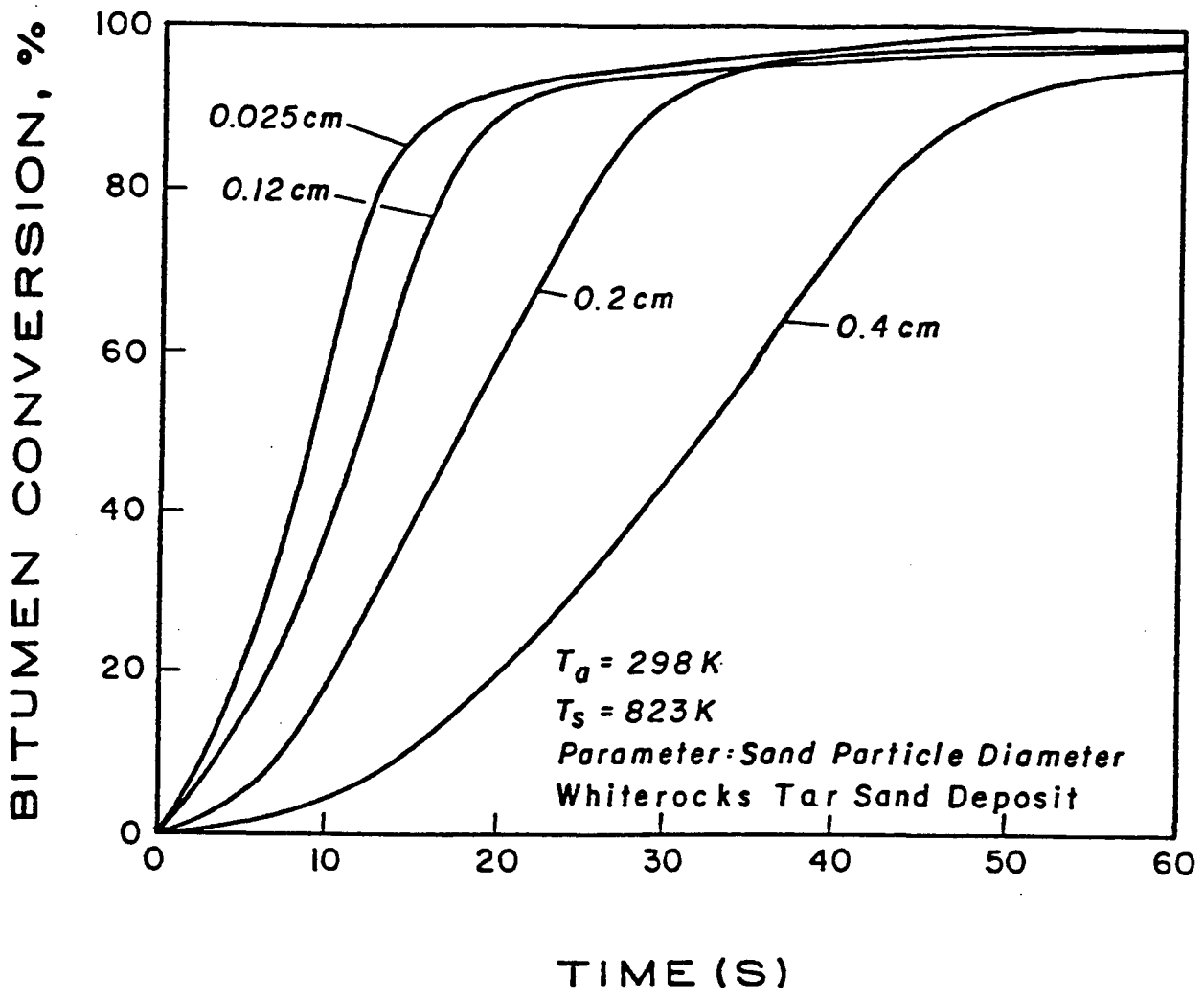

Figure 101. - **Bitumen conversion as a function of time; Whiterocks bitumen-impregnated sandstone.**

residue, C_1-C_4 hydrocarbon gases, and light and heavy oil. If it is assumed that the asphaltene species are more reactive at the pyrolysis temperatures than the non-asphaltene species, then the PR Spring Rainbow I may be more reactive than the Whiterocks bitumen because it contains higher levels of total asphaltenes; consequently, it would be expected that the Whiterocks sample would require longer times to attain the same level of conversion as the PR Spring Rainbow I samples. However, since only the larger diameter particle exhibited this behavior, mass transport may also be a factor.

The vaporized hydrocarbon species produced during the pyrolysis of the Whiterocks bitumen are, on the average, higher in molecular weight than those produced during the pyrolysis of the PR Spring Rainbow I bitumen;[26,27] that is, the more asphaltenic bitumen tends to produce higher yields of the lower molecular weight hydrocarbons. Therefore, the Whiterocks product species may exhibit lower diffusivity in the larger diameter particles such that the vaporization process in the pores may more nearly approach the equilibrium state. This would result in a net reduction in the rate of vaporization of the pyrolysis product species for the Whiterocks bitumen and an extension of the time required to achieve the same apparent level of conversion relative to the PR Spring Rainbow I sample for the large diameter particles.

As expected, the larger diameter sand particles required a longer time at the pyrolysis temperature to achieve the same level of bitumen conversion for both the PR Spring Rainbow I and Whiterocks samples. Based on bitumen fed to the cyclone pyrolysis reactor, it is expected from the fluidized bed results[33] that 60-80% of the native bitumen would be converted to a bitumen-derived liquid, 10-20% would be converted to C_1-C_4 gases, and 10-20% would be left on the sand grains as a carbonaceous residue for both the PR Spring Rainbow I and Whiterocks tar sand samples.

The calculated gas and limiting maximum sand particle residence times in the cyclone (θ), the minimum collected sand particle diameters, (d_p)min, and the maximum particle diameters for sand particles transported into the cyclone, (d_p)max, for both the 200 cm and 400 cm diameter cyclones (D_c) are presented in Table 57.

The calculations were initiated by specifying the diameter of the maximum size sand particle carried by the gas stream into the cyclone. The terminal velocity of the particle and the particle

Table 57

Entrained Particle Diameters and Cyclone Residence Times

U_t (cm s^{-1})	$(d_p)_{max}$ (cm)	θ (s)		$(d_p)_{min}$ (cm)		Re_p
		D_c = 400 cm	D_c = 200 cm	D_c = 400 cm	D_c = 200 cm	
1868	0.5	3.4	1.7	0.0016	0.0011	5020
1671	0.4	3.8	1.9	0.0017	0.0012	3593
1447	0.3	4.3	2.2	0.0018	0.0013	2333
1321	0.2	5.3	2.7	0.0020	0.0014	1270
791	0.1	7.9	4.0	0.0024	0.0017	425
396	0.05	15.9	7.9	0.0034	0.0024	106
237	0.03	26.5	13.3	0.0044	0.0031	38

Reynolds number were calculated for each specified particle diameter. The calculated residence time is for the gas in the cyclone; however, if we assume the cyclone operates at the stationary or steady state, then there would be no accumulation of sand particles within the cyclone and the calculated residence time for the gas is the limiting, maximum residence time for the sand particle in the cyclone. Finally, the diameter of the minimum sand particle, (d_p)min, collected by the cyclone was calculated. Any sand particle having a diameter less than (d_p)min will be carried out of the cyclone in the exit gas stream whereas any sand particle having a diameter greater than (d_p)min will be collected by the cyclone.

The calculated residence times indicated that for particle size diameters as small as 0.03, the 400 cm diameter cyclone can be used as a pyrolysis reactor since the residence time exceeded 18 seconds, which is the time required for a sand particle of diameter 0.025 cm to achieve 90% conversion of the bitumen. For sand particles of diameter greater than 0.1 cm, the 400 cm diameter cyclone will not provide sufficient residence time for complete conversion of the bitumen. The residence time calculated for the 200 cm diameter cyclone indicates that it would not be suitable as a pyrolysis reactor. If a riser/transport reactor is placed in series with a cyclone reactor, the particle residence time can be increased significantly and larger diameter particles can be processed for a fixed diameter cyclone.

CONCLUSIONS

The analysis of the cyclone reactor for the pyrolysis of bitumen-impregnated sandstone led to the following conclusions.

- The 400 cm diameter cyclone reactor will not provide sufficient residence time to permit complete conversion of the bitumen for bitumen-impregnated sandstone particles of diameter larger than 0.1 cm/ however, it would provide adequate residence time to achieve 90% conversion of the bitumen for bitumen-impregnated sandstone particles of diameter less than 0.03 cm. The time required for the sand particles to achieve the final temperature did not appear to be dependent upon the feed sand temperature for sand particles smaller than 1 cm in diameter.

- The residence time at the pyrolysis temperature could be increased by combining a riser or transport reactor with the cyclone reactor, thus permitting larger diameter particles to be processed.

NOMENCLATURE

B_c = width of rectangular cyclone inlet duct, cm

$\hat{C}_{p,p}$ = heat capacity of sand particle, cal $g^{-1}K^{-1}$

$\hat{C}_{p,ss}$ = heat capacity of quartzitic sandstone, cal $g^{-1}K^{-1}$(0.26 cal $g^{-1}K^{-1}$ at 373 K)

d_p = diameter of the sand particle, cm

$(d_p)_{max}$ = maximum diameter of entrained particle, cm

$(d_p)_{min}$ = minimum diameter of sand particle which is completely collected by the cyclone, cm

D_c = cyclone diameter, cm

f_C = fraction of native bitumen converted to carbonaceous residue or "coke" on the sand grains

f_{HC} = fraction of native bitumen converted to hydrocarbon liquid and to hydrocarbon gases

g = acceleration due to gravity, cm s^{-2}

k_p = thermal conductivity of the sand particles, cal $s^{-1}cm^{-1}K^{-1}$

k_{ss} = thermal conductivity of the quartzitic sand grains, cal $s^{-1}cm^{-1}K^{-1}$ ($9x10^{-3}$ cal $s^{-1}cm^{-1}K^{-1}$ at 473 K)

N_{Fo} = Fourier Number

N_t = number of turns the gas stream makes in the cyclone

$\dot{q}_c$ = heat flux vector due to conduction, cal $s^{-1}cm^{-2}$

q_r = rate of thermal energy generation or consumption per unit volume within the sand particle due to chemical reaction, cal $s^{-1}cm^{-3}$

R_p = radius of the sand particle, cm

Re_p = particle Reynolds number

t = time, s

T = temperature, K

T_a = initial, inlet temperature of the sand particle, K

T_P = average temperature of the sand particle at time t, K

T_s = constant average temperature at the surface of the sand particle, K

U_o = inlet gas stream velocity, cm s^{-1}

U_t = terminal velocity for the spherical sand particle, cm s^{-1}

α = thermal diffusivity of sand particle, cm^2 s^{-1}

ρ_g = density of fluidizing gas, g cm^{-3}

ρ_s = density of the sand grains comprising the bitumen-impregnated sandstone particles, g cm^{-3}

ρ_p = density of the sand particle, g cm^{-3}

$\phi(N_{Fo})$ = solution to the energy balance equation for spherical particle geometry

μ = viscosity of the fluidizing gas, g $cm^{-1}s^{-1}$

θ = maximum particle residence time in the cyclone, s.

SECTION C

MODIFIED HOT WATER SEPARATION TECHNOLOGY

J.D. Miller

MODIFIED HOT WATER SEPARATION TECHNOLOGY

J.D. Miller — Professor
Y.J. Yang — Graduate Student
K. Bukka — Postdoctoral Fellow

Until recently, the development of hot water separation technology for bitumen recovery from domestic tar sands has been based on an empirical approach supported, to a limited extent, by fundamental knowledge of hydrodynamics and surface chemistry. Due to different domestic tar sand properties, a special processing technique has been developed at the University of Utah in order to obtain a bitumen recovery and separation yield acceptable for industrial application. Further study of the modified hot water processing of tar sands has led to a better understanding of phenomena occurring at all interfaces involved in the separation process. These interfaces include the bitumen/sand interface during digestion, the bitumen/water interface during flotation or concentrate clean-up, and the water/sand interface during tailings sedimentation/water recycle.

The research work undertaken in this project is broadly divided into three main areas. The first area involves an attempt to understand the fundamentals of bitumen displacement from the sand surface. These activities include examination of the surface properties of bitumen, determination of the relative importance of adhesive and cohesive forces in dislodging the bitumen from sand surface, and evaluation of the hydrodynamic behavior of bitumen under simulated process conditions. The second area involved applied research on low shear digestion in a stirred tank reactor. The third area of study is involved in the selection and evaluation of diluent used in the modified hot water separation process.

FUNDAMENTALS OF BITUMEN DISPLACEMENT

A study of the bitumen-solid interface was carried out to elucidate the phase-disengagement mechanism during digestion. Motion analysis of bitumen in shear flow, involving high speed video monitoring of bitumen disengagement and shape analysis of sand fractions in the concentrate and tailings constituted an important part of the research effort. The bitumen used in the tests was extracted from Asphalt Ridge tar sand.

Motion Analysis of Bitumen in Shear Flow

A rotating disc and a rotating cylinder were used to investigate the shear disengagement of bitumen from a solid surface. A schematic diagram of the apparatus is presented in Figure 102. A bitumen-coated aluminum disc was rotated in water at different speeds, and bitumen detachment from the disc surface as a result of fluid shear was recorded using the SP2000 high speed motion analyzer video system as shown in Figure 103. The rpm of the disc at which bitumen started to be released was noted, and the shear rate and the corresponding shear stress on the bitumen were calculated from first principles.

It was seen that, for a given thickness of the bitumen layer, the quantity of liberated bitumen increased with an increase in the speed of rotation. For a given speed of rotation, the fraction of the bitumen layer that was removed increased with the thickness of the initial coating. A thin layer of bitumen always remained attached to the disc surface, indicating that the shear stress needed to cause its detachment from the disc surface is far more than that which could be provided by the fluid shear within the limits of experimentation.

For a simpler fluid dynamic analysis, a rotating cylinder system was studied. A bitumen coated cylinder was rotated in water at different speeds. The amount of bitumen disengaged from the cylinder surface because of fluid shear was determined as the difference in mass of the cylinder before and after rotation in water and then expressed as the thickness of bitumen coating the cylinder. Data presented in Tables 58-60 reveal that the amount of liberated bitumen is, first of all, a function of initial coating thickness, and then, to a much lesser degree, dependent on the rotation time and speed.

Similar to the rotating disc tests, a limiting thickness was found between 20 and 30 μm that could not be reduced further under these experimental conditions. Preliminary data on bitumen liberation kinetics are presented in Table 60. Increasing the duration of rotation to 20 minutes had no significant effect on the residual thickness.

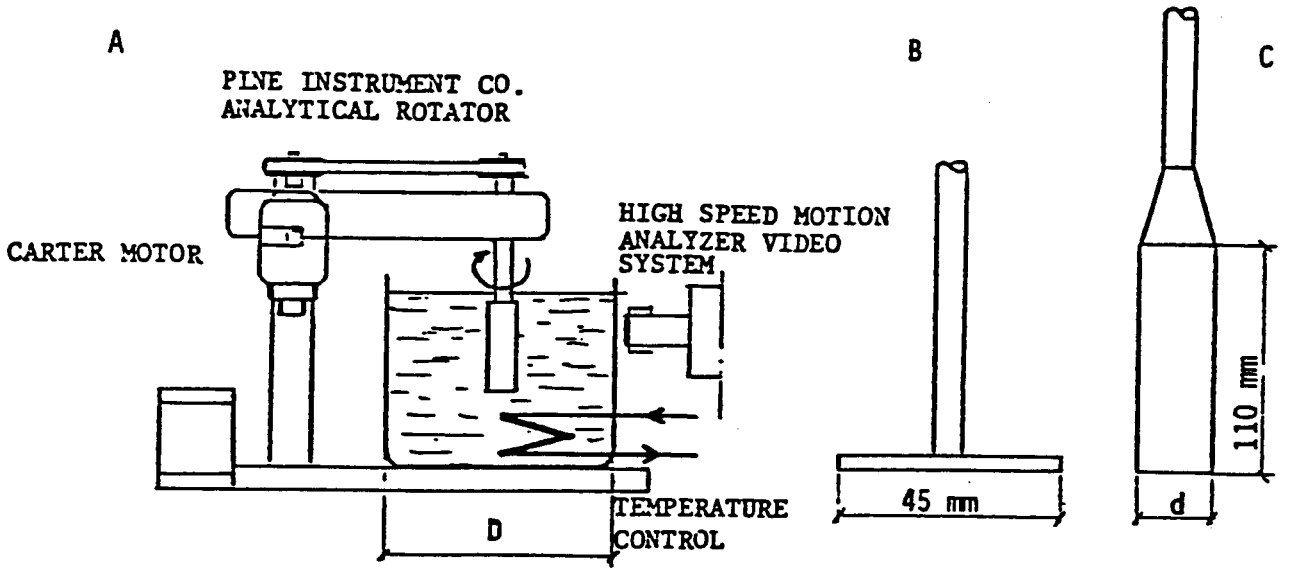

Figure 102. -
Experimental apparatus for phase-disengagement study.
A: Experimental setup
B: Aluminum disk
C: Aluminum cylinder
Range of D 10 to 30 cm; range of d 1.2 to 2.5 cm

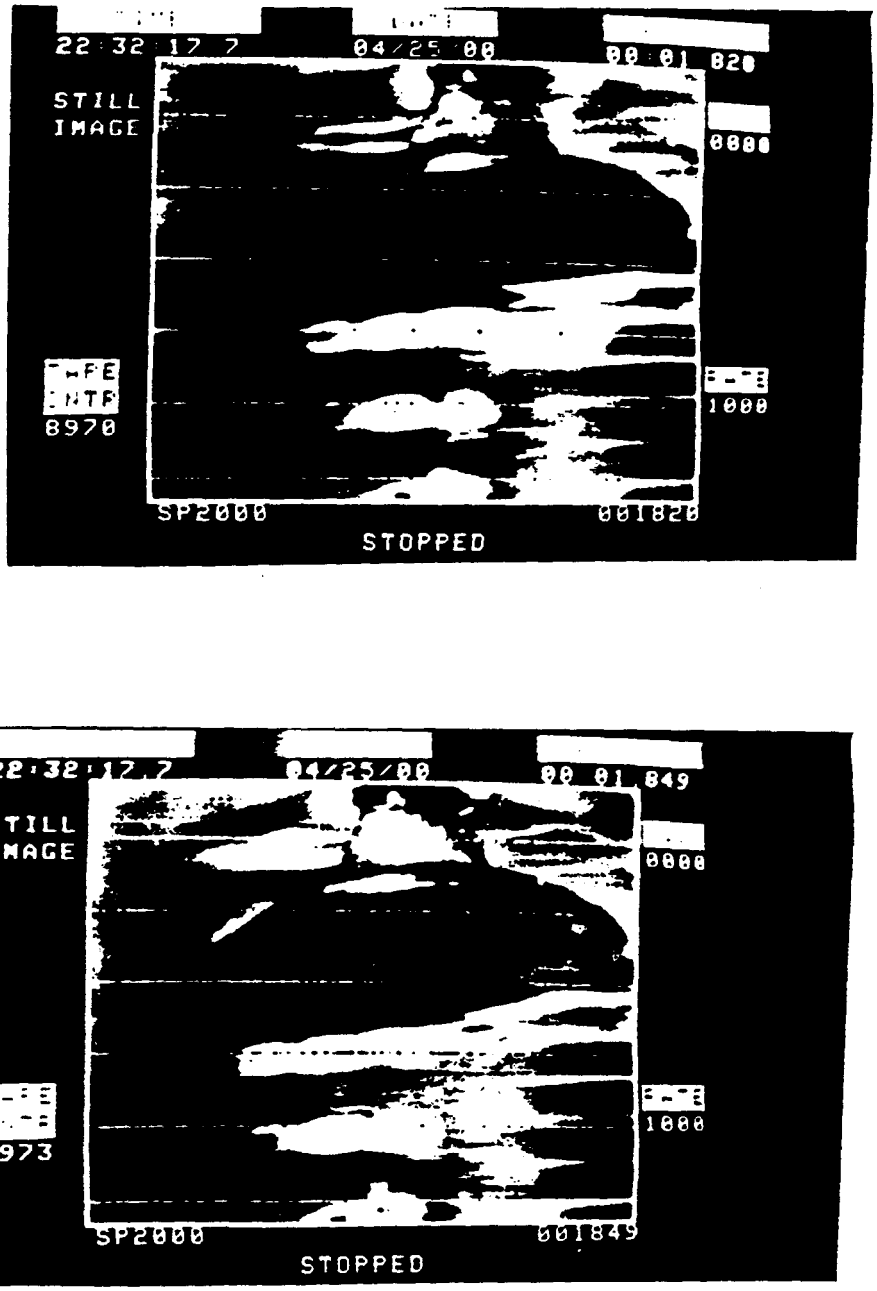

Figure 103. - High-speed photographs of bitumen disengagement from a rotating disc due to fluid shear: (a) bitumen at the point of detachment; (b) bitumen detached.

Table 58

Bitumen Liberation from a Rotating Cylinder as a Function of Time

Experimental Conditions

Reactor Geometry: D/d = 15
Temperature: 20±1 ^{o}C
Stirring Speed: 750 rpm
Bitumen Viscosity (Adjusted by Diluent Addition) at 20^{o}C: 13.6 Pas

Initial Thickness of Bitumen Layer (μm)	Amount of Bitumen Liberated (μm)	Thickness of Remaining Bitumen Layer (μm)
Time = 2 Minutes		
91.2	28.2	65.5
88.4	27.1	64.4
78.6	19.4	63.4
77.6	19.0	62.9
70.8	14.3	60.7
49.2	10.8	43.9
47.8	9.8	43.1
46.6	8.8	42.5
44.3	8.7	40.5
42.1	8.5	38.5
40.2	8.3	36.9
38.6	8.0	35.5
38.4	8.0	35.5
36.2	7.8	33.4
34.4	7.5	31.8
Time = 5 Minutes		
46.6	14.3	39.9
44.2	12.1	38.9
39.2	11.5	34.7
38.2	11.0	34.0
35.2	8.4	32.2

Table 59

Bitumen Liberation from a Rotating Cylinder at 1000 rpm

Experimental Conditions

Time: 2 minutes
Reactor Geometry: D/d = 15
Temperature: 20±1 ^{o}C
Bitumen Viscosity (Adjusted by Diluent Addition) at 20^{o}C: 13.6 Pas
Stirring Speed: 1000 rpm

Initial Thickness of Bitumen Layer (μm)	Amount of Bitumen Liberated (μm)	Thickness of Remaining Bitumen Layer (μm)
48.6	12.4	42.6
40.2	10.3	36.1
38.4	10.0	34.6
36.8	8.4	33.7
34.2	8.2	31.4

TABLE 60

Kinetics of Bitumen Disengagement from a Rotating Cylinder

Experimental Conditions

Cylinder Revolutions: 750; 1000
Reactor Geometry: D/d = 15
Temperature: 20±1 ^{o}C
Bitumen Viscosity (Adjusted by Diluent Addition) at 20^{o}C: 13.6 Pas

Initial Thickness of Bitumen Layer (μm)	Amount of Bitumen Liberated (μm)	Thickness of Remaining Bitumen Layer (μm)
Initial Bitumen Layer Thickness 67 μm, 750 rpm		
2	13.8	57.8
5	15.6	56.5
10	16.5	55.9
15	19.3	55.4
20	18.0	54.9
Initial Bitumen Layer Thickness 58 μm, 750 rpm		
2	12.6	50.7
5	13.4	50.2
10	13.9	49.9
15	14.6	49.5
20	15.2	49.2
Initial Bitumen Layer Thickness 43 μm, 1000 rpm		
2	11.4	38.1
5	12.6	37.6
10	13.4	37.2
15	14.3	36.9
20	14.8	36.6

Elliptical shape factor: ELLSF = b/a

where $a = \sqrt{\frac{4I_a}{Area}}$, $b = \sqrt{\frac{4I_b}{Area}}$

The defining equations are given by the following:

$$I_a = \frac{I_x + I_y}{2} + \left[\left(\frac{I_x + I_y}{2}\right)^2 - (I_x I_y - I_{xy}^2) \right]^{1/2}$$

$$I_b = \frac{I_x + I_y}{2} - \left[\left(\frac{I_x + I_y}{2}\right)^2 - (I_x I_y - I_{xy}^2) \right]^{1/2}$$

where

$$I_x = \int_A x^2 \, dA, \quad I_y = \int_A y^2 \, dA, \quad I_{xy} = \int_A xy \, dA$$

are used to calculate two distances perpendicular to each other based on the areal amounts of inertia, and x and y are the particle Feret distances. Shape factors approach 1 when particle projection becomes close to a circular configuration. In the size range studied, sand grains found in tailings are more regular than the sand grains which reported to the concentrate as the shape factors indicate (see Table 61).

In view of the excellent separation that can be achieved with the Asphalt Ridge tar sand, the shape factors in the region of 0.7 indicate that the sand particles can be separated with relative ease from the bitumen. On the other hand, it is envisaged that bitumen recovery from tar sands with sand shape factors smaller than 0.7 (greater irregularity of sand grains) would be much less efficient. Sand surface irregularities and roughness significantly contribute to inferior bitumen liberation with increasing bitumen viscosity. The almost rigid coating of highly viscous bitumen (e.g. >100 Pa. S at the

TABLE 61

Shape Factors for Asphalt Ridge Sand Grains (38-74 μm) from Concentrate and Tailings

GRAIN SPECIFIC PARAMETER	VALUE OF SHAPE FACTOR	
	CONCENTRATE	TAILINGS
Circular Factor	0.692	0.716
Elliptical Factor	0.713	0.753

A theoretical derivation for the shear stress at the surface of a cylinder rotating in a confined fluid field indicates that shear stress increases with rotational speed and fluid viscosity and decreases with increased diameter of the fluid container. Thus, the D/d ratio (see Figure 102) becomes a parameter of paramount importance in the study. At D/d < 3, a good simulation of the shear force field in a stirred reactor may be achieved.

In conclusion, bitumen disengagement from a coated solid surface takes place only when the shear stress due to the surrounding fluid exceeds the adhesion (between solid surface and bitumen) or cohesion (between layers of bitumen) forces per unit surface area of the coating. Experiments have shown that, whatever the initial thickness of the coated bitumen is, after disengagement there remains a residual thickness of bitumen that cannot be reduced any further. The shear stress is practically the same at different initial thicknesses. Thus the cohesion forces take on more importance at larger thicknesses, while the adhesion forces become of greater significance for bitumen layers of approximately 30 μm. In the actual situation of tar sand digestion, it is likely that the viscosity of the surrounding fluid, and hence the shear stress on the bitumen surface, would be considerably higher than that used in present tests. Abrasion of the bitumen surface may also be significant in the digester. Further, the alkaline environment in the digester may diminish the adhesive bond between the sand surface and the bitumen.

Image Analysis of Solids from Concentrates and Tailings

The shapes of 200 X 400 mesh sand grains (average size of 60μm) both from the tailings and from sand trapped in the bitumen concentrate have been studied by means of the IBAS image analyzer. The circular and elliptical shape factors were determined from about 5200 grains. By definition, the specific parameters of the sand grains are:

Circular shape factor: CIRSF = 4π Area/(Perim)^2

where Area = specific grain area

Perim = specific grain perimeter.

temperatures of processing) may never be released from the sand surface under the shear force field available during the tar sand digestion step.

Determination of Surface Properties of Bitumen

Understanding the phenomena involved in bitumen displacement from the surface of sand particles in the modified hot water separation process is of importance to the further development of the technology. A number of theories have been advanced to explain the bitumen displacement phenomena. However, complete understanding has generally not been achieved. It is clear that the adhesion forces between the surface of the sand particles and the bitumen play an important role in determining the displacement phenomena. These adhesion forces are stronger than the bitumen cohesion forces and the bitumen cannot be removed completely by fluid shear as discussed previously. As cohesion forces determine the bitumen surface tension, an attempt was made to measure the surface tension of bitumen solutions at various temperatures. The bitumen used in these studies is again that extracted from Asphalt Ridge tar sands.

Bitumen for surface tension experiments was obtained by Dean/Stark extraction of the tar sands with toluene as solvent. After complete extraction, the toluene extract was filtered through Whatman No. 42 filter paper to separate fine solids. Removal of the solvent from the solution was accomplished by distillation on a Brinkman rotary evaporator at 70°C and 4 mm Hg pressure.

The surface tension of bitumen solutions was measured with Cenco-Dunouy tensiometer. Because of the high viscosity of the extracted bitumen at room temperature, kerosene and toluene were used as diluents. The amount of bitumen in the diluents was varied from 0-60% by weight. Results from these measurements are tabulated in Table 62 and are presented in Figure 104. However, this method did not permit surface tension measurement of solutions in which the concentration of bitumen exceeded 60%. By extrapolating the surface tension values plotted in Figure 104 to 100% bitumen, a value for the pure bitumen of 40.4 and 42.1 dynes cm^{-1} have been obtained from large solutions of bitumen in kerosene and toluene respectively. Relatively large difference between the two values

Table 62

Air/Bitumen Solution Interfacial Tension at 20°C

Bitumen Solution (Wt % Bitumen)	Diluent	
	Kerosene	Toluene
0	27.8 (dynes/cm)	28.9 (dynes/cm)
5	28.2	29.6
10	28.9	29.8
15	29.7	30.7
20	30.8	31.4
25	31.9	32.4
30	32.2	32.8
35	32.7	33.4
40	33.0	33.7
45	33.4	34.9
50	33.9	35.3
53	34.4	36.1
60	35.2	36.8

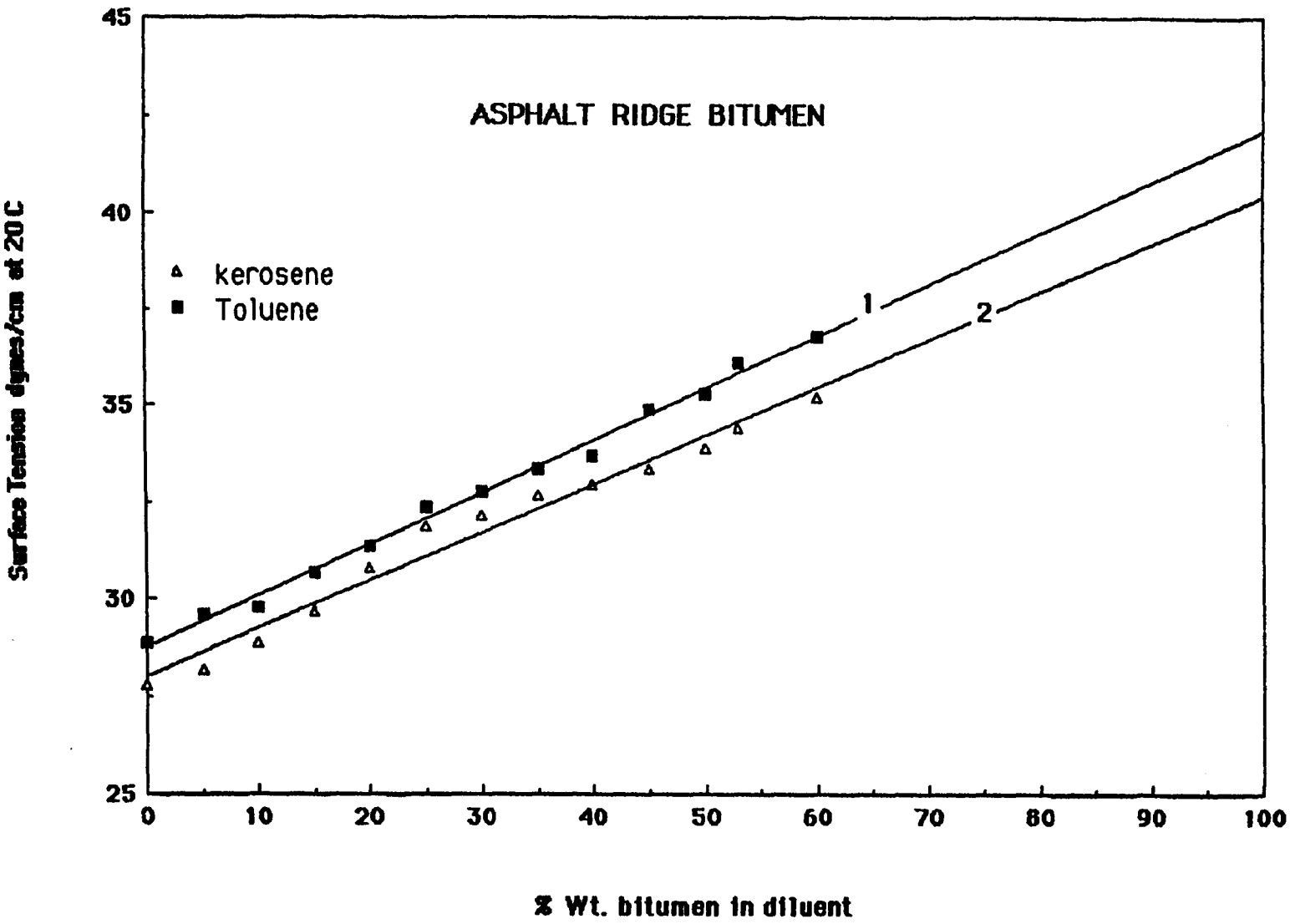

Figure 104. - Air/bitumen solution surface tension.

obtained indicates uncertainties involved in the extrapolation method. However, the average value of 41.4 dynes cm^{-1} can be used to estimate the cohesion energy of the bitumen from the following equation:

$$W_{cohesion} = 2\gamma$$

where W is the work of cohesion and γ is surface tension of the cohesion bitumen. Thus, the cohesive energy of bitumen is calculated to be 82.8 ergs cm^{-2}.

LOW SHEAR DIGESTION

Five kilogram batch samples were prepared from Athabasca, Asphalt Ridge, and Sunnyside tar sand bulk samples. When necessary, an appropriate amount of kerosene was sprayed over the sample in order to maintain a bitumen viscosity of 0.5 to 1.5 Pa. S at the temperature of processing (either 50°C or 80°C), and a sufficient penetration time was provided, as established from previous work. Bitumen recovery experiments were carried out by digestion and flotation in a 38-liter Denver type flotation cell. Solids concentration during digestion was reduced from standard practice of 75% to only 30%. A rotor-stator impeller turning at 900 rpm recirculated the slurry (the air-suction valve was closed) combining shear, impact, collision, and circulation effects, but at a much lower level of intensity than in the high intensity stirred tank reactor used previously. Experiments were not designed to obtain maximum separation efficiency for a single stage but rather to compare the separation efficiency for various tar sands at the same processing conditions. The successful use of such a lower shear force field would be of considerable value from a practical standpoint.

After 15 minutes of digestion, the flotation cell was filled with water at the same temperature and the air suction valve was opened. The resulting solids concentration dropped to 14-15% by weight. In order to study the kinetics of bitumen flotation, concentrates were collected at time intervals of 1,2,3, and 4 minutes. The hold-up volume of dispersed air in the flotation cell fluctuated between 6 and 7%.

Under low shear conditions, not much difference in total recovery was observed for many of the tar sands tested. In all cases, an ultimate recovery in excess of 90% was achieved. Data presented in Table 63 reveal that generally the percent of bitumen in concentrates I and II is still at an acceptable level (60%), excepting Sunnyside and Athabasca at 50°C. For Sunnyside tar sands, it was suggested previously that the shear force could not be transferred to the bitumen/sand interface. It is still not clear why the bitumen grade of the Athabasca concentrate at 50°C was so low.

Cumulative recovery and grade of the concentrate are presented in Figures 105-107 as a function of time. It was observed that most of the bitumen was recovered in 10 minutes for all the tar sands tested. However, when the bitumen content of the concentrate is considered, the best results are obtained after 3 minutes. Although the grade in concentrates I and II is acceptable, the recovery of bitumen is only 60% (see Asphalt Ridge at 80°C, 52°C, and Athabasca at 80°C). This value is still not acceptable from a processing standpoint, so the reduced shear hot water separation technique will require the recycle of a middling, concentrates III and IV in order to achieve a high grade product at a good recovery. A schematic representation of such a process with recycle is represented in Figure 108.

As established in previous work, bitumen viscosity is the controlling factor for the high shear force field reactor. But for lower shear force field, surface chemistry features such as zeta potential, adhesion energy, and tar sand microstructure start to play a more significant role and have to be included in the analysis and development of improved hot water separation strategies.

SELECTION AND EVALUATION OF DILUENT

Bitumens from different Utah tar sand deposits show very divergent physical properties and chemical compositions depending on the location from which they are obtained. One remarkable difference in physical properties is viscosity, a difference which prompted the development of different strategies to recover bitumen from these tar sands. This situation is in contrast to the Canadian tar sands, which have almost uniform properties and compositions regardless of their location. The

Table 63

Bitumen Concentrate Grade and Recovery for Reduced-Shear Hot-Water Separation*

Feed Source	Asphalt Ridge (10%)	Asphalt Ridge (10%)	Sunny-side (9.5%)	Sunny-side (9.5%)	Athab. (13.6%)	Athab. (13.6)
Temperature (^{o}C)	80	52	80	51	80	50
Bitumen Content (wt%)						
Concentrate I (0-1 min)	69.0	65.3	45.3	25.0	71.0	28.0
Concentrate II (1-3 min)	62.0	60.5	33.0	22.0	60.0	26.0
Concentrate III (3-6 min)	50.0	48.2	15.0	14.6	51.0	22.0
Concentrate IV (6-10 min)	43.5	42.0	12.0	11.2	36.0	19.0
Total Recovery (%)	95.8	92.9	95.9	98.5	99.0	97.0
Bitumen in Tailing (%)	0.6	0.9	1.6	2.2	0.5	1.7
Coefficient of Separation	0.86	0.78	0.57	0.46	0.86	0.48

* In all calculations, the diluent (kerosene) added has been excluded.

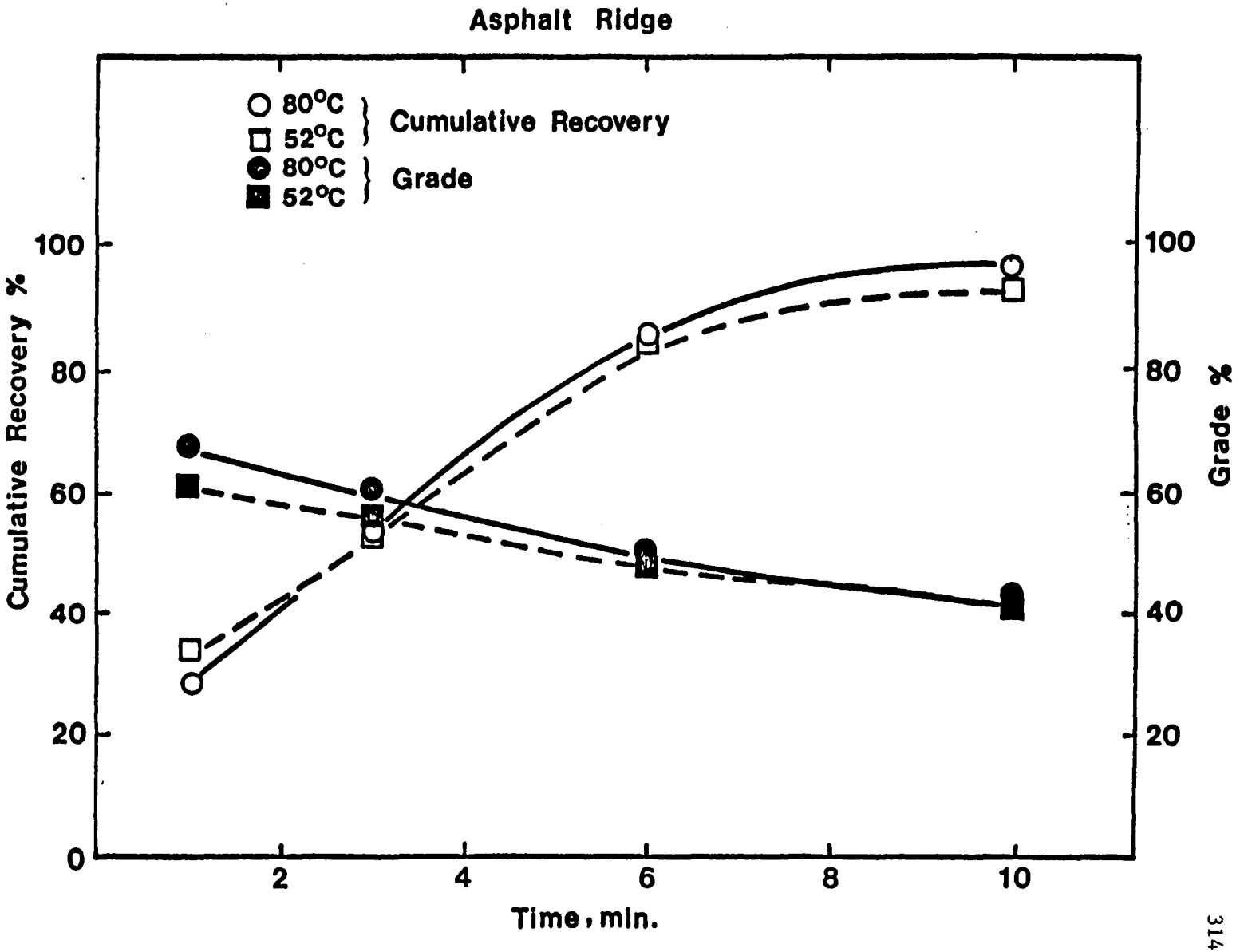

Figure 105. - Cumulative recovery of bitumen.

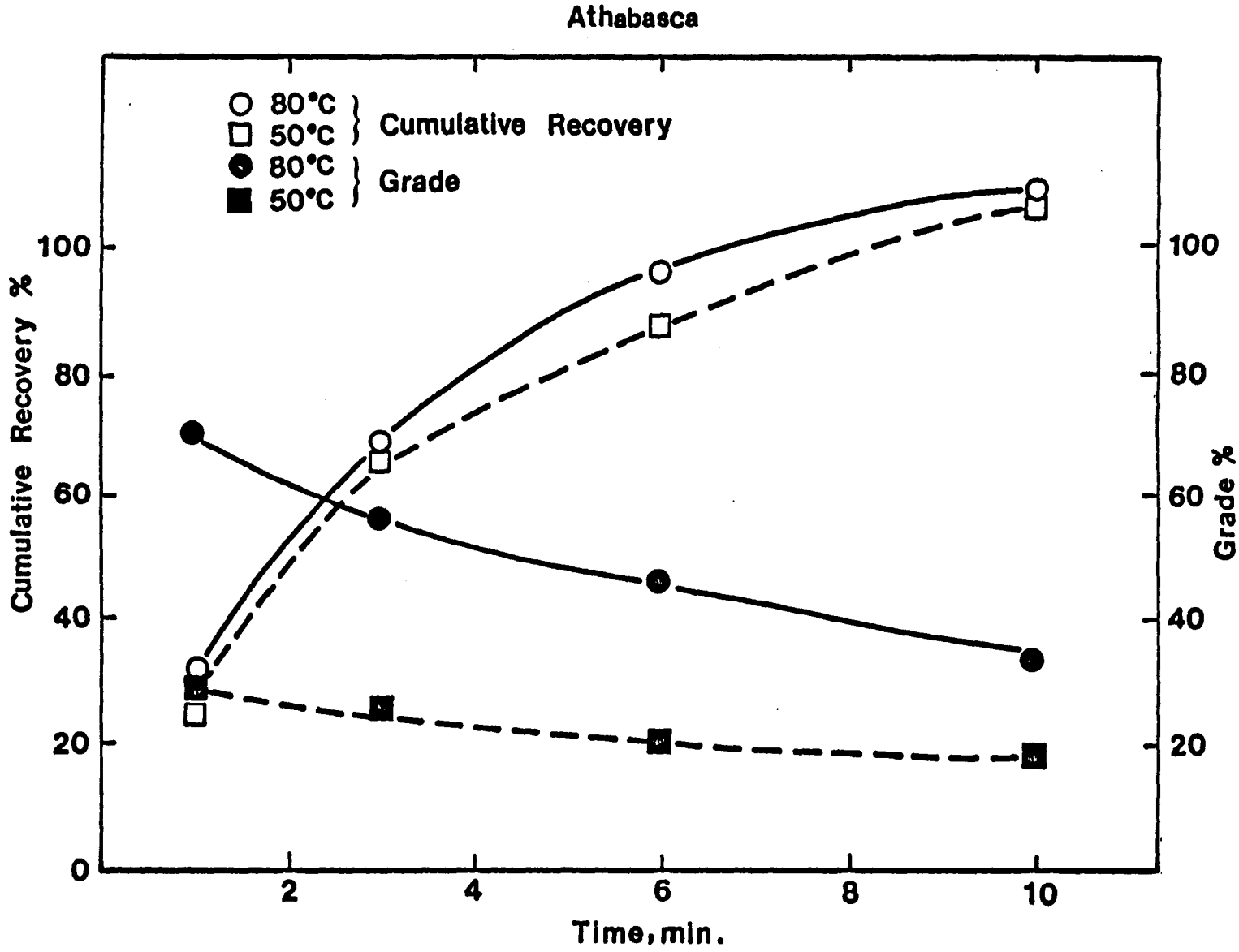

Figure 106. - Cumulative recovery of bitumen.

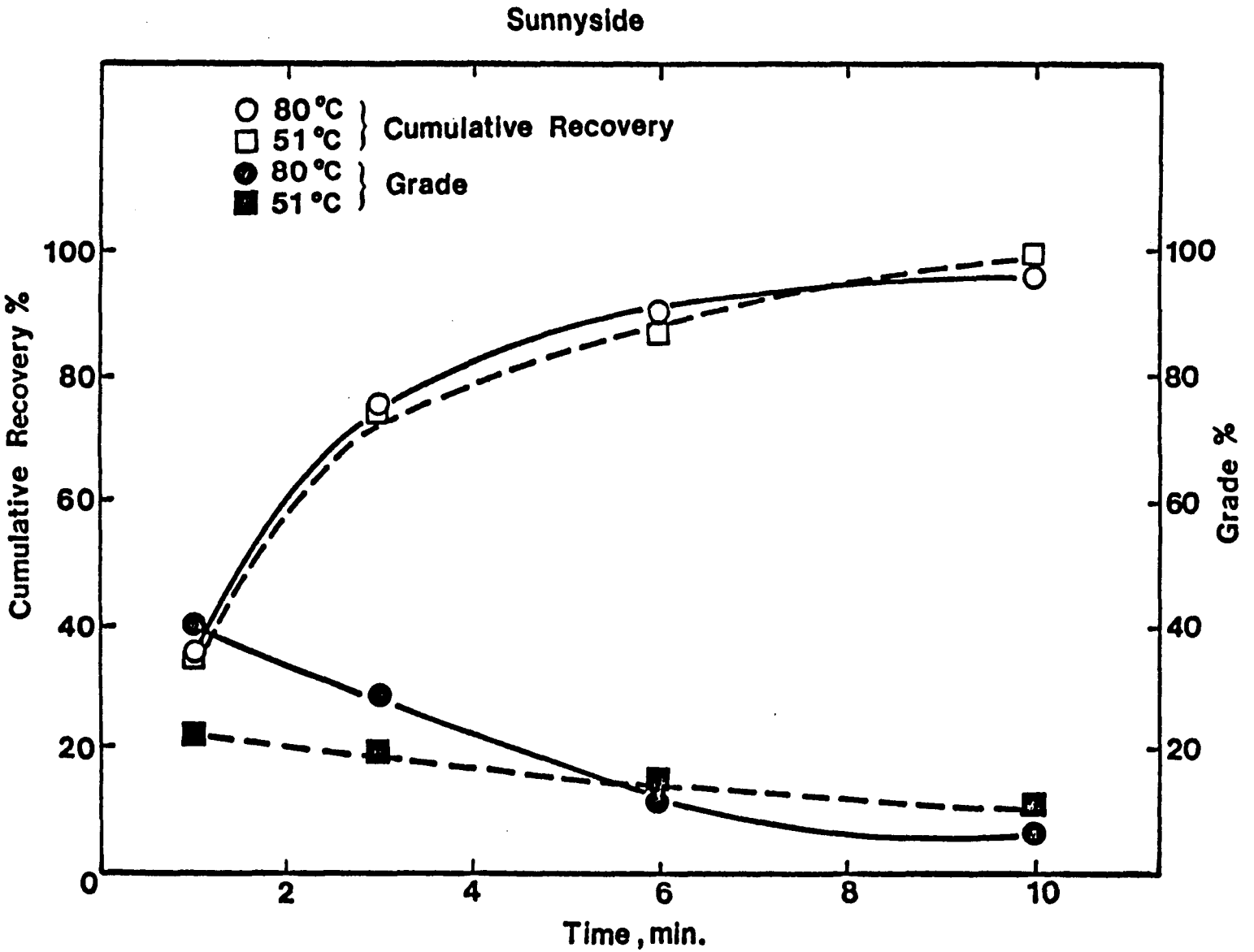

Figure 107. - Cumulative recovery of bitumen.

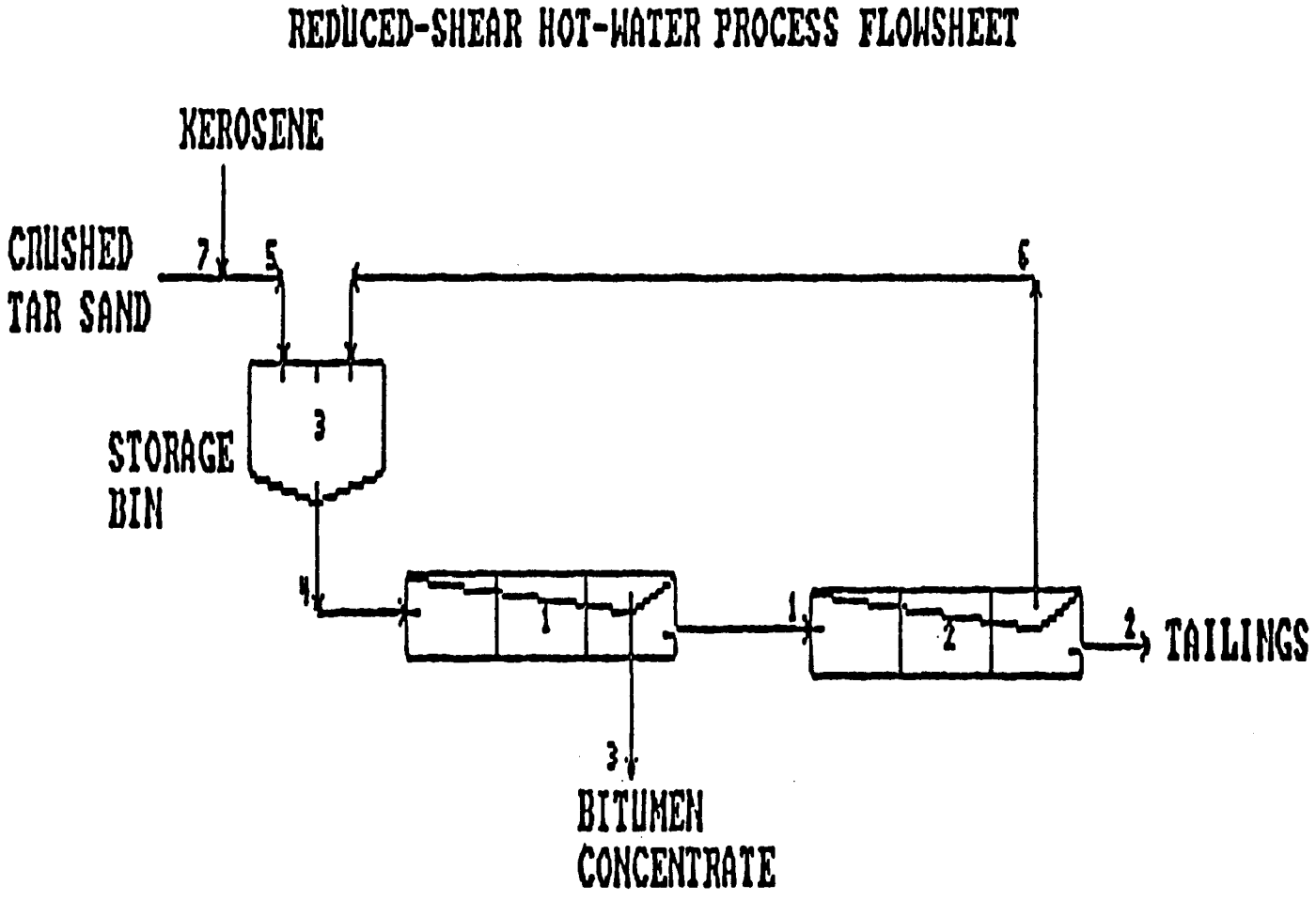

Figure 108. - Reduced-shear hot-water process flowsheet.

strategies developed for Utah tar sands include ambient temperature bitumen recovery, hot water and modified hot water separation methods. Each one of these was developed for a particular deposit and no single method can be applied universally to all deposits, although the modified hot water process is most versatile and can treat almost all tar sand types. In addition, the Utah tar sands are considered to be structurally unique in that they lack a fine layer of connate water between bitumen and sand surface as is the case for Canadian tar sands. This aqueous layer is understood to facilitate relatively easy recovery of bitumen from tar sands by hot water processing. As the bitumen in Utah deposits is in intimate contact with sand surface, greater forces are required to displace bitumen.

For convenience, the Utah tar sands have been categorized, on the basis of bitumen viscosity, into four different types. Table 64 lists the details of the criteria on which the classifications have been made. While the above-mentioned methods of bitumen recovery have been realized in lab and in pilot-plant scale operations for tar sands containing light and moderate viscosity bitumens, they are not as effective for tar sands containing bitumen of heavy and very heavy viscosities. Since a significant portion of the Utah deposits fall into this category, it is a challenge to improve the efficiency of bitumen recovery from these tar sands containing highly viscous bitumen.

Criterion for the Selection of Diluent

An important feature of modified hot water process for tar sands has been to control the viscosity of bitumen in the feed material by diluent addition. It has been determined from earlier research work that when the viscosity of bitumen in the tar sands at processing temperature is reduced to a value in the range 0.5 - 1.5 PaS recoveries were greatly improved. Addition of a diluent also facilitated higher recoveries at much lower temperatures. In these studies, kerosene has been used as a diluent. The considerations for choosing kerosene are perhaps cost and availability, which are important factors from an industrial perspective.

However, in an attempt to see whether the reduction of bitumen viscosity in tar sands can be optimized by changing the nature of the diluent, a small number of different diluents were tested. Since

Table 64

Classification of Tar Sands According to Bitumen Viscosity

Tar Sand Type	Bitumen Character	Bitumen Viscosity @ °C (Pa.S) 50	90	Recommendations for Hot Water Processing
I	Light	10^{0}	10^{-1}	Diluent unnecessary
II	Moderate	10	10^{-1}-10^{0}	Diluent optional
III	Heavy	10^{2}-10^{6}	10^{0}	Diluent necessary
IV	Very heavy	$\geq 10^{6}$	10^{3}	Tar sand not amenable to hot water separation

tar sands are processed at 50-90°C, diluents of a higher boiling point range were considered. Diluents used were cyclohexane, SC#2, SC#150, ethyleneglycoldibutylether (EGBE), and xylene. Kerosene was also included for comparison purposes. The choice of these diluents, besides being industrial solvents, was an arbitrary decision.

Viscosity Measurements of Bitumen-Diluent Mixtures

Selection of a diluent to be used in the modified hot water processing of tar sands is made from an evaluation based on its relative viscosity reducing capacity. This evaluation consisted of viscosity measurements of bitumen-diluents mixtures of several temperatures.

The bitumen samples chosen for this study were extracted from Asphalt Ridge, PR Spring, and Sunnyside tar sand deposits. These include extreme cases with regard to viscosity as Asphalt Ridge and PR Spring samples represent lower viscosity values and that of Sunnyside a much higher value.

The diluents were mixed with bitumen samples in a certain ratio which is determined by the viscosity of pure bitumen. Viscosity measurements of these bitumen-diluent mixtures were made at several temperatures in the temperature range 25-65°C. Generally a mix of 20-36% diluent in the mixture was required to bring the viscosity into the measurable range. Sunnyside bitumen sample was found to be too viscous to extend studies between three diluents. Measured viscosity data are presented in Tables 65-67.

The results shown in Tables 65-67 indicate that viscosity reduction capacities of diluents are quite varied. It also appears that the effectiveness of a diluent depends on the bitumen. For the three bitumen samples studied, the viscosity reduction capacity of diluents followed the order:

For Asphalt Ridge bitumen,

SC#150 > EGBE > Kerosene > SC#2 > Cyclohexane > Xylene.

For PR Spring bitumen,

SC#150 > Kerosene > Xylene > EGBE > SC#2 > Cyclohexane.

For Sunnyside bitumen,

Table 65

Viscosity of Asphalt Ridge Bitumen Solution at 20% W/W Diluent

Temperature ^{o}C	Viscosity (pa.s)					
	Diluent					
	Xylene	Cyclohexane	SC#2	Kerosene	EGBE	SC#150
25	--	--	--	8.53	8.35	4.00
33	16.00	12.10	8.90	4.05	3.96	2.20
41	8.82	6.47	4.85	2.23	2.14	1.26
49	5.00	3.99	2.82	1.26	1.21	0.78
57	2.80	2.12	1.67	0.76	0.74	0.51
65	1.72	1.13	1.03	--	--	0.36

Table 66

Viscosity of P.R. Spring Bitumen Solution at 36% W/W Diluent

Temperature ^{o}C	Viscosity (pa.s)					
	Diluent					
	Xylene	Cyclohexane	SC#2	Kerosene	EGBE	SC#150
25	7.44	--	15.10	2.70	11.65	2.07
33	3.96	11.40	7.90	1.55	5.91	1.21
41	2.31	5.62	4.40	0.84	2.75	0.75
49	1.42	3.12	2.72	0.46	1.71	0.48
57	0.94	1.90	1.67	0.30	0.99	0.34
65	0.74	1.26	1.07	0.22	0.57	0.25

Table 67

Viscosity of Sunnyside Bitumen Solution at 36% W/W Diluent

Temperature °C	Viscosity (pa.s)			
	Diluent			
	Cyclohexane	Kerosene	EGBE	SC#150
25	--	15.65	15.53	2.99
33	--	7.12	7.00	1.69
41	--	3.88	3.96	1.08
49	--	2.02	1.79	0.70
57	11.73	1.02	0.95	0.46
65	6.80	0.62	0.64	0.34

SC#150 > EGBE = Kerosene > Cyclohexane.

In the range of temperatures studied, the observed order of diluents does not remain the same when the bitumen sample is altered. Except for SC#150, the relative positions of other diluents are significantly changed. Lack of consistency in the order of diluents suggests that there are some specific interactions between the diluent and bitumen, which bring about further reduction in the viscosity. It also indirectly indicates that a change in the order of diluents is a result of differences in chemical compositions of the bitumens, some diluent characteristics are presented in Table 68. This is done in an attempt to relate viscosity reduction capacity of a diluent to some of its physical and chemical properties. Although it is difficult to identify any relationship with the outlined properties, it appears that for a diluent to be effective, a high boiling range and a composition with a large proportion of C8+ aromatics and some aliphatic hydrocarbons are required.

Another feature which becomes apparent from this study is that differences among the diluents, in their capacity to reduce bitumen viscosity, depends on the viscosity of pure bitumen. The results show that while a highly viscous bitumen (Sunnyside) enhances the difference between two diluents, viz., Kerosene and SC#150, low viscosity bitumen (Asphalt Ridge) lowers the difference between the same two diluents.

The effect of temperature on the viscosity of diluent-bitumen mixtures is presented in Figures 109-111. Linear relationships were obtained when ln [viscosity] was plotted against 1/T °K. The relationship is expressed as:

$$\text{Viscosity} = A\, e^{B/T}$$

In the observed order of diluents for all three bitumens listed above, it can be seen that of all the diluents used, SC#150 consistently reduces the viscosity of all three bitumen samples in a most efficient manner. Since the principal consideration for using a diluent in modified hot water process is to reduce the viscosity of bitumen in tar sands and thereby attain better yields, obviously SC#150

Table 68

Some Physical and Chemical Characteristics of Diluents

Diluent	Sp. Gravity	Boiling Point/Range Temp ^{o}C	Percentage Composition by Volume		
			Saturates	Aromatics	C8+ Aromatics
Cyclohexane	0.779	81	100	0	0
Ethyleneglycol-n-dibutylether	0.900	171	100	0	0
Kerosene	0.818	177-272	80	0	19
SC#2	0.844	138-153	18	10	79
SC#150	0.899	183-210	2	0	98
Xylene	0.871	138-140	0	26	74

1 -- y = - 20.9547 + 7.2659x R = 1.00

2 -- y = - 22.225 + 7.5772x R = 1.00

3 -- y = - 20.5897 + 6.969x R = 1.00

4 -- y = - 22.7359 + 7.4035x R = 1.00

5 -- y = - 22.8771 + 7.4382x R = 1.00

6 -- y = - 19.1432 + 6.1039x R = 1.00

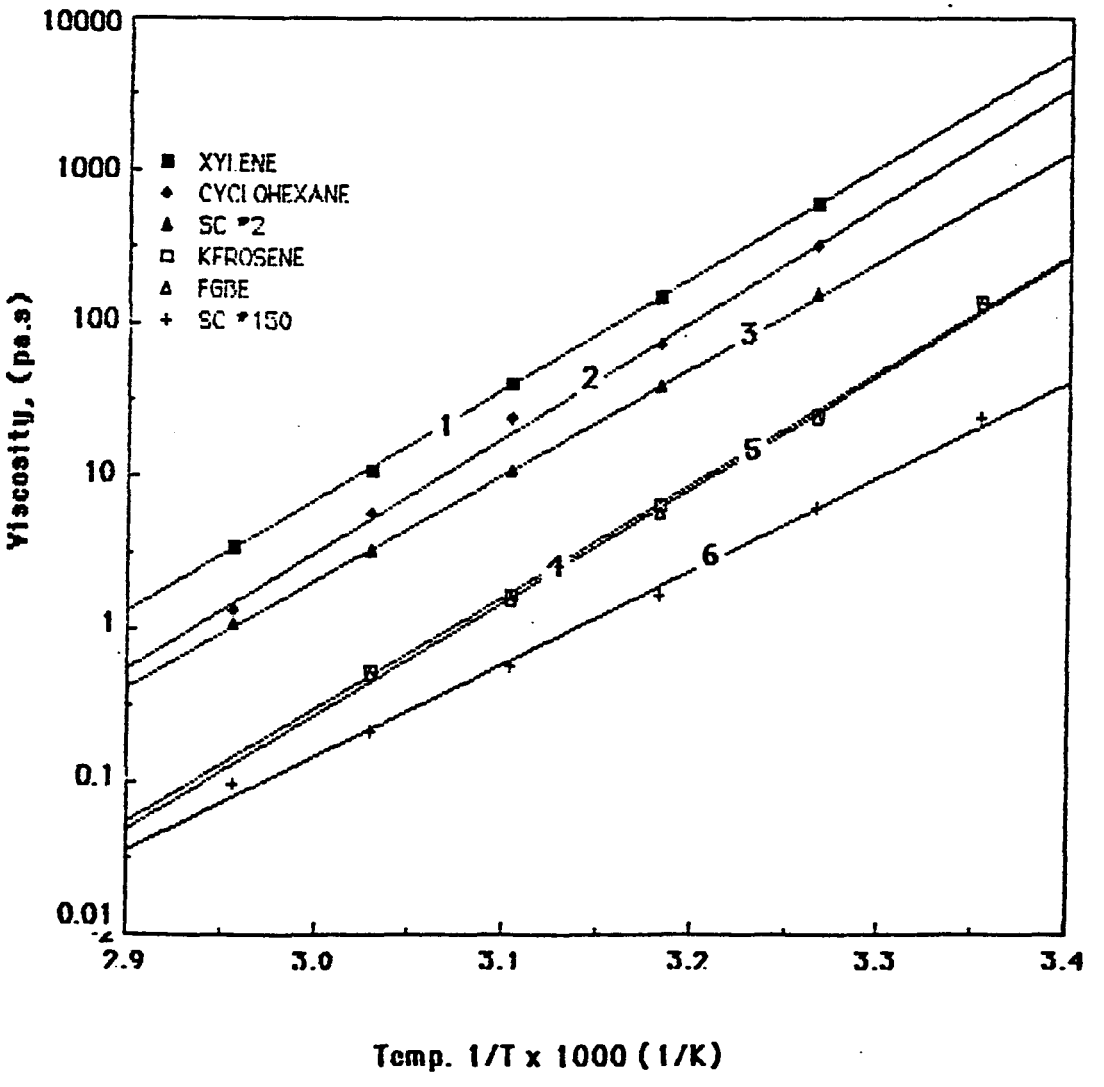

Figure 109. - Viscosity-temperature profiles of Asphalt Ridge with 20% (w/w) diluents.

1 -- y = - 17.9078 + 5.9099x R = 0.99

2 -- y = - 20.9152 + 7.127x R = 1.00

3 -- y = - 19.5718 + 6.6309x R = 1.00

4 -- y = - 20.9154 + 6.5738x R = 1.00

5 -- y = - 22.8984 + 7.5477x R = 1.00

6 -- y = - 17.2925 + 5.3558x R = 1.00

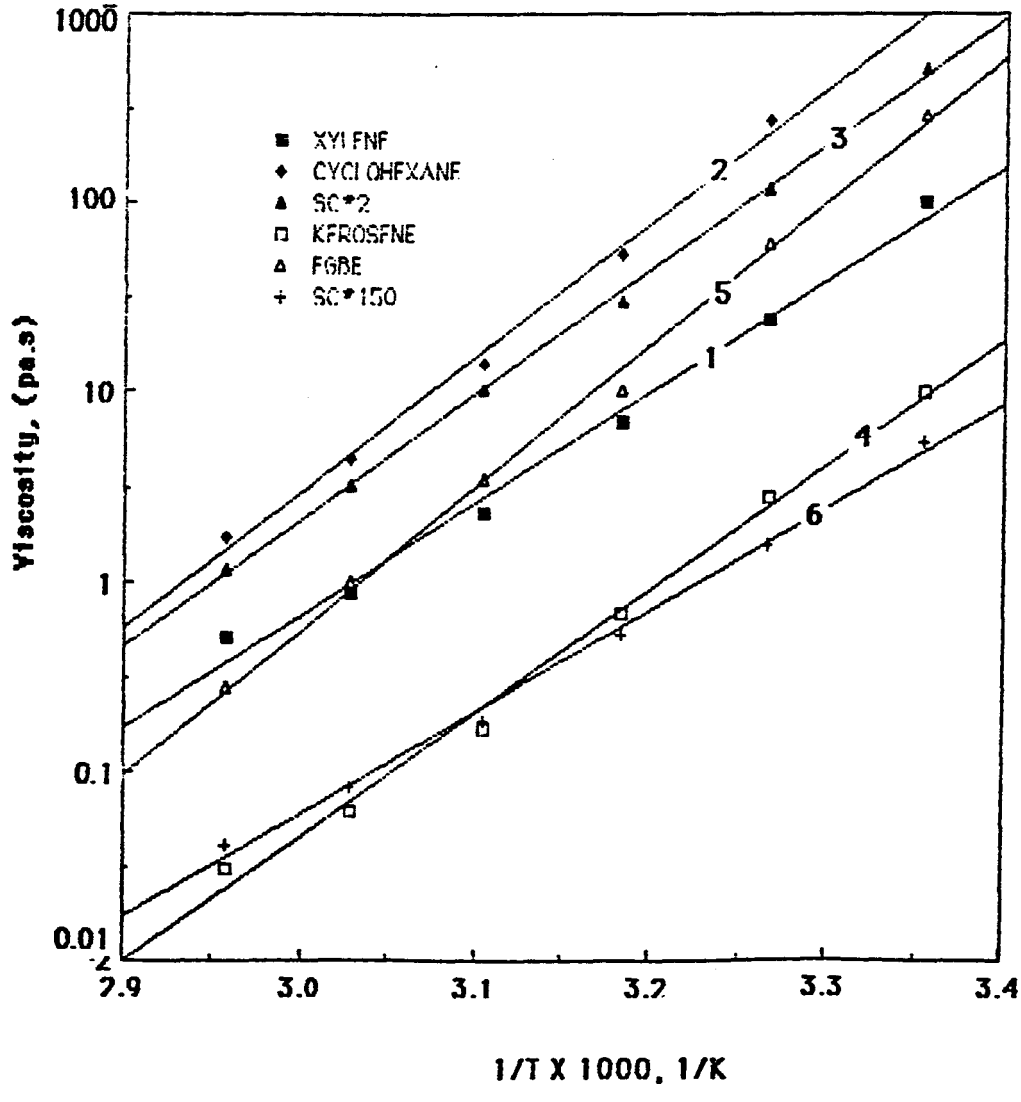

Figure 110. -Viscosity-temperature profiles of PR Spring bitumen with 36% (w/w) diluents.

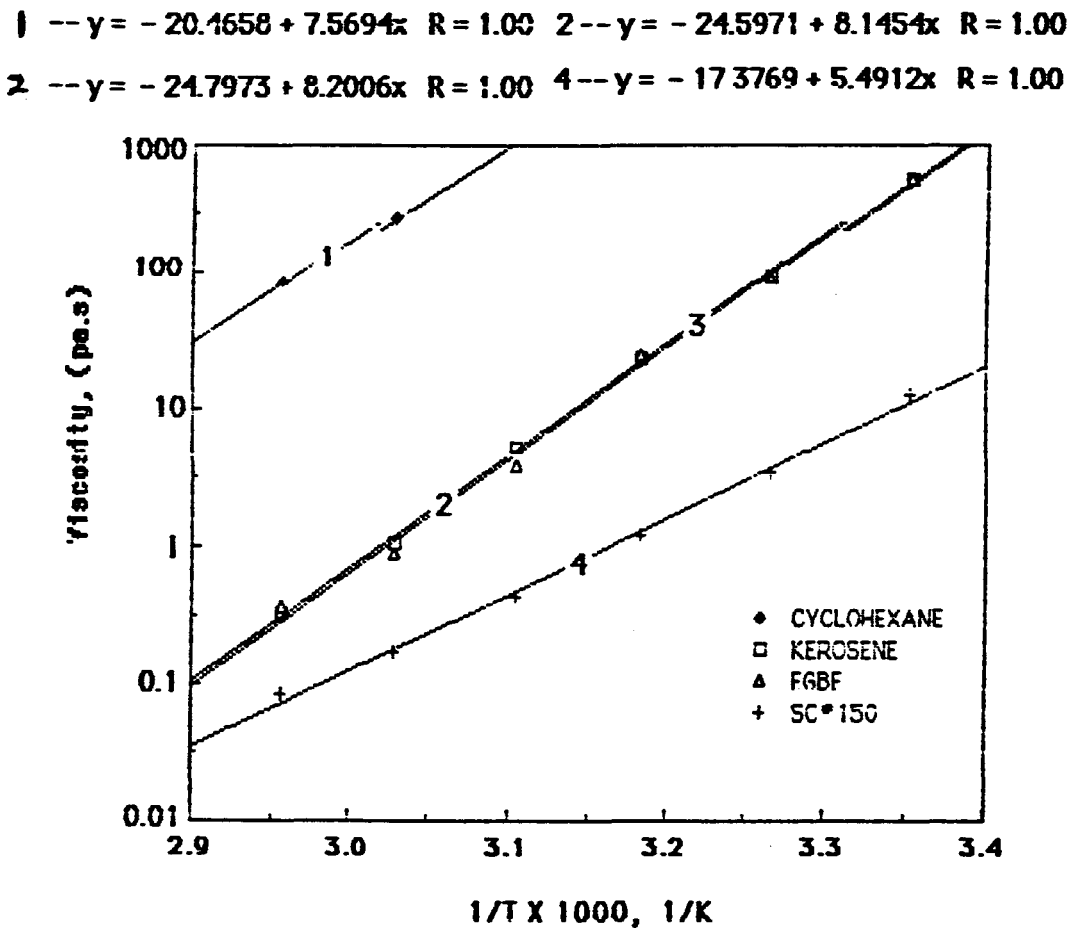

Figure 111 - Viscosity-temperature profiles of Sunnyside bitumen with 36% (w/w) diluents.

becomes a preferable diluent. Kerosene was used as a diluent in most of the earlier bitumen recovery studies. For comparison purposes, both kerosene and SC#150 were chosen as diluents for the modified hot water processing of Sunnyside tar sands. Accordingly their efficiencies in recovery and the quality of the bitumen concentrate produced are evaluated.

Evaluation of Diluent in the Modified Hot Water Processing of Sunnyside Tar Sands

Four kilogram batches of Sunnyside tar sand samples were subjected to modified hot water processing for bitumen recovery. The required amount of diluent was added to the tar sand sample and it was set aside for 24 hours to allow for diluent penetration into the sample matrix. Processing was carried out in a Denver type flotation cell as described earlier and digestion was effected with low shear energy mixing. Among the variables considered were pretreatment and processing temperatures, diluent, and percentage solids in the digestion step. Digestion was carried out at 25-30% solids for 15 minutes followed by 10 minutes of flotation at 10% solids. Digestion and flotation steps were maintained at the same temperature.

From viscosity measurements of diluent-bitumen mixtures, it was observed that SC#150 is a more efficient diluent. However, diluent concentrations in the tar sands were maintained at the same percentage level in order to distinguish the effect of diluent. Six runs and three comparisons were made between kerosene and SC#150. The results are presented in Table 69 with the values of defined variables.

The results presented in Table 69 show that at 50°C and 20% diluent concentration the recovery parameters were very poor although there are some differences in the performance of kerosene and SC#150. SC#150 appears to be marginally better. At 80°C and the same level of diluent concentration, the recovery parameters such as coefficient of separation and concentrate quality (in terms of bitumen content) are significantly improved, and the difference between the two diluents are enhanced in favor of SC#150. In the third comparison shown in Table 69, the batch experiments was

Table 69. - Summary of low-shear energy digestion test runs.

Tar Sand (Sunnyside), Kg	=	4
Wetting agent (Na_2CO_3), g	=	4
Digestion time, minutes	=	15
% solids during digestion	=	25
% solids during flotation	=	10
Duration of Pretreatment, hours	=	24

Diluents: K = kerosene
S = SC#150

	50°C				80°C	
	K(20%)	S(20%)	K(30%)	S(30%)	K(20%)*	S(20%)*
% Concentrates	57.60	58.00	46.35	35.80	41.33	310.93
% Bitumen in concentrate	15.80	16.48	20.00	25.20	20.00	28.00
% Bitumen in tailings	4.00	3.30	1.57	1.74	4.30	2.74
% Bitumen Recovery	84.30	88.00	85.83	83.50	79.60	82.80
Coefficient of separation	0.31	0.36	0.45	0.54	0.43	0.58

carried at 50°C with a 30% diluent concentration and the diluent pretreatment was carried out at 50°C. The results are almost similar to those that carried out at 80°C. It appears that temperature and diluent concentration can be altered in a complimentary manner to achieve better recoveries. In all these runs, as expected, diluent SC#150 performed better than kerosene. Further SC#150 produces significantly cleaner tailings. Nodules containing larger amounts of bitumen than the feed material, as reported earlier, were drastically reduced in the tailings for SC#150 run while they are still present in the tailings for kerosene diluent.

However, all of these improvements are somewhat masked by the typical feature of Sunnyside tar sand deposits. These are known to contain more clay and fine calcareous material than any other Utah deposits. Although bitumen disengagement from the sand surface is greatly improved in the digestion step with a better diluent, in the subsequent flotation step clay and fine sand particles rise to the surface along with the bitumen. Efforts must be made to selectively float the bitumen to the exclusion of solid particles. However, at this stage, it is not certain whether the solids reporting to the froth are laden with bitumen or rise to the surface on their own. In order to optimize the flotation process, it is essential to study the surface and electrical properties of solids associated with bitumen in the concentrate.

CONCLUSIONS AND RECOMMENDATIONS

This research project was undertaken to develop some fundamental understanding of bitumen displacement from the tar sand surface. Results from preliminary studies indicate that bitumen disengagement from a coated solid surface occurs when the applied shear stress exceeds cohesive forces that comprise the bitumen molecules. An estimate of these cohesive forces for Asphalt Ridge bitumen is made from surface tension measurements of its solutions in kerosene and toluene. It is also observed that within the experimental conditions the adhesive forces, between the bitumen and the solid surface, are too strong to displace the bitumen that is attached to the surface.

Batch experiments conducted using low shear energy digestion have shown that satisfactory bitumen recoveries can be achieved. This can potentially eliminate the high shear energy stirred reactor used earlier in the digestion step, and will be an important consideration for scale-up and commercial operations.

Image analysis of the solids derived from process concentrates and tailings shows the importance of shape factors. It is predicted that bitumen recoveries from tar sands with shape factor smaller than 0.7, which indicate shape irregularities in sand grains, would be much less efficient. Particularly such sand grains coated with a very high viscosity bitumen may never release bitumen under the conditions of digestion.

Studies have been carried out to evaluate the relative efficiencies of two diluents used in the modified hot water separation of bitumen from Sunnyside tar sands. Selection of an effective diluent for tar sands of high viscosity bitumen is an important consideration. Efficiency of a diluent is influenced by certain physical property and chemical composition. Relative efficiency of diluents can be evaluated from viscosity measurements of their solutions in bitumen.

Sunnyside tar sands containing clays and other calcareous materials have not been found to be responsive to bitumen recoveries using the modified hot water separation process. Optimization involving relatively larger amounts of efficient diluent still fails to show satisfactory results in terms of coefficient of separation. This is entirely due to the presence of clay and other fine particles. Though bitumen disengagement can be adequately achieved in the digestion step, which is indicated from the quality of tailings, in the flotation step clays and other fines rise to the surface along with the bitumen. It requires that methods have to be developed to selectively float the bitumen to the exclusion of fines in the flotation step. In order to achieve this, it is essential to study the surface and electrical properties of these fines.

SECTION D

TWO-STAGE THERMAL RECOVERY OF BITUMEN USING HEAT PIPES

J.D. Seader

TWO-STAGE THERMAL RECOVERY OF BITUMEN USING HEAT PIPES

J.D. Seader	**Principal Investigator**
T. Chakravarty	**Post-Doctoral Student**
B.K. Felix	**Graduate Student**
Guo Di	**Graduate Student**

SUMMARY

A number of facets of two-stage thermal processing of tar sands using a heat-pipe system were studied during the period covered by this report. These studies included: (1) experiments to determine the effect of pressure on hydroprocessing of oil produced by the two-stage laboratory unit, (2) preliminary designs and cost estimates for plant sizes of 15,000 and 50,000 barrels/day of oil, (3) additional designs at the 50,000 barrels/day capacity to cover a range of bitumen content, (4) lost work analyses of three different dual-bed processing systems, and (5) development of a correlation from experimental data for the minimum fluidization velocity of tar sand at high temperatures.

INTRODUCTION

An energy-efficient process for the thermal recovery of cracked bitumen from Utah tar sands is under development at the University of Utah. The process consists essentially of two steps. In the first step, mixed and suitably sized tar sand, fed into the reactor at a constant rate, is pyrolyzed at a temperature of 887°F (475°C) in an inert atmosphere. The bitumen contained in the tar sand is transformed to crude oil and fuel gas. The sand, with some coke, is obtained as a by-product. In the second step, thermal energy obtained by combusting coked sand with air at a temperature of 1067°F (575°C), is utilized in a very efficient manner by means of heat pipes to provide the necessary thermal energy for the pyrolysis and the rest of the process.

Advantages of the process[87] are:

1. Elimination of huge tailing ponds and dams associated with hot water technology.
2. Disposal of dry, thermally processed sand is relatively easy.

3. Thermal recovery of bitumen requires a minimal amount of water, which is particularly important for Utah tar sand deposits.
4. Thermal methods can process tar sand with lower bitumen content, without too much reduction in the yield of product. This method can also handle high concentrations of fines.
5. Tar sands containing particulate mineral matter and those containing consolidated sandstone matrix can be processed by this method. In general, there is flexibility with respect to variation in and nonuniformities of the mineral content in a given deposit.

A number of studies have been underway to assess the technical and economic aspects of the process. These include the ability to upgrade the oil product, the economics of the process at plant capacities of 15,000 to 50,000 barrels/day over a range of bitumen contents, the determination of the second-law efficiency and techniques to improve it, and development of design correlations for key items of equipment to ensure ability to scale-up laboratory data to full-size units.

UPGRADING OF OIL

Experiments were conducted to determine the effect of pressure on hydrotreating of synthetic crude oil produced by the energy-efficient fluidized-bed process. The experiments were performed in a 1.9 cm ID by 42 cm long 316 stainless steel trickle-bed reactor packed with 71 grams of Nalco 479 MoO-CoO catalyst. A hydrogen flow of 3000 SCF H_2/bbl of oil was maintained for all runs. The other run conditions were as follows:

Run No.	Temperature °C	Pressure psig	LHSV ml/ml-hr	Run Time hr
1	410	2300	0.56	4.5
2	410	2400	0.54	4.5
3	410	2500	0.50	4.5
4	410	2700	0.46	4.5

The main purpose of the tests was to determine the effect of hydrogen pressure on the reduction of nitrogen content in the crude oil. The properties of crude oil before and after hydrotreating were as follows:

Run No.	Sample	API Gravity	Viscosity, CPS 20°C	Weight % Composition C	N	N
1	Crude oil	19.4	1980	87.3	11.5	1.44
	Hydrotreated oil	22.5	62.4	87.8	11.1	0.78
2	Crude oil	20.1	1854	87.6	11.4	0.92
	Hydrotreated oil	23.8	44.2	87.5	11.55	0.39
3	Crude oil	20.1	1652	87.6	11.4	0.91
	Hydrotreated oil	24.1	14.6	87.5	11.95	0.41
4	Crude oil	19.8	2022	87.5	11.6	0.78
	Hydrotreated oil	24.9	58.6	87.25	12.25	0.35

The data show that although the API gravity increased and the viscosity decreased (except for Run 4) with increasing pressure, the percentage reduction in nitrogen content is hardly affected by pressure over the range of the experiments.

PRELIMINARY PROCESS DESIGNS AND ECONOMIC EVALUATIONS

The thermal process shown in Figure 112 consists of a two-stage fluidized-bed reactor in which several hundred liquid-potassium filled heat pipes thermally couple an upper pyrolysis bed with a lower combustion bed. Mined and suitably sized tar sand, fed into the upper section at a constant rate, is pyrolyzed in an inert atmosphere to volatilize and crack most of the contained bitumen. The vaporized products of the pyrolysis section are condensed to give synthetic crude oil; the rest of the bitumen, being converted to coke, is fed to the combustion bed where coke is burned with air. Finally, the residual heat in the sand leaving the burner is used to generate steam to run direct-drive steam turbines.

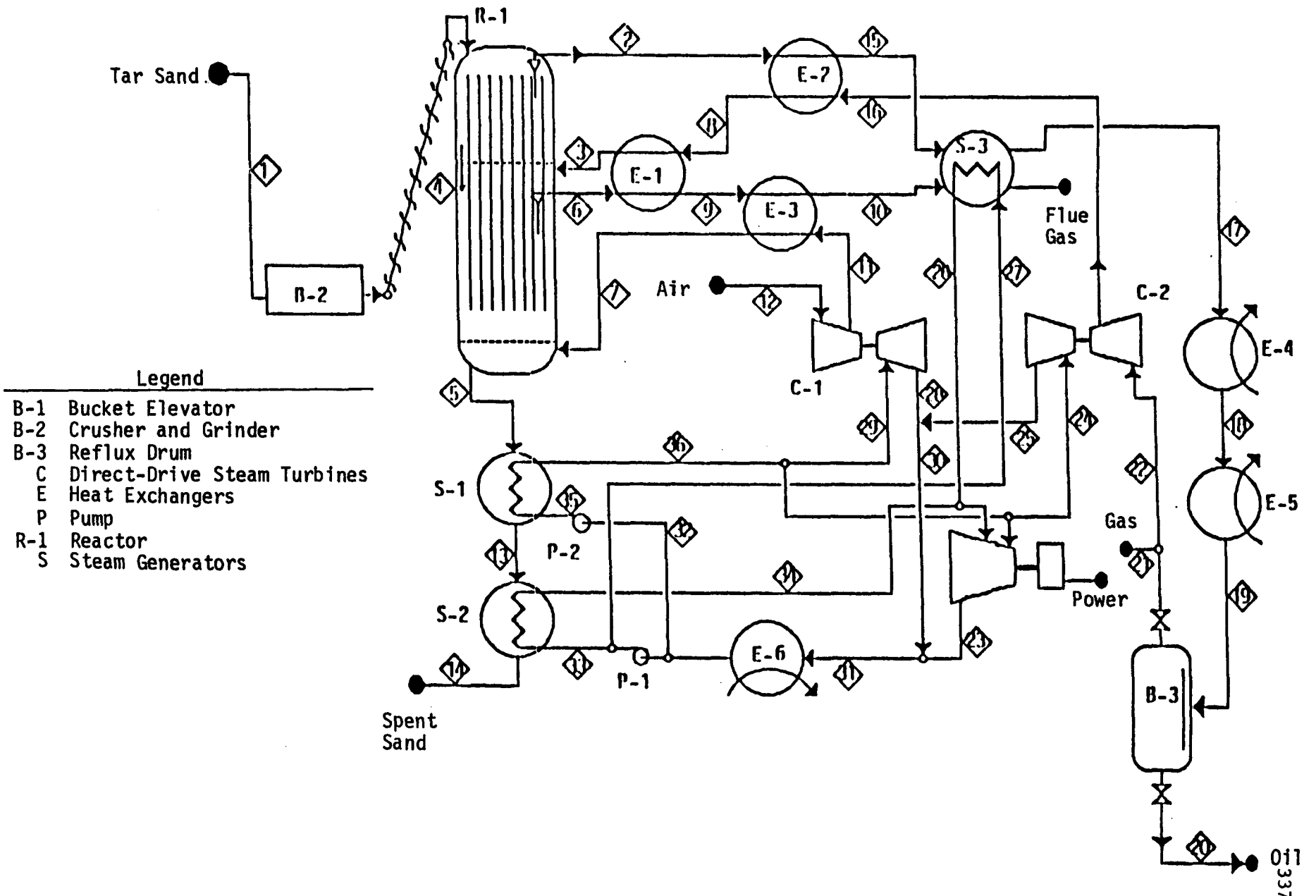

Figure 112. - **Final flow sheet for thermal recovery of oil from tar sand.**

Synthesis

The initial task was to investigate heat and power integration of the process. In terms of unit operations, the major tasks performed in the overall process are reaction, phase separation, and heat exchange. The design of the reactor is dictated by yield and residence time considerations, and that of the reflux drum by the need to condense as much liquid as possible with minimum carry-over by entrainment. If the operating conditions of these units are accepted, then the design problem that remains is to achieve the optimum economic performance out of the system of heat exchanger, coolers, and the steam and power generators.

The basic elements of the heat recovery problem are shown in Figure 113. All the exchangers, coolers, and heat engines have been stripped out of the flow diagram in Figure 112, leaving only the various heating and cooling tasks. Thus, one stream, the hot pyrolysis gas from the reactor, requires cooling from reactor exit temperature of 887°F to separator temperature of 100°F, and the recycle stream requires heating from separator temperature to reactor inlet temperature. Feed air to the burner is taken at 763°F, and so requires heating from the ambient temperature, 88°F. Two product streams from the burner, both available at 1067°F, are also cooled to 280°F to recover most of the process heat. Therefore, the data comprise a set of five streams, two requiring heating and three requiring cooling, whose end point temperatures and physical properties are known.

The design task was to find the best network of exchangers, coolers, and heat engines that handle these five streams at minimum operating and capital cost, consistent with operability. The total cost of such a network tends to be dominated by the size of the cooling water demands and the number of capital expenditure items in the network. One objective, therefore, was to produce a design that consumes the minimum utilities and uses the smallest possible number of units. Pinch technology was used to determine the optimum network which is shown in Figure 114. Schematic diagrams of the resulting mass and energy balances are given in Figures 115 to 117.

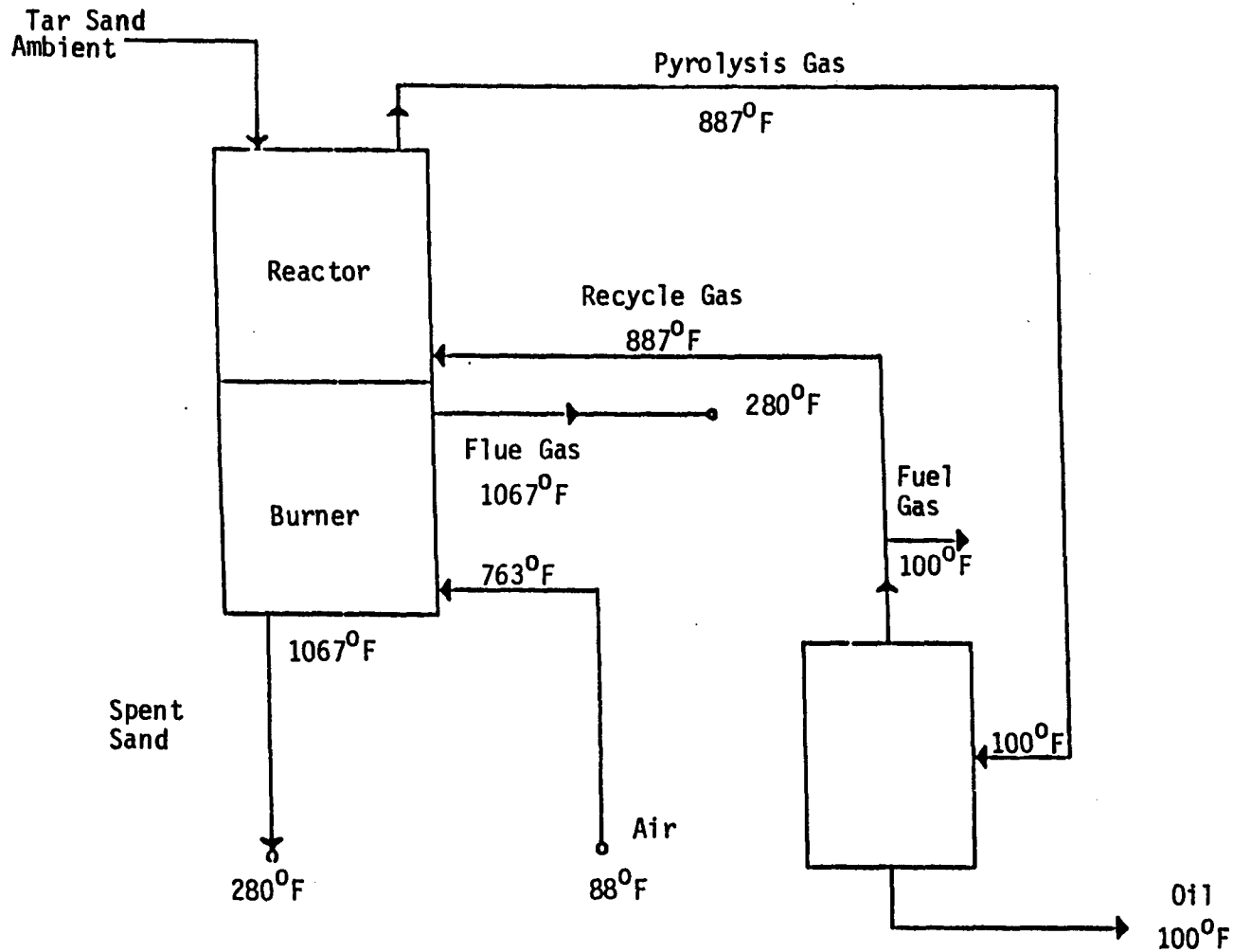

Figure 113. - Heat recovery problem.

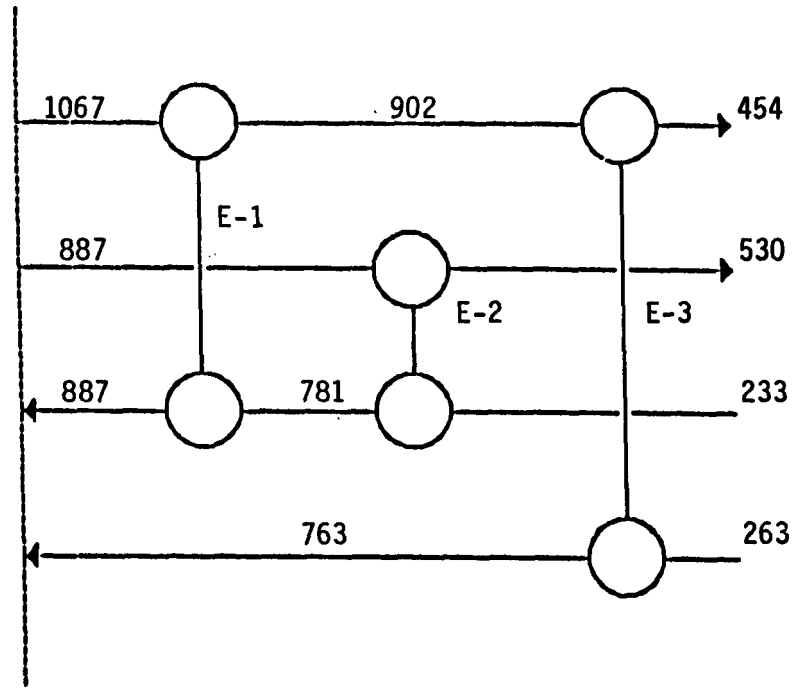

Figure 114. - Completed design for the heat recovery problem (numbers refer to stream temperatures in ^{O}F).

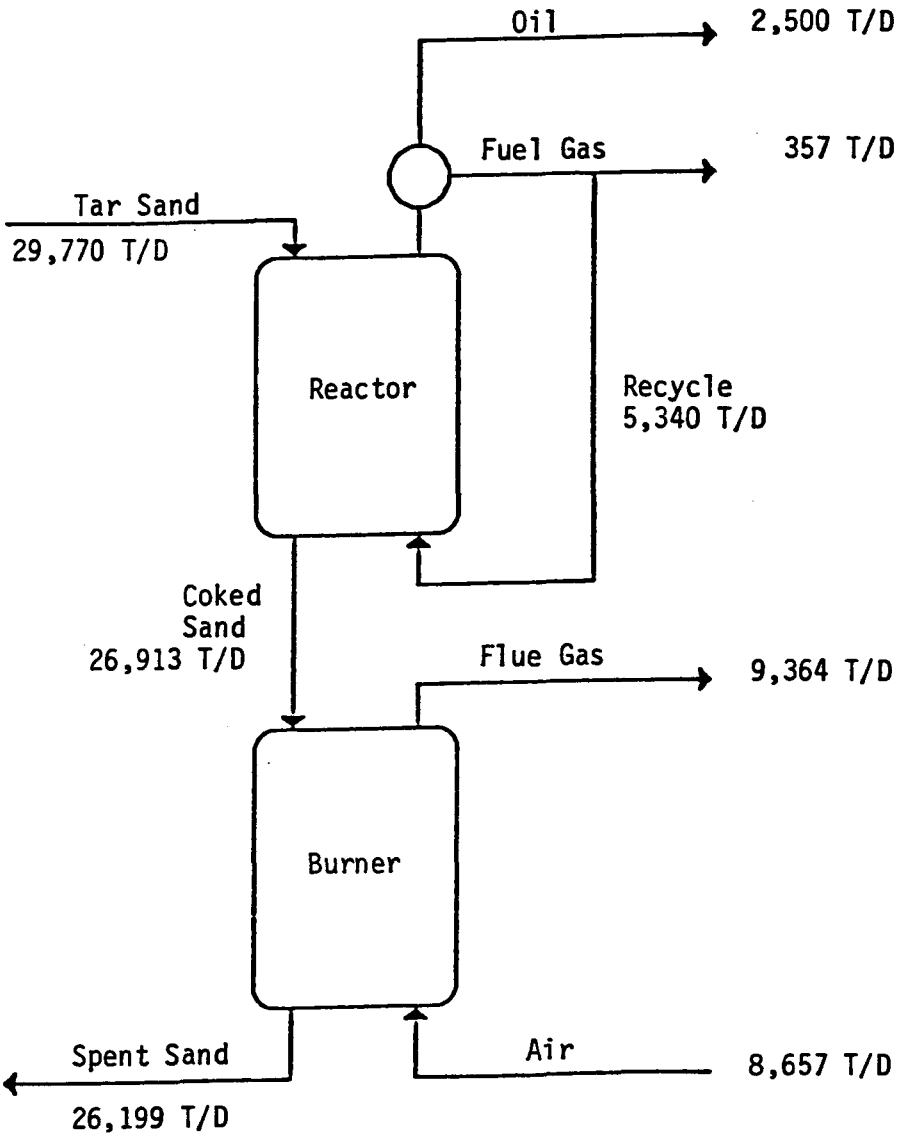

Figure 115. - **Mass balance around reactor and burner. 15,000 bbl/day of oil.**

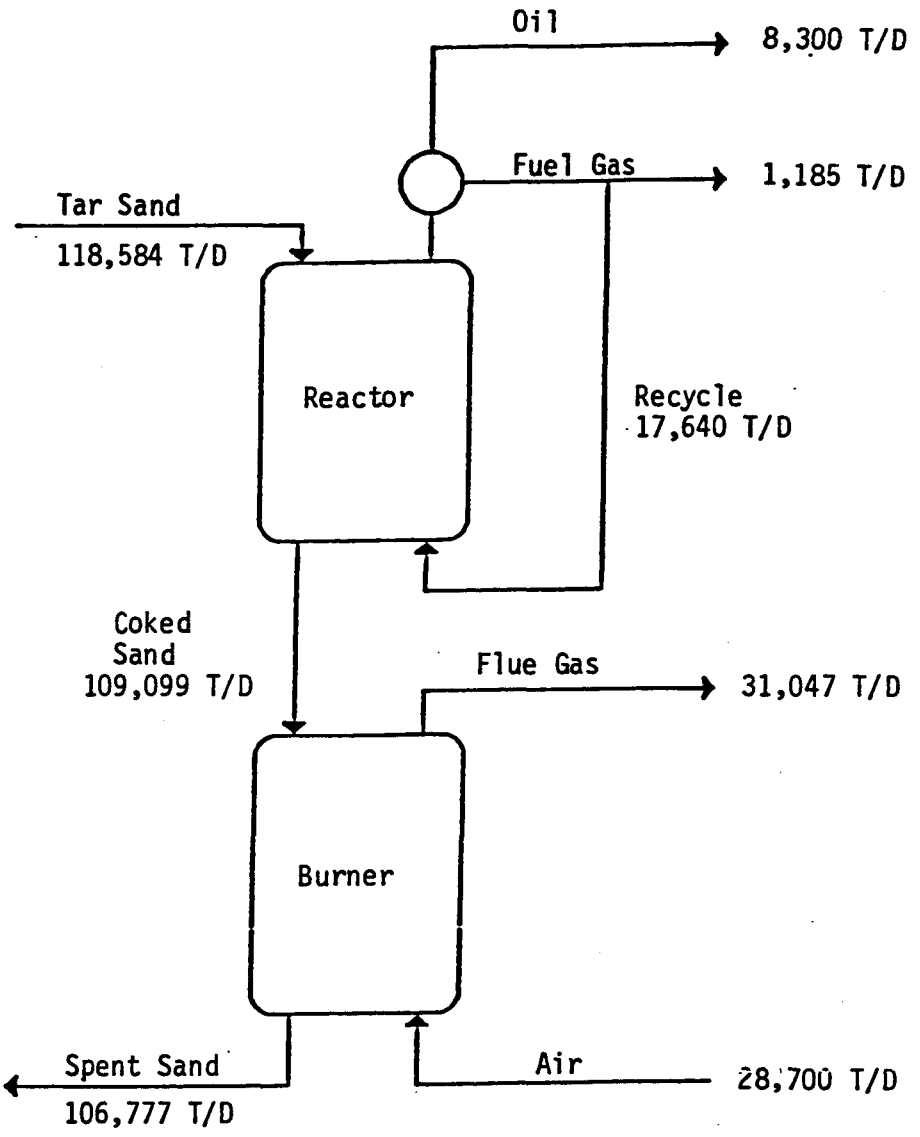

Figure 116. - **Mass balance around reactor and burner. 50,000 bbl/day of oil.**

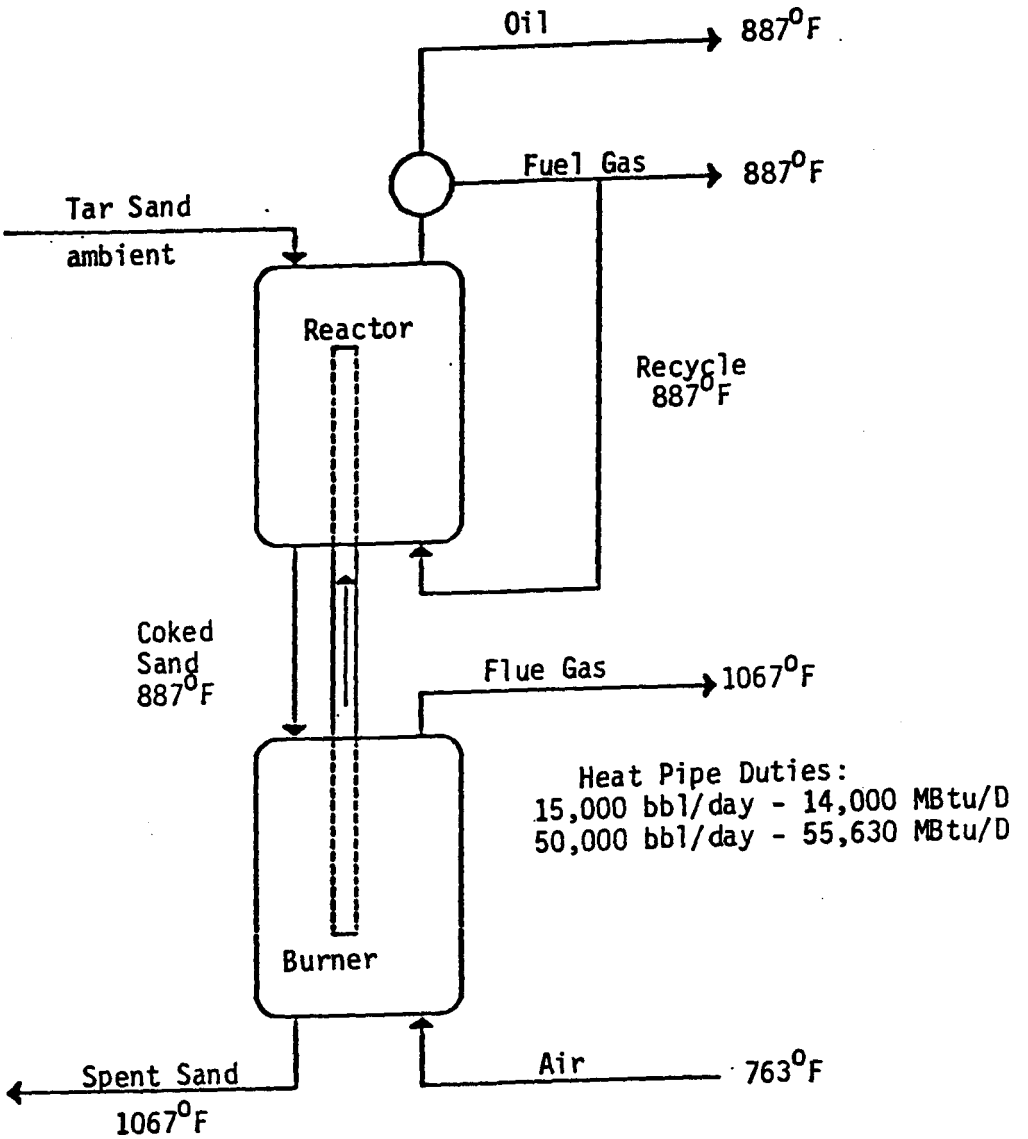

Figure 117. - **Energy balance around reactor and burner.**

Plant sizes of 15,000 bbl/day and 50,000 bbl/day based on the proposed thermal process have been considered to evaluate the economic feasibility of the design. A bitumen content in the tar sands of 12 weight percent in the 15,000 bbl/day case and 10 weight percent in the 50,000 bbl/day case was chosen to study its effects on the economics of the process.

The key factor determining the degree of success of a thermal process is the optimization of the thermal efficiency. Included in this design is an analysis of the heat exchanger network for optimizing the capital and utility costs. In the integrated process, steam is generated at two levels, high pressure (HP) and low pressure (LP). The HP steam is used in an efficient manner to compress the process gases to pressures sufficient to drive them through all the units in the process. The rest of the HP steam and all the LP steam are used to generate power. A small amount of cooling water is the only required utility for the overall process.

Design Basis

The following assumptions established the basis for the design of the proposed thermal process:

1. Bitumen, coke, fuel gas and oil compositions shown in Table 70 were obtained from the University of Utah studies on the pyrolysis of tar sand. The weight percent bitumen was taken as 12 for the plant size of 15,000 bbl/day oil, and as 10 for the plant size of 50,000 bbl/day oil. The recovery of oil was taken as 70%, together with 10% fuel gas and 20% coke.

2. Overburden was included in the mining and transportation cost of $5.00 per ton of raw tar sand feed material.

3. The plant was assumed to operate 330 days/yr.

4. The process cost was determined at plant location; marketing and transportation costs for the products were not included.

5. Disposal of processed sand and land reclamation were not incorporated in the process cost. Enthalpies and specific heat data were obtained from Jayakar (1979).[87]

TABLE 70

Bitumen, Coke, Fuel Gas, and Oil Compositions

	Weight %				
	C	H	N	S	O
Bitumen	86.1	10.9	1.0	0.5	1.5
Coke	95.5	2.9	1.0	0.6	--
Fuel Gas	71.4	21.3	1.1	1.7	4.5
Oil	85.4	11.8	1.0	0.3	1.5

Description of the Process

The process is shown in Figure 102. By means of a bucket elevator, B-1, tar sand (1) is fed into the pyrolysis reactor $-1, which comprises two stages; the upper stage constitutes the pyrolysis section and the lower stage the burner section. The upper bed is fluidized with a recycled stream of fuel gas (3) and the lower bed with air (7) which burns the coked sand (4), that flows by gravity from the upper bed. Steam is generated at two levels, high pressure (HP) (36) and low pressure (LP) (34), through the heat recovery with S-1 and S-2 by using hot spent sand (5) from the burner. Finally, the sand (14) is discharged to a landfill.

Hot gases (2) containing vaporized bitumen, cracked products, and fluidizing gas leave the reactor, R-1, and pass through the heat exchanger E-2 where the recycle stream of fuel gas (16) is preheated. Low pressure steam is generated in S-3 using the process heat in the product stream (15). The product stream (17) is then cooled with air in E-4 and water in E-5, and the condensed oil (20) is removed in the phase separator B-3.

The recycled fuel gas (22) is compressed at C-2 using HP steam generated in S-1, and preheated (16) in E-2 before finally heating it in E-1 with the combustion gases (6) leaving the burner.

Fresh air feed (12), compressed at C-1 using part of the HP steam generated in S-1, is then preheated in E-3 with the hot combustion gases (9) leaving E-1. The rest of the heat in combustion gas stream (10) is used to generate LP steam in S-3.

Part of the HP steam generated in S-1 which is left after running the compressors C-1 and C-2, and all the LP steam generated in S-2 and S-3, is then utilized to drive a turbine to generate electrical power at C-3. The water-vapor mixture leaving the compressors C-1, C-2, and C-3 is cooled with air in E-6 and pumped back to steam generators S-1 and S-2.

Apart from optimizing the heat exchanger network for minimum utility and capital costs, another attractive feature of this process is that the energy necessary to sustain the pyrolysis process is obtained from a thermally balanced reaction at the burner section in R-1 by transferring the heat to the

upper section through heat pipes filled with liquid potassium. The overall process can be conveniently divided into three different sections.

Section I: This consists of the oil and gas recovery units including the reactor unit R-1 and the phase separator, B-3.

Section II: This includes the heat exchanger network for the recovery of thermal energy in the process streams, and the utility cooling.

Section III: This includes the heat engine network run by excess process heat for compressing process streams and for power generation.

Oil and Gas Recovery Process

The reactor unit, R-1, was designed by scaling up the bench-scale data obtained in the laboratory at the University of Utah for the same process,[90] and using an empirical correlation available in the literature.[86]

A conservative residence time of 45 minutes and a temperature of 475°C for the pyrolysis section are dictated by previous work for the given yield of oil, gas, and coke. For the burner section, the temperature was chosen to be 575°C in order to have a thermally balanced process that can supply sufficient energy through heat pipes to sustain the endothermic pyrolysis process. A residence time of 70 minutes is necessary for 98% combustion of coke contained in the sand coming from the pyrolysis section.

A system of heat pipes has been chosen to transfer energy from the burner to the pyrolysis section. The advantages of this system over other common means of heat transfer are high energy flow per unit of cross-sectional area, small driving force, and uniform temperature of operation (close to isothermal operation at each end).

Heat Exchanger Network for Thermal Energy Recovery

Heat exchangers E-1 and E-2 are used to preheat the fluidizing gas of the pyrolysis section up to 887°F (pyrolysis temperature) using the combustion products of the burner section at E-1 and the gaseous product of the pyrolysis section at E-2. Because the temperature of the pyrolysis gas is still high after being cooled at E-2, it is further cooled, first by air at E-4, then by water at E-5, to 100°F to condense the oil phase, which is separated in the phase separator B-3. The oil collected in the phase separator is the principal product of the process. Of the gas obtained in the phase separator, a portion is recycled as fluidizing gas and the rest is obtained as a secondary product.

The recycle gas, required for the operation of the upper fluidized bed, is compressed to a pressure set for an average pressure drop of 3 psig at each heat exchanger and the pressure drop at the fluidized bed.

The air used to fluidize the burner section needs to be compressed to a pressure determined as above for the pyrolysis gas, accounting for the pressure drop at the heat exchanger E-3 and the fluidized bed. The air is then preheated to 763°F to have a thermally balanced overall process (Figure 112) for the reactor R-1.

Heat Engines and Heat Pumps

The purpose of this section is to utilize process heat to generate HP (250 psia) and LP (55 psia) steam to run compressors and to derive power from direct-drive steam turbines. To fully utilize the thermal energy from the hot sand leaving the burner section, a minimum temperature of 280°F was considered a reasonable limit for 55 psia steam. The generation of two levels of steam better utilizes the available energy. Part of the 250 psia steam is used to provide power necessary for the compression stages for air (C-1) and recycle gas (C-2). The balance of the 250 psia steam with all of the 55 psia steam is used to generate electrical energy at C-3. Of the total electrical energy, 35% is used to operate the pumps, elevators and crusher. The remaining electricity is available for other uses.

Steam is generated from hot sand by means of vertical heat exchangers where the sand flows by gravity. The heat in the flue gas and the pyrolysis gas is recovered in conventional heat exchangers for two systems, gas/steam and gas-liquid/steam.

Economic Evaluation

Design specifications shown in Table 71 for 15,000 bbl/day allowed us to estimate the equipment costs, the total capital investment, and the annual operating cost shown in Tables 72 and 73. From the cost data in Peters and Timmerhaus,[88] the equipment cost was estimated using the CE plant cost index and the inflation rate reported by the Congressional budget committee. Cost calculations were based on 1986 dollars. Installed equipment costs, reported in Table 71, were obtained using a Lang factor of 5. A 20% contingency factor was chosen to account for possible fluctuation in the cost of equipment.

Working capital constituted only 10% of the total investment. The total investment is insensitive to either the raw material cost or the operating cost. Costs of the raw material, utilities, and the fixed process costs are reported in dollars per barrel of synthetic crude product in Table 73. The raw material cost contributed about 75 to 80% of the total operating cost.

In order to determine the profitability of the investment, the net present value for this project was estimated. Taking 13 years as the project life, which includes 3 years for the construction of the plant, the price of the crude oil for the next ten years is forecast from the data report in the Monthly Energy Review.[91] With an estimate of the synthetic crude oil price based on the forecast, and assuming no salvage value after the ten year period, the net present value is estimated to be 27.50 million dollars.

PROCESS DESIGNS AND ECONOMIC EVALUATIONS FOR A RANGE OF TAR SAND BITUMEN CONTENTS

The process designs and economic evaluations presented in the previous section were extended, by considering the effect of bitumen content at 8, 10, and 12 weight percent levels, for a plant of 50,000 bbl/day of oil capacity. For the designs and economic analyses, bitumen, coke, fuel

TABLE 71

Equipment Cost Summary for 15,000 bbl/day

Code	Type	No of Units	Unit Size	Cost/Unit x $1000	Total Cost x $1000
R-1	Reactor	2	26 ft dia, 110 ft height 1180 heat pipes	6,645	13,290
E-1	Exchanger	2	7,442 ft^2	360	720
E-2	Exchanger	6	8,739 ft^2	360	2,160
E-3	Exchanger	3	6,639 ft^2	562	1,686
E-4	Exchanger	3	8,816 ft^2	459	1,377
E-5	Exchanger	5	6,339 ft^2	302	1,510
E-6	Exchanger	5	9,800 ft^2	528	2,640
S-1	Steam Generator	2	7,940 tubes, 10 ft x 2 in	1,587	3,174
S-2	Steam Generator	4	7,540 tubes, 10 ft x 2 in	1,412	5,648
S-3	Steam Generator	5	7,901 ft^2	737	3,685
C-1	Compressor	1	13,602 HP	13,400	13,400
C-2	Compressor	1	10,708 HP	12,000	12,000
C-3	Power Generator	1	20,100 KW	16,120	16,120
P-1	Pump	1	14.2 HP	80	80
P-2	Pump	1	82.8 HP	306	306
B-1	Bucket Elevator	2	75 HP	2,440	4,880
B-2	Crusher	2	925 HP	700	1,400
	Grinder	8	925 HP	1,000	8,000
B-3	Reflux Drum	1	6 ft dia, 24 ft height	1,854	1,854
			Subtotal		93,930
			20% contingency		18,790
			TOTAL		112,720

†Plant size: 15,000 bbl/d

TABLE 72

Total Capital Investment for 15,000 bbl/day

Item	Cost, 1000$
Equipment	112,720
Off-site Facilities, site development & Building (10% Equipment)	11,280
TOTAL	124,000
2% Contractor fee	2,480
Fixed Cost Investment	126,480
Working Capital* (2 mo operating cost)	11,000
Total Investment	137,480

† (Plant size: 15,000 bbl/d)
* (see Table 11)

TABLE 73

Annual Operating Cost for 15,000 bbl/day

	Annual Cost 1000 $/yr	$/BBL
1. Raw Material, 5 $/ton, 330 d/year	49,121	9.92
2. Variable Operating Cost		
Cooling Water, 0.11 $/1000 gal	220	0.04
Electricity, 0.065 $/KWH	-10,347	-2.09
3. Fixed Process Cost		
Direct Operation Cost (DOL): 6 men/shift, 19 $/hr	904	
Operating Supervision, 50% DOL	452	
Operating Payroll Burden, 50% DOL	452	
Operating Supplies, 20% DOL	181	
Maintenance, 5% FCI	6,330	
Plant Overhead, 50% DOL	452	
Administrative Cost, 50% DOL	452	
Taxes and Insurance, 4% FCI	5,060	
Depreciation, 10% FCI	12,650	
TOTAL FIXED PROCESS COST	26,933	5.43
TOTAL OPERATING COST	65,927	13.30

†Plant Size: 15,000 bbl/d

gas, and oil compositions as given in Figure 118 were assumed. The weight percent of bitumen in the oil-sand feed was taken as 8, 10, and 12 weight percent. As mentioned above, it was assumed that 70 weight percent of the bitumen can be recovered as oil, with 10 percent going to light fuel gases, and 20 percent to coke.

A plant size of 50,000 bbl/day of synthetic crude produced, operating 330 days per year, was assumed. The cost of mining and transporting the raw oil-sand was taken to be $5 per ton of raw oil-sand fed, but other mining costs were also evaluated. The resulting production cost does not include marketing, transportation costs of the products, disposal of processed sand, land reclamation, interest on capital investment, or profit.

The process structure shown in Figure 112 was found to be adequate. Improvements in the heat exchanger network could be made for specific feeds, but the flexibility in processing a range of bitumen content in the feed would then be lost. Such flexibility is required because feed bitumen content would be expected to vary during plant operation. Energy and material balances were made assuming that all compressors operated at efficiencies of 85% and all turbines operated at 70% efficiency. These were more realistic than earlier bases. For low bitumen content feed, it was found necessary to recycle and burn a portion of the product fuel gas to provide sufficient heat energy for the reactor. For cases of 8, 10, and 12 weight percent bitumen in the feed, fuel gas amounting to 38.2, 9.1, and 0 percent of the total fuel gas produced is recycled and burned in the combustion reactor. For all gases, the total fuel gas produced is 1186 tons per day.

Excess process steam is used to produce electricity. In-plant electric power usage was calculated to be approximately 35 percent of the electricity produced form excess process steam. The power requirement was estimated by taking the capacity of all equipment in the plant and summing the power consumption. To account for the value of product fuel gas, it was assumed that excess fuel gas is burned in a gas turbine to produce additional electricity, which is valued at an assumed market price. More power was required for the leaner tar sand, but more excess steam is produced due to the recycle combustion of a portion of the fuel gas.

Oil Sand Composition

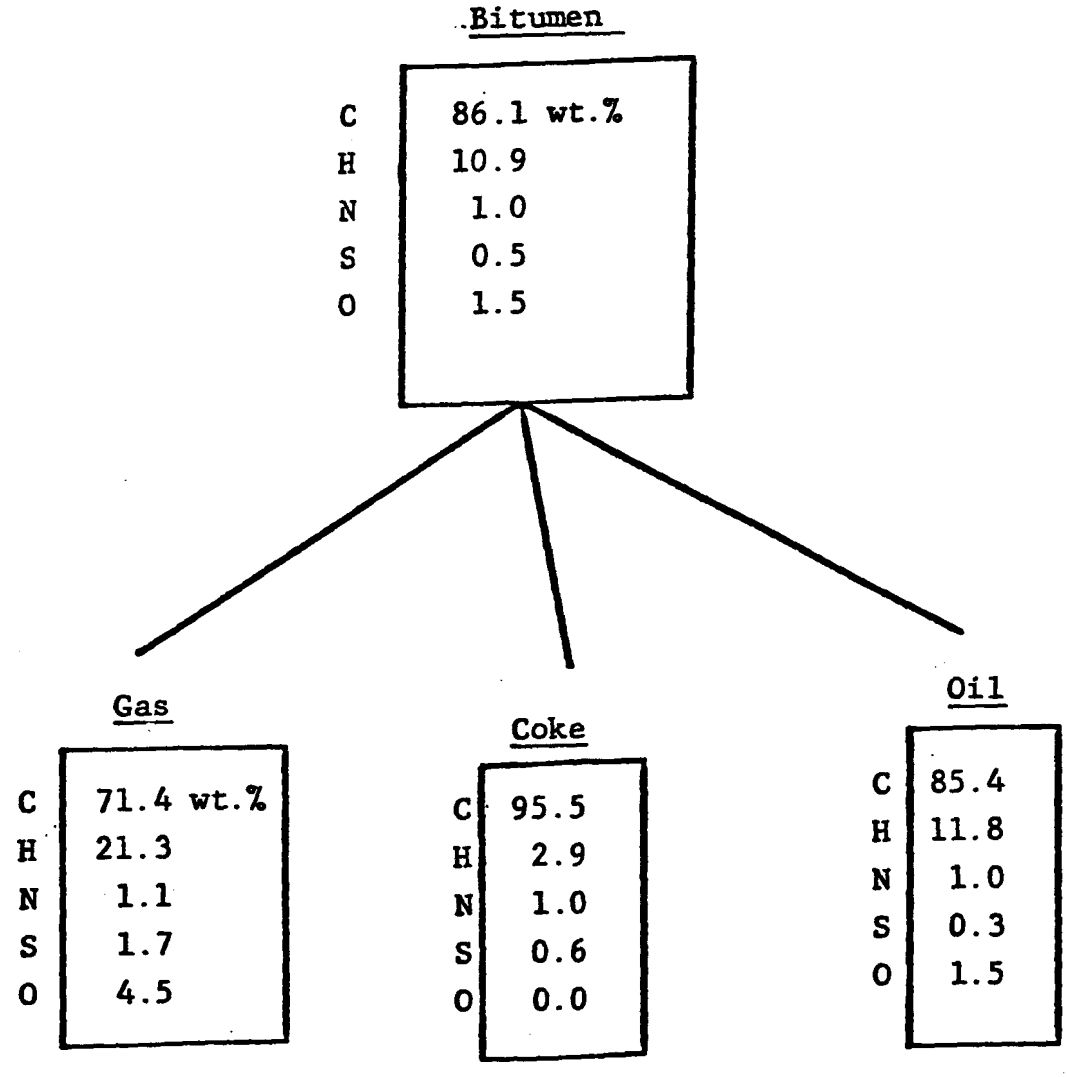

Figure 118. - Oil sand composition used for designs.

Process Description

As shown in Figure 104, raw oil sand is fed to the upper stage of the two-stage fluidized-bed reactor. Recycled light fuel gas is fed to the base of the pyrolysis bed as the fluidizing gas. A gas fluidization velocity of 2.20 ft/sec (510 lb/hr-ft^2) was chosen for the pyrolysis bed. This value is between the minimum fluidization velocity of 0.148 ft/sec and the maximum fluidization velocity of 8.37 ft/sec. A conservative residence time for sand of 45 minutes at 475°C was used.

The coked sand passes from the pyrolysis bed to the combustion bed, where air is used as the fluidizing gas. A fluidization velocity of 3.38 ft/sec (842 lb/hr ft^2) was chosen, which lies between the minimum fluidization velocity of 0.125 ft/sec and the maximum fluidization velocity of 8.14 ft/sec. A residence time of 70 min was used for the sand.

Heat pipes are used to transfer heat from the lower bed at 757°C to the upper bed at 475°C, with a heat flux of 2.83 x 10^6 Btu/ft^2-hr. For 4-inch diameter heat pipes, this yields a capacity of 247,000 BTU each.

The hot spent sand from the combustion reactor bed passes through two heat exchangers, where the excess heat is used to produce steam.

The hot gases from the pyrolysis bed pass from the reactor through a heat exchanger where the recycle gas is preheated. Then the pyrolysis gas is cooled to 138°C in a steam generator. The gas is further cooled in air coolers and the oil product is collected in a phase separator.

Process steam is used to compress the recycle fuel gas and air that are used to fluidize the reactor beds. Excess process steam is used to produce electricity in the steam turbine. It is assumed that 98 wt.% of the coke is burned in the combustion reactor with the stoichimetric quantity of oxygen. The resulting sand by-product is, therefore, quite clean and can be returned to the site as landfill.

Heat recovery from the spent sand leaving the combustion reactor depends on the concentration of bitumen in the oil sand feed. For the case of 12 wt.% bitumen in the feed, all of the steam produced by heat recovered from the sand is required at the higher pressure to provide power

to drive the two compressors. For the two cases of lower bitumen content, a greater amount of sand passes through the system and more efficient recovery of the excess heat is accomplished by producing steam at a lower pressure and temperature in a second heat exchanger downstream from the first.

Calculations of the second-law thermodynamic efficiency were also made for each of the three cases. The exergy loss and thermodynamic efficiency depend on the assumptions made about the process and to what extent the entire process is included in the calculations. The results for the entire process are summarized in Table 74. It is assumed that no steam is exported as such from the process. The dead-state temperature was taken as 77°F (25°C).

Economic Evaluations

The design specifications for each unit for a 50,000 bbl/day plant size were incorporated into a microcomputer spreadsheet to make the economic calculations. The cost basis was maintained consistent with previous work reported above. The CE plant cost index was used to bring costs up to 1986 dollars.

Production cost summaries are given in Tables 75, 76, and 77 for the three bitumen contents. The unit sizes required are generally as large as available, and, therefore, little difference in production cost for plant sizes between 15,000 and 50,000 bbl/day was found. No sparing of equipment was provided. A conservative estimate of the cost of mining raw oil sands of $5 per ton was used, though estimates range from $4 per ton to $9 per ton or higher, depending on the mining method used and the depth of the overburden and pay zone. No data from actual commercial mining of Utah oil sands are available.

Excess electricity production, including power derived from product fuel gas, was valued at 7 cents per kilowatt hour. Under the Public Utilities Regulatory Policies Act (PURPA), electricity can be sold to a utility, but rates in Utah for such secondary producer power have been low (approximately

Table 74

Results of Overall Second-Law Thermodynamic Analysis

	Bitumen Content of Feed		
	8%	**10%**	**12%**
Exergy Loss Btu/lb tar sand	303.2	312.8	352.8
Thermodynamic Efficiency, %	3.9	4.3	3.8

Table 75

Investment and Operating Cost Summary
for 8% Bitumen in Feed

Total Capital Investment	**1000$**	
Equipment	341,248	
Offsite facilities, etc. (10% equipment)	34,125	
Total	375,373	
2% contractor fee	7,507	
Fixed Cost Investment (FCI)	382,880	
Working Capital (2 months operating cost)	45,741	
TOTAL INVESTMENT	428,621	

Annual Operating Cost

	Annual Cost 1000%/yr	$/BBL
Raw Material, 5$/ton, 330 d/year	244,571	14.82
Variable Operating Cost		
Cooling Water, 0.11$/1000 gal	762	0.05
Electricity, 0.065 $/kW-hr	-4,770	-0.29
(less 35061 kW for process)		
Fixed Process Cost		
Direct Operation Cost: 6 men/shift @19$/hr	904	
Operation Supervision, 50% DOL	452	
Operating payroll burden, 50% DOL	452	
Operating Supplies, 20% DOL	181	
Maintenance, 5% FCI	19,144	
Plant Overhead, 50% DOL	452	
Administrative Cost, 50% DOL	452	
Taxes and Insurance, 4% FCI	15,315	
Depreciation, 10% FCI	38,288	
TOTAL FIXED PROCESS COST	75,640	4.58
TOTAL OPERATING COST	316,204	19.16

PRODUCT FUEL GAS COMBUSTION		
732.8 t/day		
Electric production at 30% efficiency = 3964 kW-hr/ton		
0.065 $/kW-hr	-62,308.4	
Gas turbines: 15% of capital cost @ $137 million	20,550	
TOTAL OPERATING COST	274,445	16.63

TABLE 76

Investment and Operating Cost Summary
for 10% Bitumen in Feed

10% Bitumen in Tar Sand Feed			
Total Capital Investment	**1000$**		
Equipment		288,471	
Offsite facilities, etc. (10% equipment)		28,847	
Total		317,318	
2% contractor fee		6,346	
Fixed Cost Investment (FCI)		323,665	
Working Capital (2 months operating cost)		32,205	
TOTAL INVESTMENT		355,870	
Annual Operating Cost			
		Annual Cost 1000%/yr	$/BBL
Raw Material, 5$/ton, 330 d/year		195,660	11.86
Variable Operating Cost			
Cooling Water, 0.11$/1000 gal		686	0.04
Electricity, 0.065 $/kW-hr		-6,017	-0.36
(less 28731 kW for process)			
Fixed Process Cost			
Direct Operation Cost: 6 men/shift @19$/hr		904	
Operation Supervision, 50% DOL		452	
Operating payroll burden, 50% DOL		452	
Operating Supplies, 20% DOL		181	
Maintenance, 5% FCI		16,183	
Plant Overhead, 50% DOL		452	
Administrative Cost, 50% DOL		452	
Taxes and Insurance, 4% FCI		12,947	
Depreciation, 10% FCI		32,366	
TOTAL FIXED PROCESS COST		64,389	3.90
OPERATING COST		254,717	15.44
PRODUCT FUEL GAS COMBUSTION			
1,077.7 t/day			
Electric production at 30% efficiency = 3964 kW-hr/ton			
0.065 $/kW-hr		-91,634	
Gas turbines: 15% of capital cost @ $201 million		30,150	
TOTAL OPERATING COST		193,233	11.71

TABLE 77

Investment and Operating Cost Summary for 12% Bitumen in Feed

Total Capital Investment	**1000$**	
Equipment	288,565	
Offsite facilities, etc. (10% equipment)	28,857	
Total	317,422	
2% contractor fee	6,348	
Fixed Cost Investment (FCI)	323,770	
Working Capital (2 months operating cost)	25,916	
TOTAL INVESTMENT	349,687	

Annual Operating Cost

	Annual Cost 1000$/yr	$/BBL
Raw Material, 5$/ton, 330 d/year	163,048	9.88
Variable Operating Cost		
Cooling Water, 0.11$/1000 gal	662	0.04
Electricity, 0.065 $/kW-hr	-5,094	-0.31
(less 23761 kW for process)		
Fixed Process Cost		
Direct Operation Cost: 6 men/shift @19$/hr	904	
Operation Supervision, 50% DOL	452	
Operating payroll burden, 50% DOL	452	
Operating Supplies, 20% DOL	181	
Maintenance, 5% FCI	16,189	
Plant Overhead, 50% DOL	452	
Administrative Cost, 50% DOL	452	
Taxes and Insurance, 4% FCI	12,951	
Depreciation, 10% FCI	32,377	
TOTAL FIXED PROCESS COST	64,409	3.90
TOTAL OPERATING COST	223,025	13.52

PRODUCT FUEL GAS COMBUSTION		
1,185.8 t/day		
Electric production at 30% efficiency = 3964 kW-hr/ton		
0.065 $/kW-hr	-100,826	
Gas turbines: 15% of capital cost @ $222 million	33,300	
TOTAL OPERATING COST	155,499	9.42

2.6 to 2.8 cents per kilowatt hour). A much higher rate could be realized if a company could utilize the power internally or if the power could be sold to an independent municipality.

The cost for additional equipment required to generate electricity, by utilizing the product fuel gas, was estimated as 70% of the total plant cost for a recently constructed power plant, the Hunter III power plant built by the Utah Power and Light Company.

The production cost of synthetic crude oil from tar sand, excluding interest, profit, marketing, product transportation costs, and disposal of the processed sand, ranges from $16.32 per barrel when feeding 8 wt.% bitumen, to $9.49 per barrel when feeding 12 wt.% bitumen. However, the cost of production is highly sensitive to the cost of mining the raw oil sand feed. For the case of 10 wt.% bitumen feed, for a mining cost of $5 per ton, the calculated production cost is $11.70/bbl. At $8 per ton mining cost, the production cost becomes $18.80/bbl.

The production cost is less sensitive to the value of excess electric power produced. A one-cent change from 6.5 cents per kilowatt hour results in a $.90 per barrel change in the net cost of production. A review before the Public Utilities Commission at the end of 1986 on the rate structure of electricity regarding secondary producers did not seem to improve the outlook from the secondary producers standpoint.

SECOND-LAW ANALYSES FOR COMPETING THERMAL PROCESSES

Thermal processes for the recovery of bitumen, conversion to oil, and upgrading to a refinery feedstock are inherently inefficient because the processes must be conducted at elevated temperatures. To determine quantitatively the extent to which a thermal process is inefficient from a thermodynamic standpoint, a second-law analysis can be performed based on a combined statement of the first and second laws of thermodynamics. This type of analysis involves the computation of the loss of ability of material to do useful work. The qualitative statement of the analysis is:

Lost work = Loss of availability of streams flowing in and out of the process + Net work equivalent of heat transfer into the process + Net shaft work into the process where availability = enthalpy - entropy times absolute surroundings temperature.

This type of analysis was made for three different types of thermal processes for the combined recovery and conversion of bitumen to oil. These three processes are:

1. Dual fluidized beds with extensive preheating of fluidizing gas (DBPG).
2. Dual fluidized beds with hot-sand recycle (DBSR).
3. Dual fluidized beds with heat pipes (DBHP).

Results of the second-law analysis were as follows:

Process	Lost Work, kJ/kg Tar Sand
DBPG	670
DBSR	469
DBHP	372

The results show the clear superiority of the use of heat pipes.

DEVELOPMENT OF A CORRELATION FOR MINIMUM FLUIDIZATION VELOCITY FOR SAND AT ELEVATED TEMPERATURES

This effort was part of a study to determine the optimal velocity and bed configuration for the two coupled fluidized beds used in the energy-efficient thermal process for recovery of oil from tar sands.

The correlation of Rowe and Nienow[89] is one of the few equations that is formulated to predict minimum fluidization velocity for a bed of mixed particle sizes:

$$U_c = U_1\{(\varepsilon/\varepsilon_1)^3[(1-\varepsilon_1)^{.947}/(1-\varepsilon)^{.947}]\}^{.95}[X_1+*d_1X_2)/d_2+...]^{-1.85} \quad (126)$$

where

ε_1 = voidage of a bed of particles of diameter d_1;

ε = voidage of mixture;

U_1 = minimum fluidization velocity of diameter d_1, m/s;

U_c = minimum fluidization velocity of a mixture, m/s;

$X_1, X_2, X_3 \ldots X_i$ = weight fractions of particles of diameters d_1, d_2...etc., respectively.

Because of difficulties of measuring ε_1 and ε, a modified correlation has been developed. The results are much better than those calculated by the equations of Leva[92] and Babu.[93]

This generalized equation of Rowe and Nienow[89] is applicable for: (1) Re_{mf} up to 10 and (2) all particles of the same shape. Re_{mf} in our case varies from 0.025 to 0.21 and the particles are all of similar shape. Because ε is a function of Re, we have attempted to replace ε with Re_{mf}. According to our previously reported data, $\varepsilon = C\ Re^{-0.027}$. From Leva's results,[92]

$$\varepsilon_{mf}^3 d_p^2/150(1-\varepsilon_{mf}) = 0.0007\ Re_{mf}^{-.063}. \tag{127}$$

Here, for a given particle mixture, d_p is constant. Since ε_{mf}^3 dominates the value of the left side, equation 127 reduces to $\varepsilon_{mf}^3 = CRe_{mf}^{-.063}$. Taking the cube root of both sides, we obtain

$$\varepsilon_{mf} = C\ Re^{-0.02}. \tag{128}$$

With C = 0.476, calculations for our experimental data give:

Temp., °C	Re	Measured ε	Calculated ε
23.5	0.21	0.488	0.491
200.0	0.073	0.506	0.502
400.0	0.040	0.496	0.508
600.0	0.025	0.525	0.565

The results show a maximum deviation of less than 10%, with an average deviation of only three percent. In equation 126, the term $[(1-\varepsilon_1)/(1-\varepsilon)]^{.94}$ is less important than $(\varepsilon/\varepsilon_1)^3$. Therefore, equation 126 may be simplified to:

$$U_c = U_1(\varepsilon/\varepsilon_1)^{2.85}\,[X_1 + (d_1X_2/d_2) + \ldots]^{-1.85}. \tag{129}$$

From equation 128:

$$\varepsilon/\varepsilon_1 = (Re_{mf}/Re_{mf_1})^{-.02} = (ud/u_1d_1)^{-.02}. \tag{130}$$

Substitution of equation 130 into 129 gives:

$$U_c = U_1(d/d_1)^{-0.054}[X_1+(d_1X_2)/d_2+ \ldots.]^{-1.75}. \tag{131}$$

Let G_c and G_1 represent mass velocities in the unit such that:

$$G_c/G_1 = \rho_g U_c/\rho_g U_1 = U_c/U_1.$$

Substitution into equation 131 gives

$$G_c = G_1(d/d_1)^{-.054}[X_1+(d_1X_2)/d_2 + \ldots.]^{-1.75}. \tag{132}$$

From our experimental data on particle size distribution:

Size Fraction	d_1	d_2	d_3	d_4	d_5	d_6
d_p, μm	100	150	200	250	300	500
Fraction, X	10%	20%	51%	14%	4%	1%

The average particle size is d_p = 143 μm. Substitution of these values into equation 132 gives:

$$G_c = 2.71\ G_1. \tag{133}$$

Leva's equation to estimate G_1 (minimum velocity of particle of diameter (d^1) is:[92]

$$G = 688\ \frac{d_1^{1.85}\rho_g(\rho_s - \rho_g)]^{.94}}{\mu_g^{.88}} \tag{134}$$

where

$d_1 = 100\mu m = 3.281*10^{-4}$ feet = 0.003937 in

$\rho_s = 166.7$ lb/ft^3

The results for the minimum mass velocity in lb/hr-ft^2 are:

	G_{mf}			
T, °C	**Measured**	**Eq. (133)**	**Leva**	**Babu**
23.5	19.50	24.17	17.11	28.02
200.0	10.00	11.25	7.97	12.19
400.0	6.80	6.67	4.71	6.88
600.0	5.00	4.50	3.19	4.50

From the comparison, equation 133, based on equation 131, predicts better values than the correlations of Leva or Babu.[92,93]

REFERENCES

1. Oblad, A.G., P.I., "Recovery of Oil from Utah's Tar Sands," Final Report for Contract DE-AT-81LC10332, 1979-1983.

2. Oblad, A.G., P.I., "Recovery of Oil from Utah's Tar Sands," Final Report for Contract DOE EY 77-S-03-1762, 1977-1979.

3. Bunger, J.W., and Cogswell, D.E., "Characteristics of Tar Sand Bitumen Asphaltenes as Studied by Conversion of Bitumen by Hydropyrolysis," Ch. 13 of Chemistry of Asphaltenes, J.W. Bunger, N.C. Li (eds.), Advances in Chemistry Series - 1985, American Chemical Society, 1981.

4. Bunger, J.W., Cogswell, D.E., Wood, R.E., and Oblad, A.G., "Hydropyrolysis - Potential for Primary Upgrading, in Oil Shale, Tar Sands, and Related Materials, Harry Stauffer, ed., ACS Symposium Series - 163, Chapter 25, pp. 369-380.

5. Bunger, J.W., "Upgrading Utah Tar Sand Bitumen to Syncrude," Proceedings WRI-DOE Tar Sand Symposium, Western Research Institute, Vail, Colorado, June 26-29, 1984.

6. Bunger, J.W., Tsai, C.H., and Russell, C.P., "Competing Reactions During Hydropyrolysis Upgrading of Tar Sand Bitumen and Residual Material," Proceedings - WRI-DOE Tar Sand Symposium, Western Research Institute, July 7-10, 1986.

7. Bunger, J.W., and Oblad, A.G., "Upgrading of Bitumen by Hydropyrolysis--A Process for Low Coke and High Syncrude Yields," Proceedings III International Conf. on Heavy Crude and Tar Sands. UNITAR/UNDP Information Centre, July 22-31, 1985, pp. 1717-1726.

8. Bunger, J.W., "Reactions of Hydrogen During Hydropyrolysis Processing of Heavy Crudes," Preprints, Division of Petroleum Chemistry, ACS, 30 (3), 594-554 (1985).

9. Bunger, J.W., "Inhibition of Coke Formation in Hydropyrolysis of Residual Oils," Preprints, Division of Petroleum Chemistry, ACS, 30 (3), 549-554 (1985).

10. Bunger, J.W., Cogswell, D.E., and Oblad, A.G., Am. Chem. Soc. Div. Fuel Chem. Prepr., Miami Beach, Sept. 1978, 23 (4), 98.

11. Shabtai, J.S., Ramakrishnan, R., and Oblad, A.G., "Hydropyrolysis of Model Compounds," in "Thermal Hydrocarbon Chemistry," Oblad et al., ed., Adv. in Chem. Ser., 183, 297-329, 1979.

12. Bunger, J.W., "Processing Utah Tar Sand Bitumen," Ph.D. Dissertation, University of Utah, Salt Lake City, Utah, 1979.

13. Bunger, J.W., and Oblad, A.G., "Upgrading of Bitumen by Hydropyrolysis--a Process for Low Coke and High Syncrude Yields," Proceedings, 3rd International Conference on Heavy Crudes and Tar Sands, UNITAR/UNDP, July 22-31, 1985, pp. 1717-1726.

14. Oblad, A.G., et al., "Recovery and Hydropyrolysis of Oil from Utah's Tar Sands," Final Report, #DE-AS20-82LC10942 (1985).

15. Bunger, J.W., "Evidence for the Thermal Hydrogenation of Aromatics During Hydropyrolysis," Presented before the 185th National Meeting, Amer. Chem. Soc., Seattle, Mar. 20-25, 1983.

16. Ramakrishnan, R., "Hydropyrolysis of Coal Derived Liquids and Related Model Compounds," Ph.D. Dissertation, University of Utah, Salt Lake City, Utah, 1978.

17. Wen, Y.H., "Hydropyrolysis of Partially Hydrogenated Synfuels and Related Naphthenoaromatic Compounds," Ph.D. Dissertation, University of Utah, Salt Lake City, Utah, 1986.

18. The source and description of TS-IIC oil is given in L.A. Johnson et al., J. Petr. Tech., pp. 295-304, Feb. 1980.

19. Bunger, J.W., Thomas, K.P., and Dorrence, S.M., "Compound Types and Properties of Utah and Athabasca Tar Sand Bitumen," Fuel, (1979), 58 (3), 183.

20. Oblad, A.G., et al., "Recovery and Upgrading of Oil from Utah's Tar Sands," Second Annual Report 1985-86, DE-FG20-84LC11057 (1987).

21. Bajus, M., and Vesely, V., "Steam Cracking of Hydrocarbons. 2. Pyrolysis of Methylcyclohexane," Ind. Eng. Chem. Product Res. Dev., 1979, 18(2), 135-142.

22. Knight, S.A., "Analysis of Aromatic Petroleum Fractions by Means of Absorption Mode Carbon-13 NMR Spectroscopy," Chemistry and Industry, (1967), 11, 1920.

23. Dickinson, E.M., "Structure Comparison of Petroleum Fractions Using Proton and ^{13}C n.m.r. Spectroscopy," Fuel, (1980), 49 (5), 2980.

24. Gillet, S., and Rubini, P., "Quantitative C-13 and Proton n.m.r. Spectroscopy of Crude Oil and Petroleum Products. 1. Some Rules for Obtaining a Set of Reliable Structural Parameters," Fuel, (1981), 60 (3), 221.

25. Gupta, P.L., et al., "Estimation of Average Structural Parameters of Petroleum Crudes and Coal-Derived Liquids by ^{13}C and ^{1}H n.m.r.," Fuel, (1986), 65 (4), 515.

26. Kershaw, J.R., and Kelly, B.A., "The Chemical Nature of Flash Pyrolysis Tars. An N.M.R. Study," Fuel Proc. Tech., (1983), 7, 145-159.

27. Snape, C.E., "Assignment of Aliphatic Carbon Peaks in the ^{13}C n.m.r. Spectra of Coal Liquefaction Products," Fuel, (1982), 61 (8), 775.

28. Netzel, D.A., and Miknis, F.P., "NMR Study of U.S. Eastern and Western Shale Oils Products by Pyrolysis and Hydropyrolysis," Fuel, (1982), 66 (11), 1101.

29. Dalling, D.K., et al., "Application of C-13 and Proton NMR to the Average Structure Analysis of Athabasca, Santa Rose, and Asphalt Ridge Tar Sand Bitumens," Symposium on WRI-DOE Tar Sand, at Vail, Colorado, 2-4 June, (19840.

30. Oblad, A.G., et al., "Recovery and Upgrading of Oil from Utah Tar Sands," First Annual Report 1984-85, DE-FG20-84LC11057 (1986).

31. Venkatesan, V.N., "Fluid Bed Thermal Recovery of Synthetic Crude from Bituminous Sands of Utah," Ph.D. Dissertation, University of Utah, Salt Lake City, Utah (1979).

32. Wang, J., "The Production of Hydrocarbon Liquids from a Bitumen-Impregnated Sandstone in a Fluidized Bed Reactor," M.S. Thesis, University of Utah, Salt Lake City, Utah (19830.

33. Dorius, J.C., "The Pyrolysis of Bitumen-Impregnated Sandstone from the PR Spring (Utah) Deposit in a Fluidized Bed," Ph.D. Dissertation, University of Utah, Salt Lake City, Utah (1985).

34. Shun, D., "The Fluidized Bed Pyrolysis of Bitumen-Impregnated Sandstone from the Circle Cliffs Deposit," Ph.D. research in progress (1985).

35. Middleton, W.R., "Gradient Elution Chromatography Using Ultraviolet Monitors in the Analytical Fractionation of Heavy Petroleums," Anal. Chem., 39, 1839 (1967).

36. Callen, R.B., Bendoraitis, J.G., Simpson, C.H., and Voltz, S.E., "Upgrading Coal Liquids to Gas Turbine Fuels. I. Analytical Characterization of Coal Liquids," Ind. Eng. Chem. Prod Res. Dev., 15, 222 (1976).

37. Utley, J., "The Application of Gradient Elution Chromatography to the Analysis of Bitumens and Bitumen-Derived Liquids," Senior Project Final Report, Department of Fuels Engineering, University of Utah, Salt Lake City, Utah (1983).

38. Johnson, L.A., Marchant, L.C., and Cupps, C.Q., "Properties of Utah Tar Sands--North Seep Ridge Area, P.R. Spring Deposit," Laramie Energy Research Center/RI-75/6 (1976).

39. Ritzma, H.R., "Oil-Impregnated Rock Deposits of Utah," Utah Geological and Mineralogical Survey, Map 47, (1979) (2 Pages).

40. Glassett, J.M. and Glassett, J.A., "The Production of Oil from Intermountain West Tar Sands Deposits," Final Report, U.S. Dept. of the Interior, Bureau of Mines, Contract No. 50,241,129 (1976).

41. Wood, R.E. and Ritzma, H.R., "Analyses of Oil Extracted from Oil-Impregnated Sandstone Deposits in Utah," Utah Geological and Mineralogical Survey, Special Studies 39, Salt Lake City, Utah (1972).

42. Gwynn, J.W., "Instrumental Analysis of Tars and Their Correlations in Oil-Impregnated Sandstone Beds, Uintah and Grant Counties, Utah," Utah Geological and Mineralogical Survey, Special Studies 37, Salt Lake City, Utah (1971).

43. Peterson, P.R., "Informational Core Drilling in Utah's Oil-Impregnated Sandstone Deposits, Southeast Uintah Basin, Uintah County, Utah," Utah Geological and Mineralogical Survey, Report of Investigation No. 88, (1974).

44. Pyrolysis: Theory and Industrial Practice, Albright, L.F., Crynes, B.L., and Corcoran, W.H., ed., Academic Press New York, New York, Chapter 4 (1983).

45. Drushell, H.V., Personal Communication, July 11, 1983.

46. Carberry, J.J., Chemical and Catalytic Reaction Engineering, McGraw-Hill Book Co., Inc., New York (1976).

47. Carberry, J.J., Personal Communication, October 29, 1984.

48. Box, G.E.P. and Wilson, K.B., "On the Experimental Attainment of Optimum Conditions," J. Royal Stat. Soc., Sec. B, 13 (1), 1 (151).

49. Box, G.E.P. and Wilson, K.B., "Multifactor Experimental Designs for Exploring Response Surfaces," Ann. Mathm. Stat., 195 (1957).

50. Speight, J.G., Personal Communication, July 23, 1984.

51. Wood, R.E., and Ritzma, H.R., "Analyses of Oil Extracted from Oil-Impregnated Sandstone Deposits in Utah," Utah Geological and Mineral Survey, Special Studies, 39, 1-19 (1972).

52. Campbell, J.A., and Ritzma, H.R., "Geological and Petroleum Resources of the Major Oil-Impregnated Sandstone Deposits of Utah," Utah Geological and Mineral Survey, Special Studies 50, 1-24 (1979).

53. Ritzma, H.R., "Oil Impregnated Sandstone Deposits, Circle Cliffs Uplift (Utah)," Utah Geological Association Henry Mountains Symposium, 343-351 (1980).

54. Kayser, R.B., "Bituminous Sandstone Deposits Asphalt Ridge," Utah Geological and Mineral Survey, Special Studies 19, Salt Lake City, Utah, (1966), 45.

55. Kuuskraa, V.V., and Hammershaimb, V.A., editors, "Major Tar Sand and Heavy Oil Deposits of the United States," Interstate Oil Compact Commission, Oklahoma City (1984).

56. Ball, D., Marchant, L.C., and Goldburg, A,. editors, "The IOCC Monograph Series: Tar Sands," Interstate Oil Compact Commission, Oklahoma City (1984).

57. Richardson, J.F., "Incipient Fluidization and Particulate Systems," in Fluidization, J.F. Davidson and D. Harrison, eds., Chapter 2, Academic Press, Inc., London, (1971).

58. Probstein, R.F., and Hicks, R.E., Synthetic Fuels, pp 28, McGraw-Hill, New York (1982).

59. Ritzma, H.R., "Oil-Impregnated Rock Deposits of Utah," Utah Geological and Mineral Survey, Map 47 (2 pages), University of Utah, Salt Lake City, Utah (1979).

60. Resnik, B.S., Dike, D.H., English, L.M., and Lewis, A.G., "Evaluation of Tar Sand Mining Volume I - An Assessment of Resources Amenable to Mine Production," Final Report, Contract No. DE-AC22-80PC30201, U.S. Department of Energy (1981).

61. Sepulveda, J.E., and Miller, J.D., "Extraction of Bitumen from Utah Tar Sands by a Hot Water Digestion-Flotation Technique," Mining Eng. 30, 1311 (1978).

62. Hupka, J., Miller, J.D., and Oblad, A.G., "Diluent-Assisted Hot Water Processing of Tar Sands," AOSTRA J. Res., 3, 95 (1987).

63. Miller, J.D., and Misra, M., "Concentration of Utah Tar Sands by an Ambient Temperature Flotation Process," Int. J. Mineral Process. 9, 269 (1982).

64. Venkatesan, V.N., Hanson, F.V., and Oblad, A.G., "A Fluidized-Bed Thermal Pyrolysis Process for the Recovery of a Bitumen-Derived Liquid from the Bitumen-Impregnated Sandstone Deposits of Utah," AIChE Symposium Series 78 (216), 42 (1982).

65. Rameler, R.W., "The Production of Synthetic Crude Oil from Oil Sand by Application of the Lurgi-Ruhrgas Process," Can. J. Chem. Eng., 48 (10), 552 (1970).

66. Weiss, H.J., "Direct Coking of Tar Sands by the L-R Process," paper presented at the Symp. on Production, Processing and Characterization of Heavy Oils, Tar Sand Bitumens, Shale Oils and Coal Derived Liquids, Salt Lake City, Utah (1981).

67. Miller, J.D., and Misra, M., "Hot Water Process Development for Utah Tar Sands," Fuel Proc. Tech. 6, 27-59 (1982).

68. Lin, L.C., Hanson, F.V., and Oblad, A.G., "A Preliminary Mathematical Model of the Pyrolysis of Bitumen-Impregnated Sandstone in a Fluidized Bed," Proceedings DOE-WRI Tar Sands Symposium, ( ).

69. Fan, L.S., Fan, L.T., Tojo, K., and Walawender, W.P., "Volume Reaction Model for Pyrolysis of a Single Solid Particle Accompanied by a Complex Reaction," Can. J. Chem. Eng., 56, 603 (1977).

70. Satterfield, C.N., Mass Transfer in Heterogeneous Catalysis, M.I.T. Press, Cambridge, Massachusetts (1970).

71. Bird, R.B., Stewart, W.E., and Lightfoot, E.N., Transport Phenomena, John Wiley & Sons, Inc., New York (1960).

72. Sneddon, I.N., Fourier Transforms, McGraw-Hill Book Co., New York (1951).

73. Sneddon, I.N., The Use of Integral Transforms, McGraw-Hill Book Co., New York (1972).

74. Ozisik, M.N., Heat Conduction, John Wiley & Sons, Inc., New York (1980).

75. Do, D.D., "Modeling of Oil Shale Pyrolysis in a Fluid-Bed Retort," Fuel Processing Technology, 10, 57 (1985).

76. McCabe, W.L., and Smith, J.C., Unit Operations of Chemical Engineering, 4th edn., McGraw-Hill, New York (1985).

77. Krieth, F., and Bohn, M.S., Principles of Heat Transfer, 4th edn., Harper and Row, New York (1986).

78. Carslaw, H.S., and Jaeger, J.C., Conduction of Heat in Solids, second edition, Oxford University Press, London (1959).

79. Camp, F.W., The Tar Sands of Alberta, Canada, 2nd ed., Cameron Engineers, Inc., Denver, Colorado (1974).

80. Hanson, F.V., 1983. Personal communication of data determined in Laboratory of Coal Science, Synthetic Fuels and Catalysis, Department of Fuels Engineering, University of Utah.

81. Robie, R.A., Hemingway, B.S., and Fisher, J.R., 1978. Thermodynamic properties of minerals and related substances at 298.15K and 1 bar (10^5 pascals) pressure and at higher temperatures. Geol. Survey Bull., 1452, Washington, D.C.

82. Barbour, R.V., Dorrence, S.M., Vollmer, T.L., and Harris, J.D., "Pyrolysis of Utah Tar Sands - Products and Kinetics," Preprints, Div. Fuel Chem., Amer. Chem. Soc., 21 (7), 278-283 (1976).

83. Lin, L.C., "The Kinetics and Mathematical Model of the Pyrolysis of Bitumen-Impregnated Sand Stone Particles," Ph.D. Dissertation, University of Utah, Salt Lake City, Utah, 1988.

84. Weast, R.C,. Editor, "CRC Handbook of Chemistry and Physics," 55th Edition, CRC Press, Cleveland (1974-1975).

85. Perry, R.H., and Chilton, C.H., Editors, "Chemical Engineers Handbook, 5th Edition, McGraw-Hill Book Co., Inc., New York (1973).

86. Kunii, D., and Levenspiel, O., "Fluidization Engineering," John Wiley & Sons, Inc., New York (1969).

87. Jayakar, K., "Thermal Recovery of Oil from Tar Sands," Ph.D. Dissertation, University of Utah, 1979.

88. Peters, M.S., Timmerhaus, K.D., Plant Design and Economics for Chemical Engineers, 3rd ed., McGraw-Hill, 1980.

89. Rowe, P.N. and Nienow, A.W., "Minimum Fluidization Velocity of Multi-Component Particle Mixtures," Chem. Eng. Sci., 30 1365 (1975).

90. Smart, L., "Thermal Processing of Utah Tar Sands," M.S. Thesis, University of Utah, 1984.

91. Monthly Energy Review, April 1985, Energy Information Administration, Washington, D.C., United States Department of Energy.

92. Leva, M., "Fluidization," McGraw-Hill, New York, 1959.

93. Babu, S.P., Shah, B., Talwalker, A., Chem. Eng. Progress Symposium Series, V. 74, 176 (1978) p 176.